

A COMPARISON OF THE USE OF CLASSICAL AND MODERN CONTROL  
DESIGN TECHNIQUES FOR IMPROVING THE LATERAL-DIRECTIONAL  
POWERED APPROACH FLYING QUALITIES OF THE F-14 AIRCRAFT

by

Joseph A. Renfrow

Thesis submitted to the Faculty of the  
Virginia Polytechnic Institute and State University  
in partial fulfillment of the requirements for the degree of

MASTER OF SCIENCE

in

Mechanical Engineering

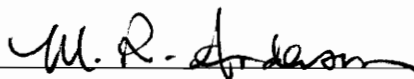
APPROVED:



H. H. Robertshaw, Chairman



H. H. Cudney



M. R. Anderson

December, 1994

Blacksburg, Virginia

C.2

LD  
5055  
V855  
1994  
R422  
c.2

A COMPARISON OF THE USE OF CLASSICAL AND MODERN CONTROL  
DESIGN TECHNIQUES FOR IMPROVING THE LATERAL-DIRECTIONAL  
POWERED APPROACH FLYING QUALITIES OF THE F-14 AIRCRAFT

by

Joseph A. Renfrow

Committee Chairman: Dr. Harry H. Robertshaw  
Mechanical Engineering

ABSTRACT

Due to the limitations of its analog flight control system, the F-14 aircraft exhibited several major flying qualities deficiencies. To correct these deficiencies, the Department of the Navy instigated a program to replace the analog system with digital flight control computers incorporating enhanced control laws. A new control law was designed for the powered approach configuration (landing phase) using classical control techniques, and demonstrated greatly improved flying qualities in piloted simulator testing. To determine if further increases in system performance were realizable, an advanced multivariable control system was designed. Although the multivariable control law design resulted in excellent flying qualities, a significant improvement was not realized over the classically designed system and therefore should not be considered for implementation into the actual flight control software.

## **Acknowledgments**

I would like to thank my advisor Dr. Harry Robertshaw for being patient with me over the years as I balanced the demands of work, school, and family.

I would also like to thank my past and present supervisors at the Manned Flight Simulator for supporting my quest for higher education.

Finally, I am eternally grateful to my wonderful wife Jinna for the sacrifices she made which enabled me to successfully complete this project, and for doing such a wonderful job of raising our son Robert.

# Table of Contents

Abstract.....	ii
Acknowledgements.....	iii
Table of Contents.....	iv
List of Figures.....	vii
List of Tables.....	xi
Nomenclature.....	xii
I. Introduction.....	1
1.1 Background.....	1
1.2 Literature Review.....	6
1.3 Contributions of the Thesis.....	8
1.4 Outline of the Thesis.....	9
II. F-14 Aircraft Model Description.....	10
2.1 Simulation Description.....	10
2.2 Nonlinear Equations of Motion.....	14
2.3 Linear Aircraft Dynamics Model.....	15
III. Aircraft Flight Control Requirements and Analysis Methods.....	20
3.1 Introduction.....	20
3.2 Flying Qualities.....	20
3.3 Flying Qualities Specifications.....	22
3.4 Low Order Equivalent Systems.....	25
3.5 SISO Robustness.....	27
3.6 MIMO Robustness.....	27
IV. Analysis of the Production Control System.....	31
4.1 Introduction.....	31
4.2 System General Description.....	31
4.2.1 Lateral Control System Description.....	32
4.2.2 Directional Control System Description.....	36
4.3 Piloted Simulation Evaluation.....	41
4.3.1 Bank Angle Captures.....	41
4.3.2 Runway Lineup Corrections.....	42
4.4 Off-line Nonlinear Simulation Evaluation.....	45

	4.4.1	Response to Pilot Control Inputs.....	45
	4.4.2	Response to Atmospheric Turbulence.....	50
	4.5	Open-loop Stability Analysis.....	50
	4.6	Summary.....	53
V.		PA ARI Control Law Design.....	61
	5.1	Introduction.....	61
	5.2	Design Objectives.....	61
	5.3	PA ARI Description.....	62
	5.4	Sideslip Rate Estimator Design.....	65
	5.5	Feedback Loop Design Techniques.....	68
	5.5.1	Roll Rate Feedback Gain Design.....	73
	5.5.2	Estimated Sideslip Rate Feedback Gain Design.....	77
	5.6	Feedforward Path Designs.....	94
	5.6.1	Lateral Stick to Spoiler Gearing.....	94
	5.6.2	Lateral Stick to Rudder.....	97
	5.6.3	Roll Rate Command Model.....	100
	5.7	SISO Robustness.....	103
	5.8	MIMO Robustness.....	111
	5.9	Response to Atmospheric Turbulence.....	114
	5.10	Equivalent Systems Analysis.....	114
	5.11	Piloted Simulation Evaluation.....	119
	5.11.1	Bank Angle Captures.....	119
	5.11.2	Runway Lineup Corrections.....	119
	5.12	Summary.....	120
VI.		Multivariable Model Following (MMF) Control Law Design.....	121
	6.1	Introduction.....	121
	6.2	Design Objectives.....	121
	6.3	General Description.....	122
	6.4	Maneuver Command Generator.....	124
	6.4.1	Roll Rate Command Model.....	124
	6.4.2	Sideslip Command Model.....	127
	6.4.3	Yaw Rate Command due to Roll Rate Command.....	127
	6.4.4	Yaw Rate Command due to Roll Angle Command.....	129
	6.4.5	Yaw Rate Command due to Sideslip Rate Command..	129

6.4.6	Response to Pilot Inputs.....	130
6.5	Design Plant Model.....	134
6.5.1	Control Selector Design.....	135
6.5.2	Transformation to Sensor Coordinates.....	137
6.6	Feedforward Dynamic Inversion.....	139
6.6.1	Solution of the Dynamic Inversion Problem.....	139
6.6.2	Application to the MMF Control Law.....	139
6.7	Linear Quadratic Regulator Design.....	146
6.7.1	Solution of the LQR Problem.....	146
6.7.2	Application to MMF Control Law.....	147
6.8	Reduced Order Observer with Loop Transfer Recovery.....	163
6.8.1	Design Procedure.....	163
6.8.2	Robustness Analysis.....	169
6.8.3	Transient Response.....	169
6.9	Consolidated MMF Control System.....	179
6.9.1	“Fly-by-Wire” Implementation.....	179
6.9.2	Integration with the Mechanical Control System.....	187
6.10	High Order Stability Robustness Analysis.....	194
6.11	Equivalent Systems Analysis.....	205
6.12	Nonlinear Simulation Evaluation.....	209
6.13	Summary.....	216
VII.	Summary and Conclusions.....	217
	References.....	220
	Vita.....	224

## List of Figures

1.1	F-14 Tomcat.....	4
2.1	Nonlinear Simulation Structure.....	12
2.2	Linear Model Extraction Process.....	13
2.3	Aircraft Body-Axis System.....	16
2.4	Aircraft Dynamics Linear Model.....	19
3.1	MIMO Additive Uncertainty Representation.....	29
3.2	MIMO Multiplicative Uncertainty Representation.....	29
4.1	Aerodynamic Control Surfaces.....	33
4.2	F-14 Control System Architecture.....	34
4.3	Lateral Axis Control System.....	35
4.4	Spoiler Control System.....	37
4.5	AFCS Lateral Stick to Spoiler Gearing.....	38
4.6	Individual Spoiler Surface Deflection vs Lateral Stick.....	39
4.7	Directional Axis Control System.....	40
4.8	Runway Lineup Correction Task.....	43
4.9	Response to Lateral Stick Input.....	46
4.10	Roll Rate and Sideslip Responses for Various Lateral Stick Inputs...	48
4.11	Roll Rate vs Lateral Stick and Max. Sideslip vs Max. Roll Rate.....	49
4.12	AFCS Response to Lateral Turbulence Velocity.....	51
4.13	Open-loop Analysis Model.....	52
4.14	Frequency Response with Loop Opened at Roll Rate Gyro.....	54
4.15	Frequency Response with Loop Opened at Yaw Rate Gyro.....	55
4.16	Frequency Response with Loop Opened at Lateral Acceleration.....	56
4.17	Frequency Response with Loop Opened at Roll Series Servo.....	57
4.18	Frequency Response with Loop Opened at Yaw Series Servo.....	58
4.19	Root-locus with Loop Opened at Roll Series Servo.....	59
4.20	Root-locus with Loop Opened at Yaw Series Servo.....	60
5.1	Roll PA ARI Overview.....	63
5.2	Yaw PA ARI Overview.....	63
5.3	Roll PA ARI Control System.....	64
5.4	Yaw PA ARI Control System.....	66
5.5	Roll Angle Complementary Filter.....	69
5.6	Sideslip Rate Estimator.....	70
5.7	Sideslip Rate Estimator Frequency Response Validation.....	71
5.8	Design Plant Model.....	72
5.9	PA ARI Open-loop Synthesis Model.....	74
5.10	Closed-loop PA ARI.....	75
5.11	Roll Rate Feedback Root-locus.....	76
5.12	Beta-dot Feedback Root-locus ( $\zeta_{dr}=0.7$ ).....	79
5.13	PA ARI Response to Lateral Stick ( $\zeta_{dr}=0.7$ ).....	80



5.14	PA ARI Response to Rudder Pedal ( $\zeta_{dr}=0.7$ ).....	82
5.15	Beta-dot Feedback Root-locus ( $\zeta_{dr}=1.0$ ).....	84
5.16	PA ARI Response to Lateral Stick ( $\zeta_{dr}=1.0$ ).....	85
5.17	PA ARI Response to Rudder Pedal ( $\zeta_{dr}=1.0$ ).....	87
5.18	Beta-dot Feedback Root-locus ( $\zeta_{dr}>1.0$ ).....	89
5.19	PA ARI Response to Lateral Stick ( $\zeta_{dr}>1.0$ ).....	90
5.20	PA ARI Response to Rudder Pedal ( $\zeta_{dr}>1.0$ ).....	92
5.21	PA ARI Lateral Stick to Spoiler Gearing.....	95
5.22	Roll Rate Response vs Lateral Stick.....	96
5.23	LSRI Rudder Command vs Lateral Stick.....	98
5.24	Sideslip Responses to Lateral Stick and Max. Sideslip vs Max. Roll Rate.....	99
5.25	Roll Rate, Roll Rate Cmd, and Roll Series Servo Response to Lateral Stick.....	101
5.26	Roll Rate Command vs Lateral Stick.....	102
5.27	Open-loop PA ARI for Robustness Analysis.....	105
5.28	Frequency Response with Loop Opened at Roll Rate Gyro.....	106
5.29	Frequency Response with Loop Opened at Yaw Rate Gyro.....	107
5.30	Frequency Response with Loop Opened at Lateral Accelerometer...	108
5.31	Frequency Response with Loop Opened at Roll Series Actuator.....	109
5.32	Frequency Response with Loop Opened at Yaw Series Actuator.....	110
5.33	MIMO Robustness with Loop Open at Sensors.....	112
5.34	MIMO Robustness with Loop Open at Actuators.....	113
5.35	AFCS vs PA ARI Response to Atmospheric Turbulence.....	115
5.36	Equivalent System Frequency Response Validation / Lateral Stick Input.....	117
5.37	Equivalent System Frequency Response Validation / Rudder Pedal Input.....	118
6.1	MMF Control Structure.....	123
6.2	Maneuver Command Generator Structure.....	125
6.3	Roll Rate Command Model.....	126
6.4	Sideslip Command Model.....	128
6.5	Detailed Maneuver Command Generator.....	131
6.6	MCG Response to Lateral Stick Half Doublet.....	132
6.7	MCG Response to Rudder Pedal Step.....	133
6.8	Combined Control Selector and Plant.....	137
6.9	Dynamic Inversion Control Law.....	140
6.10	Combined MCG, Dynamic Inversion, and Design Plant Model.....	141
6.11	Combined MCG and Dynamic Inversion Response to Lateral Stick.....	142
6.12	Combined MCG and Dynamic Inversion Response to Rudder Pedal.....	144
6.13	Performance and Robustness Specification.....	148

6.14	Open-loop Plant Singular Values.....	149
6.15	Plant Augmented with Integrals of Phi and Beta.....	150
6.16	Augmented Plant Singular Values.....	151
6.17	LQR Input Return Ratio Singular Values.....	154
6.18	LQR MIMO Stability Robustness.....	155
6.19	Regulator Root-locus.....	157
6.20	Closed-loop LQ Regulator.....	158
6.21	LQR Response to Roll Angle Step Command.....	159
6.22	LQR Response to Sideslip Angle Step Command.....	161
6.23	Closed-loop LQG System.....	168
6.24	LQG System with Loop Opened at Plant Input.....	170
6.25	LQR vs LQG/LTR Input Return Ratio Singular Values.....	171
6.26	LQG/LTR System with Loop Opened at Plant Output.....	172
6.27	LQG/LTR Output Return Ratio Singular Values.....	173
6.28	LQG/LTR Output MIMO Robustness.....	174
6.29	LQR vs LQG/LTR Response to Roll Angle Command.....	175
6.30	LQR vs LQG/LTR Response to Sideslip Command.....	177
6.31	Stage 1 MMF Control Architecture.....	181
6.32	Modified LQ Regulator Structure.....	182
6.33	Stage 1 MMF Response to Lateral Stick.....	183
6.34	Stage 1 MMF Response to Rudder Pedal.....	185
6.35	MMF with Mechanical Path Compensation.....	188
6.36	Stage 2 MMF Closed-loop System.....	189
6.37	Stage 2 MMF Response to Lateral Stick.....	190
6.38	Stage 2 MMF Response to Rudder Pedal.....	192
6.39	Open-loop MMF Control System.....	195
6.40	MMF Open-loop Frequency Response with Loop Opened at Differential Spoiler.....	196
6.41	MMF Open-loop Frequency Response with Loop Opened at Differential Stabilizer.....	197
6.42	MMF Open-loop Frequency Response with Loop Opened at Rudder.....	198
6.43	MMF Open-loop Frequency Response with Loop Opened at Roll Rate.....	199
6.44	MMF Open-loop Frequency Response with Loop Opened at Roll Angle.....	200
6.45	MMF Open-loop Frequency Response with Loop Opened at Yaw Rate.....	201
6.46	High Order MMF Actuator Plane MIMO Stability Robustness.....	203
6.47	High Order MMF Sensor Plane MIMO Stability Robustness.....	204
6.48	MMF LOES Frequency Response Validation / Lateral Stick Input..	206
6.49	MMF LOES Frequency Response Validation / Rudder Pedal Input.	207
6.50	Nonlinear MMF Response to Lateral Stick.....	210

6.51	Nonlinear MMF Response to Rudder Pedal.....	212
6.52	MMF vs PA ARI Response to Atmospheric Turbulence.....	214
6.53	Response to Lateral Stick Half-Doublet showing effect of Variation of MCG Roll Command Time Constant.....	215

## List of Tables

2.1	Design Flight Condition Parameters.....	18
3.1	Cooper-Harper Rating Scale.....	21
3.2	Flying Qualities Specification Definitions.....	23
3.3	Spiral Mode Minimum Time to Double Amplitude.....	24
3.4	Maximum Roll Mode Time Constant.....	24
3.5	Minimum Dutch Roll Frequency and Damping.....	24
3.6	Maximum Equivalent Time Delay.....	24
3.6	LOES Parameters.....	26
4.1	Handling Qualities Ratings for the Production AFCS.....	45
5.1	PA ARI SISO Gain and Phase Margins.....	104
5.2	PA ARI MIMO Gain and Phase Margins.....	111
5.3	PA ARI Equivalent System Analysis Results.....	116
5.4	AFCS vs PA ARI Handling Qualities Ratings Comparison.....	120
6.1	MMF SISO Gain and Phase Margins.....	194
6.3	MMF Equivalent System Analysis Results.....	208

## Nomenclature

Symbol	Definition	Units
A	state matrix	
AFCS	Automatic Flight Control System	
$\alpha$	angle-of-attack	deg
$A_y$	lateral acceleration	ft/sec <sup>2</sup>
B	input distribution matrix	
$\beta$	sideslip angle	deg
C	output distribution matrix	
CASTLE	Controls Analysis and Simulation Test Loop Environment	
D	direct feedthrough matrix	
DFCS	Digital Flight Control System	
Dsp, $\delta_{sp}$	differential spoiler	deg
Da, $\delta_a$	differential stabilizer	deg
Dr, $\delta_r$	rudder	deg
Dlat, $\delta_{lat}$	lateral stick	inch
Dped, $\delta_{ped}$	rudder pedal	inch
g	gravitational constant	ft/sec <sup>2</sup>
$I_x$	moment of inertia about the x-axis	slug-ft <sup>2</sup>
$I_y$	moment of inertia about the y-axis	slug-ft <sup>2</sup>
$I_z$	moment of inertia about the z-axis	slug-ft <sup>2</sup>
$I_{xz}$	product of inertia about the x-axis	slug-ft <sup>2</sup>
L	rolling moment	ft-lbs
LME	Linear Model Extraction	
LQG	Linear Quadratic Gaussian	
LQR	Linear Quadratic Regulator	
LTR	Loop Transfer Recovery	
M	pitching moment	ft-lbs
m	aircraft mass	lb-sec <sup>2</sup> /ft
MFS	Manned Flight Simulator	

MIMO	Multi-input, Multi-output	
MMF	Multivariable Model Following	
N	yawing moment	ft-lbs
NAWCADPAXRIV	Naval Air Warfare Center - Aircraft Division at Patuxent River, MD	
P	roll rate	deg/sec
PA	Powered Approach	
PA ARI	Power Approach Automatic Rudder Interconnect	
Q	pitch rate	deg/sec
R	yaw rate	deg/sec
SISO	Single-input, Single-output	
U	x-axis velocity	ft/sec
V	y-axis velocity	ft/sec
$V_T$	total velocity	ft/sec
W	z-axis velocity	ft/sec
X	x-axis force	lbs
Y	y-axis force	lbs
Z	z-axis force	lbs
$\Theta$	pitch angle	deg
$\Phi$	roll angle	deg
$\Psi$	heading angle	deg
$\omega$	natural frequency	rad/sec
$\zeta$	damping ratio	

# Chapter I

## Introduction

### 1.1 Background

From the time of the Wright brothers' first successful flight of a human piloted, heavier-than-air, powered aircraft in 1903 until the end of World War II, aircraft primary flight control systems were mechanized using direct mechanical links between the pilot controls and the aerodynamic control surfaces. Early aerodynamic configurations sacrificed stability in order to maximize controllability, and thus required significant pilot compensation to maintain stabilized flight [1.1]. As aircraft designers became more aware of mathematical techniques for predicting aircraft stability and control characteristics, aircraft flying qualities improved accordingly. Due to the limited airspeed and altitude flight envelopes of these relatively stable, piston powered aircraft their simple mechanical control systems were more than adequate [1.2].

With the dawn of the jet age, aircraft performance increases made the use of simple mechanical controls impossible. The forces required to move the aerodynamic surfaces of jet aircraft flying at high speed would be too great for human powered controls. To alleviate this problem aircraft designers connected the pilot control linkages to hydraulic actuators which drove the aerodynamic control surfaces. Since the forces on the

aerodynamic control surfaces were not transmitted back to the pilot, these systems were called irreversible control systems.

As the flight envelope of new aircraft designs continued to expand, the resulting extreme variations in dynamic response characteristics made open-loop mechanical/hydraulic control systems inadequate. Advances in closed-loop servo mechanism technology which occurred during World War II became increasingly applied to the aircraft control problem. These systems were mechanized using analog control logic to convert aircraft attitude, rate, and acceleration measurements into electro-hydraulic servo actuator commands. The position of the servo actuator was then mechanically summed into the pilot's mechanical linkage which controlled the main hydraulic surface actuators.

The electronics technology that existed in the 1950's and 60's combined with the conservative nature of the aircraft industry restricted the typical production fighter aircraft stability augmentation system to simple, low authority architectures with minimal gain scheduling or dynamic compensation. Due to their relative simplicity, flight control systems could not be optimized across the entire operating envelope. Typically, the high speed region of the flight envelope was emphasized in the design process more heavily than the low speed region. This was to ensure satisfactory flying qualities and stability margins in the aircraft's primary mission related flight regime.

At low speed flight conditions such as powered approach (PA) where the dynamic pressure acting on the aircraft control surfaces was reduced, the absence of gain scheduling in some aircraft meant that the



effective loop gain of the feedback system was reduced substantially. The resulting dynamic response and flying qualities were thus dependent on the aircraft's inherent stability characteristics. Aerodynamic configurations optimized for high speed flight typically possessed poor low speed characteristics.

The Grumman F-14 Tomcat, shown in figure 1.1, is a prime example of the problem described above. Entering operational service in 1972 as the United States Navy's premier air superiority fighter and aircraft carrier theater defense platform, the F-14's analog flight control system was designed using standard 1960's techniques. Despite the fact that the F-14 aerodynamic configuration is an advanced design employing variable sweep wings which allows the aircraft to reach speeds in excess of Mach 2 with the wings fully aft and permits relatively slow landing speeds with the wings in the forward position, the PA lateral-directional flying qualities are marginal [1.3, 1.4].

The F-14 PA flying qualities exhibit three primary deficiencies: 1) large adverse sideslip in response to lateral stick inputs, 2) a lightly damped Dutch-roll mode and 3) a nonlinear lateral stick to roll rate response. These characteristics significantly degrade the pilot's ability to make accurate lateral line-up corrections during the terminal phases of an aircraft carrier or airfield landing approach.

In the early 1980's, NASA Langley Research Center designed and flight tested an improved lateral directional PA control system for the F-14 [1.4, 1.5]. This system was a modified version of an up-and-away (UA) control law being tested by NASA and the US Navy [1.6] which was

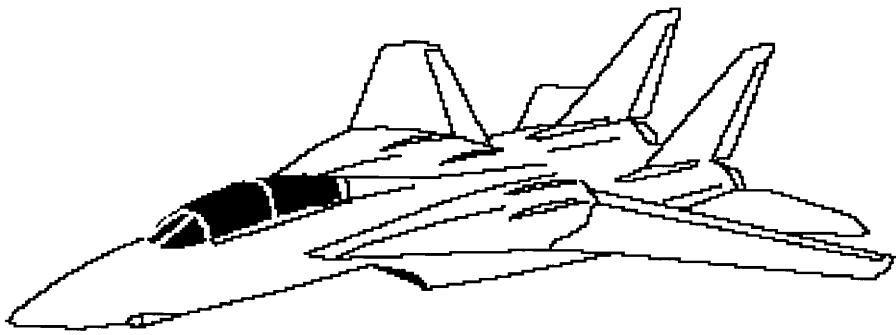


Figure 1.1 F-14 Tomcat

designed to improve high angle of attack flying qualities and reduce the susceptibility of the aircraft to control induced departures. Although this control law resulted in improved PA flying qualities, some undesirable characteristics remained. Due to funding constraints, the improved control system was not incorporated into production aircraft.

Finally, in 1992 the Naval Air Systems Command initiated a program to replace the F-14 analog flight control computers with digital flight control computers. With the increased flexibility afforded by the digital computers, control law enhancements could now be realized which would correct the deficiencies of the current F-14 aircraft. The Naval Air Warfare Center Aircraft Division (NAWCAD) at Patuxent River was tasked as the lead activity in the development, integration, and testing of the new F-14 Digital Flight Control System (DFCS).

The PA control law developed for the F-14 DFCS was called the Power Approach Automatic Rudder Interconnect (PA ARI). Due to the aggressive program schedule, limited amount of flight test time available (i.e., limited number of "gain tuning" flights), and concerns over flight control computer processing power, a requirement of the PA ARI control law design was to keep the system as simple as possible. As a result, the system was designed using current industry standard control design methods such as root-locus and Bode plots.

Due to the inherent simplicity of the PA ARI control design, it was desired to assess the performance of the system by comparing it to a more advanced control architecture. A multivariable model following (MMF) control law was therefore designed which utilized a maneuver command

generator and dynamic inversion to achieve feedforward model following control, with feedback error suppression provided by a proportional plus integral linear quadratic regulator. A reduced order observer possessing exact Loop Transfer Recovery (LTR) was used to provide feedback of unmeasured states. The resulting closed-loop performance, flying qualities, and SISO and MIMO robustness characteristics were compared to that achieved by the classically designed PA ARI control law.

## 1.2 Literature Review

From its introduction in 1960 by Kalman until the early 1980's, optimal multivariable control theory found few applications in the aircraft control industry. Some of the reasons for this reluctance included the difficulty in relating the physical design requirements to the mathematical problem formulation, the complexity of the resulting controllers, and an apparent lack of robustness to modeling uncertainty [1.7]. The mid 1980's and early 90's have seen a resurgence in the number of applications of modern control theory to aircraft control design problems throughout the literature. The key event that sparked this renewed interest in aircraft modern control synthesis was the incorporation of classical control concepts for loop shaping and robustness into the modern control framework [1.8]. Techniques such as Linear Quadratic Gaussian with Loop Transfer Recovery (LQG/LTR),  $H^\infty$ , and  $\mu$ -synthesis have made multivariable loop shaping a routine exercise.

One of the earliest successful applications of modern control theory applied to a production aircraft system was the Boeing 767 lateral autopilot [1.7]. The original autopilot had been designed using classical control theory, and exhibited a small amplitude limit cycle oscillation which was objectionable to passengers. Repeated attempts to remedy the problem using root-locus techniques failed, so a full-state linear quadratic (LQ) approach was attempted. The resulting controller provided robustness against the uncertainties which caused the limit cycle in the classically designed system, and has since been incorporated on all production 767 aircraft.

A successful application of LQG/LTR to aircraft control was the Air Force STOL (Short TakeOff and Landing) and Maneuver Technology Demonstrator (S/MTD) Program [1.9]. The test vehicle for this program was a modified F-15 which utilized two-dimensional thrust vectoring nozzles and forward mounted canards. The S/MTD utilized an integrated flight and propulsion control system designed by Honeywell. The Honeywell approach was to use LQG/LTR for feedback loop robustness and disturbance rejection, and feedforward command shaping to provide desired response to pilot inputs (flying qualities). Balanced model order reduction was used to reduce the resulting compensator order to an equivalent proportional plus integral control structure. Although modern control theory was deemed necessary for the S/MTD to achieve its design requirements, a program requirement was to keep complexity to a minimum.

A well known theoretical application of LQG theory to aircraft flight control design was performed by Thompson, Coleman, and Blight [1.10]. Their design achieved decoupled regulation of roll rate and sideslip angle using aileron and rudder surface commands. The control structure consisted of an integral linear quadratic model following regulator and an integral Kalman estimator. Desired loop shapes were achieved by using frequency shaped performance outputs in the quadratic cost function. Although the desired performance and robustness was achieved, the controller was of high order and an iterative procedure was used for the computation of the explicit model feedforward gain matrix.

Dynamic inversion control has been increasingly applied to theoretical aircraft control studies in recent years. Reference [1.11] provides a thorough review of this technique. An early application of dynamic inversion was demonstrated by Chetty and Henschel [1.12], who applied the technique to the DFVLR in-flight-simulator testbed known as ATTAS (Advanced Technologies Testing Aircraft System). The ATTAS control law utilized a feedforward command model which generated commanded trajectories for the aircraft states and state derivatives. These were input to an inverse of the aircraft linear state equation to produce the control signal that resulted in aircraft response tracking of the commanded states. The error between the commanded and measured response variables were fed back through proportional plus integral compensation to assure accurate closed-loop tracking. Flight test results demonstrated excellent tracking of the command model by the aircraft.

### **1.3 Contributions of the Thesis**

The main contribution of this thesis is the development of an improved lateral-directional control law using classical control techniques for the F-14 aircraft in PA configuration which will greatly enhance the aircraft flying qualities over the current system. The relative “optimality” of the system will be demonstrated by comparing its characteristics to a more advanced system designed using optimal multivariable design techniques.

### **1.4 Outline of the Thesis**

Chapter II describes the F-14 nonlinear simulation model and the linear models used for the design and analysis efforts.

Chapter III gives details on the flying qualities and stability robustness requirements for aircraft flight control systems.

In Chapter IV, the motivation for designing enhanced control laws for the F-14 is revealed by demonstrating the poor characteristics of the existing analog flight control system in the powered approach configuration.

In Chapter V, the PA ARI control law being incorporated into the F-14 Digital Flight Control System is designed and analyzed, and then evaluated using piloted simulation.

Chapter VI demonstrates the effectiveness of a combined dynamic inversion and LQG/LTR approach for the synthesis of a lateral-directional control law for the F-14.

Chapter VII contains the summary and conclusions.

## Chapter II

### F-14 Simulation Model Description

#### 2.1 Nonlinear Simulation Description

A high fidelity, six degree-of-freedom, nonlinear simulation model of the F-14 aircraft has been developed at NAWCADPAXRIV. The simulation consists of a number of F-14 specific FORTRAN modules such as aerodynamics, propulsion, weight and inertia, and control systems which interface to a library of generic aircraft simulation modules known as CASTLE, or Controls Analysis and Simulation Test Loop Environment [2.1]. CASTLE was developed in the mid 1980's to address the Navy's requirement to support the test and evaluation of many aircraft platforms, using common software to perform generic requirements. The generic CASTLE modules include but are not limited to the following:

- six degree-of-freedom equations of motion
- standard atmosphere
- turbulence models
- menu-driven user interface
- real-time laboratory communications
- analysis functions:
  - trim, maneuver generator, linear model extraction (LME)



A block diagram of the F-14 nonlinear simulation is shown in figure 2.1. Reference [2.2] provides an in-depth description of the complete simulation model.

The F-14 nonlinear simulation can be utilized in a variety of ways to support flight control system design and analysis tasks. Real-time pilot-in-the-loop is the most spectacular technique. A modern, state-of-the-art simulation laboratory has been established at the Manned Flight Simulator (MFS) at NAWCADPAXRIV which provides all necessary simulation hardware and computer resources required for the manned simulation task. The simulation also provides extensive batch mode capabilities, such as arbitrary equilibrium point determination (trim), maneuver generation and data storage, plotting, and linear model extraction (LME). LME is a generic CASTLE function which computes linear state-space models of any desired simulation subsystem. The linear models are computed by individually adding perturbations ( $\delta$ ) to the subsystem inputs ( $u$ ) and states ( $x$ ), and recording the changes ( $\Delta$ ) in the state derivatives ( $\dot{x}$ ) and outputs ( $y$ ). Integration of all subsystem states is suppressed during the LME process. This process is shown in figure 2.2. The linear model matrices are then defined as:

$$A = \frac{\dot{\Delta x}}{\delta x} \quad B = \frac{\dot{\Delta x}}{\delta u} \quad C = \frac{\Delta y}{\delta x} \quad D = \frac{\Delta y}{\delta u} \quad (2.1)$$

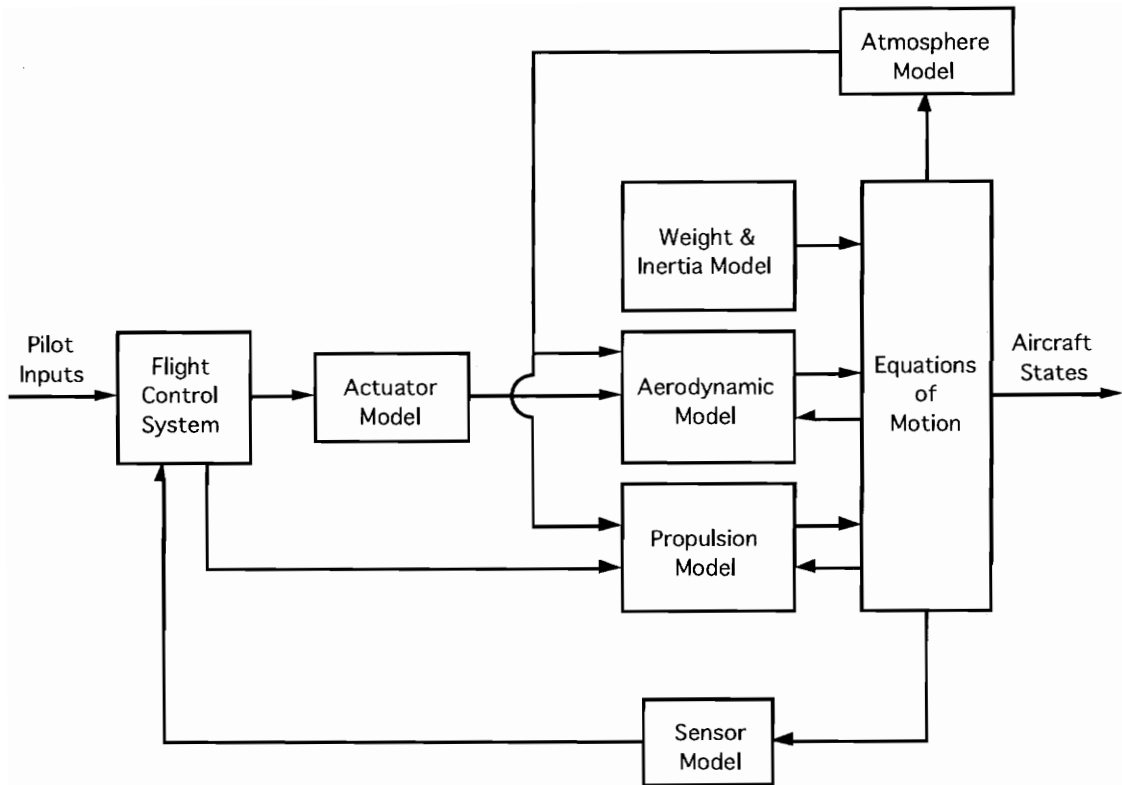


Figure 2.1 Nonlinear Simulation Structure

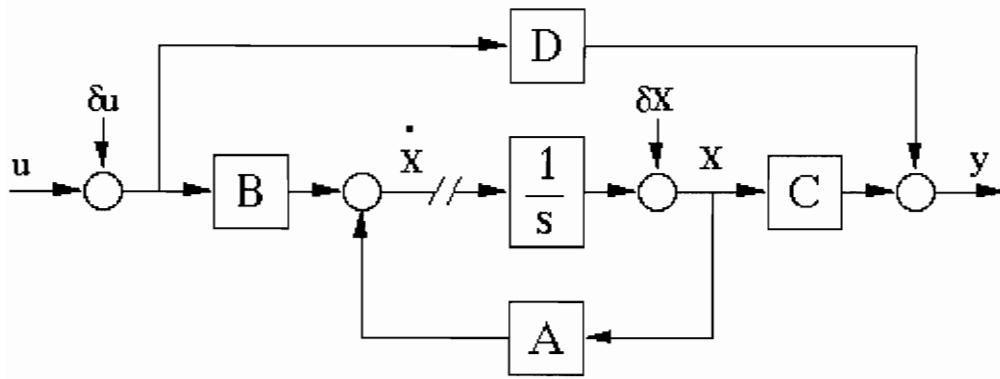


Figure 2.2 Linear Model Extraction Process

## 2.2 Nonlinear Equations of Motion

The equations of motion contained in CASTLE are derived from Newton's Second Law of motion. The equations are 6 degrees-of-freedom non-linear differential equations. The details of this development are given by Etkin [2.3]. The force equations are:

$$\begin{aligned}
 \dot{U} &= RV - QW - g \sin \Theta + \frac{X}{m} \\
 \dot{V} &= PW - RU + g \cos \Theta \sin \Phi + \frac{Y}{m} \\
 \dot{W} &= QU - PV + g \cos \Theta \cos \Phi + \frac{Z}{m}
 \end{aligned} \tag{2.2}$$

The moment equations are:

$$\begin{aligned}
 \dot{P} &= - \left[ \frac{I_z - I_y}{I_x} \right] QR + \frac{I_{xz}}{I_y} \left( \dot{R} + PQ \right) + \frac{L}{I_x} \\
 \dot{Q} &= \left[ \frac{I_z - I_x}{I_y} \right] PR - \frac{I_{xz}}{I_y} \left( P^2 - R^2 \right) + \frac{M}{I_y} \\
 \dot{R} &= - \left[ \frac{I_y - I_x}{I_z} \right] PQ + \frac{I_{xz}}{I_z} \left( \dot{P} - QR \right) + \frac{N}{I_z}
 \end{aligned} \tag{2.3}$$

The Euler angular velocities are:

$$\begin{aligned}
 \dot{\Phi} &= P + (Q \sin \Phi + R \cos \Phi) \tan \Theta \\
 \dot{\Theta} &= Q \cos \Phi - R \sin \Phi \\
 \dot{\Psi} &= (Q \sin \Phi + R \cos \Phi) \sec \Theta
 \end{aligned} \tag{2.4}$$

The aerodynamic angles are the angle-of-attack ( $\alpha$ ) and sideslip angle ( $\beta$ ), which are defined as:

$$\begin{aligned}\alpha &= \tan^{-1}\left(\frac{W}{U}\right) \\ \beta &= \sin^{-1}\left(\frac{V}{V_T}\right)\end{aligned}\quad (2.5)$$

The total velocity vector is defined as:

$$V_T = \sqrt{U^2 + V^2 + W^2}\quad (2.6)$$

The forces, moments, rates, angles, and velocities which make up (2.2) through (2.6) are shown in Figure 2.3.

### 2.3 Linear Aircraft Dynamics Model

Most of the analysis and design tasks performed in this thesis are based on linear dynamic system models of the form:

$$\dot{\mathbf{x}} = \mathbf{Ax} + \mathbf{Bu}\quad (2.7)$$

The Linear Model Extraction capability of CASTLE is used to obtain the linearized aircraft equations of motion. For lateral-directional dynamics, these equations are:

$$\begin{bmatrix} \dot{v} \\ \dot{p} \\ \dot{r} \\ \dot{\phi} \end{bmatrix} = \begin{bmatrix} Y_v & Y_p & Y_r - U_0 & g \cos \Theta_0 \\ L_v & L_p & L_r & 0 \\ N_v & N_p & N_r & 0 \\ 0 & 1 & 0 & 0 \end{bmatrix} \begin{bmatrix} v \\ p \\ r \\ \phi \end{bmatrix} + \begin{bmatrix} Y_{\delta_{sp}} & Y_{\delta_a} & Y_{\delta_r} \\ L_{\delta_{sp}} & L_{\delta_a} & L_{\delta_r} \\ N_{\delta_{sp}} & N_{\delta_a} & N_{\delta_r} \\ 0 & 0 & 0 \end{bmatrix} \begin{bmatrix} \delta_{sp} \\ \delta_a \\ \delta_r \end{bmatrix}\quad (2.8)$$

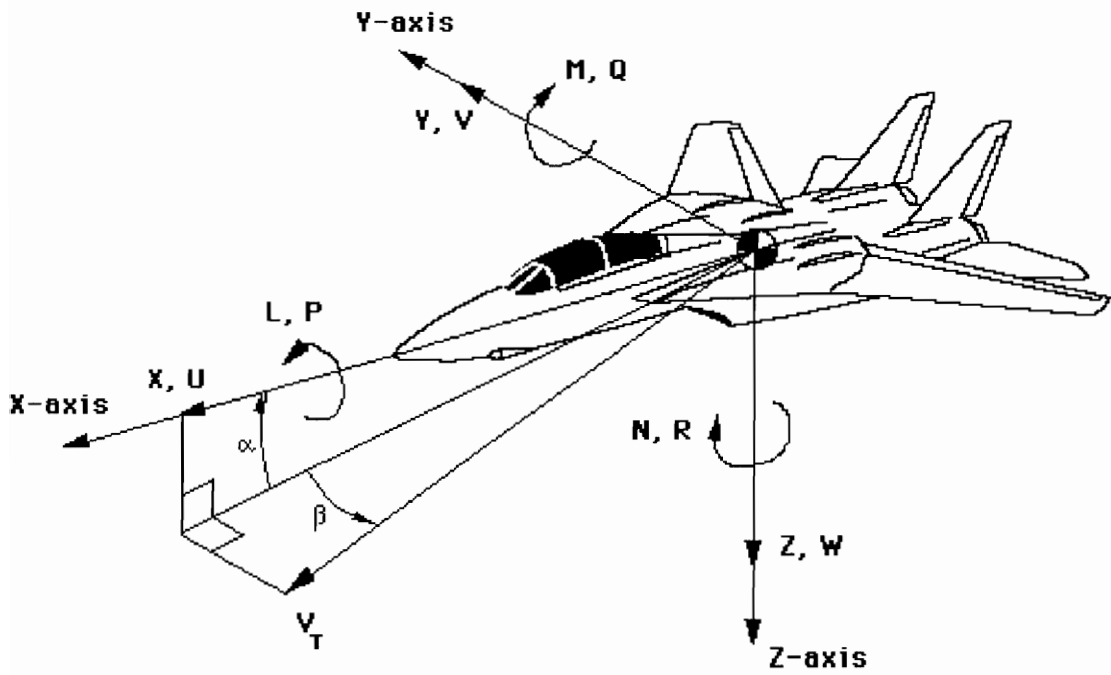


Figure 2.3 Aircraft Body-Axis System

The state variables are:

$v$  = Lateral Velocity (ft/sec)

$p$  = Roll Rate (rad/sec)

$r$  = Yaw Rate (rad/sec)

$\phi$  = Roll Angle (rad)

The controls inputs are:

$\delta_{sp}$  = Differential Spoiler (deg)

$\delta_a$  = Differential Stabilizer (deg)

$\delta_r$  = Rudder (deg)

The design flight condition being analyzed is the nominal powered approach configuration, as shown in Table 2.1. The stores configuration specified in Table 2.1 is referred to as "2x4", which is a combination of two Sparrow missiles, two Sidewinder missiles, two Phoenix missiles, and two external fuel tanks. This configuration was selected because it possesses the poorest lateral-directional stability characteristics, and should minimize the sensitivity of resulting control designs to off-nominal stores configurations. The DLC (direct lift control) status will be explained further in chapter IV. Figure 2.4 gives the state-space model matrices for the design flight condition.

Table 2.1 Design Flight Condition Parameters

Parameter	Value
Calibrated Airspeed	137.3 knots
Angle-of-Attack	10.5 degrees
Altitude	100 feet
Gross Weight	54,000 lbs
Landing Flaps	Down (35 deg)
DLC Status	Engaged
Center of Gravity Location	10.9 % mac
Stores Configuration	2x4



$$A = \begin{bmatrix} -0.1129 & -233.5377 & 44.1579 & 31.6331 \\ 0.0027 & -0.2520 & -0.1407 & 0 \\ -0.0206 & 0.6524 & -1.3283 & 0 \\ 0 & 0.1853 & 1.0000 & 0 \end{bmatrix}$$

$$B = \begin{bmatrix} 0 & 0.0622 & 0.1012 \\ -0.0016 & -0.0052 & -0.0112 \\ -0.0193 & -0.0467 & 0.0036 \\ 0 & 0 & 0 \end{bmatrix}$$

Figure 2.4 Aircraft Dynamics Linear Model

## Chapter III

# Aircraft Flight Control System Requirements and Analysis Methods

### 3.1 Introduction

The goal of an aircraft flight control system is to manipulate the aerodynamic control surfaces such that the aircraft performs the desired maneuvers with minimal pilot workload. To achieve this end, the flight control system must satisfy both flying qualities requirements as well as stability robustness requirements.

### 3.2 Flying Qualities

Flying qualities are the pilot's opinion of the relative ease for which a given task or mission can be performed. This opinion is a combination of the aircraft response mode characteristics, cockpit design, weather conditions, and pilot skill level. The current standard for piloted evaluation of aircraft flying qualities is the Cooper-Harper rating scale [3.1]. The Cooper-Harper rating scale, shown in Table 3.1, combines a numerical rating (called an HQR, or handling quality rating) with descriptions of aircraft characteristics and required pilot compensation. HQR's from 1 to 3 are considered satisfactory. HQR's from 4 to 6 are considered adequate, but improvement is required. HQR's from 7 to 10 are considered unacceptable.

Table 3.1 Cooper-Harper Rating Scale

Aircraft Characteristics	Demands on the Pilot in Selected Task or Required Operation	HQR
Excellent; highly desirable	Pilot compensation not a factor for desired performance	1
Good; negligible deficiencies	Pilot compensation not a factor for desired performance	2
Fair; some mildly unpleasant deficiencies	Minimal pilot compensation required for desired performance	3
Minor but annoying deficiencies	Desired performance requires moderate pilot compensation	4
Moderately objectionable deficiencies	Adequate performance requires considerable pilot compensation	5
Very objectionable but tolerable deficiencies	Adequate performance requires extensive pilot compensation	6
Major deficiencies	Adequate performance not attainable with maximum pilot compensation. Controllability not in question.	7
Major deficiencies	Considerable pilot compensation is required for control	8
Major deficiencies	Intense pilot compensation is required to retain control	9
Major deficiencies	Control will be lost during some portion of required operation	10

### 3.3 Flying Qualities Specifications

A considerable amount of research has been devoted to the correlation of aircraft response characteristics to the Cooper-Harper rating scale [3.2]. This research has resulted in the development of military specifications governing the modal characteristics of aircraft. The specification used for the F-14 DFCS program is MIL-F-8785C, "Military Specification for the Flying Qualities of Piloted Airplanes" [3.3]. MIL-F-8785C defines boundaries, or "levels" that relate a particular aircraft modal property to the Cooper-Harper rating scale. In order to determine the flying quality level for a particular modal property, the aircraft classification and mission flight phase must be defined. The aircraft classifications, flight phases, and flying quality levels in relation to the Cooper-Harper ratings are shown in Table 3.2.

The F-14 aircraft flying in powered approach configuration is classified as a type IV aircraft flying in Category C flight phase. The corresponding lateral-directional modal requirements as defined in MIL-F-8785C are shown in Tables 2.3, 2.4, and 2.5. The goal of the flight control system designer is to insure the equivalent closed-loop modal characteristics fall within the Level 1 boundaries specified in Tables 2.3 through 2.6.

In addition to specifications on modal characteristics, MIL-F-8785C specifies the allowable equivalent time delay of the closed-loop system. The equivalent time delay is defined as the time required for the aircraft to achieve maximum angular acceleration following a pilot step input. This delay can seriously degrade the pilots ability to perform high gain tracking tasks, and lead to pilot-induced-oscillations (PIO). Table 3.6 defines the equivalent time delay requirements.

Table 3.2 Flying Qualities Specification Definitions

Airplane Classes	Definition
Class I	Small, light airplanes
Class II	Medium weight, low-to-medium-maneuverability airplanes
Class III	Large, heavy, low-to-medium-maneuverability airplanes
Class IV	High-maneuverability airplanes
Flight Phases	Definition
Category A	Nonterminal flight phases generally requiring rapid maneuvering
Category B	Nonterminal flight phases normally accomplished using gradual maneuvers without precision tracking, although accurate flight-path control may be required
Category C	Terminal flight phases normally accomplished using gradual maneuvers and usually requiring accurate flight-path control
Flying Quality Levels	Definition
Level 1 (Cooper-Harper 1-3)	Flying qualities adequate for the mission flight phase
Level 2 (Cooper-Harper 4-6)	Flying qualities adequate to accomplish the mission flight phase, but some increase in pilot workload or degradation in mission effectiveness exists
Level 3 (Cooper-Harper 7-9)	Flying qualities such that the airplane can be controlled safely, but pilot workload is excessive, or mission effectiveness is inadequate, or both.

Table 3.3 Spiral Mode Minimum Time to Double Amplitude

Level	Min Time to Double Amplitude (seconds)
1	12.0
2	8.0
3	4.0

Table 3.4 Maximum Roll Mode Time Constant

Level	Max Roll Mode Time Constant (seconds)
1	1.0
2	1.4
3	--

Table 3.5 Minimum Dutch Roll Frequency and Damping

Level	$\zeta_{dr}^*$	$\zeta_{dr}\omega_{ndr}^*$ (rad/sec)	$\omega_{ndr}$ (rad/sec)
1	0.08	0.15	1.0
2	0.02	0.05	0.4
3	0.0	--	0.4

\* The governing damping requirement is that yielding the larger value of  $\zeta_{dr}$

Table 3.6 Maximum Equivalent Time Delay

Level	Maximum Equivalent Time Delay (seconds)
1	0.10
2	0.20
3	0.30

### 3.4 Low Order Equivalent Systems

The modal parameters specified in Tables 2.3 through 2.5 are based on 4th order lateral-directional rigid body dynamics. When highly augmented aircraft are being analyzed, which include actuator dynamics, sensor dynamics, and control system dynamics, the frequency and damping of a particular rigid-body mode in the high order system may not provide a realistic measure of the flying qualities of the aircraft. This can be especially true for model following control systems, where forward path dynamics can completely mask the dynamics of the feedback loop. To address this issue, the concept of low-order-equivalent-systems (LOES) was developed to analyze the flying qualities of complex flight control systems. The LOES is determined by approximating the frequency response of the original high-order system with a 4th order model which meets the model structure requirements of the flying qualities specification. A modal analysis of this equivalent model then yields the parameters required for military flying qualities specification compliance analysis. The required equivalent model forms for determining lateral-directional flying qualities are shown below:

$$\frac{\phi}{\delta_{\text{lat}}}(s) = \frac{K_{\phi}(s^2 + 2\zeta_{\phi}\omega_{\phi}s + \omega_{\phi}^2)e^{-\tau_{\text{lat}}s}}{\left(s + \frac{1}{\tau_s}\right)\left(s + \frac{1}{\tau_R}\right)(s^2 + 2\zeta_{\text{dr}}\omega_{\text{dr}}s + \omega_{\text{dr}}^2)} \quad (3.1)$$

$$\frac{\beta}{\delta_{\text{ped}}}(s) = \frac{(A_{\beta_3}s^3 + A_{\beta_2}s^2 + A_{\beta_1}s + A_{\beta_0})e^{-\tau_{\text{ped}}s}}{\left(s + \frac{1}{\tau_s}\right)\left(s + \frac{1}{\tau_R}\right)(s^2 + 2\zeta_{\text{dr}}\omega_{\text{dr}}s + \omega_{\text{dr}}^2)} \quad (3.2)$$

The parameters in equations (3.1) and (3.2) which are specified in MIL-8785C are given in Table 3.6 below:

Table 3.6 LOES Parameters

Parameter	Definition
$\tau_s$	spiral mode time constant (sec)
$\tau_R$	roll mode time constant (sec)
$\omega_{dr}$	Dutch-roll frequency (rad/sec)
$\zeta_{dr}$	Dutch-roll damping ratio
$\tau_{lat}$	lateral axis equivalent time delay (sec)
$\tau_{ped}$	directional axis equivalent time delay (sec)

The technique for determining the LOES for analysis of the F-14 flying qualities consists of the following four step process:

- 1) direct truncation of uncontrollable and unobservable states
- 2) residualization of high frequency states
- 3) balanced model reduction
- 4) computation of equivalent time delay

This effectiveness of this process has been demonstrated on extremely complex aircraft systems with well over 100 states [3.4].



### 3.5 SISO Robustness

Although single-input single-output (SISO) robustness tests are known to be optimistic because they only account for parameter variations in one loop, these methods are still the current standard for evaluating military aircraft flight control systems. The current specification for SISO robustness is MIL-F-9490D, "Flight Control Systems - Design, Installation, and Test of Piloted Aircraft, General Specification For" [3.5]. The robustness requirements of MIL-F-9490D are listed below:

- Gain Margin: 6 dB
- Phase Margin: 45 degrees

The compliance with MIL-F-9490D is determined by closing all feedback loops except for one, and calculating the frequency response for that open loop. This process is repeated for all inputs and outputs of the plant (actuator commands and sensor feedbacks).

### 3.6 MIMO Robustness

SISO robustness analysis is a necessary step to satisfy the military flight control system design requirements. However, when the system is multivariable, SISO methods cannot guarantee stability of the closed-loop system if parameter variations occur simultaneously in more than one feedback path. In order to gain additional confidence in the SISO analysis results, a multi-input multi-output (MIMO) analysis is conducted to determine the effect of uncertainty occurring in all loops simultaneously. The two most common uncertainty formulations are the additive and multiplicative uncertainties, shown below in figures 3.1 and 3.2.  $G(s)$  is the

nominal open-loop system (with loops broken at the plant inputs or outputs) and  $\Delta(s)$  is a frequency dependent uncertainty. As shown in figure 3.1, the system transfer function “seen” by the additive uncertainty is:

$$S(s) = (I + G(s))^{-1} \quad (3.3)$$

while figure 3.2 shows the transfer function “seen” by the multiplicative uncertainty is:

$$T(s) = G(s)(I + G(s))^{-1} \quad (3.4)$$

The quantities  $S(s)$  and  $T(s)$  are known as the sensitivity function and complementary sensitivity function, respectively. Conservative multivariable gain and phase margin estimates have been developed [3.6, 3.7] based on  $S$  and  $T$  using the small gain theorem and the MIMO Nyquist Stability Criterion. The resulting multivariable stability margin estimates based on  $S$  are:

$$GM = \frac{1}{1 \pm \frac{1}{\|S\|_{\infty}}} \quad (3.5)$$

$$PM = \pm 2 \sin^{-1} \left( \frac{1}{2\|S\|_{\infty}} \right) \quad (3.6)$$

While the multivariable stability margin estimates based on  $T$  are:

$$GM = 1 \pm \frac{1}{\|T\|_{\infty}} \quad (3.7)$$

$$PM = \pm 2 \sin^{-1} \left( \frac{1}{2\|T\|_{\infty}} \right) \quad (3.8)$$

where  $\|S\|_{\infty}$  and  $\|T\|_{\infty}$  are the infinity norm of  $S$  and  $T$ , and are equal to the peak value of the maximum singular value of  $S$  and  $T$  over all frequencies.

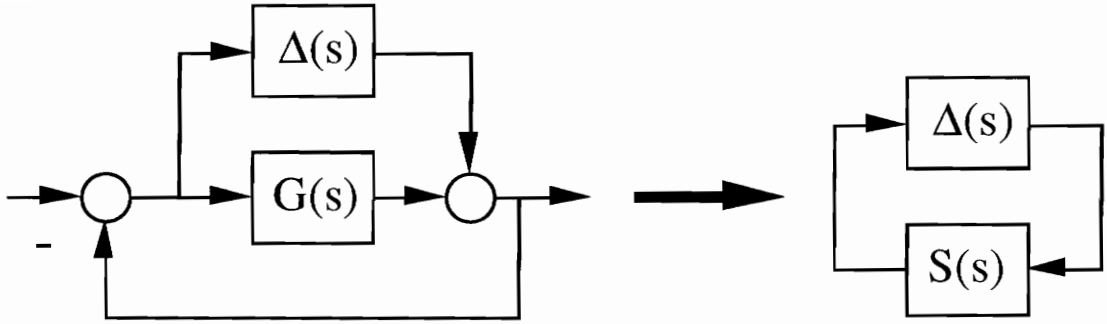


Figure 3.1 MIMO Additive Uncertainty Representation

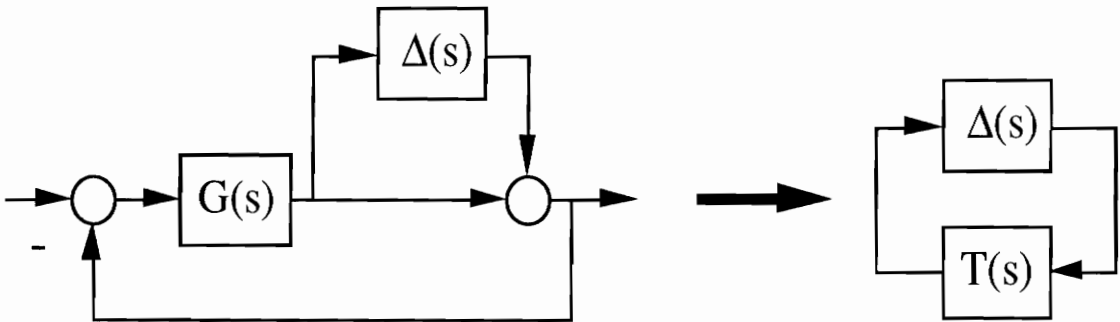


Figure 3.2 MIMO Multiplicative Uncertainty Representation

Each of the above techniques produce guaranteed, although conservative margins which indicate the amount of simultaneous gain and phase variation that can occur in all the feedback loops without destabilizing the system. The conservatism inherent in this analysis stems from the fact that system phase information is not used in the derivation of the margins. Since both techniques produce guaranteed margins, a degree of conservatism can be removed by selecting the most optimistic estimate produced by both methods. A key assumption in the application of this technique is that the nominal closed-loop system is stable.

## **Chapter IV**

### **Analysis of the Production AFCS**

#### **4.1 Introduction**

As described in chapter I, the current F-14 aircraft flying qualities was deficient in the powered approach regime due to the design limitations of the analog automatic flight control system (AFCS). To provide motivation for the design of enhanced control laws for the F-14 digital flight control system (DFCS), the deficiencies of the current system were analyzed. Piloted simulation evaluation provided the most obvious demonstration of the AFCS flying qualities deficiencies. Following the piloted evaluations, off-line nonlinear simulations were conducted to quantify the problems observed by the pilots. Linear analysis of the AFCS feedback loops was then performed to relate the flying qualities problems to the feedback loop stability and performance characteristics.

#### **4.2 System General Description**

The production F-14 flight control system consists of a mechanical primary flight control system and an analog automatic flight control system (AFCS). The AFCS consists of a three-axis analog stability augmentation system (SAS) and a spoiler control system. The primary flight control system converts pilot longitudinal stick inputs into symmetric horizontal stabilizer deflection, lateral stick inputs into differential stabilizer deflection, and

rudder pedal inputs into rudder deflection. The three-axis SAS consists of the pitch SAS, roll SAS, and yaw SAS. Each SAS axis is dual channel (produces two identical output commands) and processes pilot inputs and aircraft state information. Each output channel controls a series servo actuator (Channels A and B) which is mechanically summed into the pilot's mechanical command to form the total command to the control surface actuators. Additional roll control power is provided by the spoilers, which are located along the top surface of each wing. The spoilers are electrically controlled via lateral stick commands. Figure 4.1 identifies the aerodynamic control surfaces of the F-14 airplane. The mechanical, SAS, and spoiler control system architecture is shown in figure 4.2.

#### **4.2.1 Lateral Control System Description**

The lateral axis control system is shown in figure 4.3. It consists of the lateral stick to differential stabilizer mechanical path, the roll SAS, and the spoiler control system. The mechanical path can command up to  $\pm 7$  degrees of differential stabilizer. The Roll SAS operates on lateral stick and roll rate inputs to produce roll series actuator commands, which provide up to  $\pm 5$  degrees additional authority. The roll SAS lateral stick path, referred to as the roll CAS, consists of a 0.5 second lag filter and 2.14 gain. The roll rate feedback gain is implemented as a non-linear function which is designed to increase the damping for roll rates in excess of 135 deg/sec. Both the roll CAS and roll rate feedback paths were optimized for high speed flight.

In powered approach configuration with flaps down, the majority of the roll control power is accomplished by differentially deflecting the spoilers.

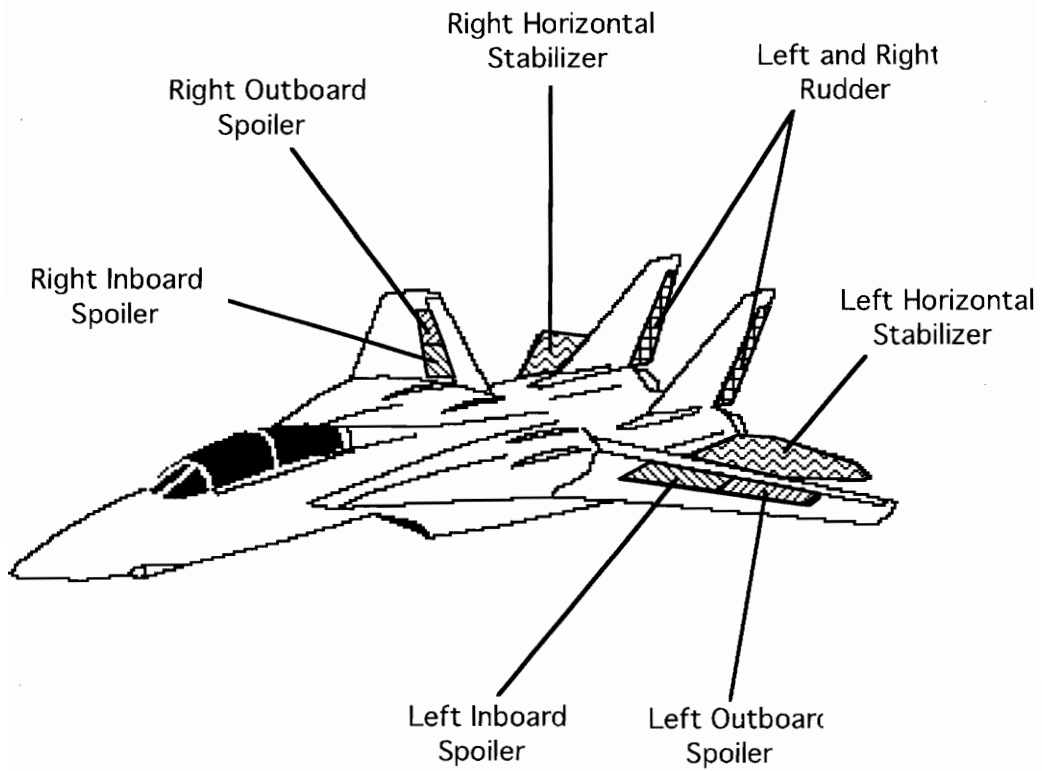


Figure 4.1 F-14 Aerodynamic Control Surfaces

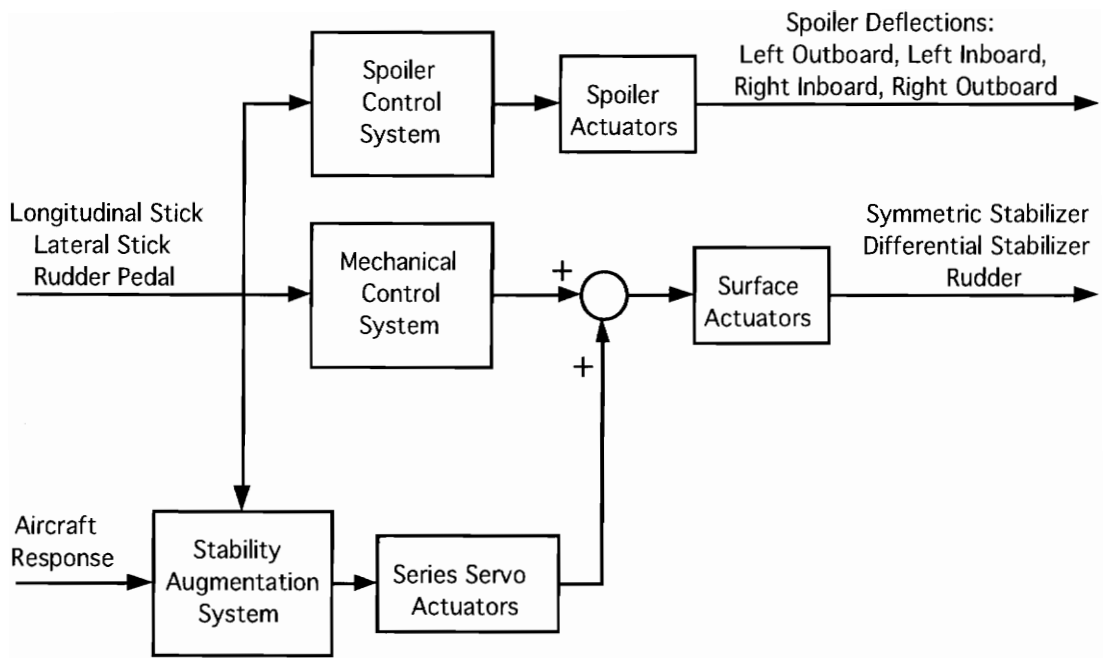


Figure 4.2 F-14 Control System Architecture



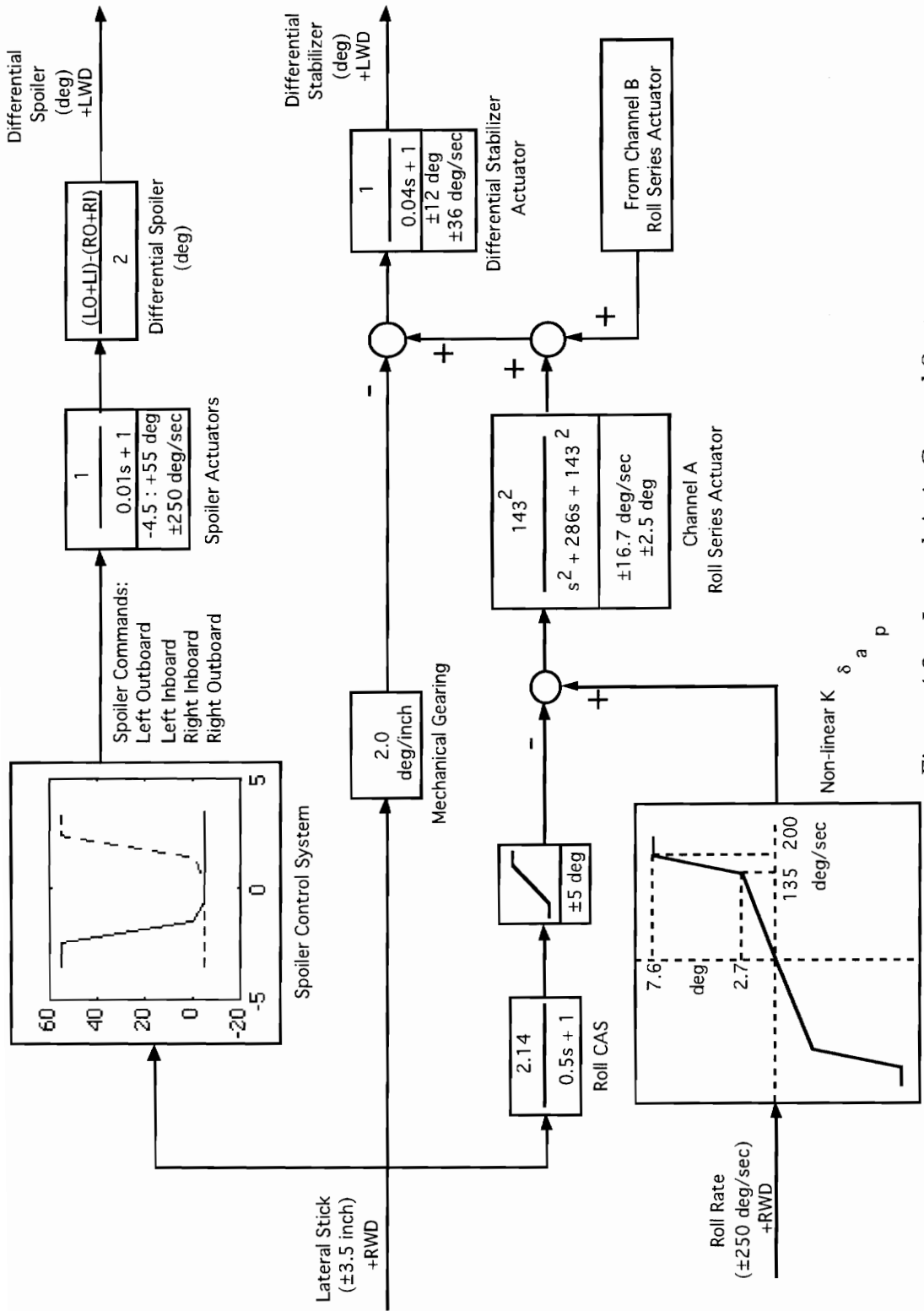


Figure 4.3 Lateral Axis Control System

For lateral stick inputs, the outboard spoilers on the side of the stick input (i.e., right stick commands right spoilers) are deflected upwards from the lower position of -4.5 degrees (flush against the wing), to a maximum angle of 55 degrees, while the opposite side spoilers remain flush to the wing. The inboard spoilers will also do the same, unless the Direct Lift Control (DLC) system is engaged. If DLC is engaged, the left and right inboard spoilers are biased up to 17.5 degrees. From this biased position, the inboard spoilers are deflected differentially for roll control and symmetrically for vertical flight path control. The complete spoiler control system is shown in figure 4.4. Figure 4.5 shows the lateral stick to spoiler gearing which is shown on the spoiler control system diagram. The individual spoiler surface deflection versus lateral stick displacement relationship for the DLC engaged and disengaged configurations is shown in figure 4.6.

#### **4.2.2 Directional Control System Description**

The directional axis control system is shown in figure 4.7. It consists of the rudder pedal to rudder surface mechanical path and the yaw SAS. The mechanical path can command the rudder up to its maximum authority of  $\pm 30$  degrees. The dual-channel Yaw SAS operates on lateral acceleration and yaw rate inputs to produce yaw series actuator commands, which have a total authority of  $\pm 19$  degrees. The yaw rate feedback path utilizes a 2.0 second washout filter and 0.5 gain to improve the damping of the Dutch-roll mode. The washout is required to neutralize the yaw series servo command during a steady-state turn. The lateral acceleration feedback path is amplified by a gain which is a function of lateral stick deflection, and filtered by a 0.05

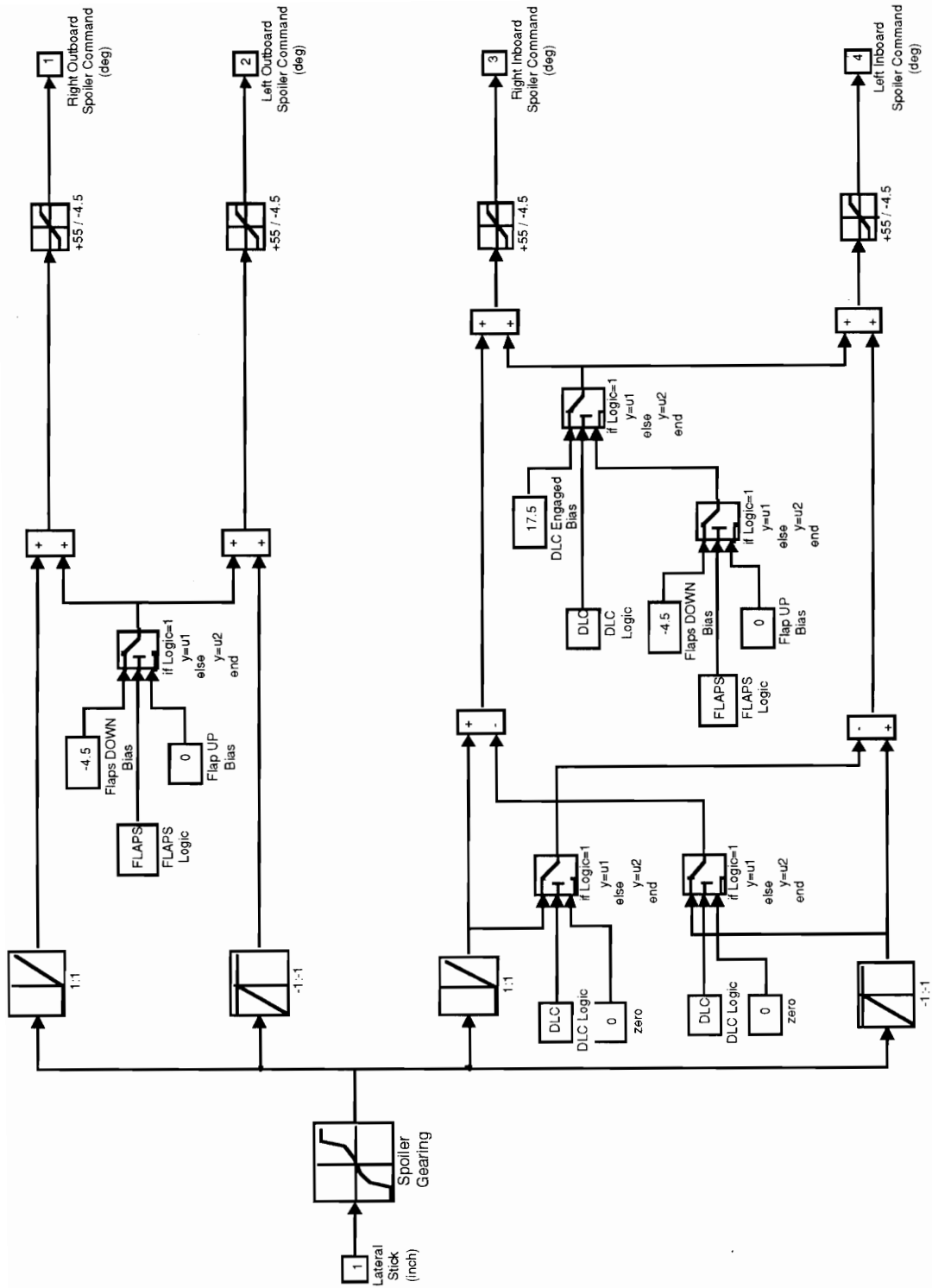


Figure 4.4 Spoiler Control System

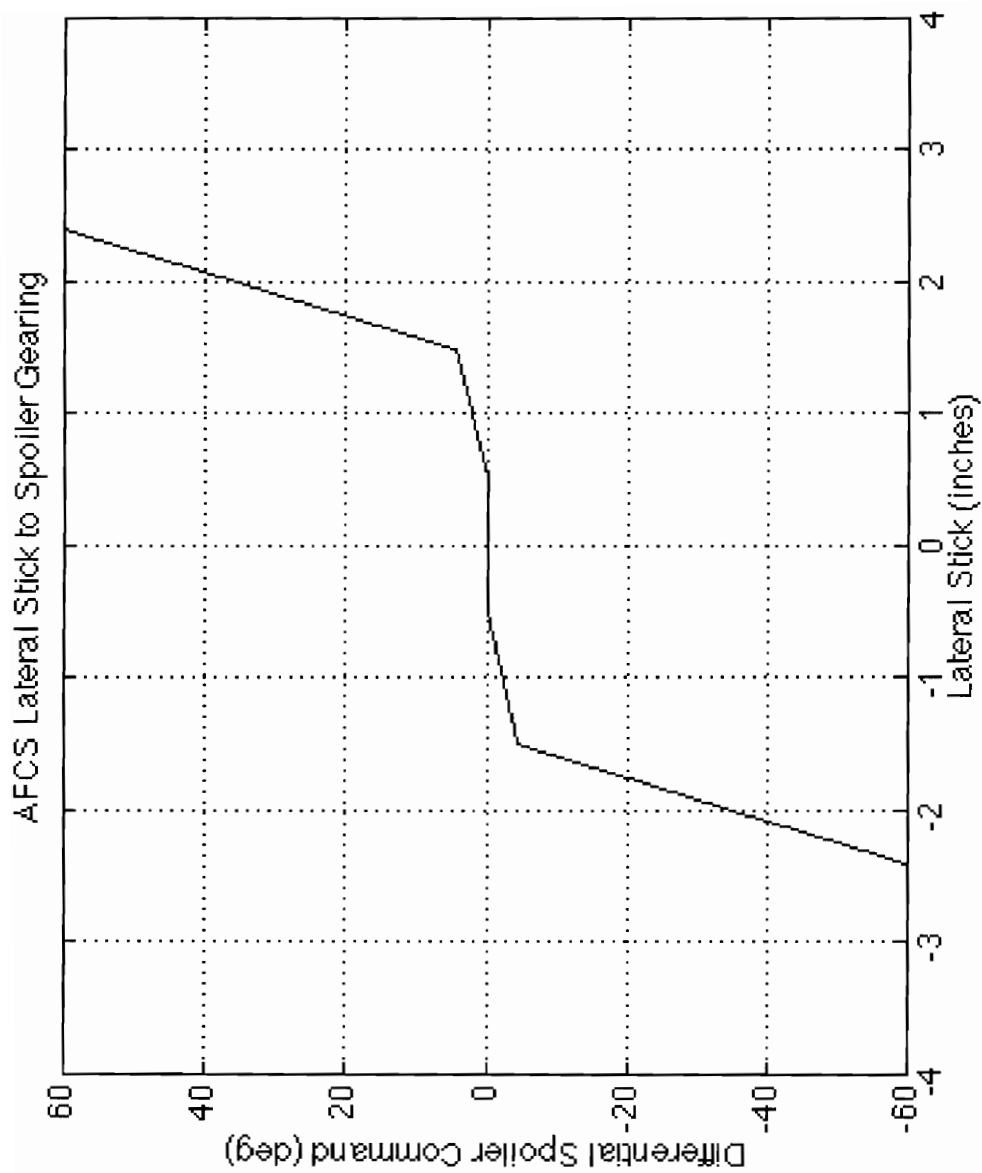


Figure 4.5 AFCS Lateral Stick to Spoiler Gearing

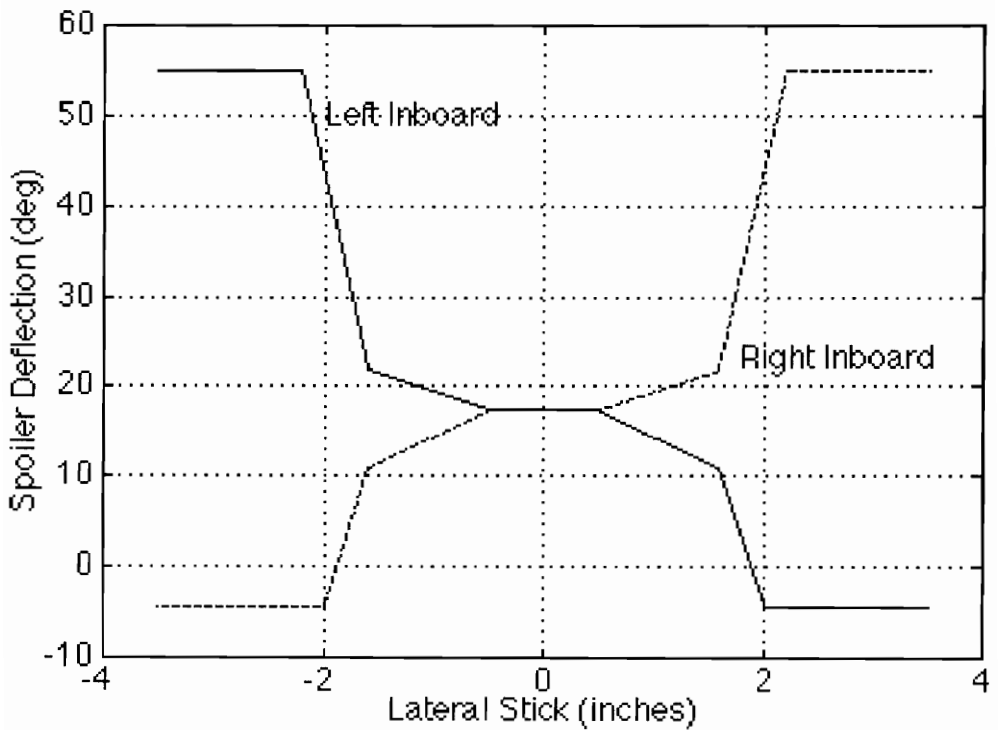
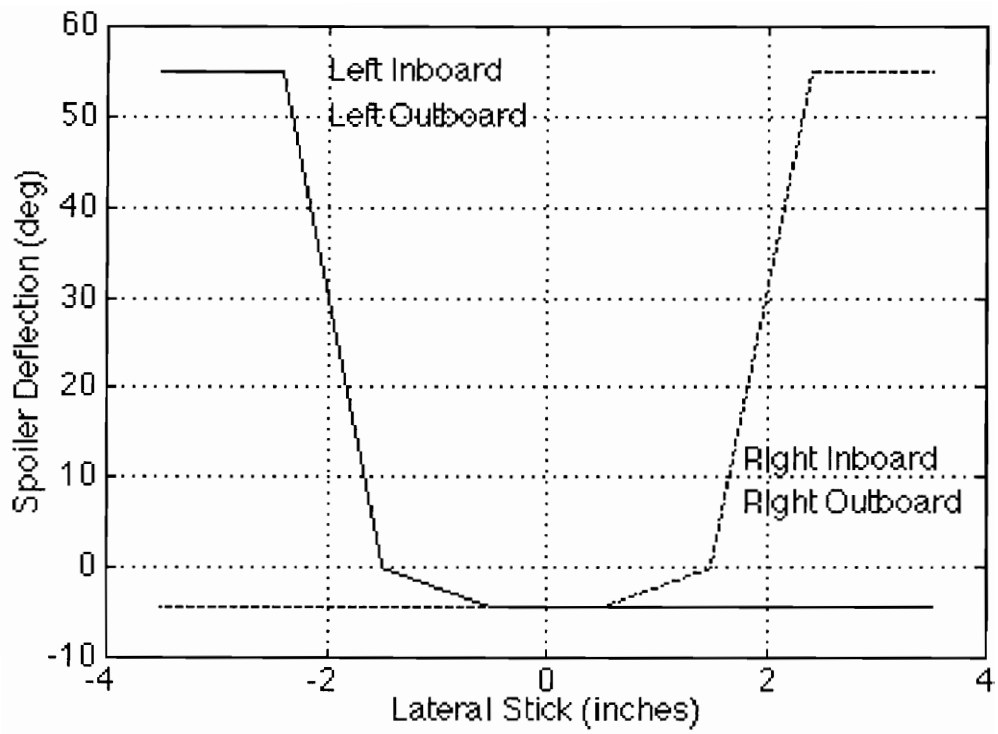


Figure 4.6 Individual Spoiler Surface Deflection vs Lateral Stick

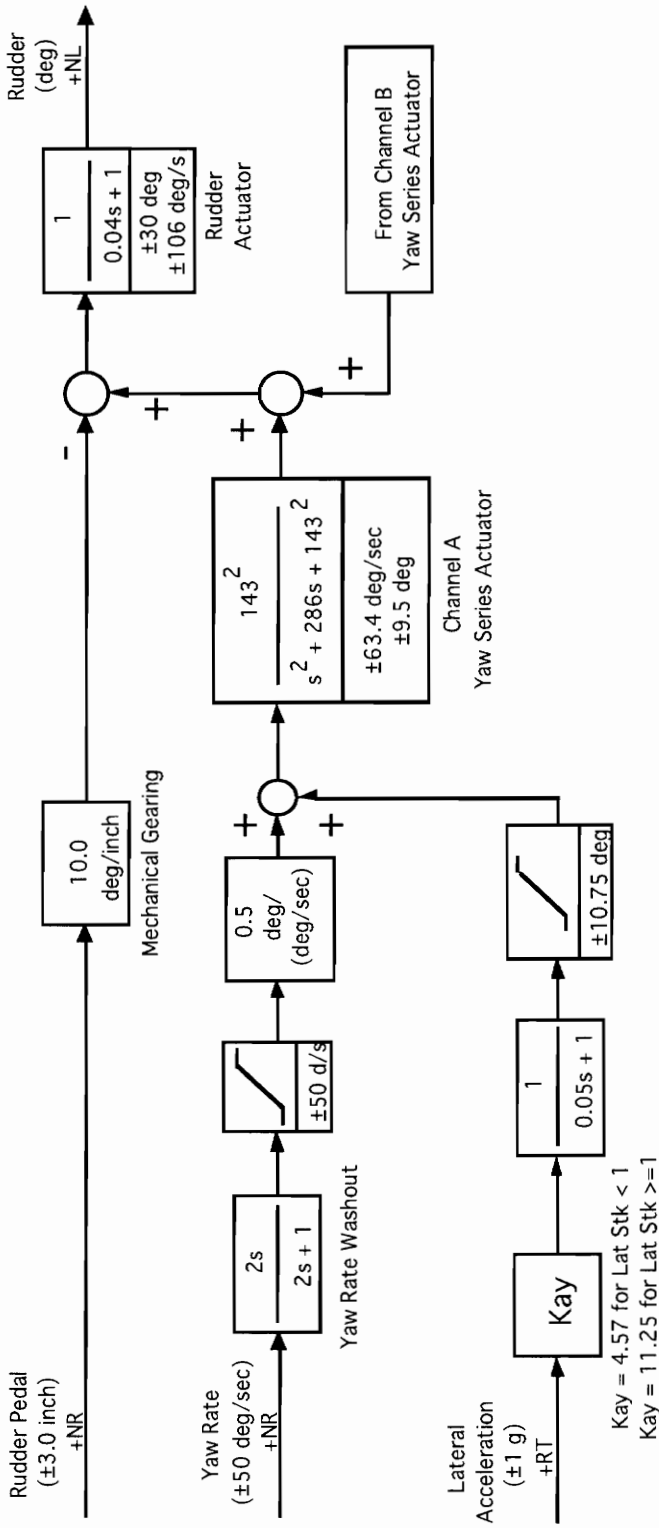


Figure 4.7

Directional Axis Control System

second lag. Lateral acceleration feedback is used for turn coordination and sideslip reduction. Since large lateral stick inputs tend to produce more sideslip (and therefore lateral acceleration) than small inputs, the lateral acceleration feedback gain is boosted to compensate for these inputs.

### **4.3 Piloted Simulation Evaluation**

In support of the PA ARI development effort, the characteristics of the production AFCS were evaluated during a comprehensive piloted simulation study conducted at NAWCAD [4.1]. The model used for this evaluation was the F-14 nonlinear FORTRAN simulation implemented into the CASTLE simulation environment described in Chapter II. The evaluation was performed by multiple Navy and Grumman pilots. In the powered approach regime, the primary tasks performed were bank angle captures and runway lineup corrections. The tasks were designed to highlight the deficiencies of the production AFCS. Pilot handling qualities ratings (HQR's) were the primary method of system performance evaluation.

#### **4.3.1 Bank Angle Captures**

The bank angle (or roll angle) capture task involved the pilot using lateral stick inputs to roll the aircraft to a specified bank angle. The initial condition for these tasks was an initial steady state bank angle from which the pilot rolled the aircraft through wings level and captured the bank angle in the opposite direction. The maneuver amplitudes studied were  $\pm 10$ ,  $\pm 30$ , and  $\pm 45$  degrees. Smooth, gradual inputs as well as sharp, aggressive inputs were

studied. The primary objective of this task was to evaluate the roll rate sensitivity and predictability (linearity).

The average pilot HQR for these tasks was 6 (Very objectionable but tolerable deficiencies - adequate performance requires extensive pilot compensation). The primary reason for the poor ratings was due to the excessive adverse sideslip induced by the rolling maneuver. The sideslip excursions excited the lightly damped Dutch-roll mode, and the resulting coupled lateral-directional oscillations significantly degraded the pilot's ability to capture the desired bank angle. Several lateral stick corrections were required to dampen the oscillations and stabilize at the desired bank angle. The task also demonstrated a significant nonlinear roll rate sensitivity to lateral stick inputs which degraded the pilot's ability to establish a desired roll rate and to stop the roll rate at the desired bank angle.

#### **4.3.2 Runway Lineup Corrections**

The prime task of the manned simulation evaluation was the execution of airfield and carrier landings requiring significant lineup corrections to acquire runway centerline. This task simulates an instrument approach in bad weather where the pilot does not visually acquire the runway until after descending below a given altitude limit. Once the runway is sighted, the pilot must apply the required corrections to bring the aircraft in line with the runway centerline.

The runway lineup task was performed with 50 and 100 foot lateral offsets, with the correction being applied at an altitude of 200 feet. At the nominal approach airspeed of 137 knots, the pilot had approximately 15



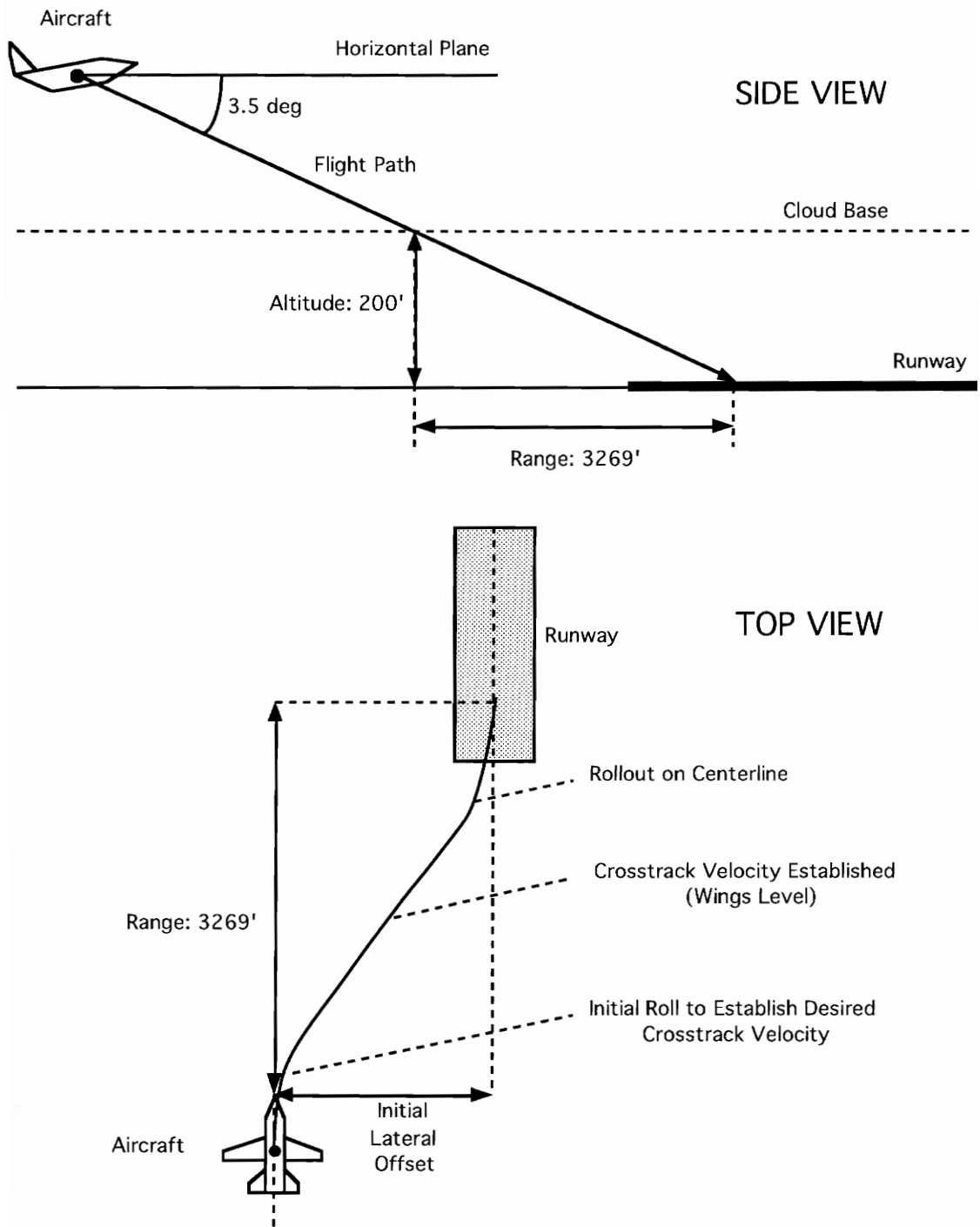


Figure 4.8 Runway Lineup Correction Task

seconds to make the necessary corrections to achieve a successful touchdown. The maneuver required is an S-turn requiring precise control of roll rate (and thus roll angle) and heading angle. The aircraft is first rolled to a desired bank angle. As the aircraft turns, the cross track velocity (the time rate-of-change of the lateral offset distance) increases. Once the desired cross track velocity is achieved, the aircraft is returned to wings level. As the aircraft nears the runway centerline, the pilot commands bank angle in order to eliminate the cross track velocity. As the cross track velocity nears zero, the aircraft is rolled to wings level on the runway centerline. A two view schematic of this scenario is presented in figure 4.8.

The pilots found the runway lineup correction task to be very demanding. Large (greater than 1.5 inches) lateral stick inputs were required to generate the necessary roll response required to establish the desired cross track velocity. These inputs tended to generate large amounts of adverse sideslip which excited the Dutch-roll mode. The resulting coupled roll and yaw oscillations and nonlinear roll response characteristics made establishment of the desired cross track velocity difficult and obscured the pilot's perception of the aircraft's horizontal flight path. Adequate performance was only achievable when the rudder pedals were used during the rolling maneuvers to provide turn coordination and Dutch-roll damping. The average HQR resulting from this task was 6. Table 4.1 below summarizes the HQR's obtained from the simulation evaluation of the production AFCS for the bank angle and runway lineup tasks.

Table 4.1 Handling Qualities Ratings for the Production AFCS

Task	Average HQR
Bank Angle Capture	6
Runway Lineup	6

#### 4.4 Off-line Nonlinear Simulation Evaluation

##### 4.4.1 Response to Pilot Control Inputs

The same nonlinear FORTRAN simulation model used in the piloted simulation evaluation was used in an off-line batch mode to investigate the problems reported by the pilots. Figure 4.9 shows the response to a 1 inch lateral stick half-doublet at the design flight condition specified in Table 2.1. The oscillations in the roll and yaw axis responses are quite apparent, as well as the large adverse sideslip. This adverse sideslip results primarily from kinematic coupling. Adverse sideslip due to kinematic coupling is caused when an aircraft at moderate to high angle-of-attack (AOA) rolls about the body x-axis. Under these conditions, a considerable amount of the angle-of-attack is converted to sideslip. To prevent this AOA to sideslip conversion, the pilot must coordinate the lateral stick input with rudder pedal, thereby performing a coordinated roll about the velocity vector (otherwise known as a stability axis roll).

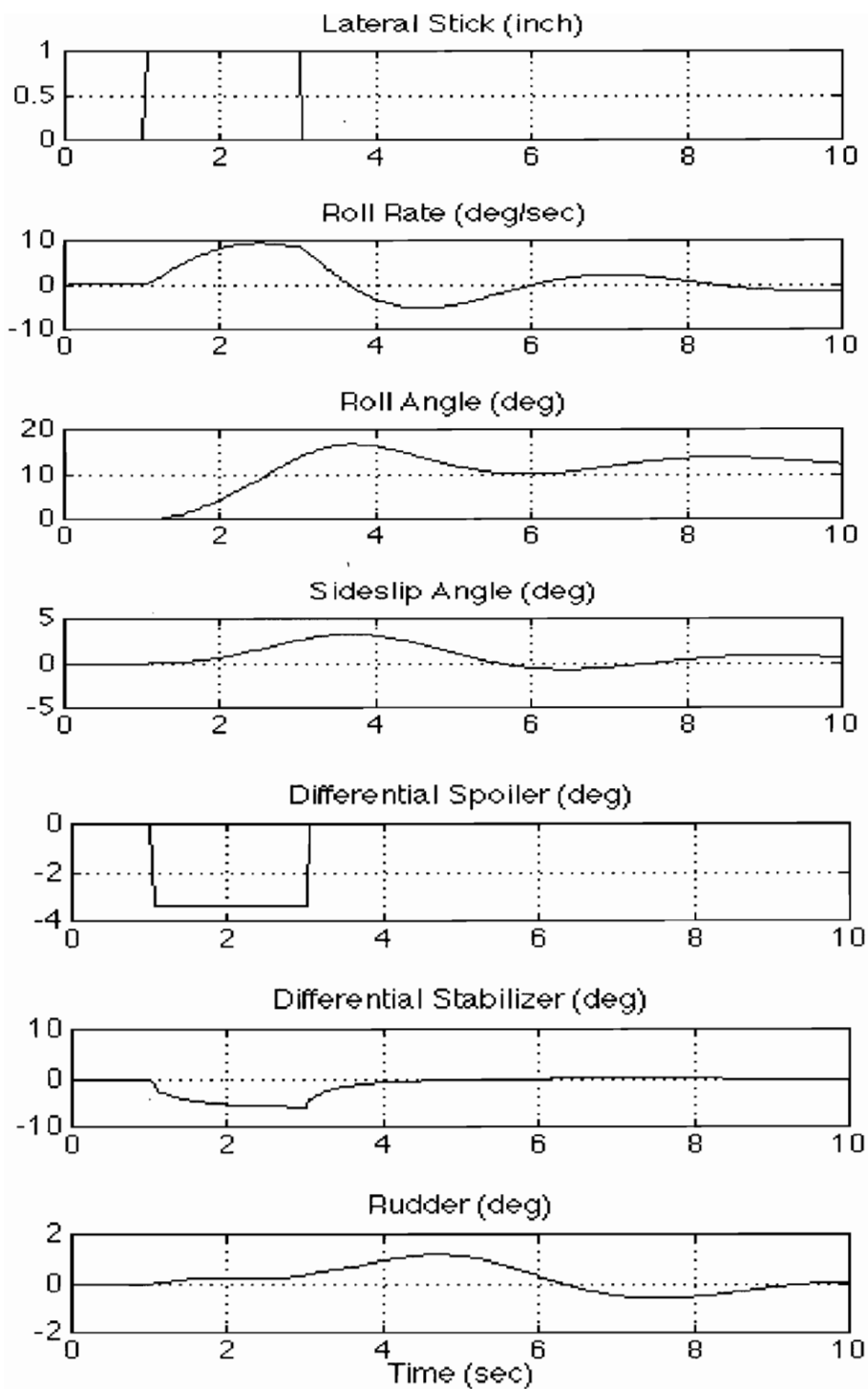


Figure 4.9 AFCS Response to Lateral Stick Step

The nonlinearity of the lateral stick to roll rate response as well as the adverse sideslip characteristics were analyzed by running the nonlinear FORTRAN simulation with a series of lateral stick inputs, ranging in size from 0.5 inches to the maximum deflection of 3.5 inches, in 0.5 inch increments. Figure 4.10 shows the resulting roll rate and sideslip angle responses. There is an obvious increase in the roll rate response between 1.5 and 2.0 inches of lateral stick. The top plot in figure 4.11 shows the maximum roll rate attained versus the lateral stick amplitude. The slope of the roll rate response is much steeper in the range from 1.5 to 2.0 inches of lateral stick. This re-enforces the conclusion drawn from figure 4.10 regarding the nonlinearity of the roll rate response. This sensitivity increase can be directly attributed to the shape of the production lateral stick to spoiler gearing shown in figure 4.5. Figure 4.5 shows a large slope change in differential spoiler command at 1.5 inches of stick. This undesirable characteristic was forced upon the original design due to analog hardware implementation restrictions.

The bottom plot in figure 4.11 shows the resulting maximum sideslip excursion versus the maximum roll rate obtained from the lateral stick maneuvers. This slope of the plot can be used as an indicator of the system turn coordination properties. A perfectly coordinated aircraft would have a slope of 0 degrees sideslip per deg/sec roll rate. The slope computed for the AFCS is approximately 0.35 deg/(deg/sec) for small roll rate maneuvers.

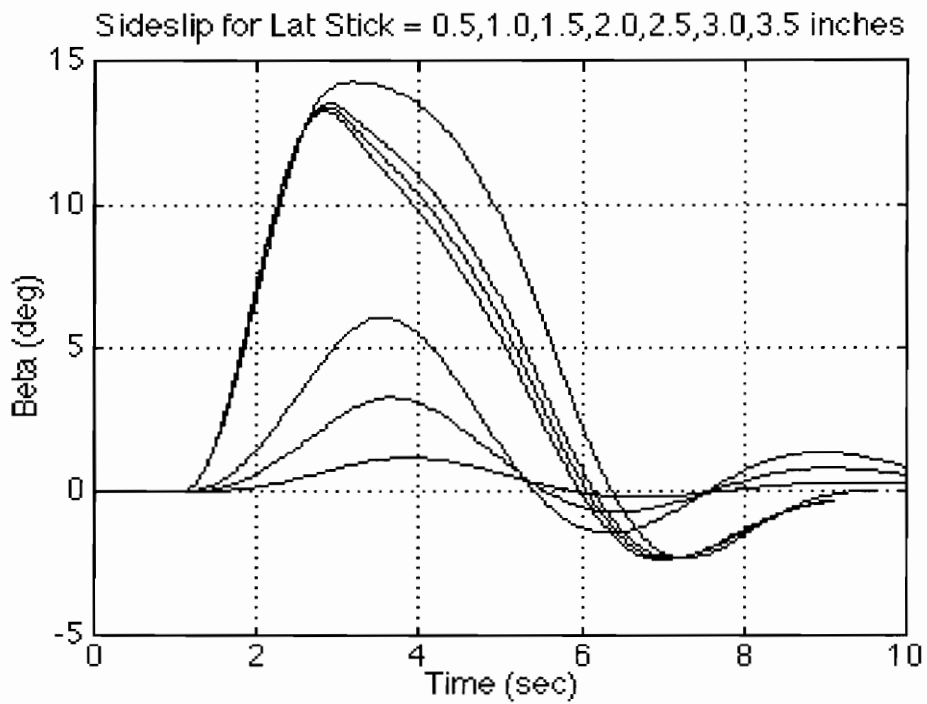
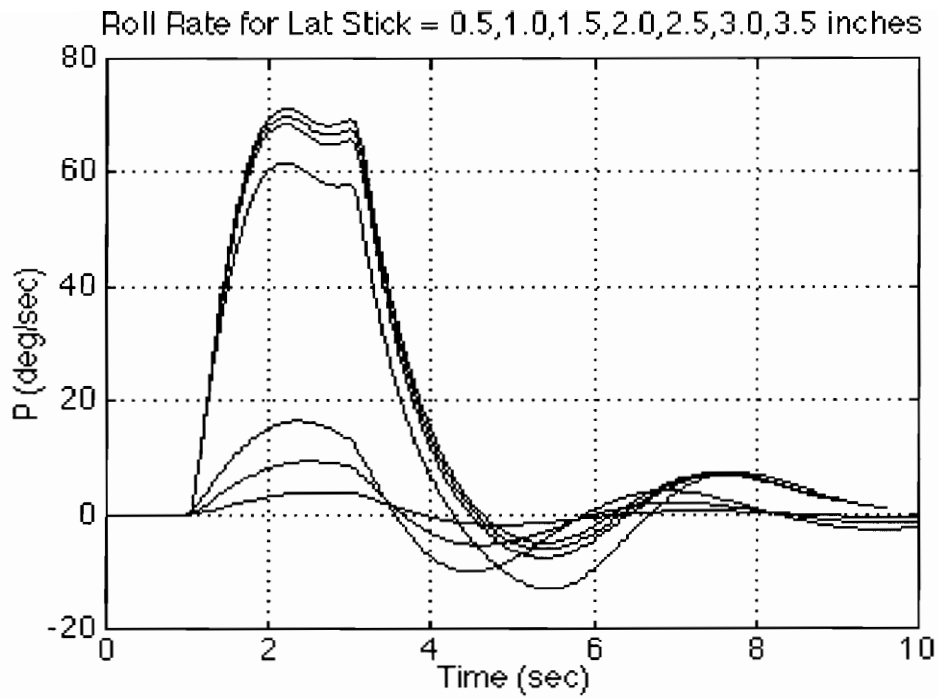


Figure 4.10 Roll Rate and Sideslip Responses for Various Lateral Stick Inputs

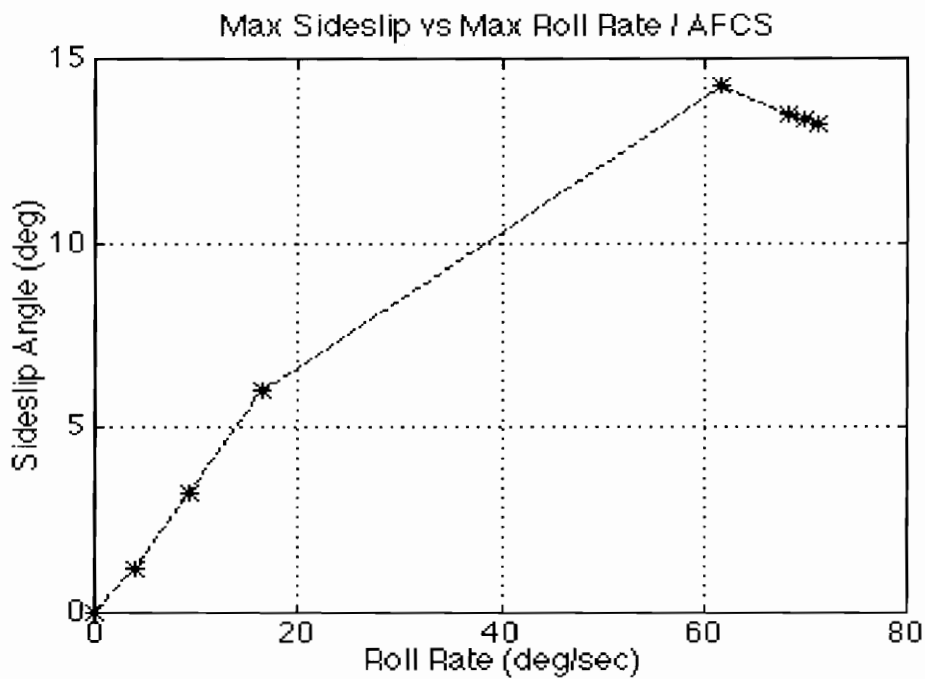
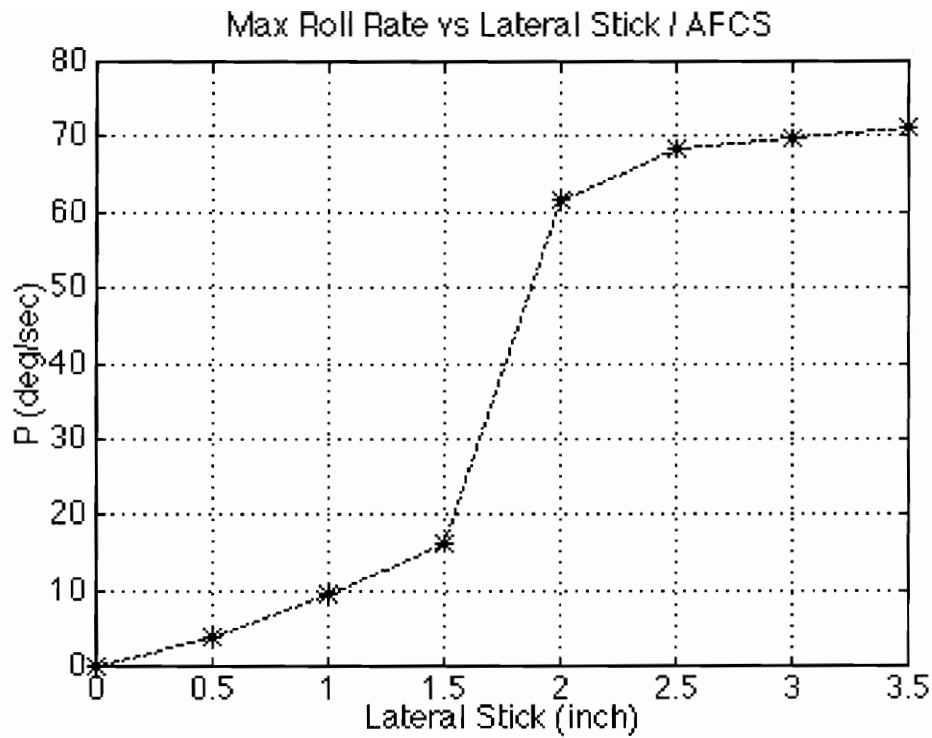


Figure 4.11 Roll Rate vs Lateral Stick and Max. Sideslip vs Max. Roll Rate

#### **4.4.2 Response to Atmospheric Turbulence**

The atmospheric turbulence model built into the MFS CASTLE simulation environment was used to evaluate the disturbance rejection properties of the AFCS control system. CASTLE contains both the Dryden and the Von-Karman forms of turbulence models. A detailed derivation of these models is presented in Etkin [2.3]. The evaluation performed in this work utilized the Von-Karman turbulence model. The turbulence intensity was set to 5 on a scale of 1 to 10. The analysis consisted of initializing the simulation at the design flight condition and running for 10 seconds with no control inputs while introducing a lateral velocity turbulence component. Figure 4.12 shows the result of turbulence on the aircraft straight and level tracking characteristics. The aircraft roll and heading angles are disturbed considerably by the turbulence, while the control surfaces show very little activity.

#### **4.5 Open-loop Stability Analysis**

The failure of the production control system to adequately compensate for the poor characteristics of the bare airframe was made readily apparent when an open-loop stability analysis was conducted. Frequency responses were computed for the lateral and directional axes with the control system loops opened at the sensor plane and the actuator plane, as shown in figure 4.13. The analysis model included all known high-frequency dynamics such as sensors and actuator dynamics. The loop of interest was analyzed by closing all the other loop breaks, leaving the SISO system of interest. The



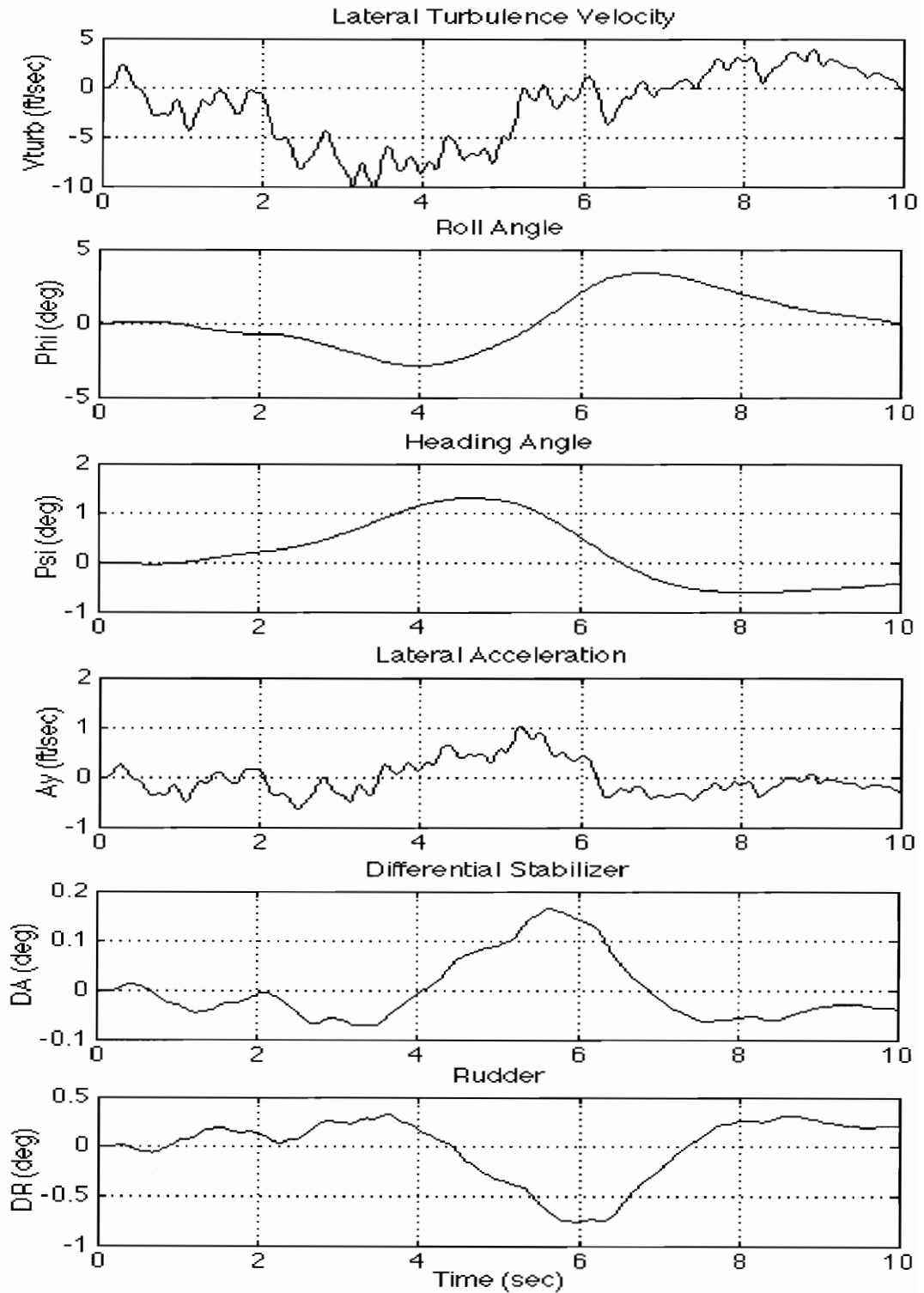


Figure 4.12 AFCS Response to Lateral Turbulence Velocity

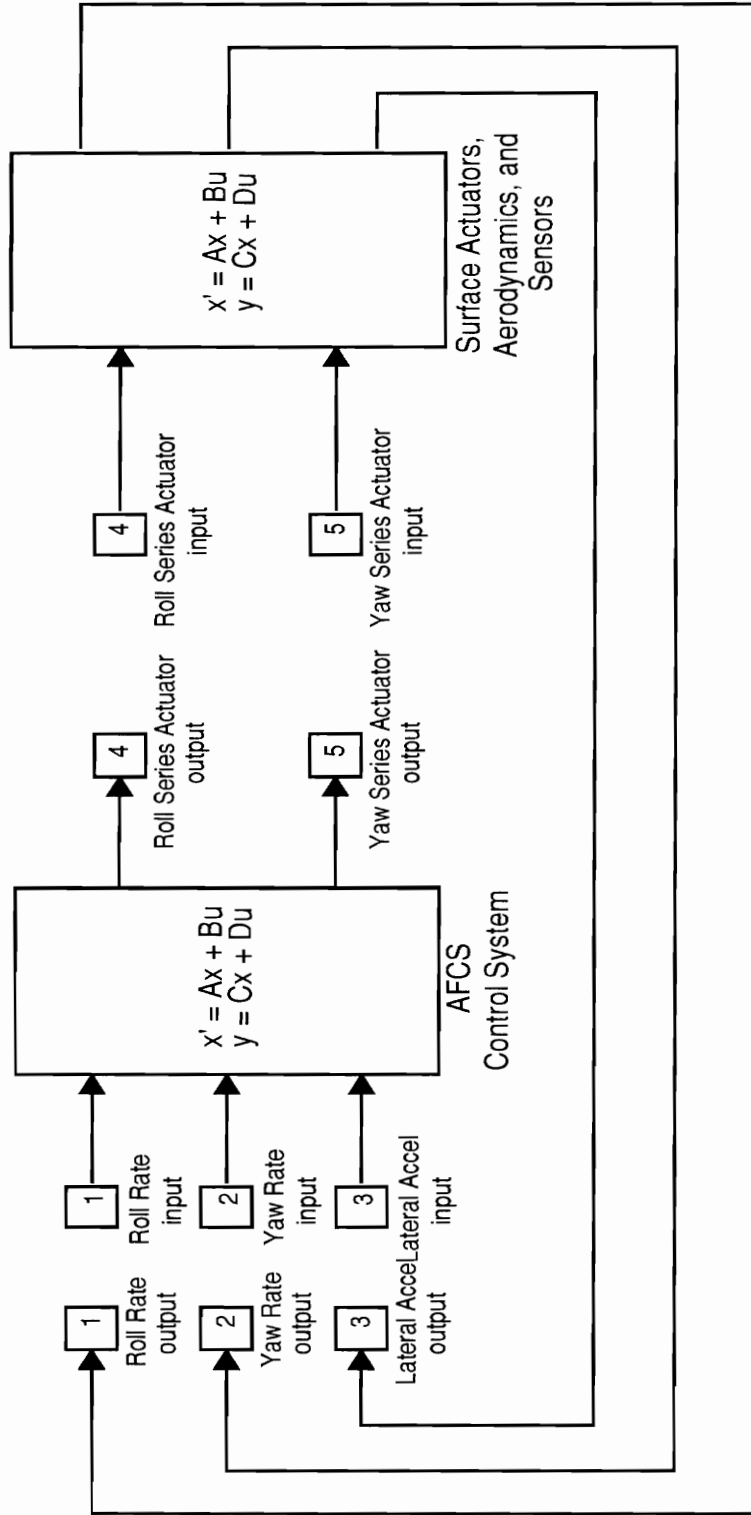


Figure 4.13  
AFCS Open-loop Analysis Model

bode plots for all actuator and sensor loop breaks are shown in figures 4.14 through 4.18. Due to the low gain in all loops, stability robustness was not in question. However, the feedback loops provided practically no disturbance rejection or command tracking capability, as demonstrated by the nonlinear simulation response to turbulence. As explained in Chapter I, the analog control system implementation did not permit gain scheduling across the flight envelope. The gains were optimized for high speed flight, so when the aircraft is in the low-speed landing configuration where the control surface effectiveness is reduced, the control system loop gain is reduced accordingly.

A root-locus analysis was also conducted of the lateral and directional control systems with the loops opened at the actuator plane only. The root-locus with the loop opened at the roll series servo is shown in figure 4.19. The closed-loop poles were virtually equal to the open-loop poles, which again demonstrates the low level of augmentation afforded by this feedback loop. The root-locus with the loop opened at the yaw series servo is shown in figure 4.20. A moderate increase in Dutch-roll damping was produced by the yaw SAS, from  $\zeta=0.11$  to  $\zeta=0.28$ .

#### **4.6 Summary**

Piloted simulation, nonlinear simulation analysis, and linear stability analysis of the production AFCS control system confirmed the known flying qualities deficiencies of the aircraft in the powered approach configuration. The deficiencies were shown to be due to the nonlinear lateral stick to spoiler gearing, the lack of automatic coordinating rudder due to lateral stick inputs, and the low feedback gains which do not sufficiently augment the bare airframe characteristics in the low-speed PA regime.

AFCS Bode Plot / FCS Mode: PA\_SAS / Loop Open at PBDEG  
Case 1: Vcal=137.3, AOA=10.5, DLC ON, Flaps DOWN, Loading: 2x4, CG=10.9 %

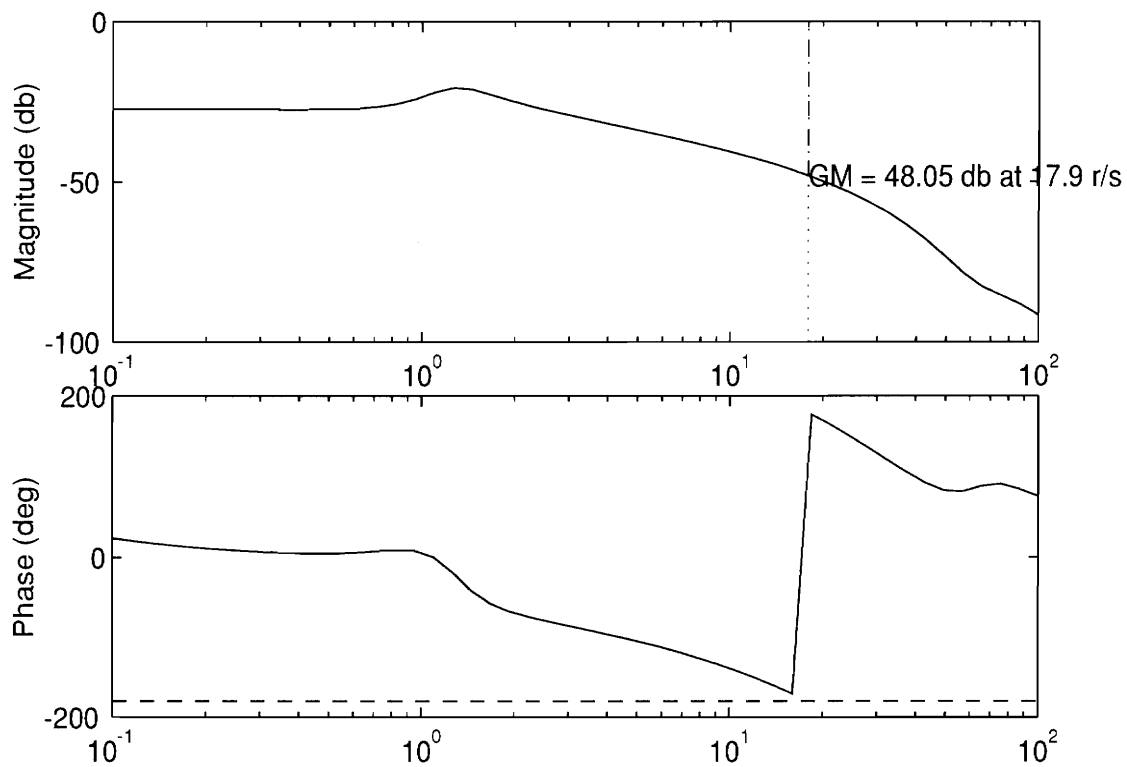


Figure 4.14 Frequency Response with the Loop Opened at Roll Rate

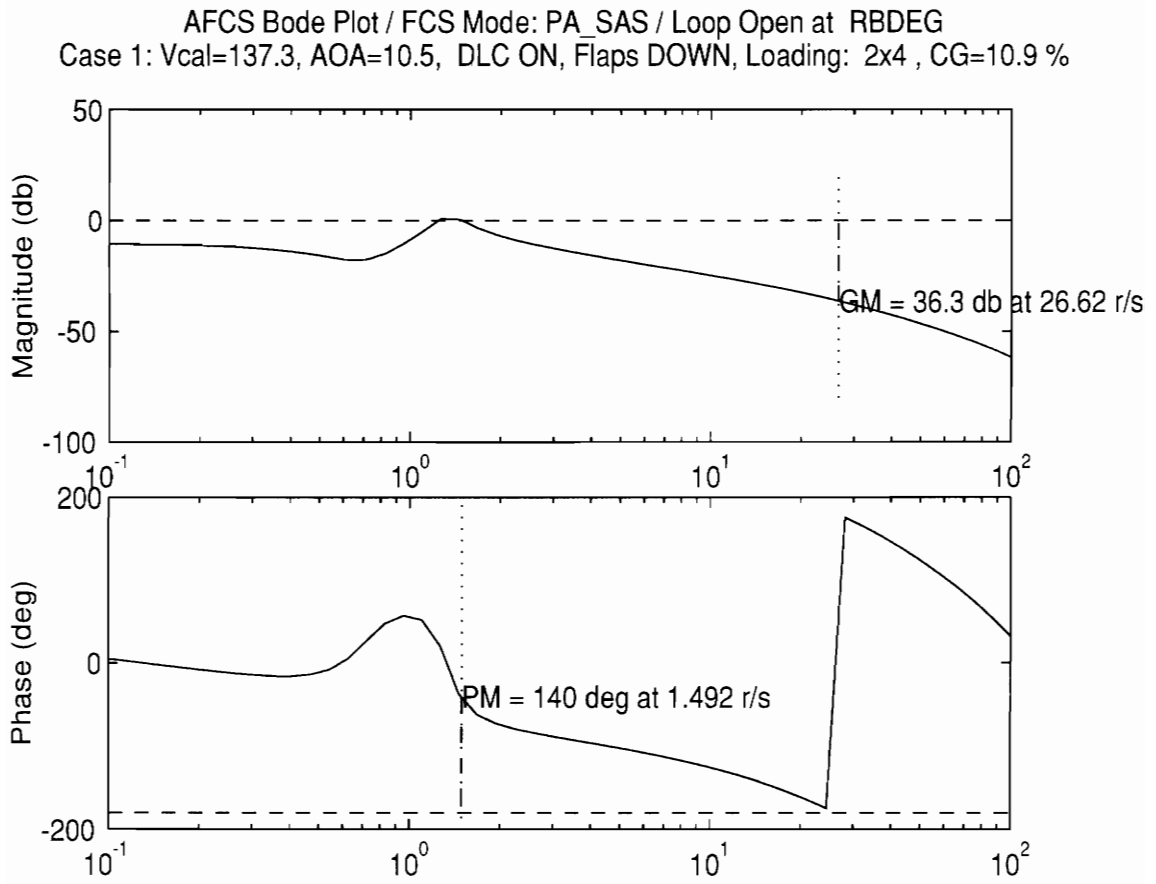


Figure 4.15 Frequency Response with the Loop Opened at Yaw Rate

AFCS Bode Plot / FCS Mode: PA\_SAS / Loop Open at AY  
Case 1: Vcal=137.3, AOA=10.5, DLC ON, Flaps DOWN, Loading: 2x4, CG=10.9 %

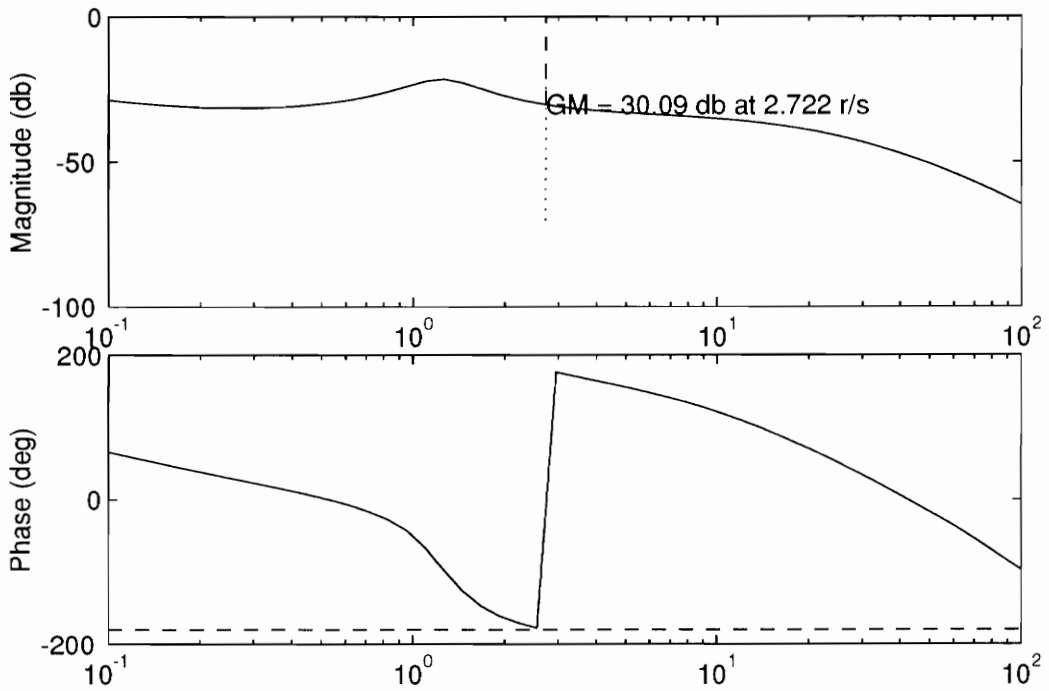


Figure 4.16 Frequency Response with the Loop Opened at Lateral Acceleration

AFCS Bode Plot / FCS Mode: PA\_SAS / Loop Open at DA  
Case 1: Vcal=137.3, AOA=10.5, DLC ON, Flaps DOWN, Loading: 2x4, CG=10.9 %

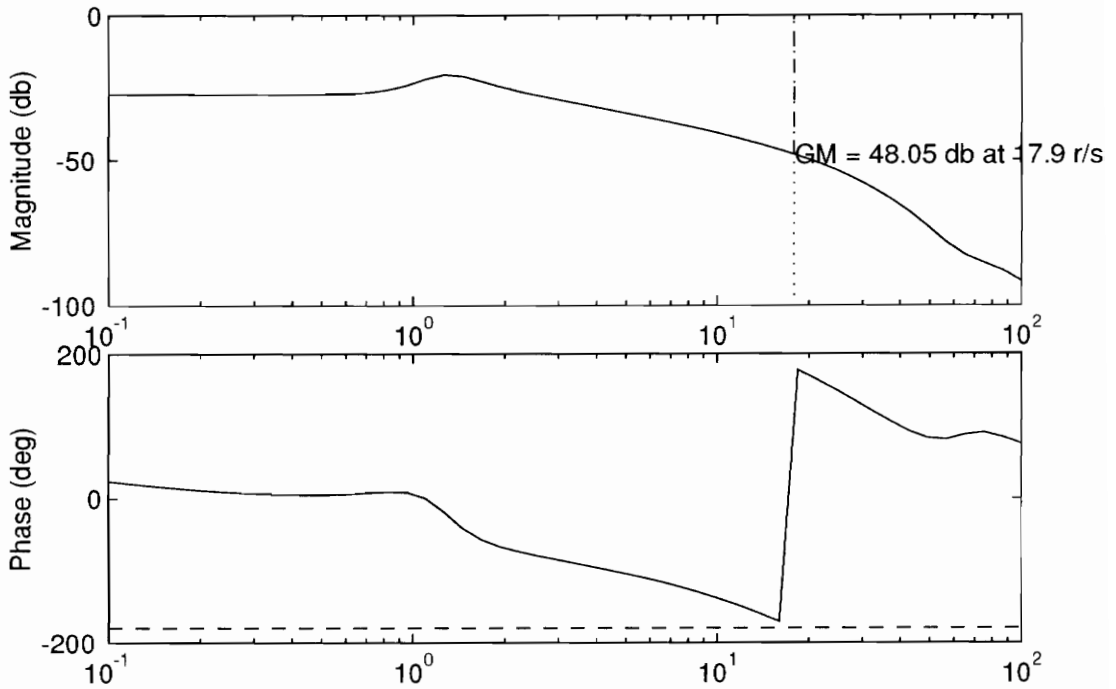


Figure 4.17 Frequency Response with the Loop Opened at Roll Series Servo

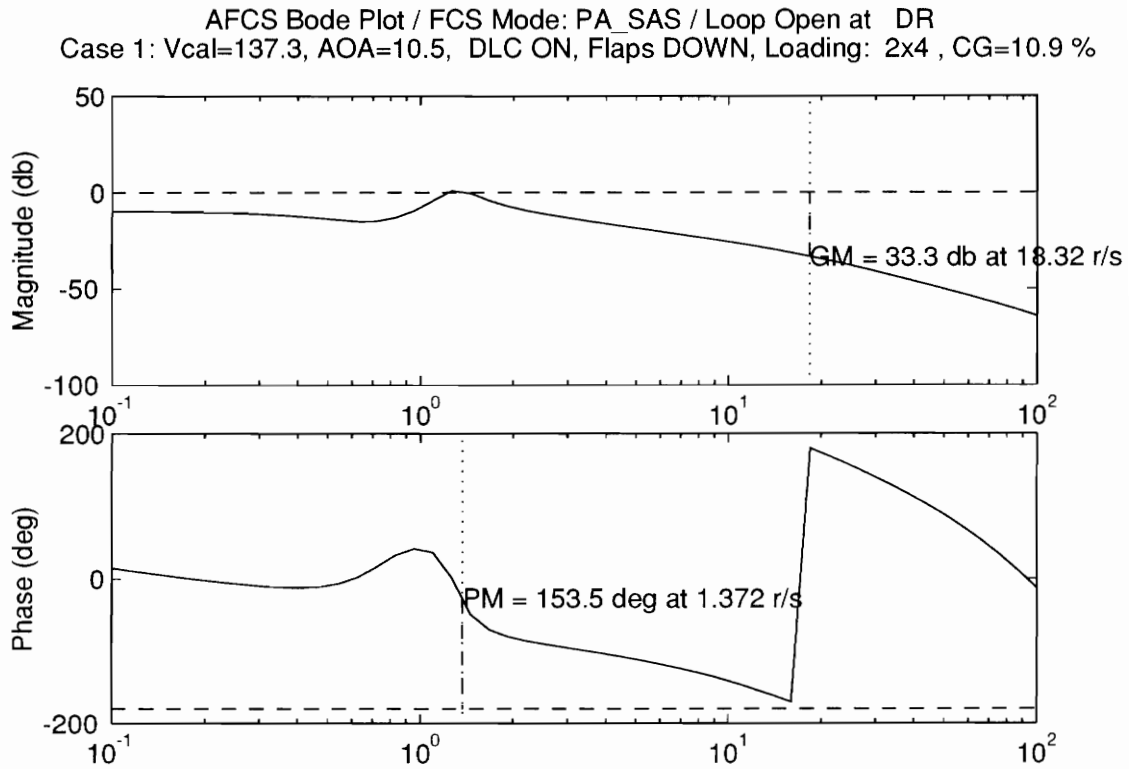


Figure 4.18 Frequency Response with the Loop Opened at Yaw Series Servo



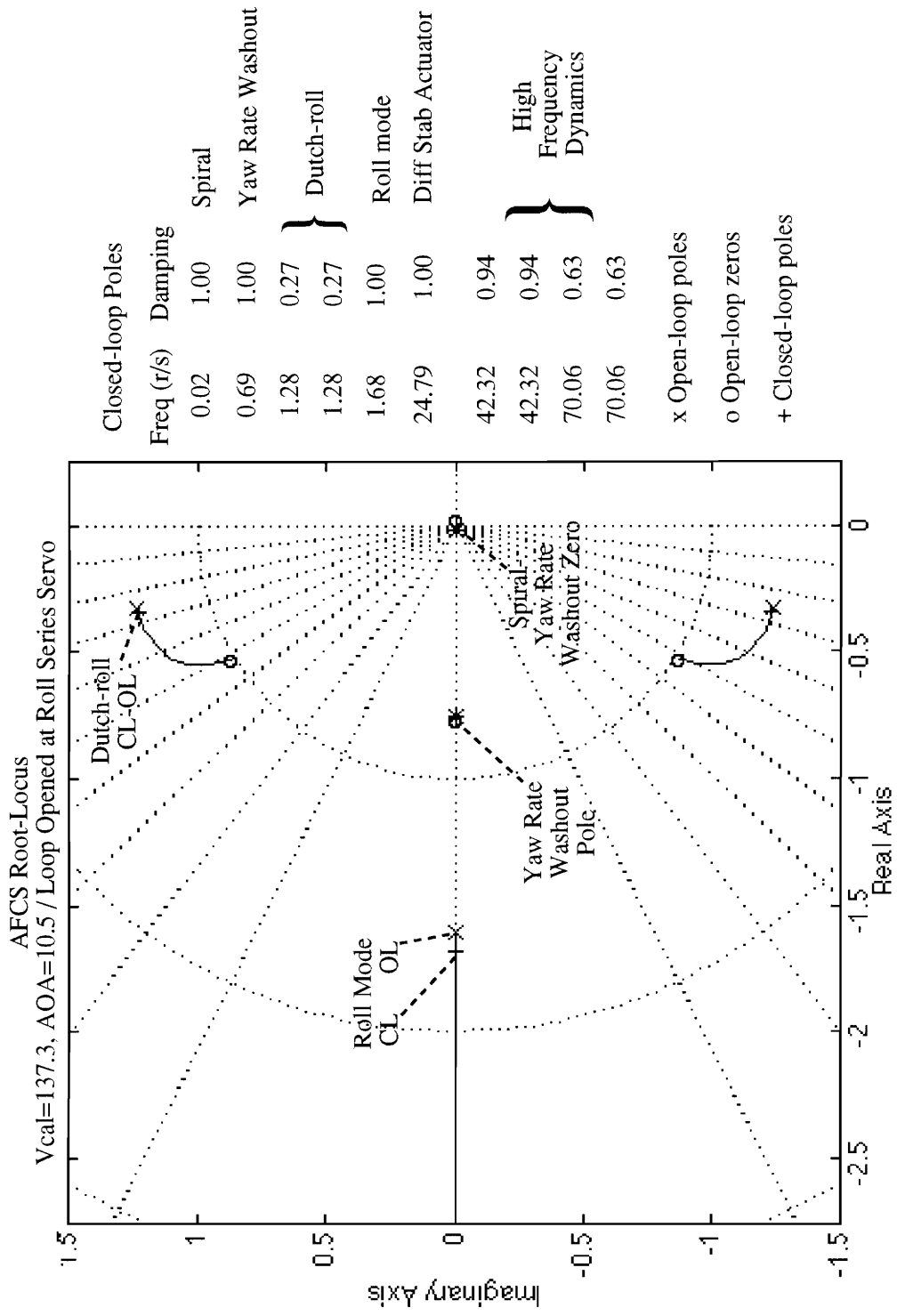


Figure 4.19 Root-locus with Loop Opened at Roll Series Servo

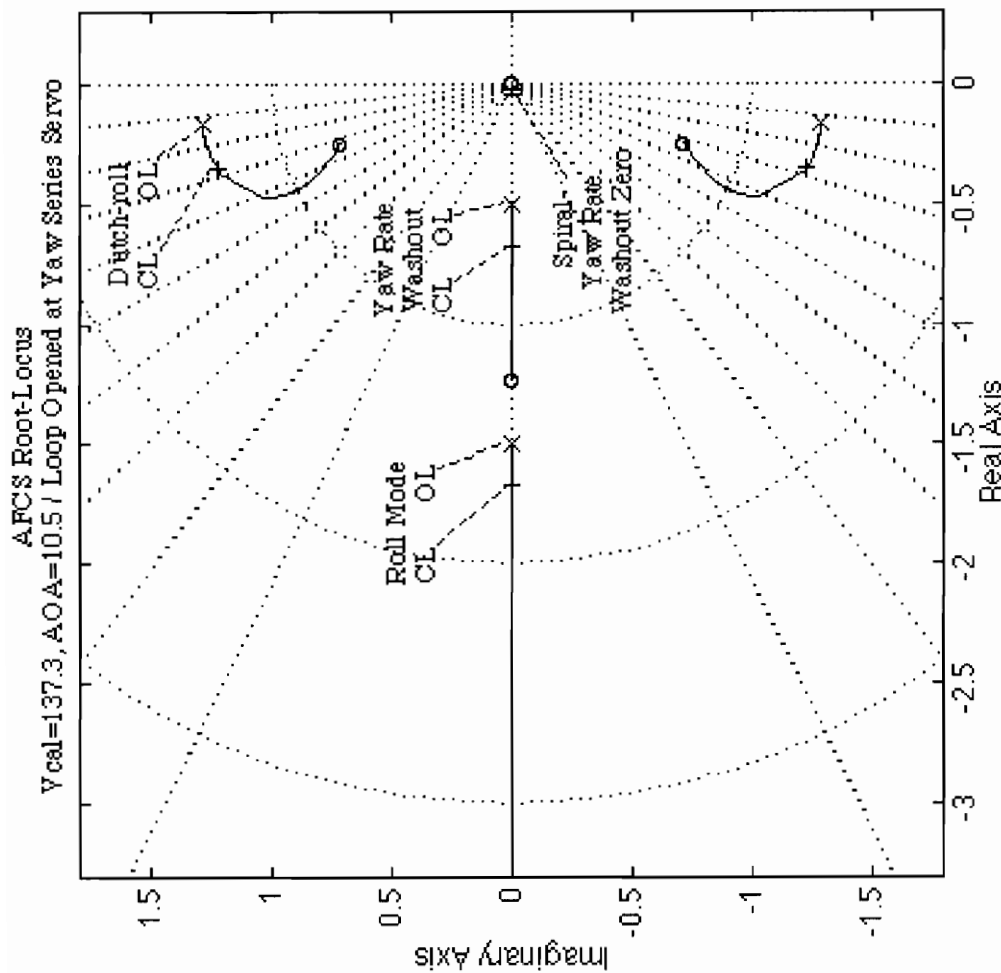


Figure 4.20 Root-locus with Loop Opened at Yaw Series Servo

## Chapter V

### PA ARI Control System Design

#### 5.1 Introduction

The Power Approach Automatic Rudder Interconnect (PA ARI) control law was designed to improve the lateral-directional flying qualities of F-14 aircraft in the powered approach regime. The control laws were designed using a combination of linear single-input, single-output (SISO) methods in combination with off-line and piloted nonlinear simulation optimization. The robustness of the design was insured by performing SISO as well as multi-input, multi-output (MIMO) stability analysis of all feedback loops. Flying qualities were demonstrated by a comprehensive pilot-in-the-loop simulation evaluation and equivalent systems analysis.

#### 5.2 Design Objectives

The PA ARI control law was designed to correct the deficiencies of the production AFCS control laws. The PA ARI was designed to meet or exceed the MIL-F-8785C requirements for Level I flying qualities and provide a handling quality rating (HQR) from 1 to 3 for any task within the PA operating envelope. The specific design objectives of the PA ARI control law were:

- 1) Increase Dutch-roll damping
- 2) Reduce sideslip excursions for lateral stick inputs (improve turn coordination)
- 3) Improve roll response predictability

The following control system functions are proposed to satisfy the design objectives:

- 1) Estimated sideslip rate (beta-dot) to rudder feedback
- 2) Lateral stick to rudder interconnect
- 3) a) Re-designed lateral stick to spoiler gearing  
b) Roll rate command/tracking system

A functional overview of the roll and yaw PA ARI control laws are shown in figures 5.1 and 5.2. These diagrams only represent the control law functions which will reside in the digital computer software. The mechanical primary control system was not altered for the digital flight control system upgrade program.

### **5.3 PA ARI Description**

The detailed roll PA ARI control law, including mechanical paths, is shown in figure 5.3. The key features of this system are the modified spoiler gearing and roll rate command system. The modified spoiler gearing function in combination with the mechanical differential stabilizer is designed to provide the desired roll rate in response to lateral stick inputs, thereby eliminating the need to use the roll series servos to generate roll rate. The

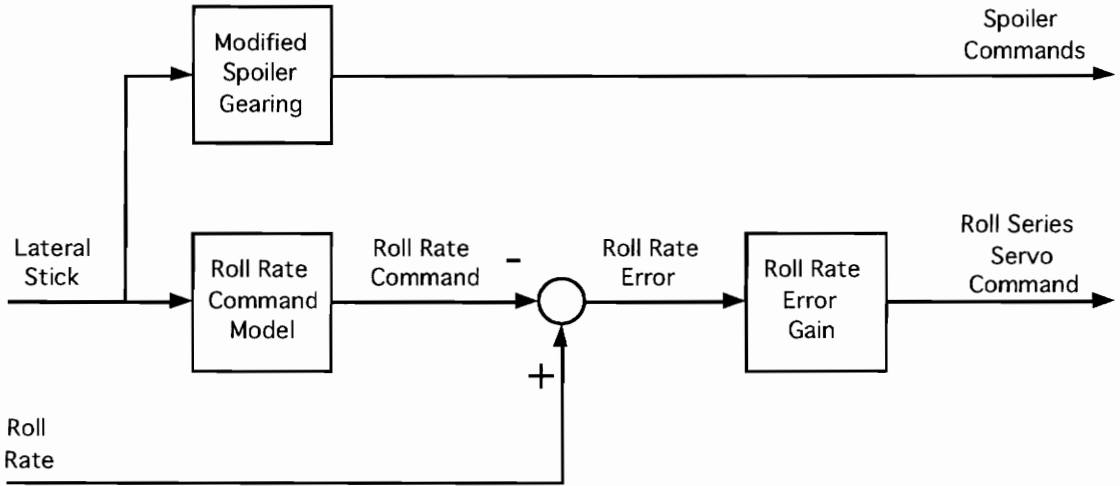


Figure 5.1 Roll PA ARI Overview

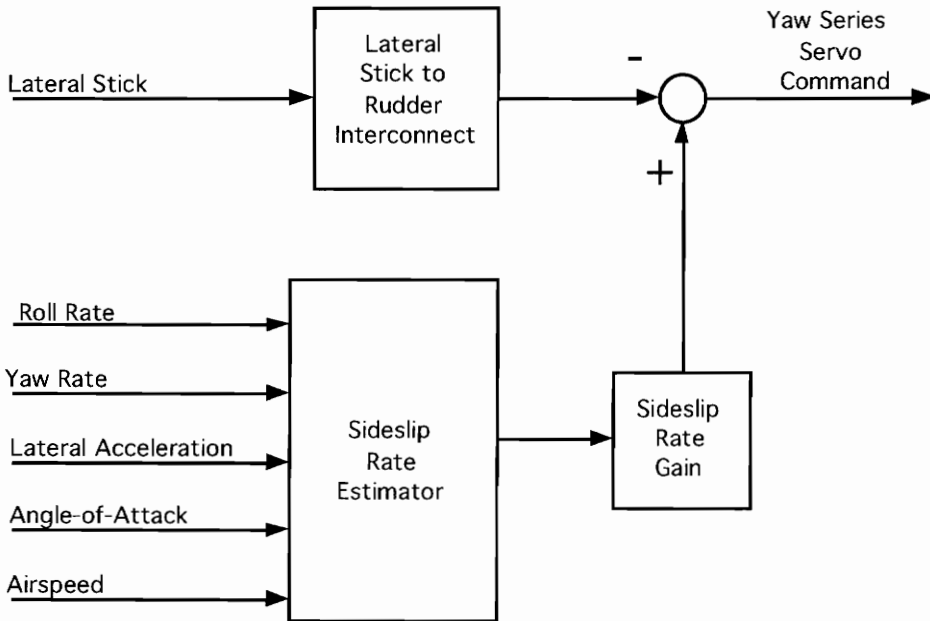


Figure 5.2 Yaw PA ARI Overview



estimated roll rate response to lateral stick inputs is implemented in the roll rate command gain and lag in figure 5.3. A roll rate error is then formed between the commanded roll rate and the roll rate feedback signal. The error is amplified by a gain and sent to the roll series servos, which in turn command differential stabilizer to adjust the aircraft roll rate and track the command model. The gain is scheduled with low-pass filtered angle-of-attack, which provides an effective indicator of the aircraft trim airspeed but with more sensor redundancy than the airspeed measurement system.

The detailed yaw PA ARI control law, including mechanical paths, is shown in figure 5.4. The key features of this system are the sideslip rate (beta-dot) estimator and the lateral stick to rudder interconnect (LSRI). The details of the sideslip rate estimator are given in section 5.3. The LSRI is designed to provide the necessary anticipatory rudder deflection to achieve coordinated rolling maneuvers with minimal sideslip excursions. Both the LSRI and sideslip rate feedback gains are scheduled with filtered angle-of-attack.

#### 5.4 Sideslip Rate Estimator Design

The single most enhancing feature of the PA ARI control law is the estimated sideslip rate (beta-dot) feedback. The beta-dot calculation is derived from the lateral force 6-DOF equation of motion, given by (2.2):

$$\dot{V} = PW - RU + g \cos \Theta \sin \Phi + \frac{Y}{m} \quad (5.1)$$

For small values of beta-dot, the following relationship holds:

$$\dot{V} \approx V_T \dot{\beta} \quad (5.2)$$

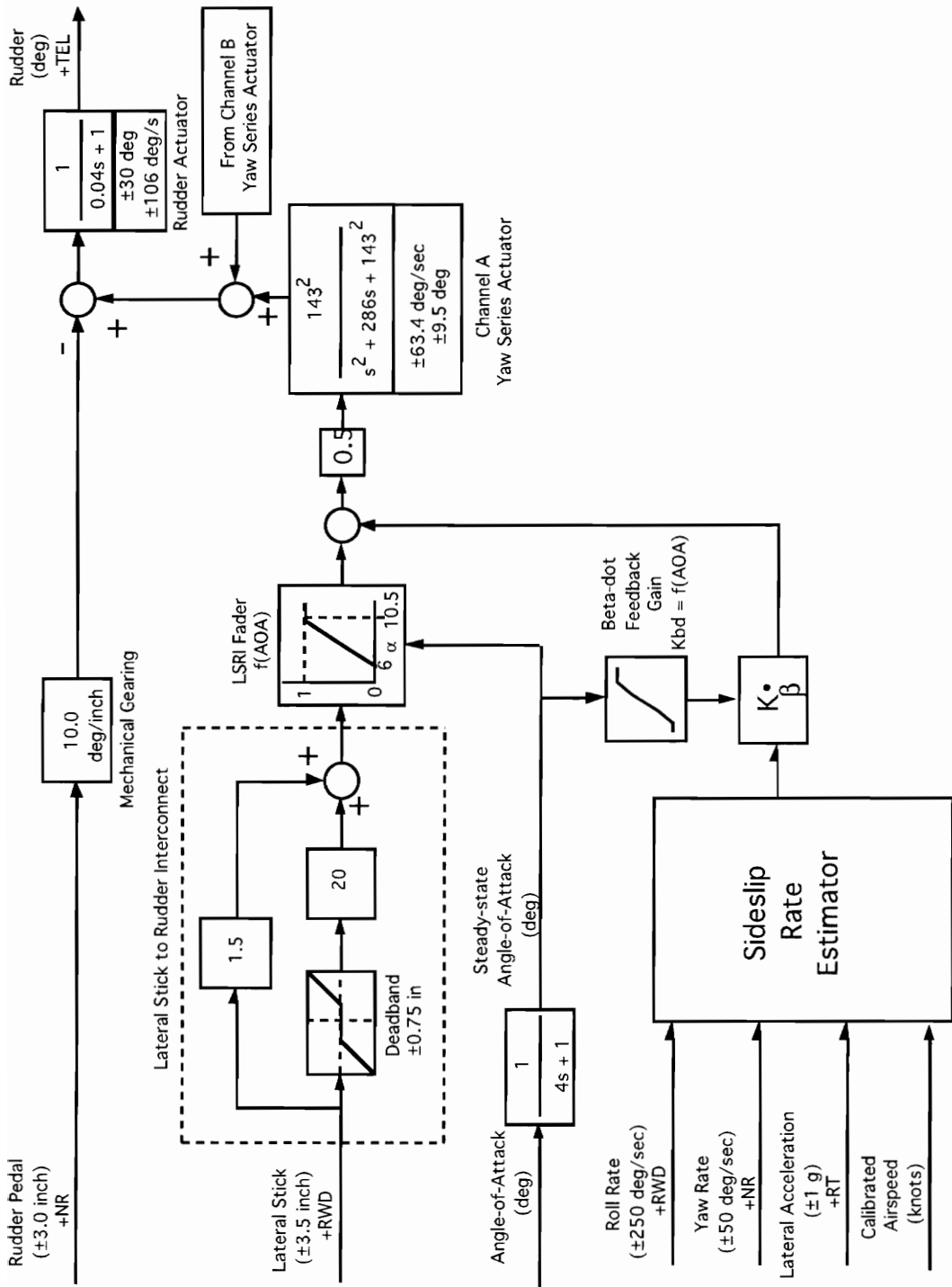


Figure 5.4 Yaw PA ARI Control System



The following relationships are exact:

$$W = V_T \sin \alpha, \quad U = V_T \cos \alpha, \quad A_y = \frac{Y}{m} \quad (5.3)$$

Substituting (5.2) and (5.3) into (5.1) results in:

$$V_T \dot{\beta} = P V_T \sin \alpha - R V_T \cos \alpha + g \cos \Theta \sin \Phi + A_y \quad (5.4)$$

Dividing both sides by  $V_T$  and assuming that  $\cos \Theta = 1$  results in:

$$\dot{\beta} = P \sin \alpha - R \cos \alpha + \frac{g \sin \Phi + A_y}{V_T} \quad (5.5)$$

All of the parameters on the right hand side of (5.5) are available to the F-14 flight control computer. However, due to the present redundancy management scheme roll angle ( $F$ ) is a simplex input. The design goal of the PA ARI system is to be fail operational, therefore, this input cannot be used. To provide the roll angle input, an estimator is constructed that combines a low frequency estimate with a high frequency estimate in the form of a complementary filter. The low frequency estimate of roll angle is derived from (5.5) by assuming the aircraft is in a steady-state turn, with zero roll rate and a constant sideslip angle. This results in:

$$0 = -R \cos \alpha + \frac{g \sin \Phi + A_y}{V_T} \quad (5.6)$$

Rearrangement of (5.6) yields:

$$\hat{\Phi}_{L.O} = \sin^{-1} \left( \frac{V_T R \cos \alpha - A_y}{g} \right) \quad (5.7)$$

The high frequency estimate of roll angle is simply the integration of the aircraft roll rate:

$$\hat{\Phi}_{HI}(s) = \frac{P}{s} \quad (5.8)$$

The low and high frequency estimates are then frequency weighted as follows:

$$\hat{\Phi}(s) = \left( \frac{10s}{10s+1} \right) \hat{\Phi}_{HI} + \left( \frac{1}{10s+1} \right) \hat{\Phi}_{LO} \quad (5.9)$$

The weighting frequency of 10 rad/sec corresponds to the value used in the current F-18 sideslip rate estimator. Equation (5.9) is a complementary filter estimate of roll angle. This expression can be simplified by substituting (5.8) into (5.9) to give:

$$\hat{\Phi}(s) = \frac{\hat{\Phi}_{LO} + 10P}{10s+1} \quad (5.10)$$

A block diagram of the complementary filter structure is shown in figure 5.5. The complementary filter can be integrated into equation (5.5) to form the complete sideslip rate estimator, as shown in figure 5.6. The accuracy of the estimator was validated by performing a frequency response comparison between the estimated sideslip rate and the aerodynamic model sideslip rate as shown in figure 5.7.

## 5.5 Feedback Loop Design Techniques

The roll rate and estimated sideslip rate feedback gains were computed using root-locus techniques to perform successive loop closure. Since the control law will be employed in a digital computer, the feedback gain design was conducted using discrete time plant models. The design plant model

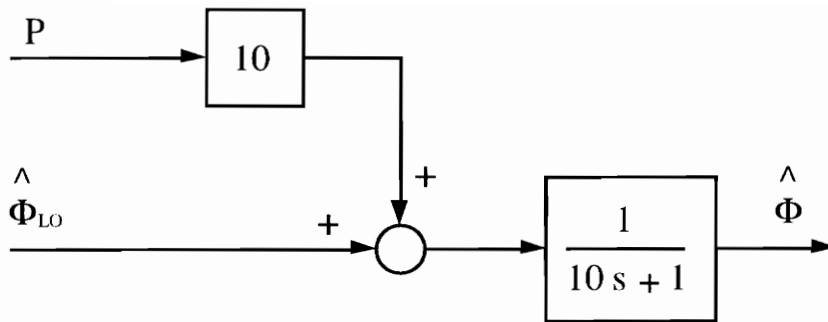


Figure 5.5 Roll Angle Complementary Filter

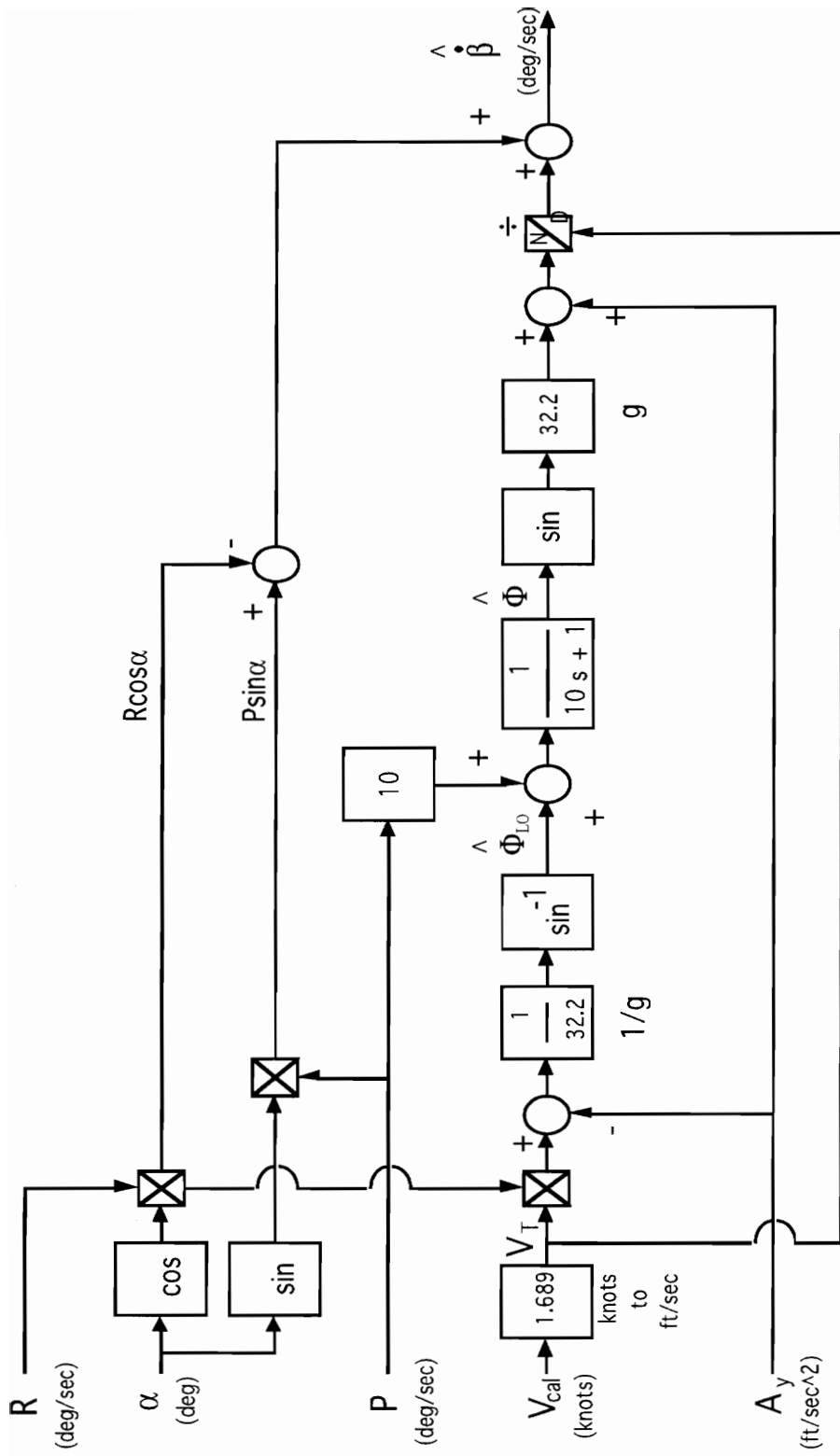


Figure 5.6 Sideslip Rate Estimator

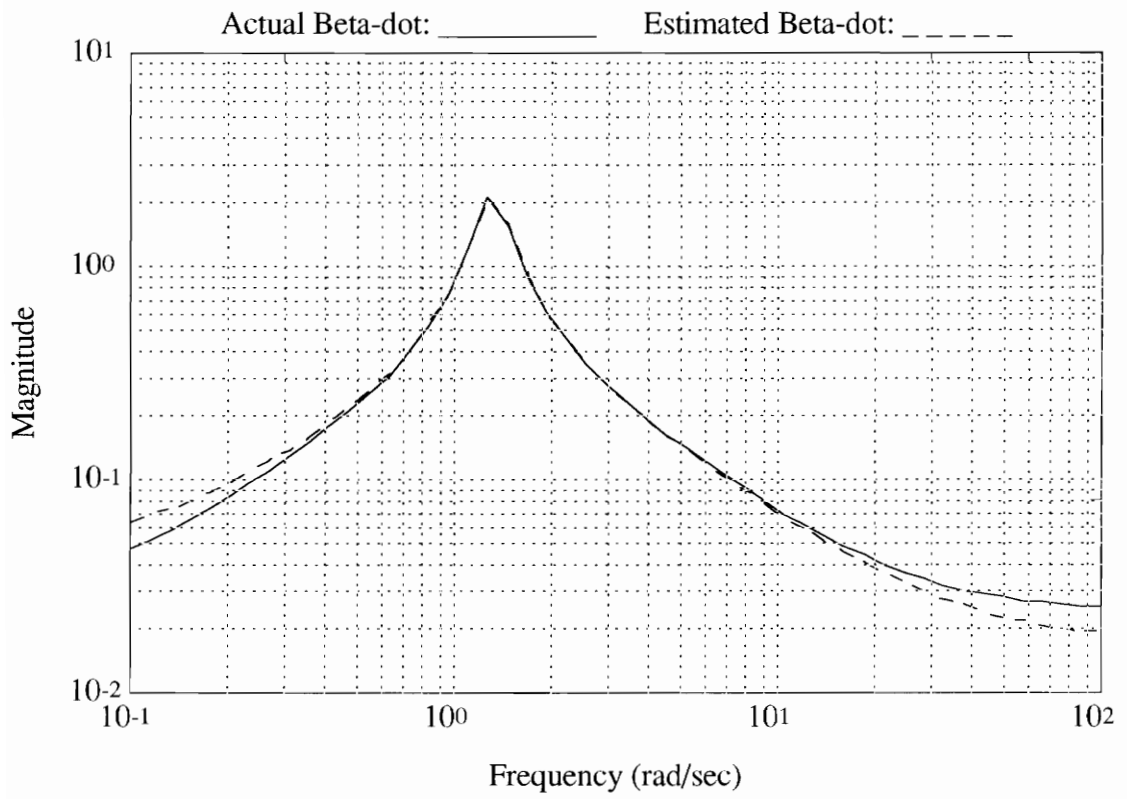


Figure 5.7 Sideslip Rate Estimator Frequency Response Validation

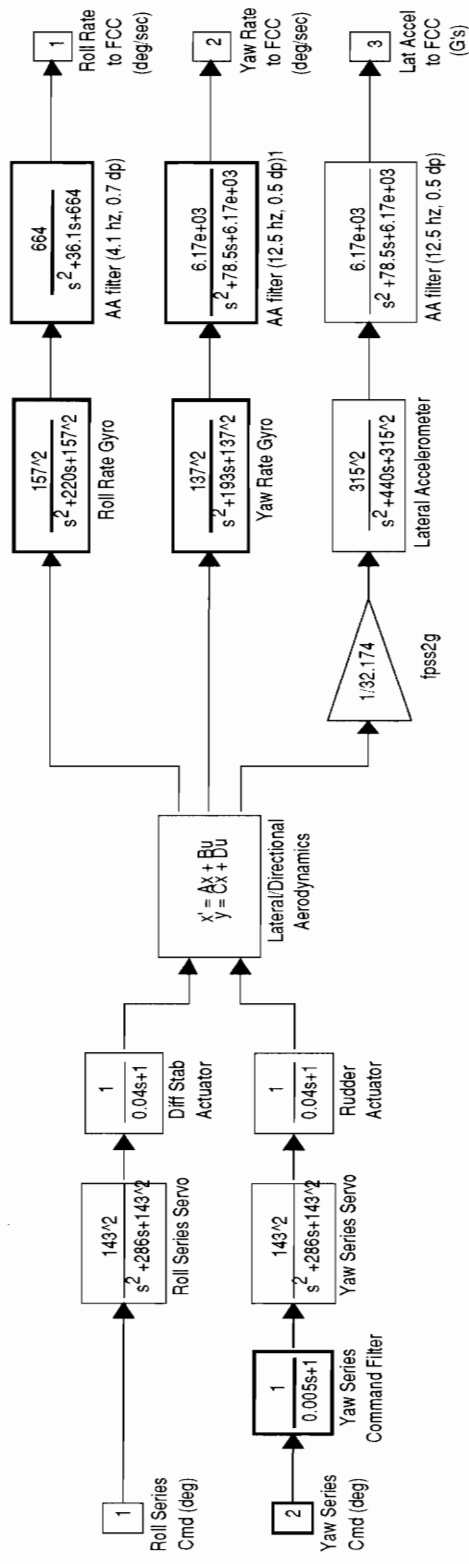


Figure 5.8

Design Plant Model

included all known high frequency dynamics, such as actuator dynamics, sensor dynamics, and anti-aliasing filter dynamics. The design plant model was discretized at a 50 hz sample rate, and a pure time delay of 0.01 seconds was added to account for the time difference between the digital flight control computer input A/D conversion and output D/A conversion. The continuous domain design plant model is shown in figure 5.8.

Tustin's method was used to implement the control law digital filters since this is what will be implemented in the flight hardware. For gain selection analyses, an open-loop model was required with the loop breaks at the feedback gain locations. Figure 5.9 shows the open-loop synthesis model used in the feedback gain selection process. The order of feedback loop closure was 1) roll rate and 2) estimated sideslip rate. This choice was based on the relative bandwidth of the two loops, as will be shown in sections 5.5.1 and 5.5.2. After the gains were designed, the time response of the system was evaluated using the closed-loop model shown in figure 5.10.

### **5.5.1 Roll Rate Feedback Gain Design**

The roll rate feedback gain root locus is shown in figure 5.11. This is a z-plane root locus, with the axis scales reduced to show only the low frequency dynamics of interest. The equivalent s-plane closed-loop poles are listed in the right hand column. The design goal of this loop was to set the gain as high as possible without risking instability. The loop gain was selected such that the open-loop roll mode couples with the differential stabilizer actuator mode and forms a complex pair with a natural frequency

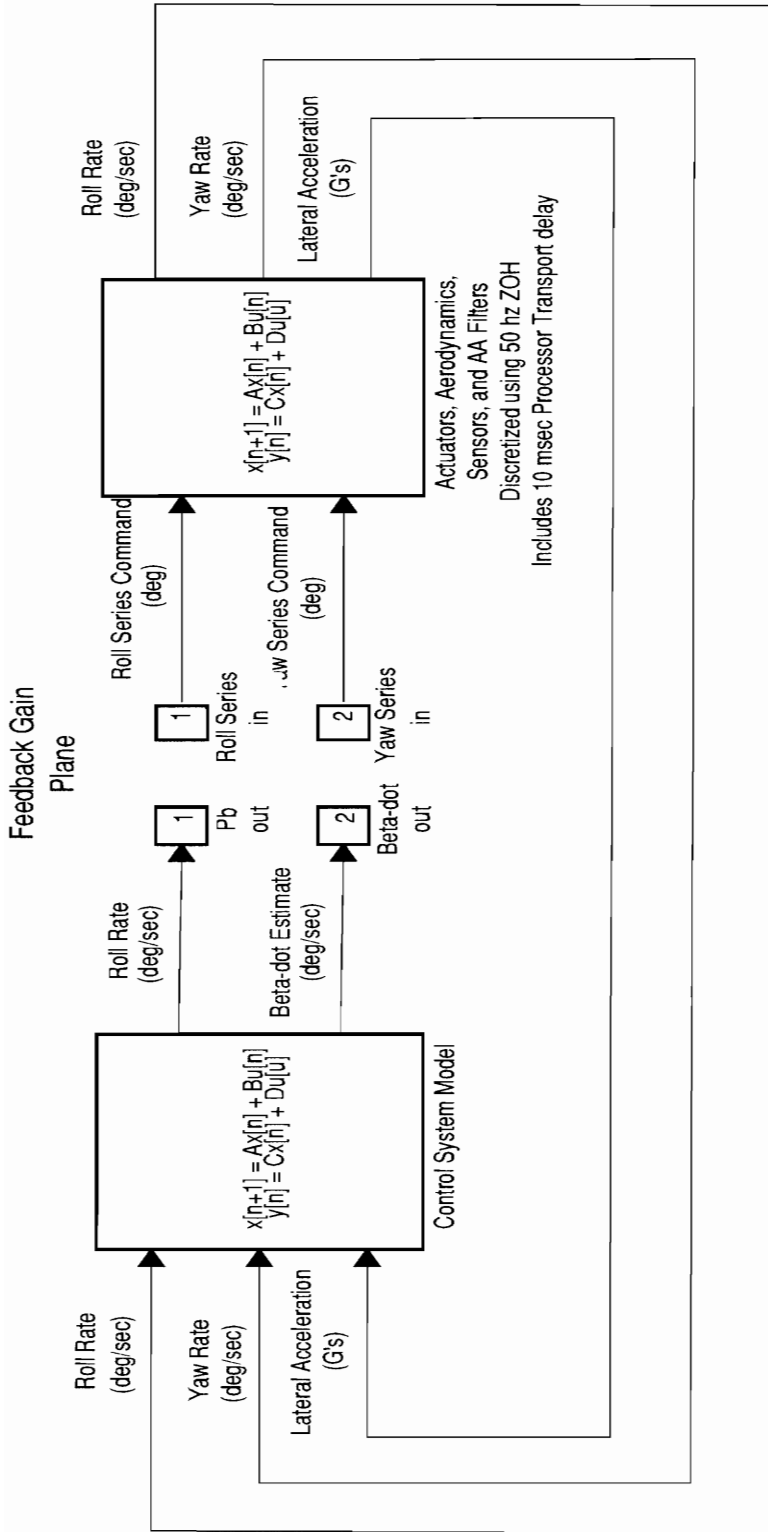


Figure 5.9 PA-ARI Open-loop Synthesis Model



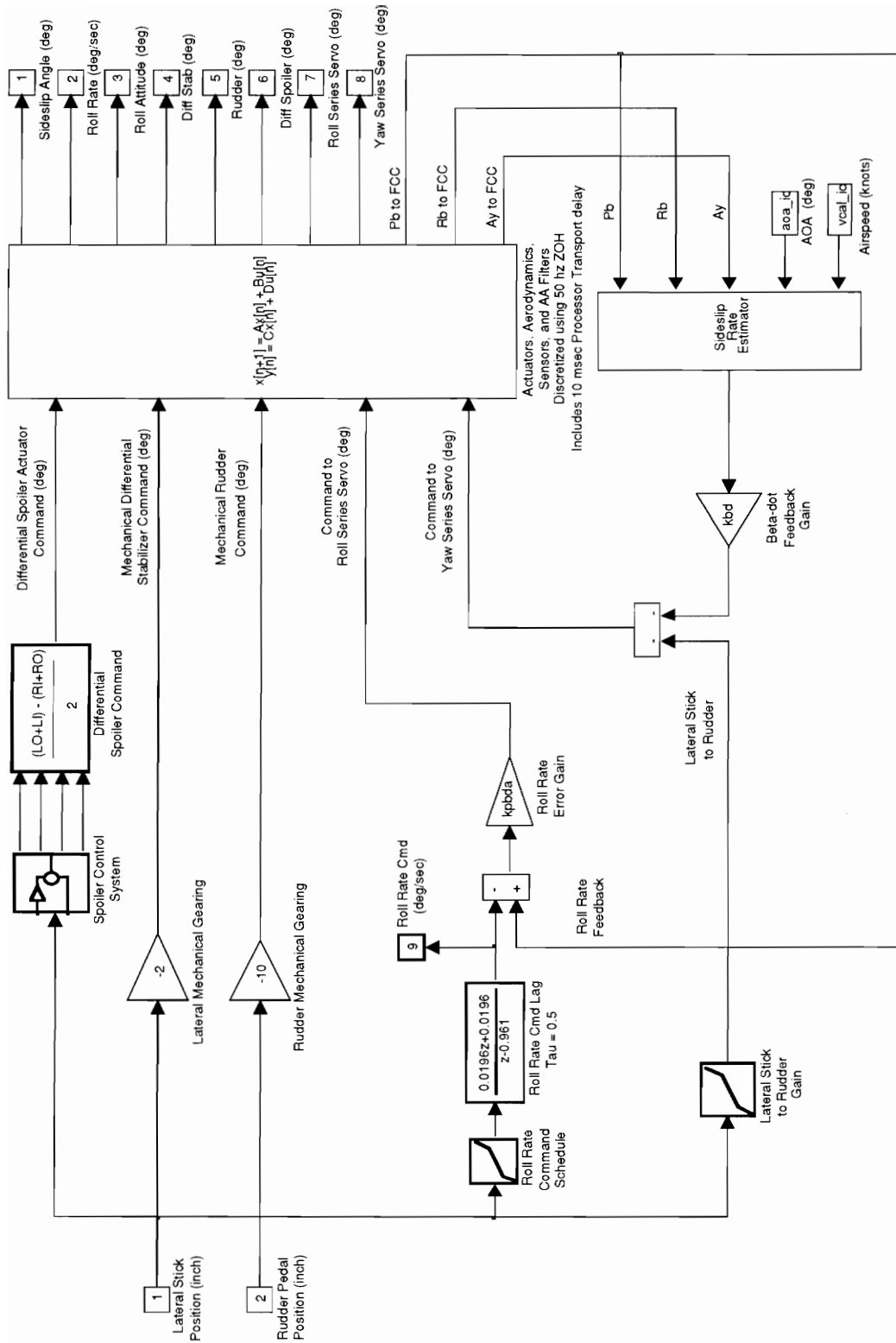


Figure 5.10 Closed-loop P.A. ARI

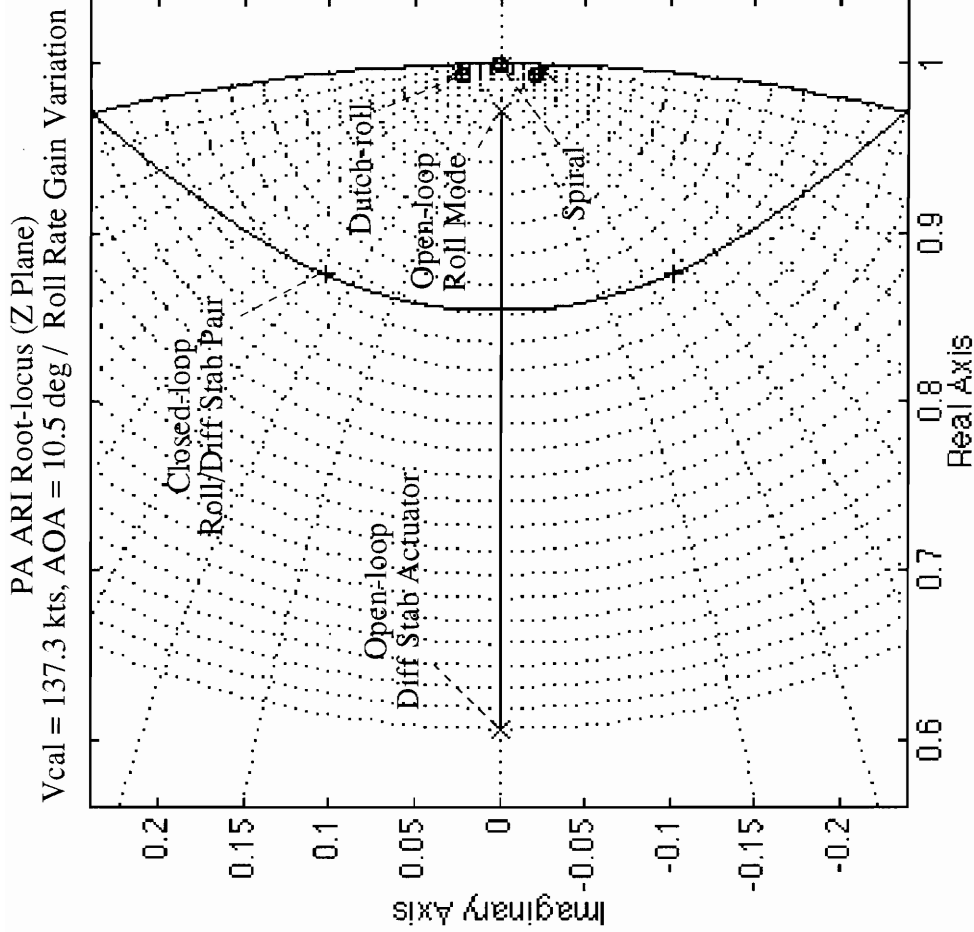


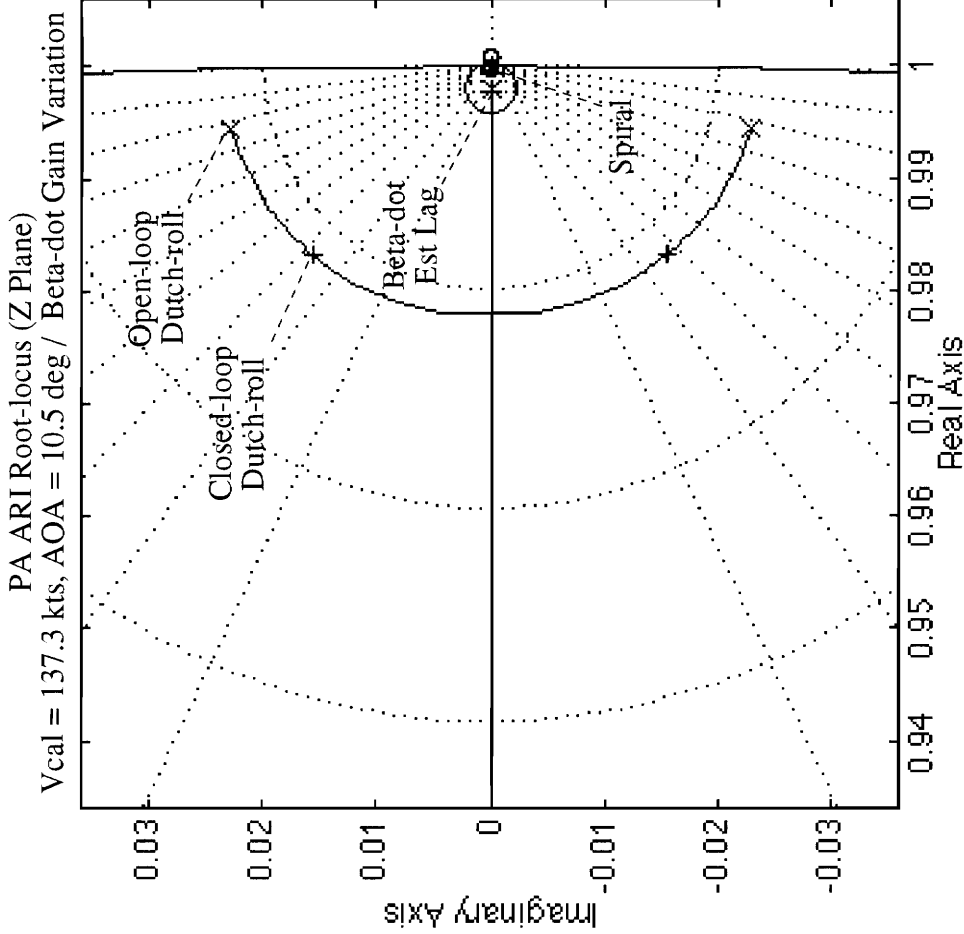
Figure 5.11 Roll Rate Feedback Root-locus

of 8.5 rad/sec and a damping ratio of 0.73. The rationale behind this unorthodox roll mode design is that the large majority of the aircraft rolling moment is produced by differential spoiler deflection. The primary function of the roll rate error path is to reduce errors between the roll rate command model and the roll rate feedback. The command model gain and lag shown in figure 5.3 were designed to match the roll response produced by the spoilers and mechanical differential stabilizer. Therefore, the roll rate error signal will be small for pilot inputs and the closed-loop response will appear to be first order. The high loop gain assures the aircraft will track the command model which will provide the pilot with good roll predictability during lateral maneuvering as well as provide good disturbance rejection characteristics.

### **5.5.2 Estimated Sideslip Rate Feedback Gain Design**

After computing the roll rate feedback loop gain, the roll rate loop in figure 5.9 was closed leaving only the estimated sideslip rate ( $\dot{\beta}$ ) feedback loop open. The goal of the  $\dot{\beta}$  feedback was to increase the damping of the Dutch-roll mode and to help minimize sideslip angle excursions resulting from lateral stick inputs and other yaw axis disturbances. A reasonable preliminary design was to set the Dutch-roll damping ratio to about 0.7, as shown by the root-locus in figure 5.12. The linear closed-loop response to lateral stick and rudder pedal inputs for this gain configuration are shown in figures 5.13 and 5.14, respectively. As expected, the responses are well behaved. Figure 5.15 shows the root-locus where the  $\dot{\beta}$  gain was increased to a level which results in a Dutch-roll damping ratio of 1.0.

The resulting closed-loop response to a lateral stick input in figure 5.16 shows that sideslip angle excursions were reduced for the higher gain case. The increased damping also results in a more sluggish sideslip response to pedal inputs, as shown by figure 5.17. Experiments with the beta-dot feedback gain in piloted simulation studies revealed that flying qualities for lateral axis maneuvering tasks were enhanced by increasing the gain, the upper limit being determined by high frequency robustness and noise attenuation considerations. As the loop gain was increased, the Dutch-roll mode became two real roots, as shown by figure 5.18. The sideslip response to a lateral stick half-doublet was fast and essentially deadbeat for this case, as shown in figure 5.19. The unfortunate side effect of this configuration was made apparent when rudder pedal inputs were considered, as shown in figure 5.20. The sideslip response to rudder pedal inputs was dominated by the slower Dutch-roll root and became extremely sluggish. The best compromise between sideslip suppression for lateral stick inputs and directional axis responsiveness was determined to be the configuration with the Dutch-roll damping ratio equal to 1.



Loop Gain:	1.494	
Freq ( $\tau/s$ )	Damping	
0.00	-1.00	Spiral
0.11	1.00	Beta-dot Est Lag
1.18	0.71	Dutch-roll
1.18	0.71	
8.50	0.72	Roll/Diff Stab
8.50	0.72	
20.36	1.00	Rudder Actuator
78.71	0.49	High Frequency Dynamics
78.71	0.49	
104.60	0.79	
104.60	0.79	
x		Open-loop poles
o		Open-loop zeros
+		Closed-loop poles

Figure 5.12 Beta-dot Feedback Root-locus ( $\zeta_{dr}=0.7$ )

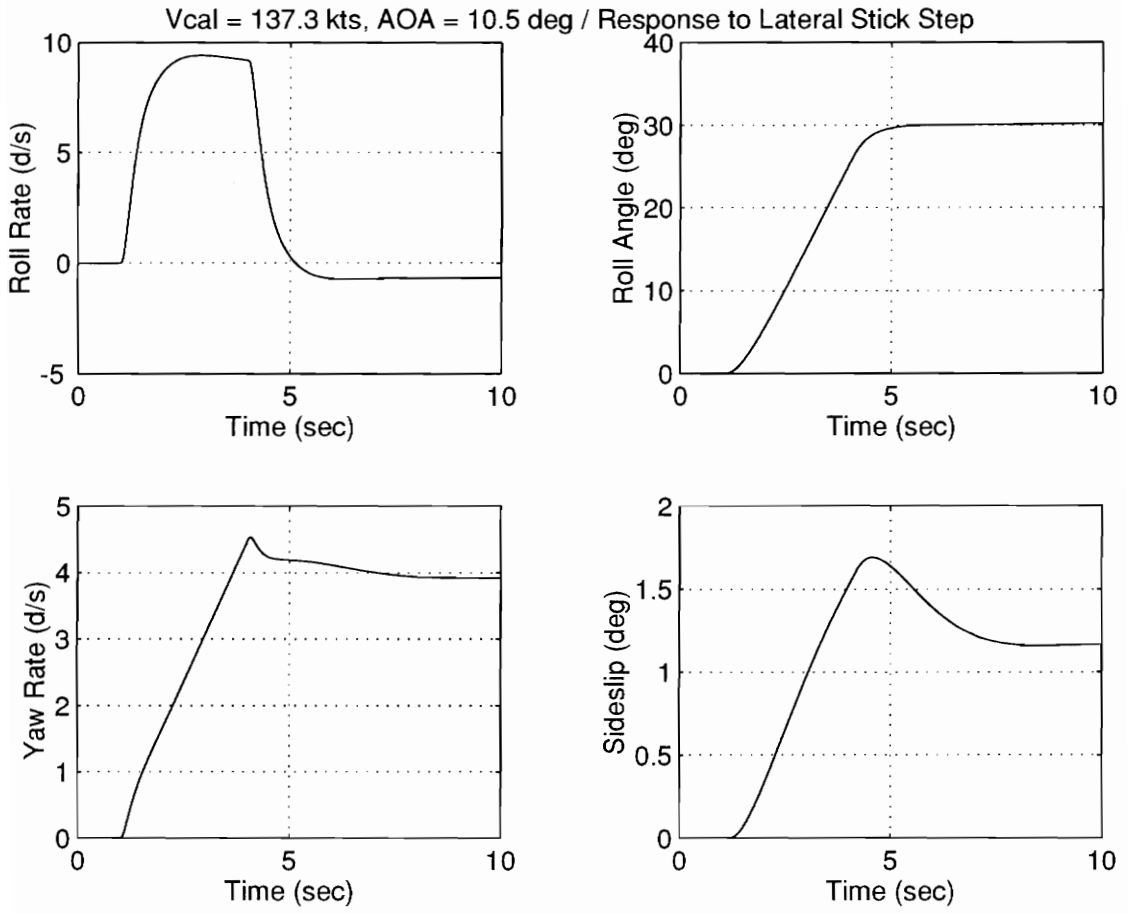


Figure 5.13 PA ARI Response to Lateral Stick ( $\zeta_{dr} = 0.7$ )

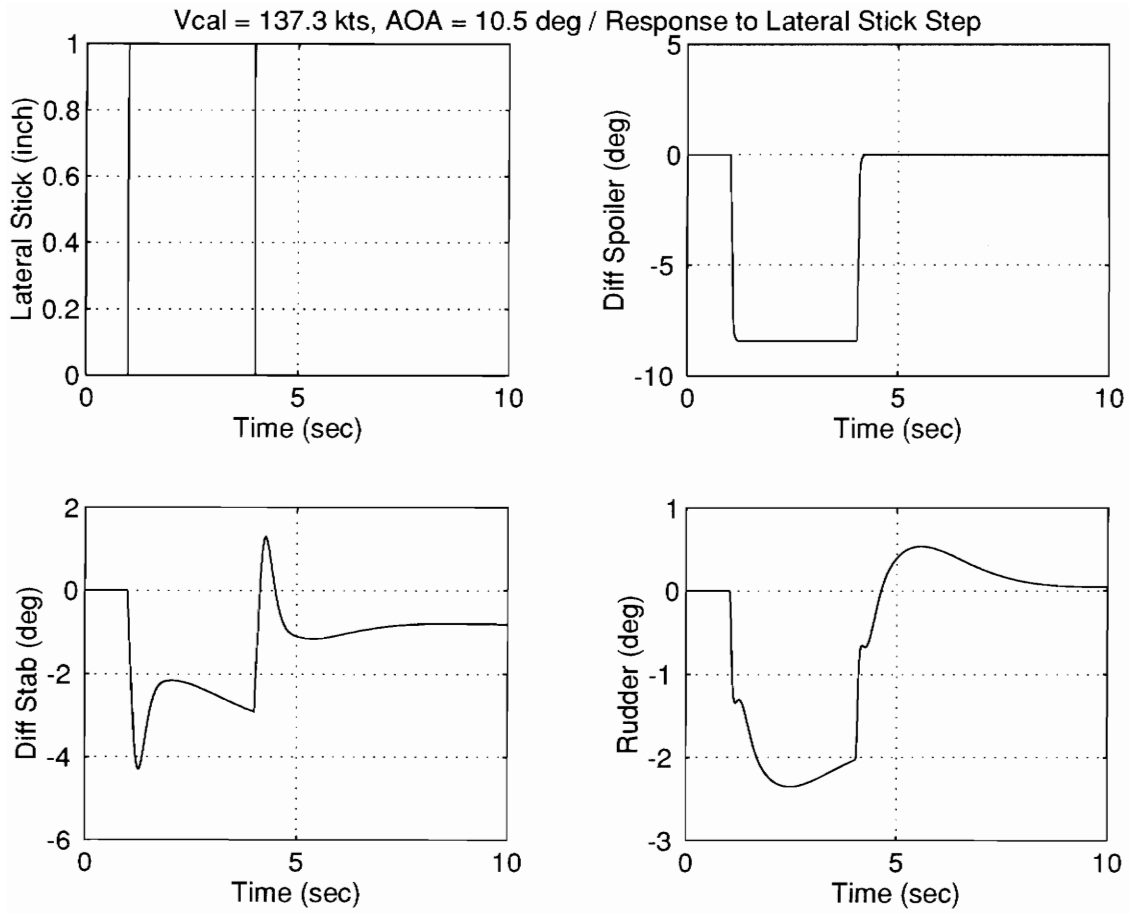


Figure 5.13 (Continued) PA ARI Response to Lateral Stick ( $\zeta_{dr} = 0.7$ )

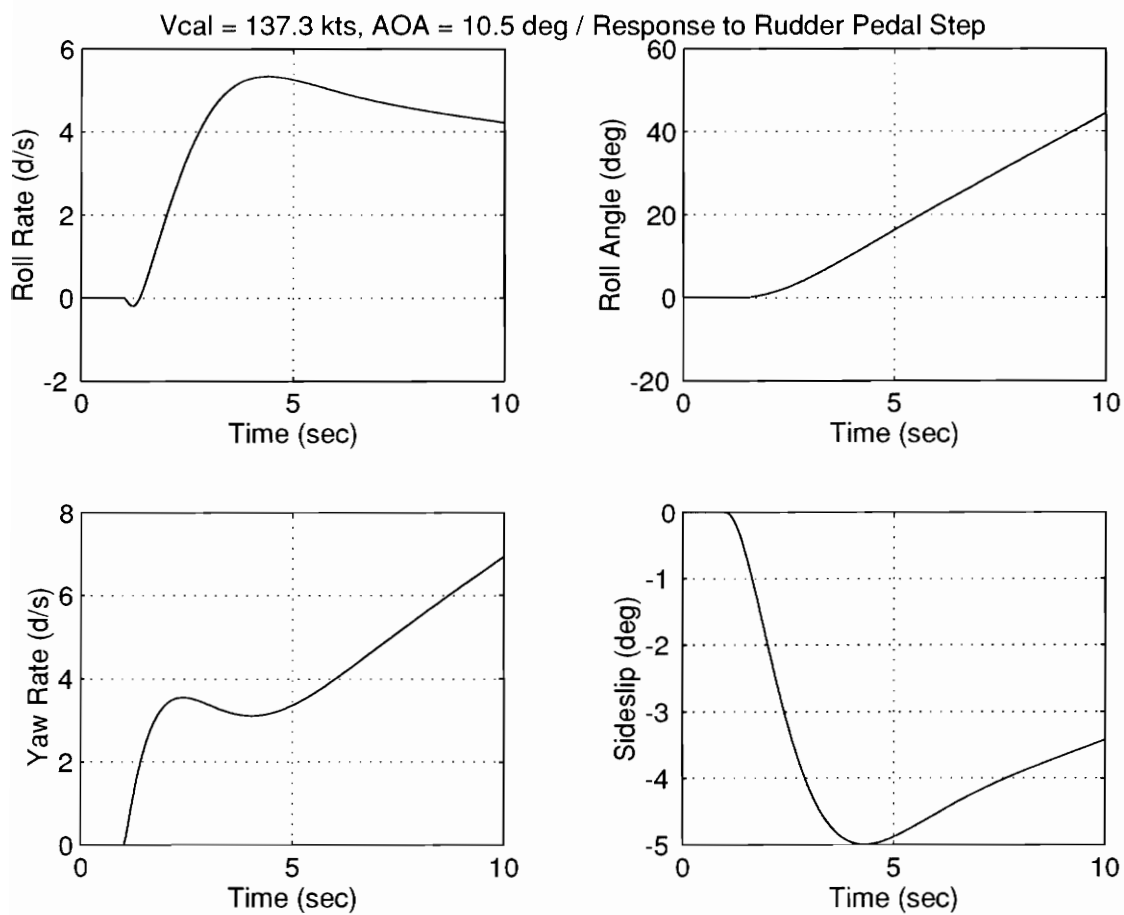


Figure 5.14 PA ARI Response to Rudder Pedal ( $\zeta_{dr} = 0.7$ )



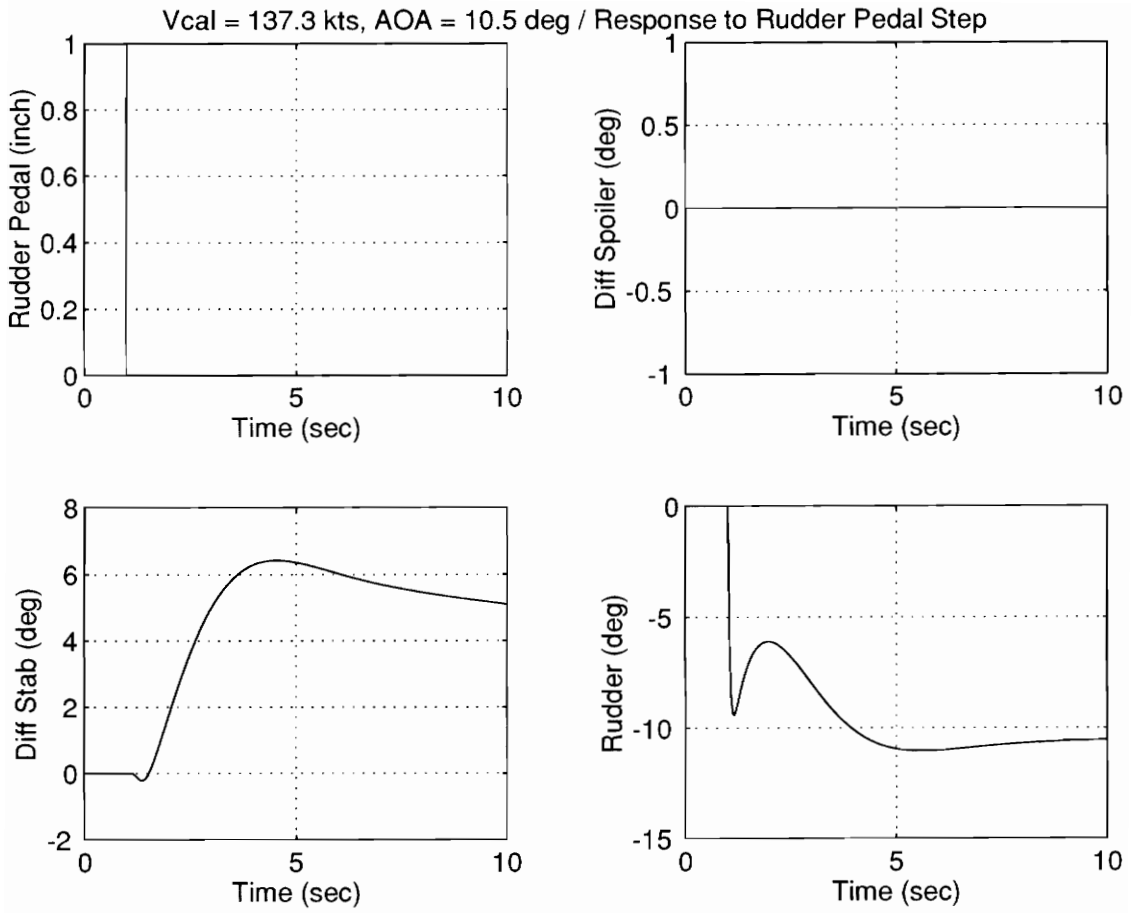


Figure 5.14 (Continued) PA ARI Response to Rudder Pedal ( $\zeta_{dr} = 0.7$ )

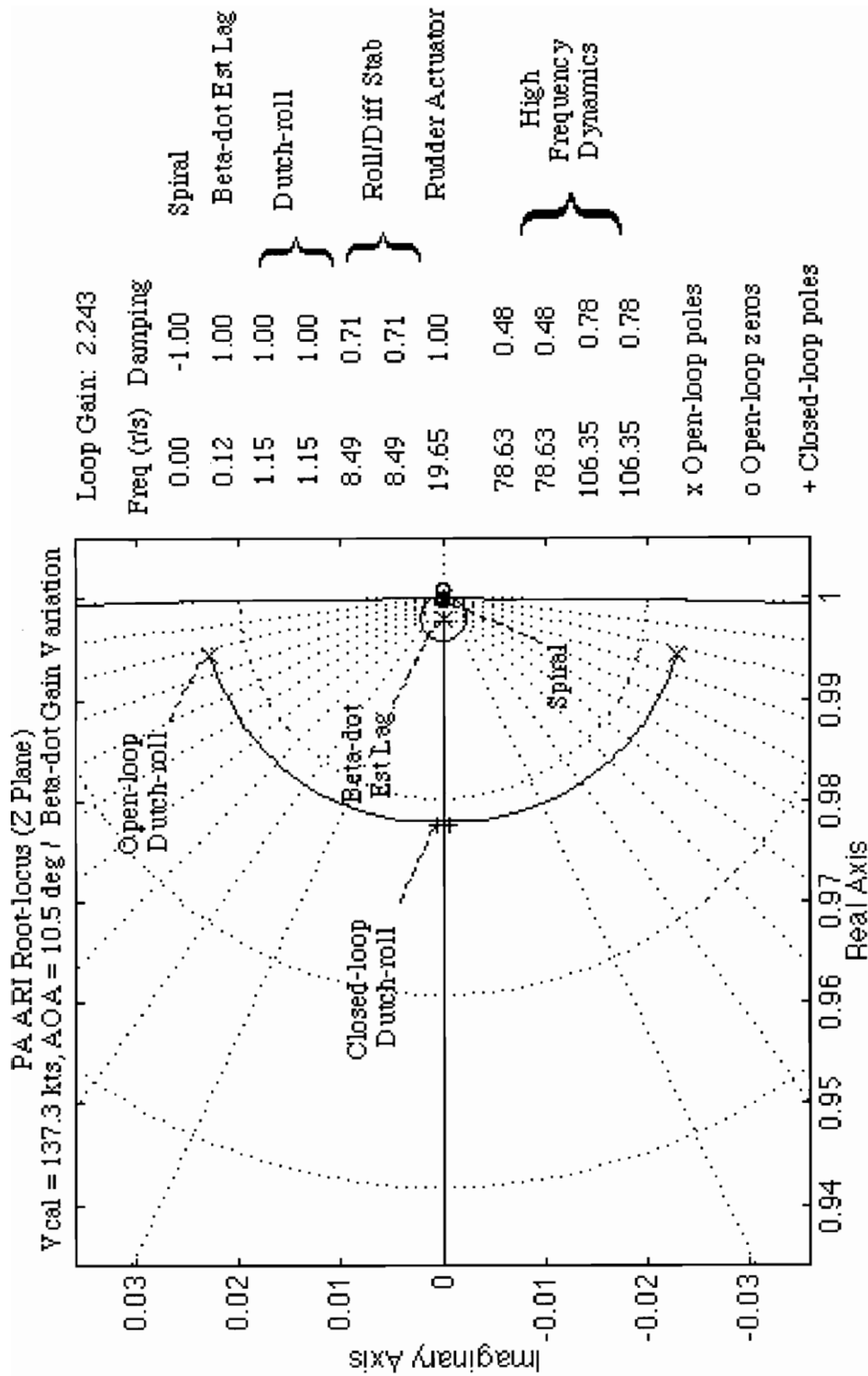


Figure 5.15 Beta-dot Feedback Root-locus ( $\zeta_{dr}=1.0$ )

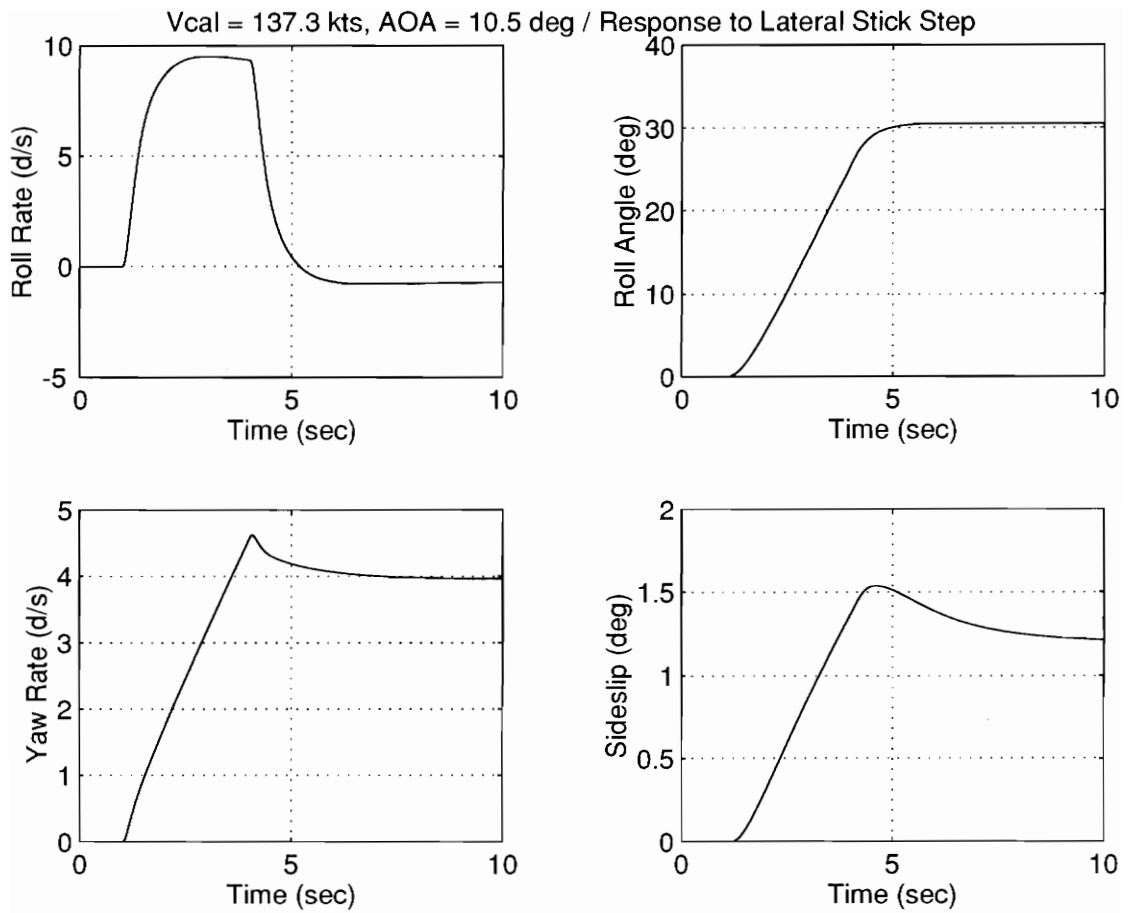


Figure 5.16 PA ARI Response to Lateral Stick ( $\zeta_{dr} = 1$ )

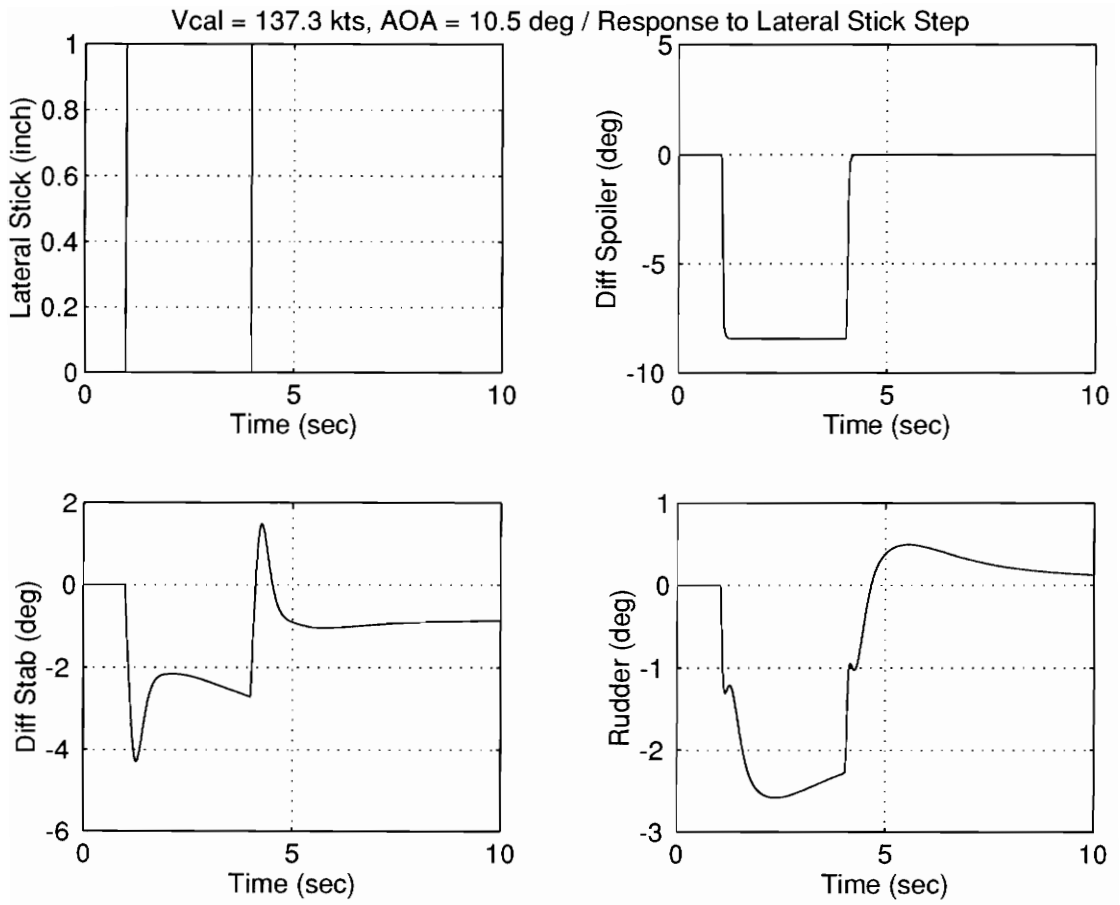


Figure 5.16 (Continued) PA ARI Response to Lateral Stick ( $\zeta_{dr} = 1$ )

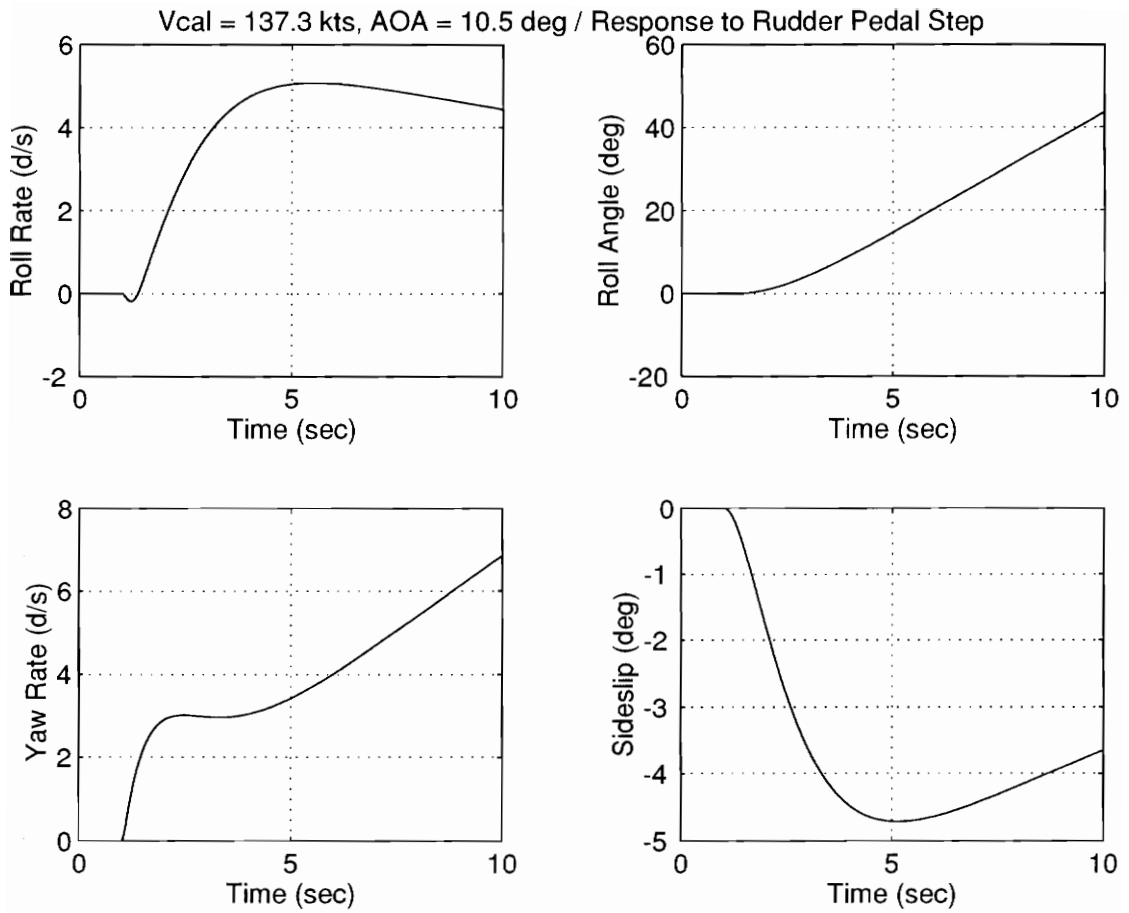


Figure 5.17 PA ARI Response to Rudder Pedal ( $\zeta_{dr} = 1$ )

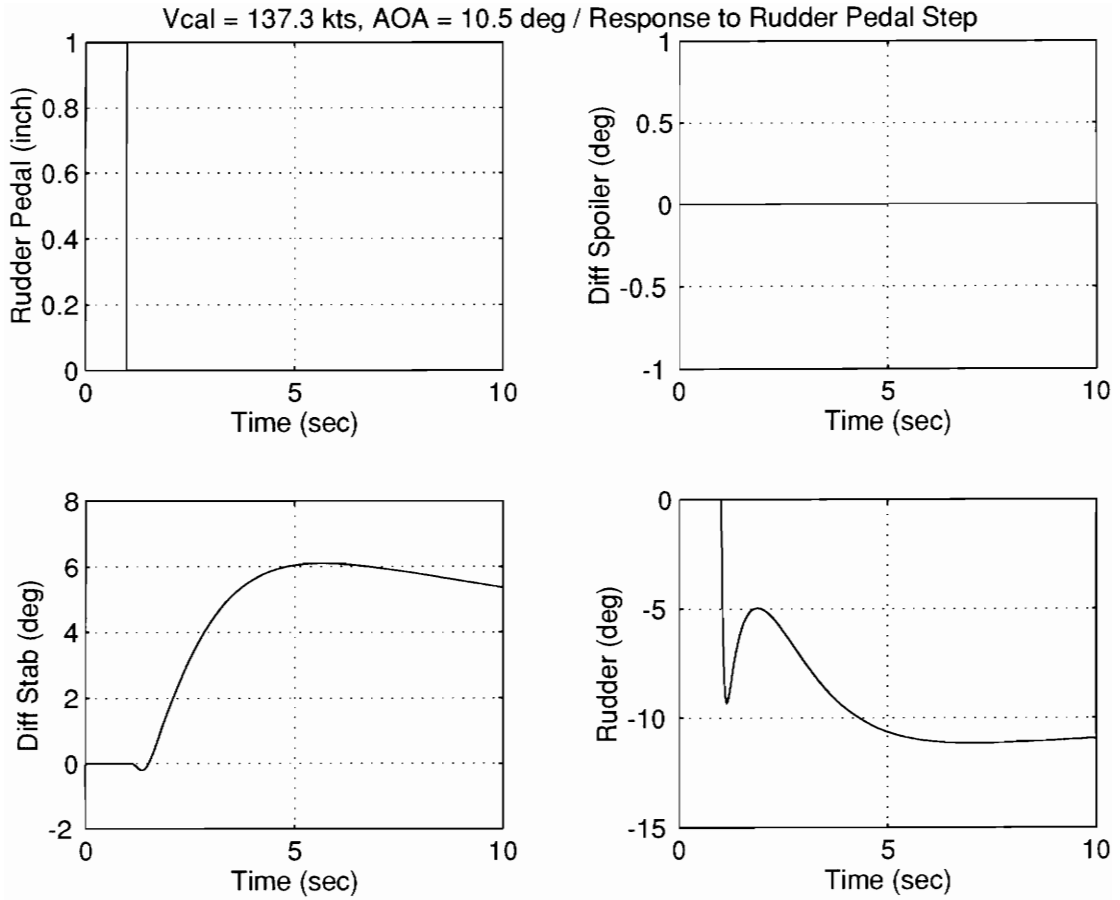
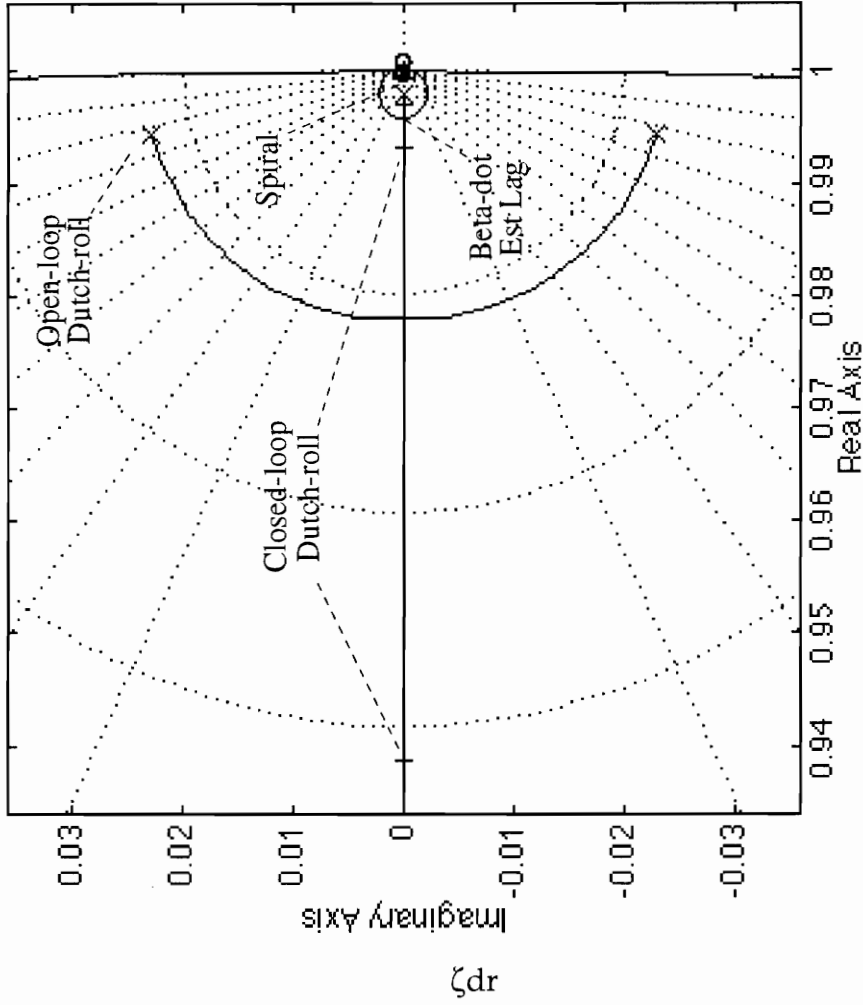


Figure 5.17 (Continued) PA ARI Response to Rudder Pedal ( $\zeta_{dr} = 1$ )

PA ARI Root-locus (Z Plane)  
 Vcal = 137.3 kts, AOA = 10.5 deg / Beta-dot Gain Variation



Loop Gain: 3.784

Freq (r/s)	Damping	
0.00	-1.00	Spiral
0.15	1.00	Beta-dot Est Lag
0.33	1.00	} Dutch-roll
3.34	1.00	
8.56	0.68	} Roll/Diff Stab
8.56	0.68	
18.33	1.00	Rudder Actuator
78.54	0.47	} High Frequency Dynamics
78.54	0.47	
109.39	0.77	
109.39	0.77	

x Open-loop poles

o Open-loop zeros

+ Closed-loop poles

Figure 5.18 Beta-dot Feedback Root-locus ( $\zeta_{dr} > 1$ )

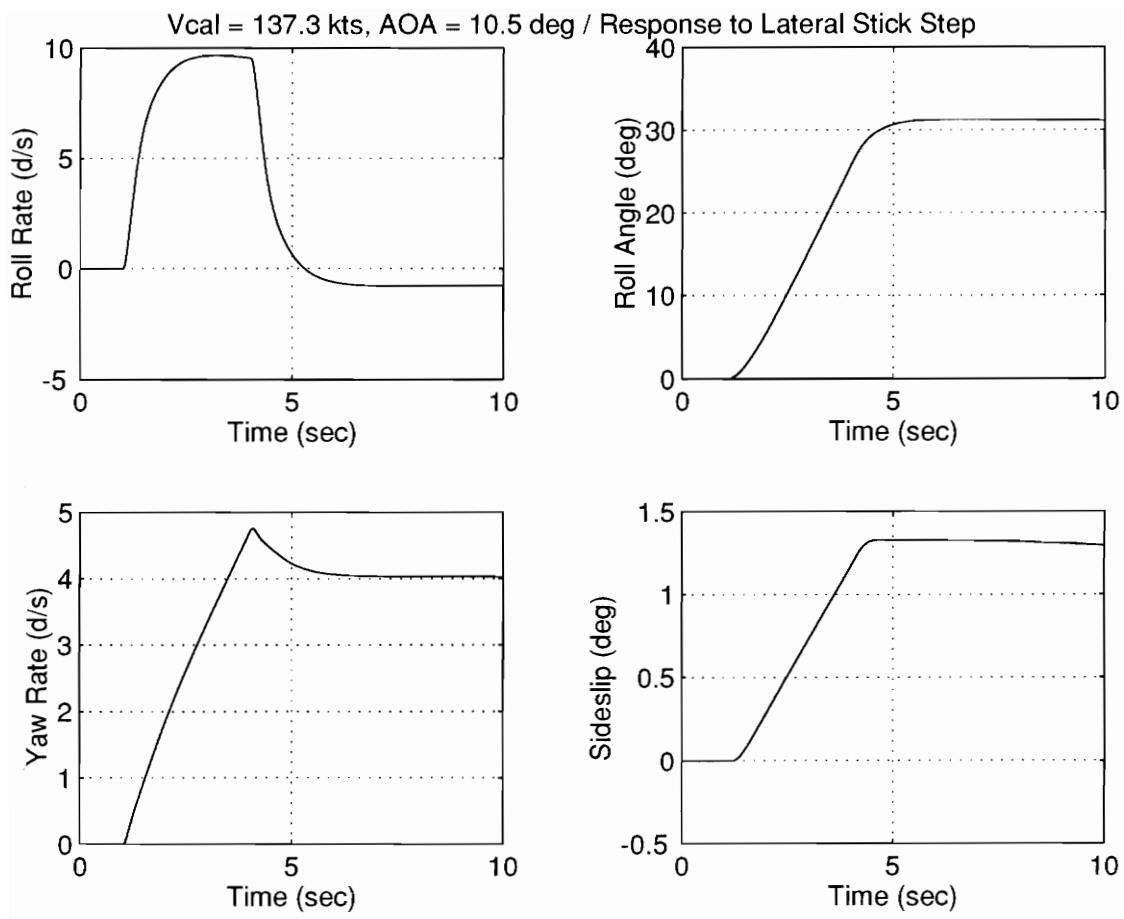


Figure 5.19 PA ARI Response to Lateral Stick ( $\zeta_{dr} > 1$ )



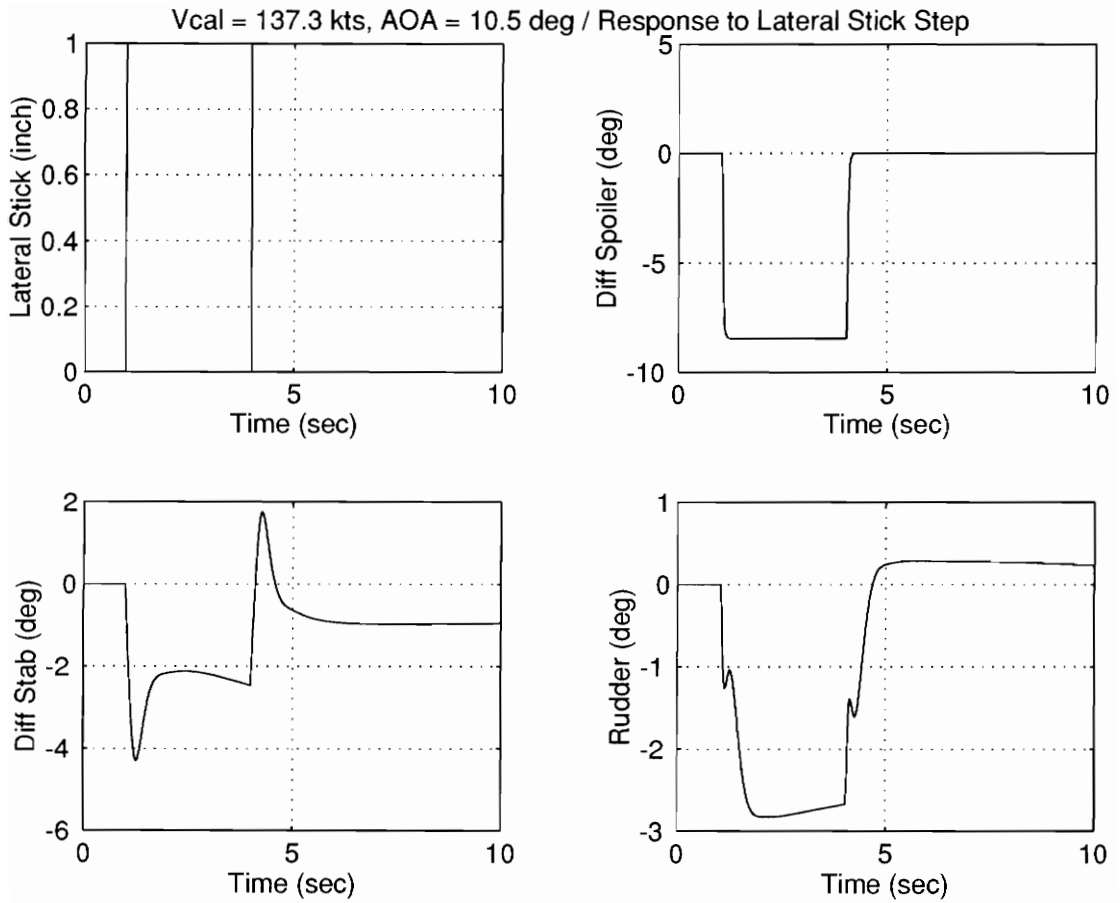


Figure 5.19 (Continued) PA ARI Response to Lateral Stick ( $\zeta_{dr} > 1$ )

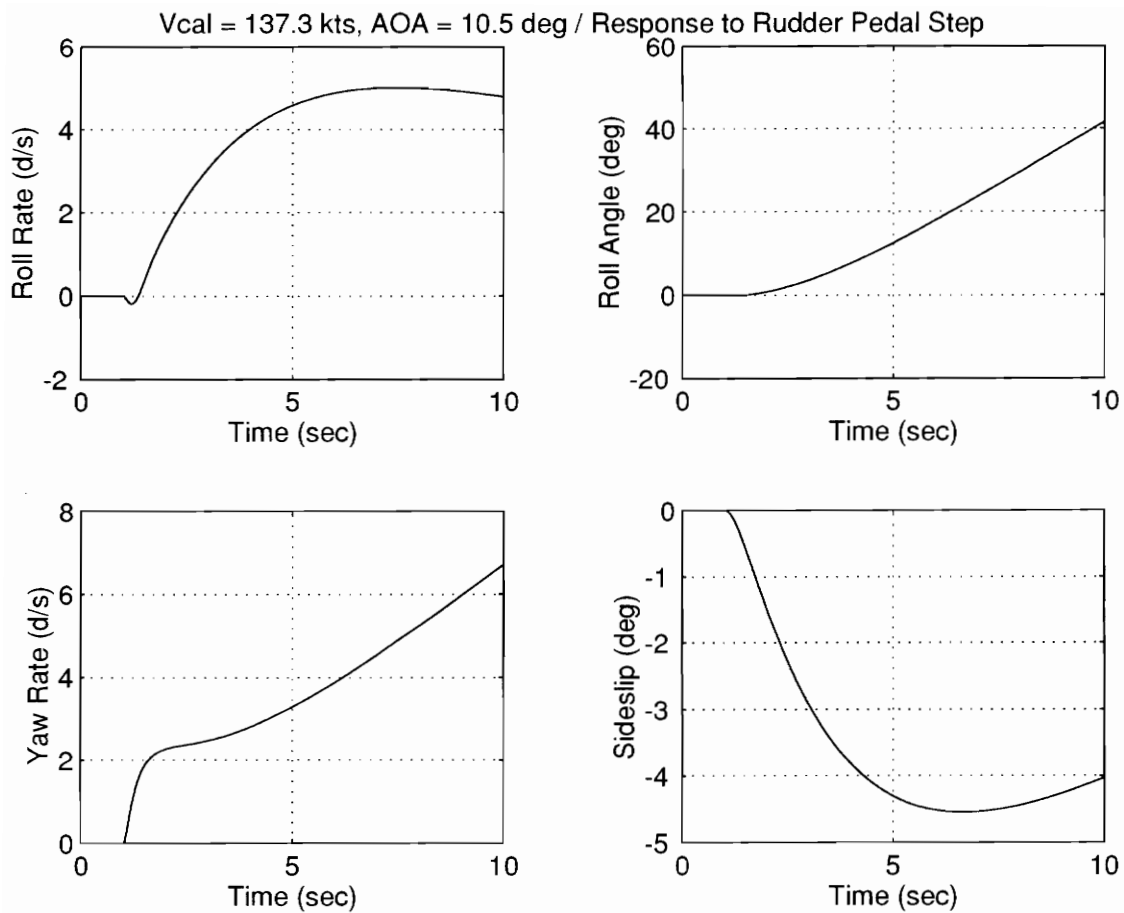


Figure 5.20 PA ARI Response to Rudder Pedal ( $\zeta_{dr} > 1$ )

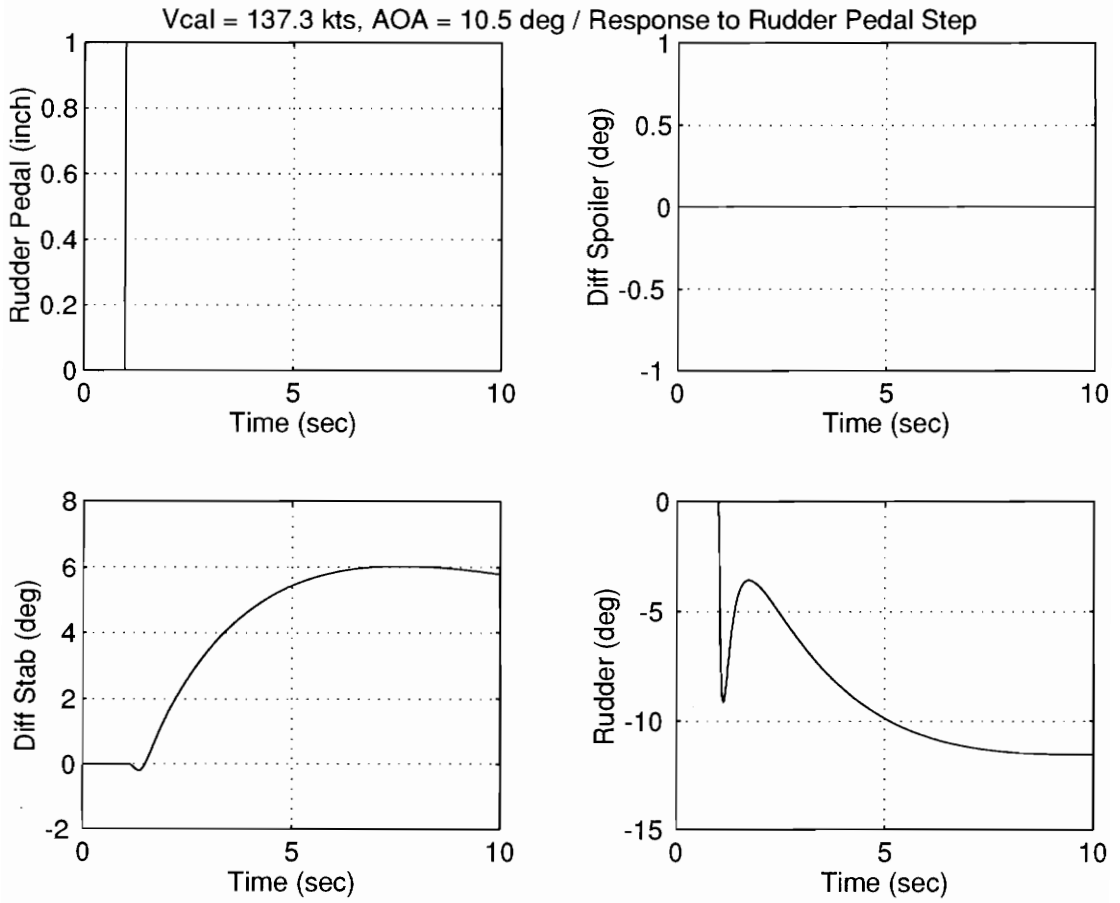


Figure 5.20 (Continued) PA ARI Response to Rudder Pedal ( $\zeta_{dr} > 1$ )

## 5.6 Feedforward Path Designs

The forward paths of the PA ARI control system consist of the lateral stick to spoiler gearing, the lateral stick to rudder interconnect (LSRI), and the roll rate command model. These functions were designed primarily by trial and error using the nonlinear FORTRAN simulation.

### 5.6.1 Lateral Stick to Spoiler Gearing

In powered approach configuration, the spoilers provide a much larger percentage of rolling moment than does the differential stabilizer. Roll control predictability is therefore highly dependent on the characteristics of the lateral stick to spoiler gearing. As detailed in section 5.2, the lateral stick to spoiler gearing used in the AFCS resulted in a highly nonlinear roll rate response vs lateral stick deflection. To improve the predictability of the roll rate response, the spoiler gearing was modified as shown in figure 5.21. The redesigned spoiler gearing eliminates the 0.5 inch deadband in the original design, and reduces the magnitude of the slope increases at each breakpoint. This results in a more responsive aircraft for small lateral stick inputs, and provides a more linear lateral stick to roll rate response relationship. Figure 5.22 shows the time histories of the roll rate response for various lateral stick step input amplitudes as well as the maximum roll rate response versus lateral stick input amplitude. The PA ARI demonstrates a far more linear lateral stick to roll rate relationship than was achieved by the AFCS. The response for small stick inputs (less than 0.5 inches) is somewhat lower than for medium to large amplitude inputs. The reduced sensitivity for small inputs results in enhanced precision tracking characteristics, as reported in reference [5.1].

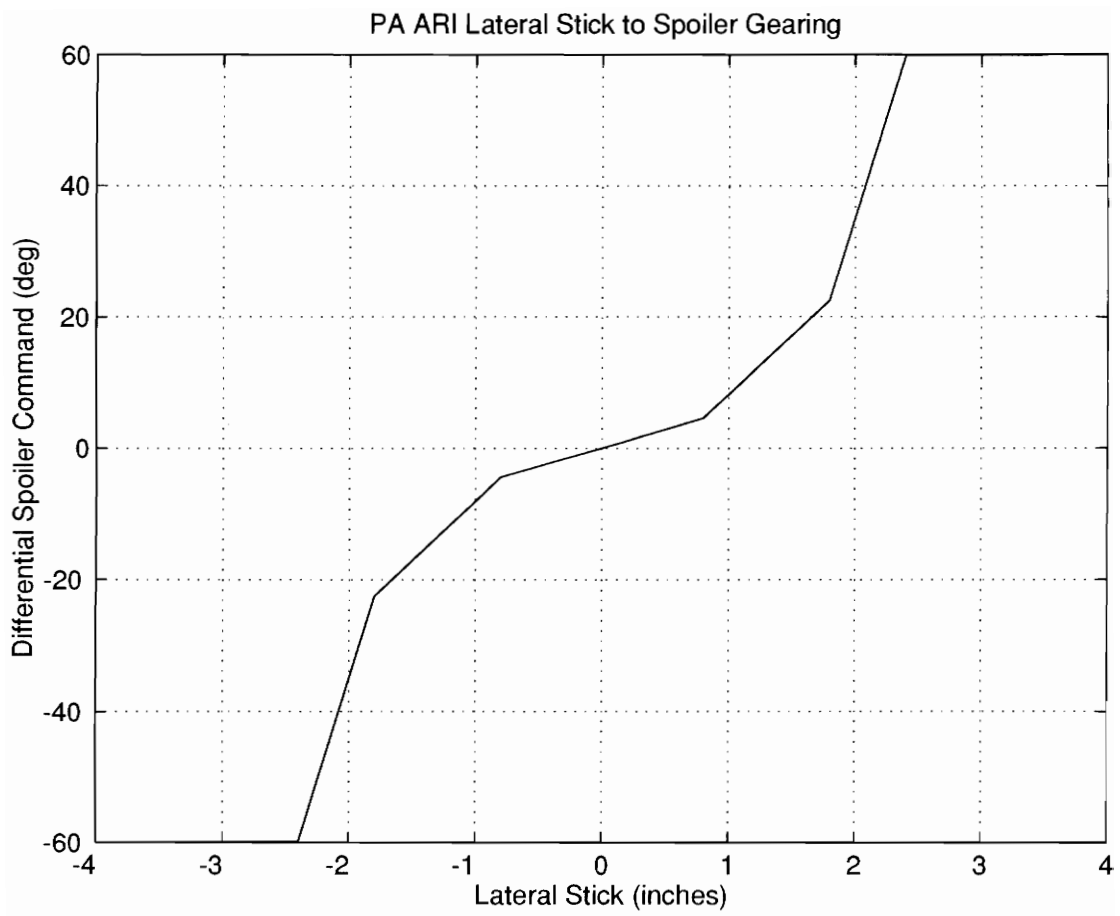


Figure 5.21 PA ARI Lateral Stick to Spoiler Gearing

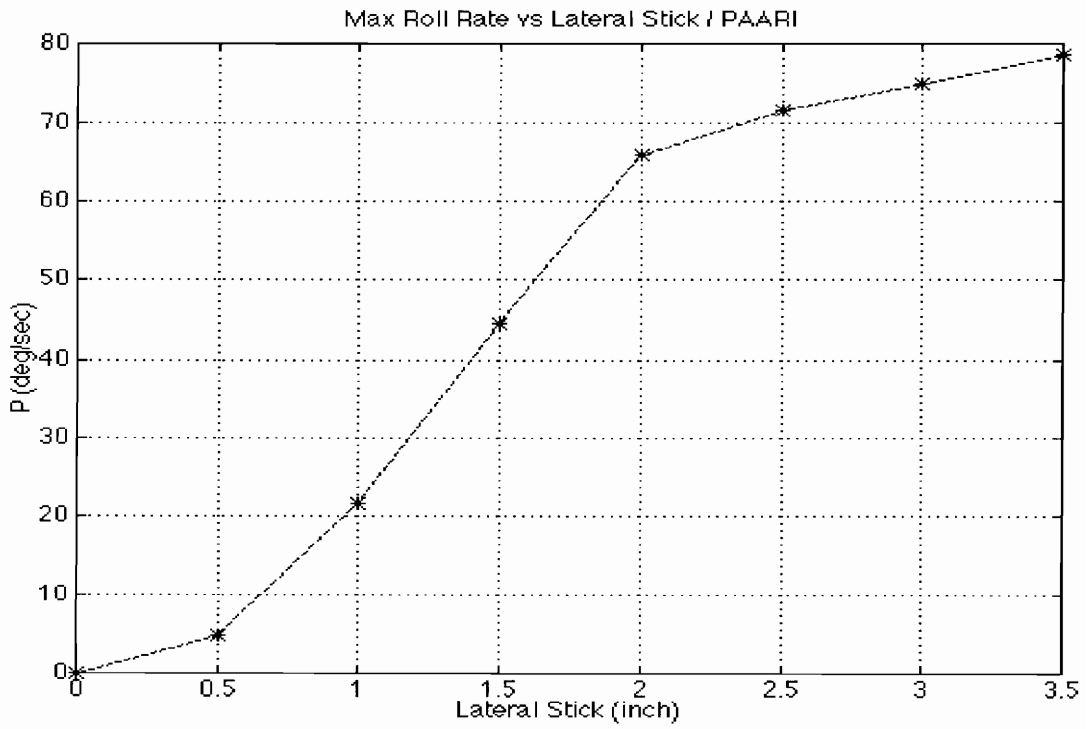
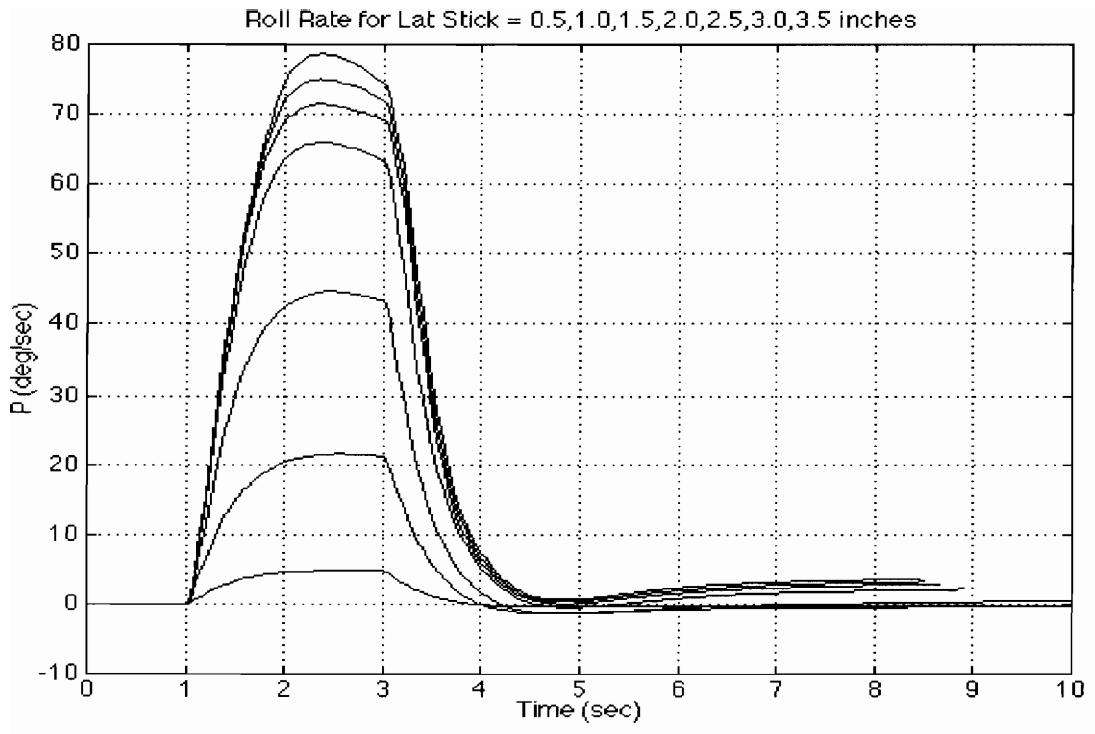


Figure 5.22 Roll Rate Response vs Lateral Stick

## 5.6.2 Lateral Stick to Rudder

A prime design goal of the PA ARI was to reduce the transient adverse sideslip response induced by lateral stick inputs. A proven technique for achieving this goal is to incorporate a lateral stick to rudder interconnect (LSRI). By automatically commanding rudder deflection while performing a roll maneuver, the aircraft can be made to roll about the velocity vector with little sideslip angle, as opposed to rolling about the body x-axis, which induces adverse sideslip through kinematic coupling. NASA incorporated an LSRI into their proposed F-14 PA control law [1.4, 1.5]. Since that system was only a modified version of an existing analog system, the LSRI was limited to a constant gain. The result was an aircraft that was reasonably coordinated for large inputs, but too proverse (over coordinated) for small inputs. Proverse yaw in response to lateral stick inputs can lead to pilot induced oscillations (PIO) and should be avoided. A nonlinear two-slope architecture with an angle-of-attack fadeout was therefore incorporated into the PA ARI, and refined through extensive piloted simulation testing. The final configuration selected for the LSRI is shown in figure 5.23, as well as the rudder response for various amplitude lateral stick steps. Since the authority of each yaw series actuators is only  $\pm 9.5$  degrees, saturation occurred for lateral stick inputs in excess of 1.58 inches. Due to the enhanced roll rate response of the PA ARI which required relatively small lateral stick inputs for typical PA tasks, saturation of the LSRI was not a major concern. The sideslip response for various amplitude lateral stick steps and the maximum sideslip response versus maximum roll rate is shown in figure 5.24. The data shows

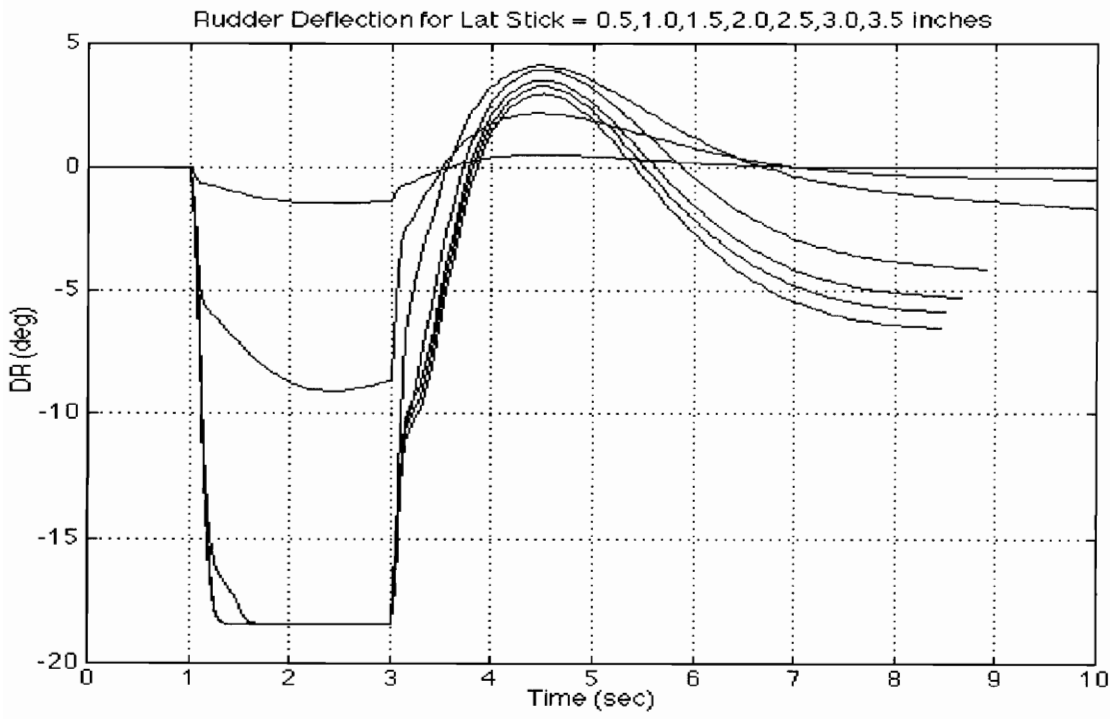
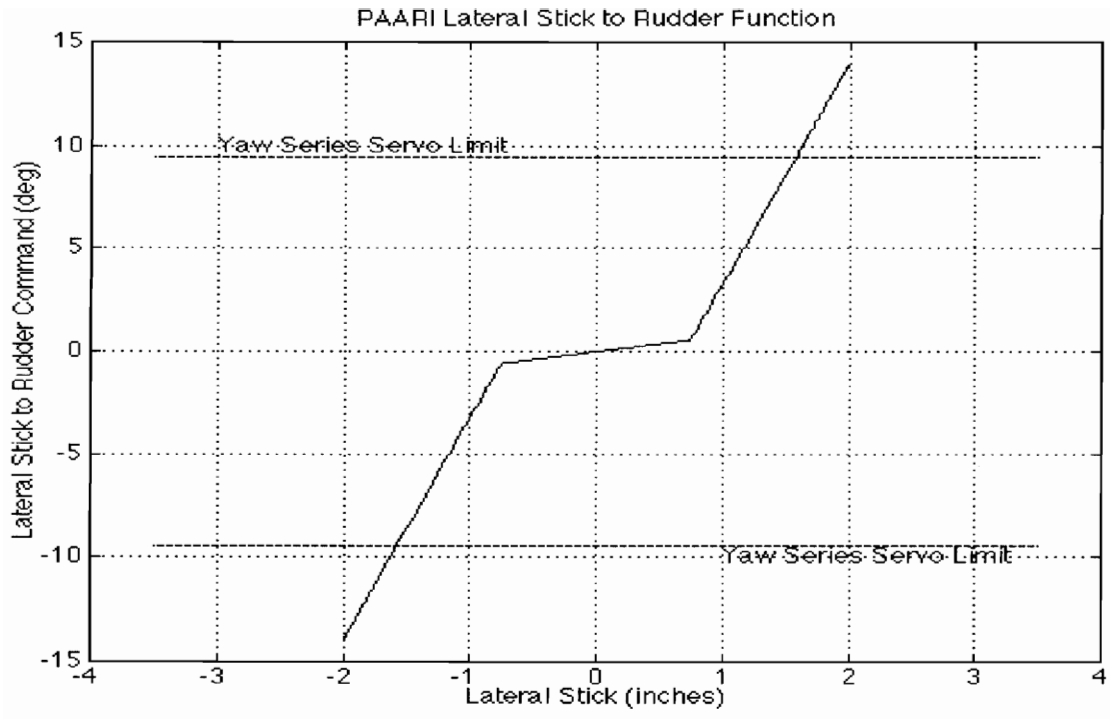


Figure 5.23 LSRI Rudder Command vs Lateral Stick



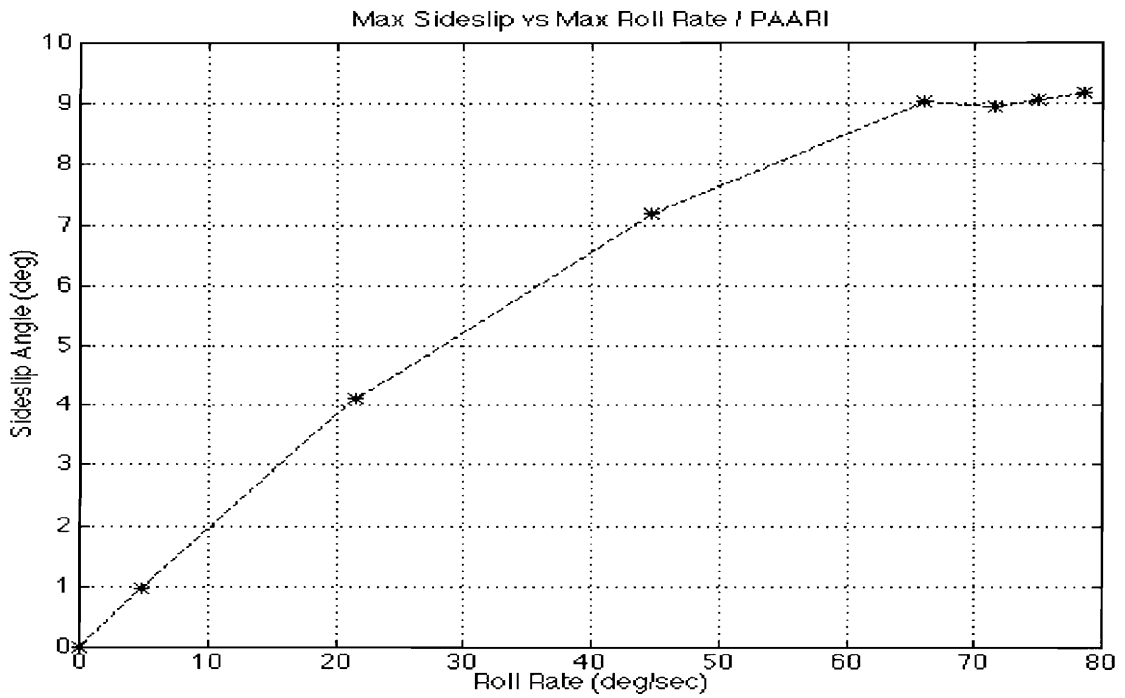
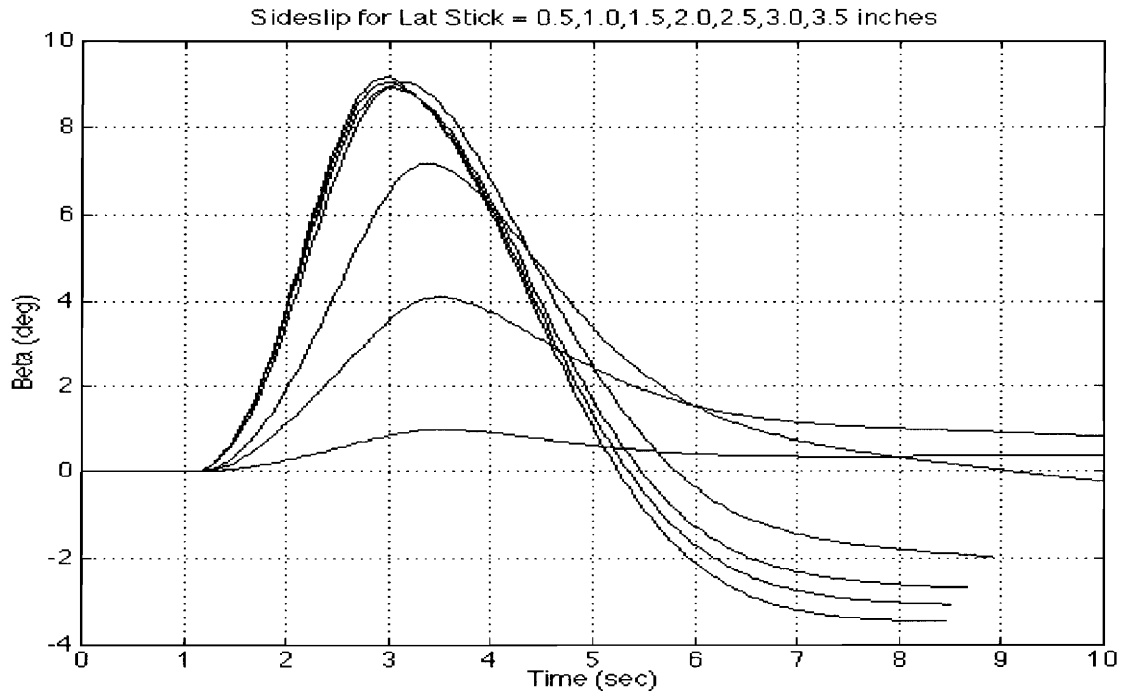


Figure 5.24 Sideslip Responses to Lateral Stick and Max Sideslip vs Max Roll Rate

the sideslip per unit roll rate was only 0.18 deg/(deg/sec), as opposed to 0.35 deg/(deg/sec) for the AFCS.

### 5.6.3 Roll Rate Command Model

The last component of the system to be designed was the roll rate command model in the Roll PA ARI, figure 5.3. This is the final design task of the iterative design process because minor refinements in it have the least impact on the closed-loop response characteristics. The basic roll rate response characteristics were determined primarily by the lateral stick to spoiler gearing, and to a lesser degree by the LSRI. The goal of the roll rate command design was to approximately match the “open-loop” roll response with a first order lag and nonlinear function table. The command model was designed by running the nonlinear FORTRAN model with lateral stick steps of various amplitudes, and matching the gain and time constant of the command model to the aircraft roll rate response. This results in small roll rate response errors for lateral stick inputs, which translates into reduced roll series servo actuator activity. The command model gain and time constant were optimized exclusively for the nominal design flight condition shown in Table 2.1. Figure 5.25 shows the roll rate command model gain schedule, while figure 5.26 shows the commanded versus actual roll rate and the roll series servo actuator response to a 0.5 inch lateral stick step.

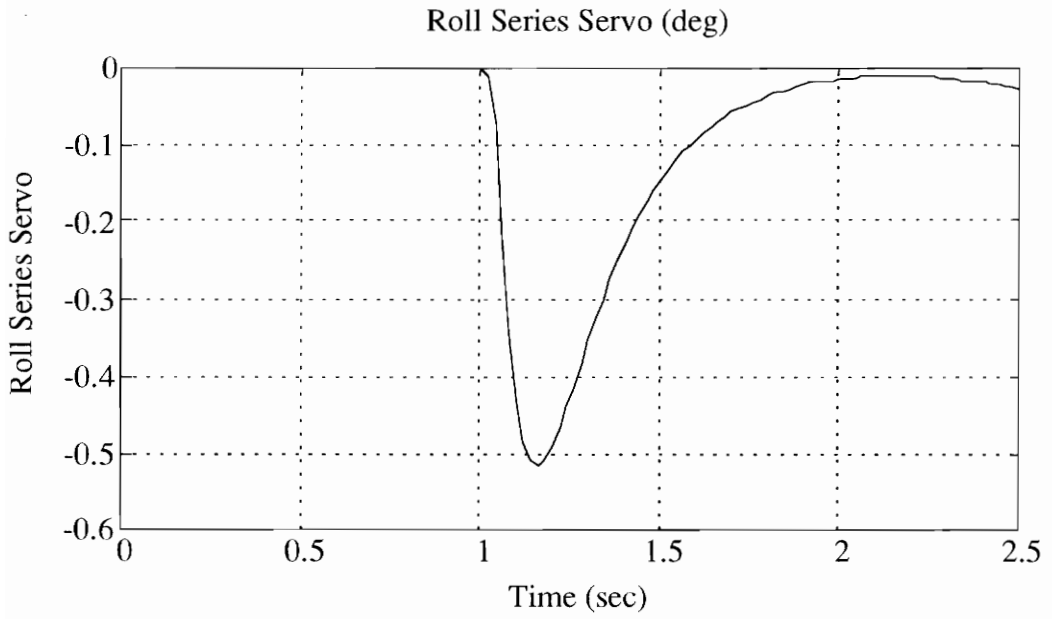
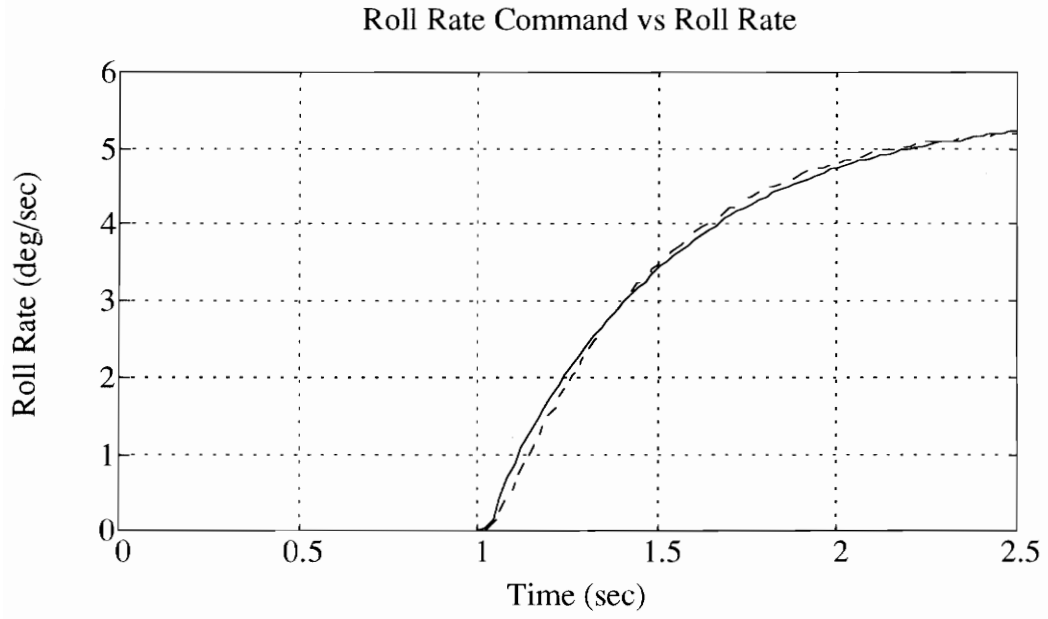


Figure 5.25 Roll Rate, Roll Rate Command, and Roll Series Servo Response to Lateral Stick Step

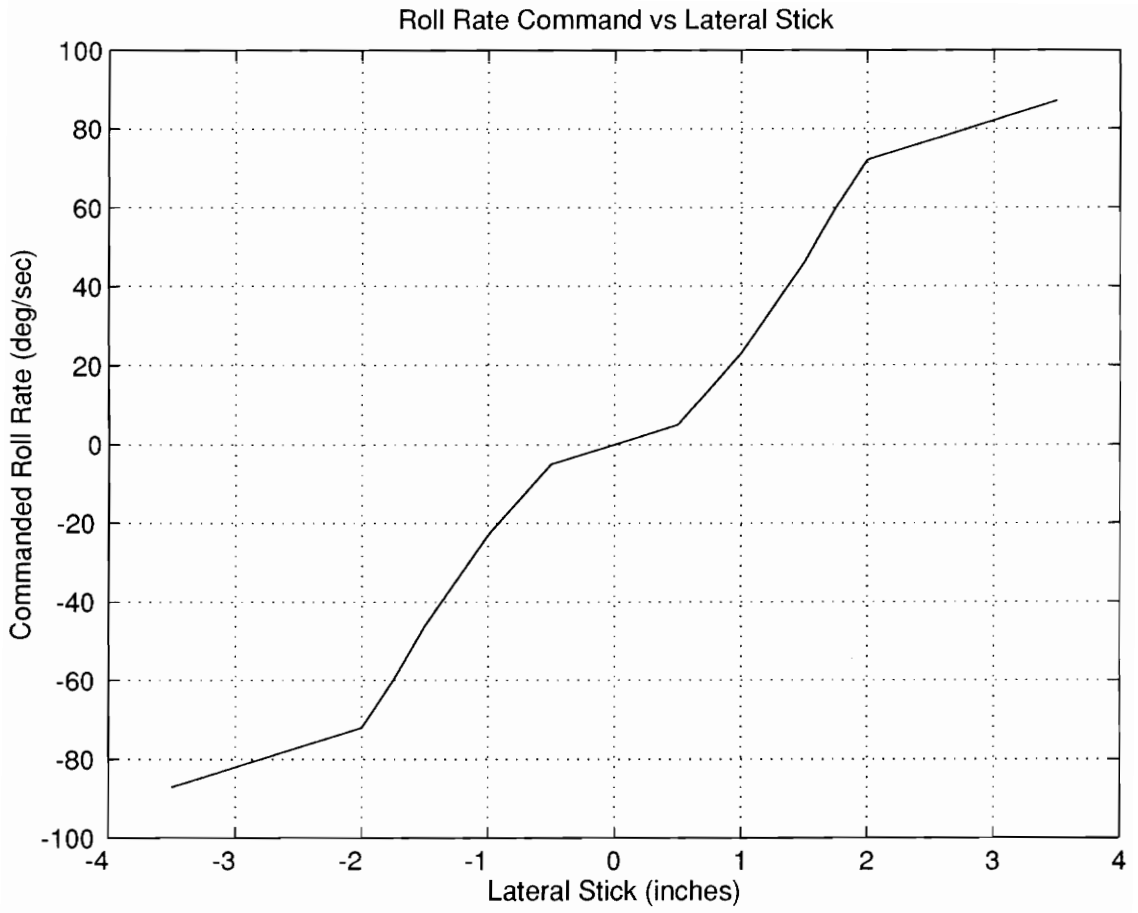


Figure 5.26 Roll Rate Command versus Lateral Stick

## 5.7 SISO Robustness

A hard requirement of the PA ARI design effort was to insure that all single-loop gain and phase margins meet or exceed the following requirements, as defined by MIL-F-9490D:

- Gain Margin  $\geq 6.0$  dB
- Phase Margin  $\geq 45$  degrees

The stability margins were calculated at each sensor feedback and actuator command signal. The five loops analyzed were:

- roll rate sensor
- yaw rate sensor
- lateral accelerometer
- roll series servo command
- yaw series servo command

The open-loop system with all loops open is shown in figure 5.27. The linearized open-loop model was then manipulated to close all loops except the one being analyzed, and the frequency response computed. This process was repeated for all five loops. Figures 5.28 through 5.32 show the bode plots for each loop, with the gain and phase margins included. All feedback loops passed the stability margin requirements specified by MIL-F-9490D. Table 5.1 summarizes the PA ARI SISO stability margin results.

Table 5.1 PA ARI SISO Gain and Phase Margins

Loop	Gain Margin (db)	Phase Margin (deg)
Roll Rate	12.54	85.22
Yaw Rate	26.30	120.9
Lateral Acceleration	23.73	N/A
Roll Series Actuator	12.67	89.12
Yaw Series Actuator	25.49	119.6

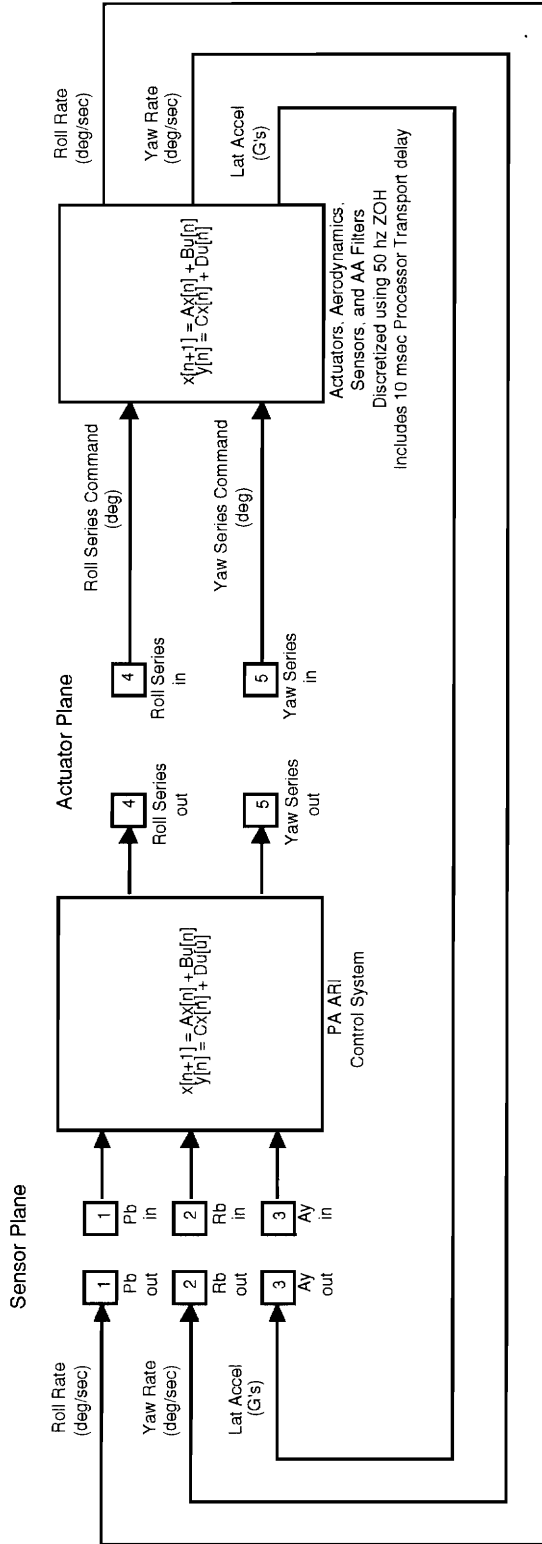


Figure 5.27 Open-loop PA ARI for Robustness Analysis

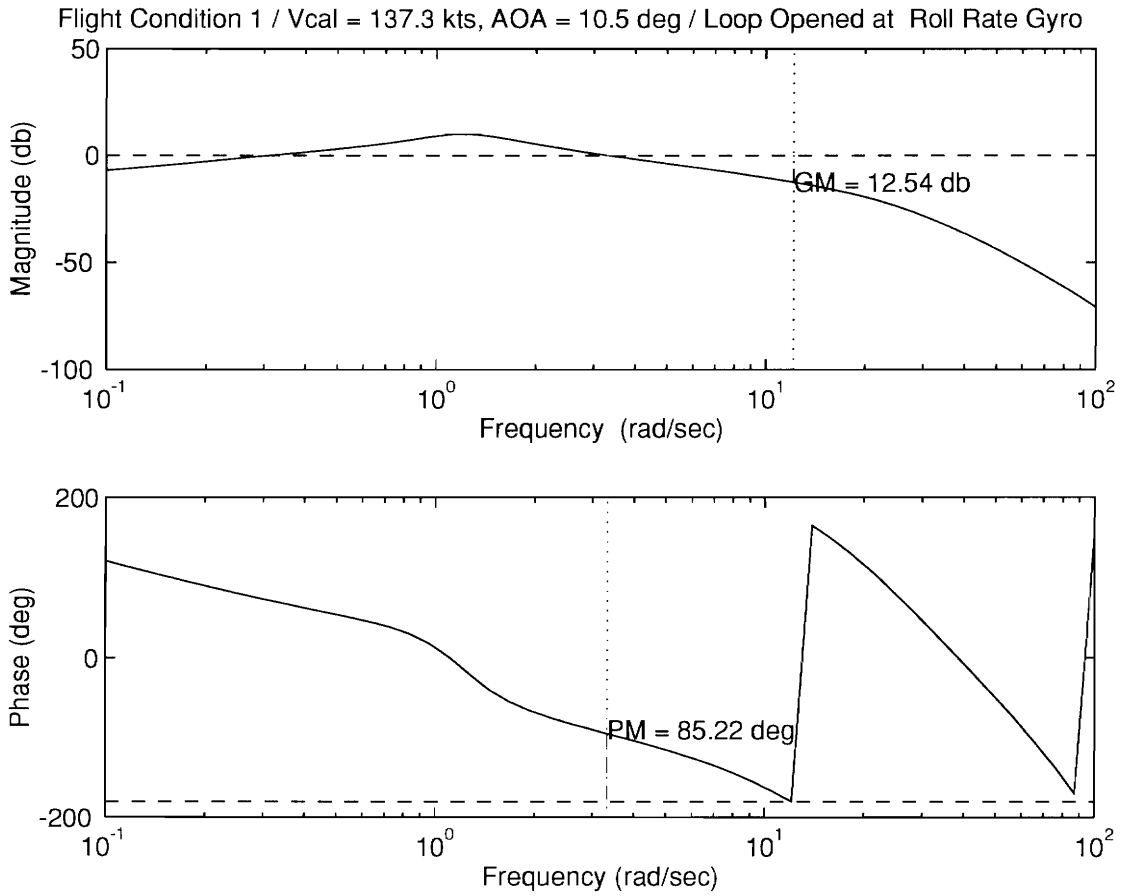


Figure 5.28 Frequency Response with Loop Opened at Roll Rate Gyro



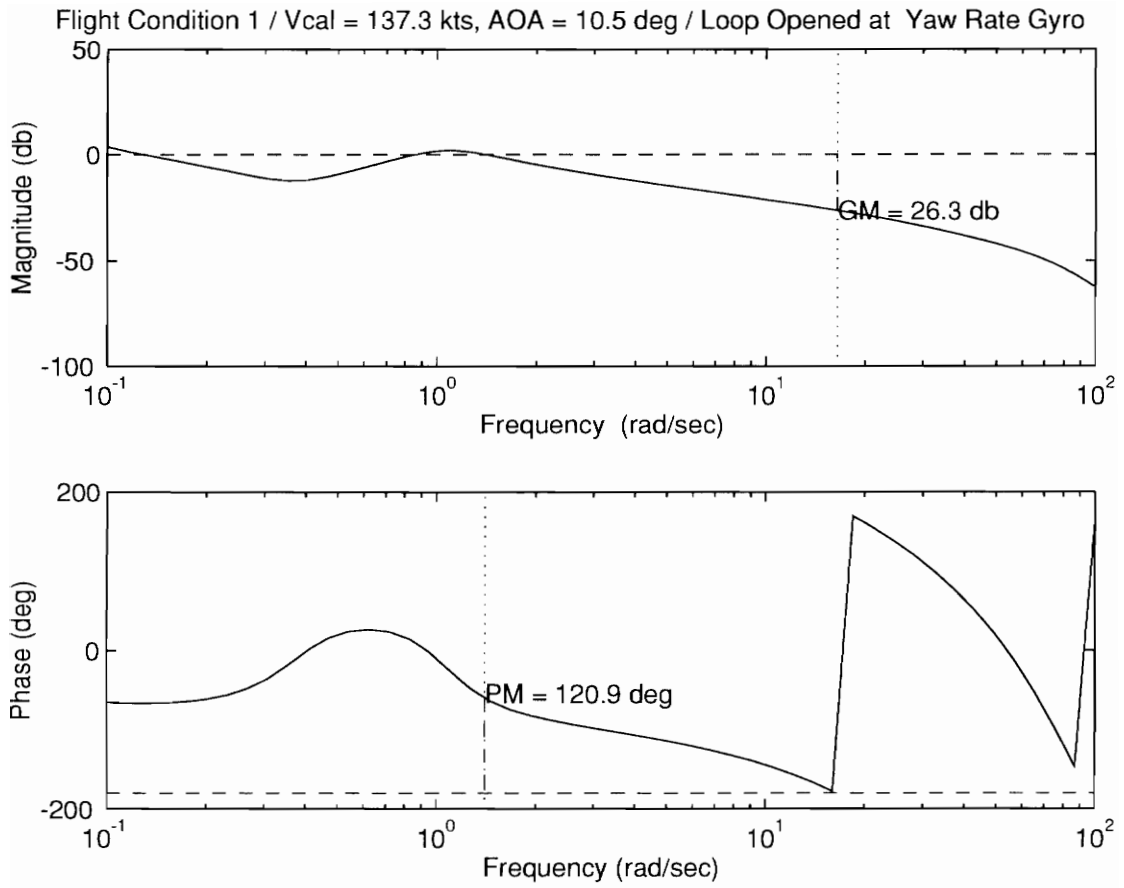


Figure 5.29 Frequency Response with Loop Opened at Yaw Rate Gyro

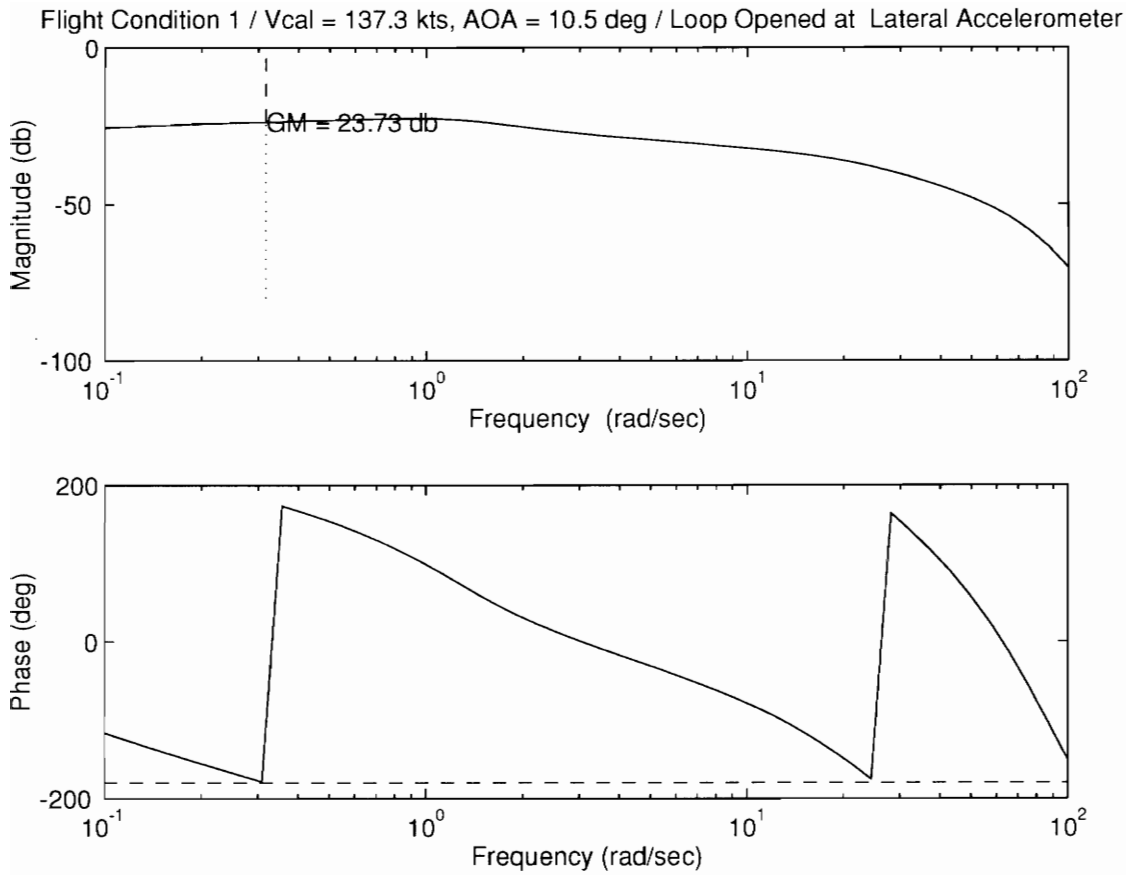


Figure 5.30 Frequency Response with Loop Opened at Lateral Accelerometer

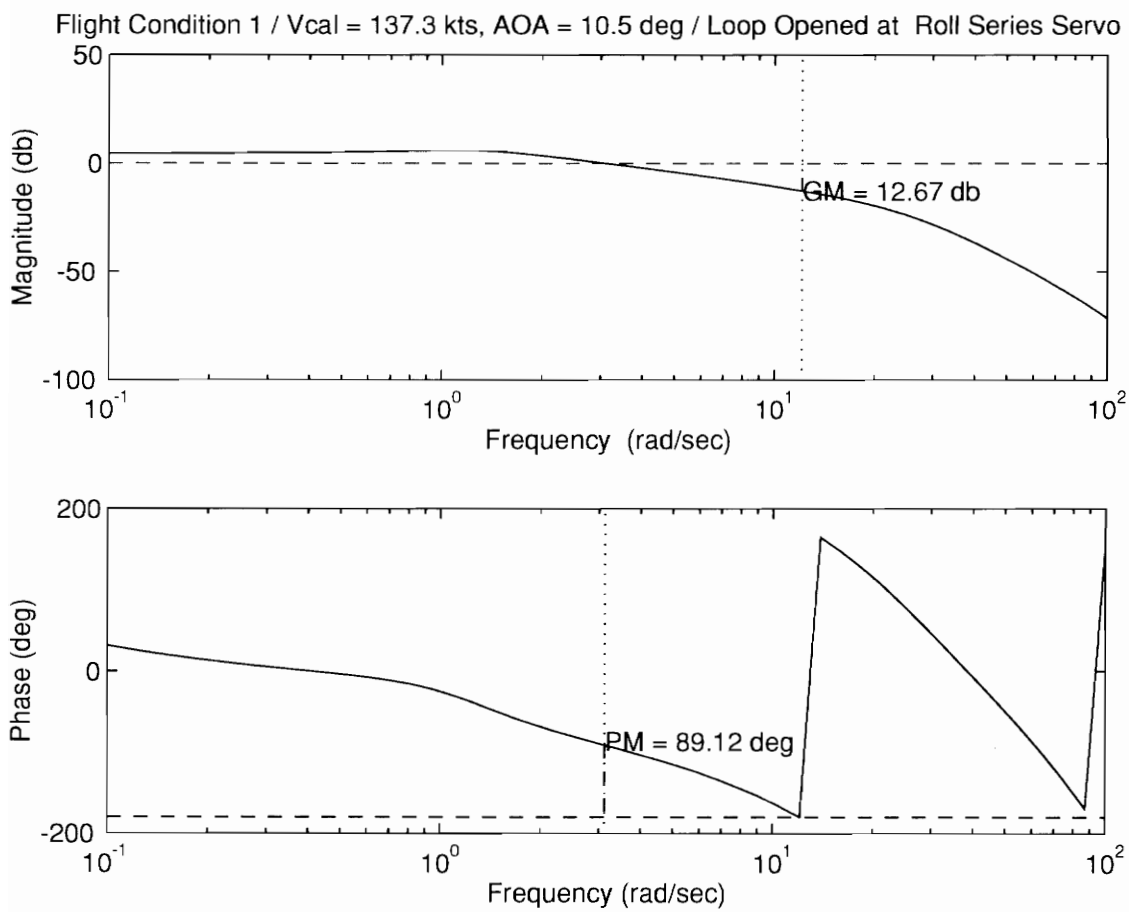


Figure 5.31 Frequency Response with Loop Opened at Roll Series Actuator

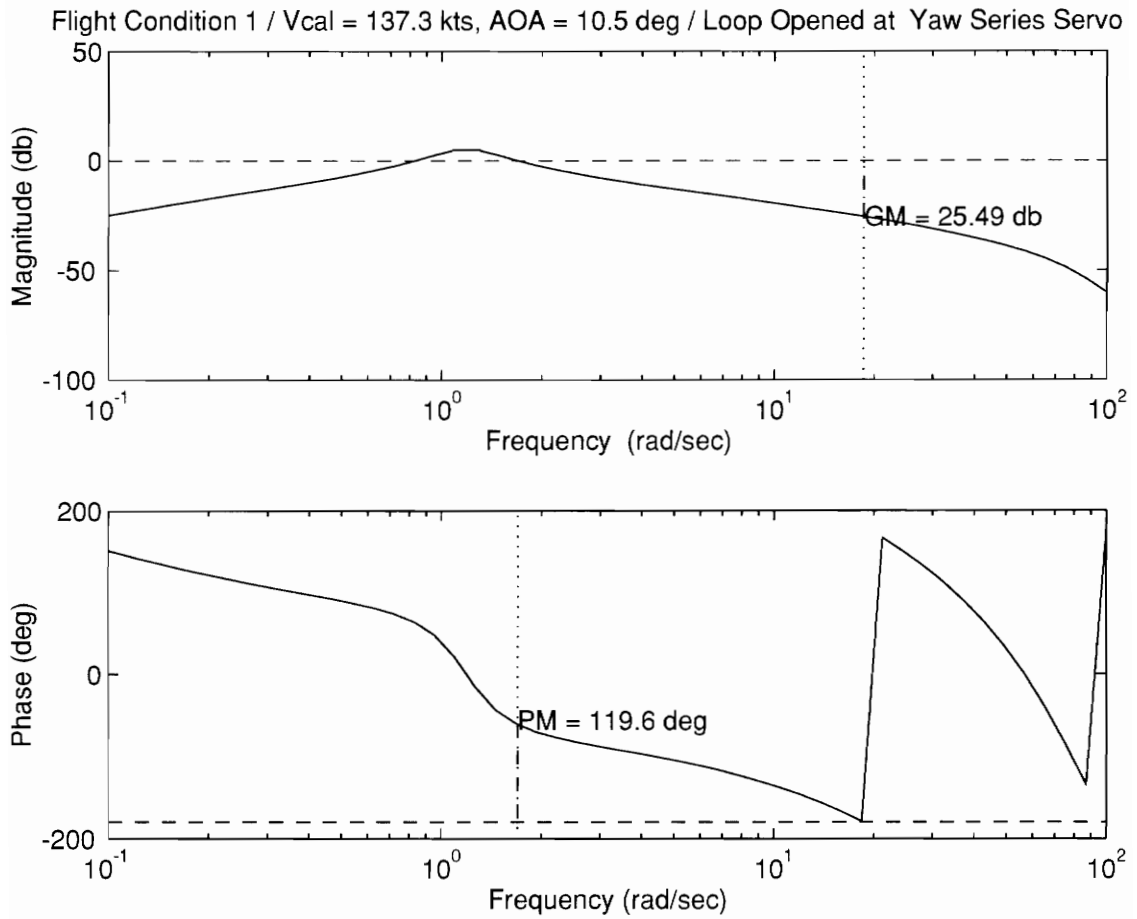


Figure 5.32 Frequency Response with Loop Opened at Yaw Series Actuator

## 5.8 MIMO Stability Robustness

Because of the inherent optimism in SISO analysis methods, a multi-input multi-output (MIMO) stability analysis was conducted on the PA ARI control system. The MIMO robustness properties were evaluated at the sensor plane and the actuator plane. The quantities utilized for this analysis were the sensitivity function (S) and the complementary sensitivity function (T) and their associated gain and phase margin estimates, as described in chapter III. Figure 5.33 shows the maximum singular values of S and T and the resulting MIMO stability margins with the loop opened at the sensor plane, while figure 5.34 shows the same results for the loop opened at the actuator plane. The results show that the system is considerably less robust to uncertainties occurring at the sensors than at the actuators. The prime factor influencing this result is that the sensor plane consists of 3 signal paths (roll rate, yaw rate, and lateral acceleration), while the actuator plane has only 2 paths (roll series servo and yaw series servo). Uncertainty affecting 3 paths simultaneously has a larger impact on closed-loop stability than uncertainty affecting only 2 paths simultaneously. Table 5.2 summarizes the PA ARI MIMO robustness results.

Table 5.2 PA ARI MIMO Gain and Phase Margins

Loop Break Plane	GM (db)	PM (deg)
Sensors	+1.31 /-1.31	±8.04
Actuators	+10.8 /-4.67	±41.66

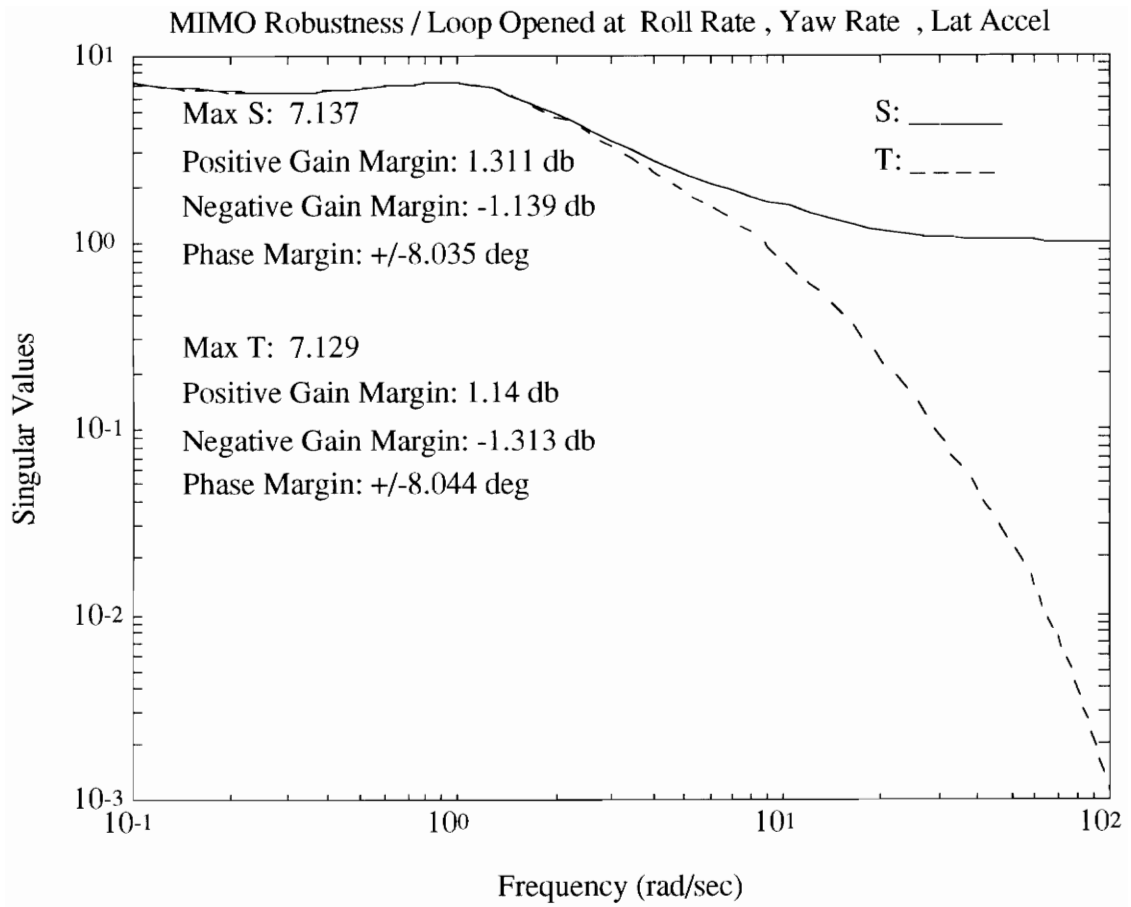


Figure 5.33 MIMO Robustness with Loop Open at Sensors

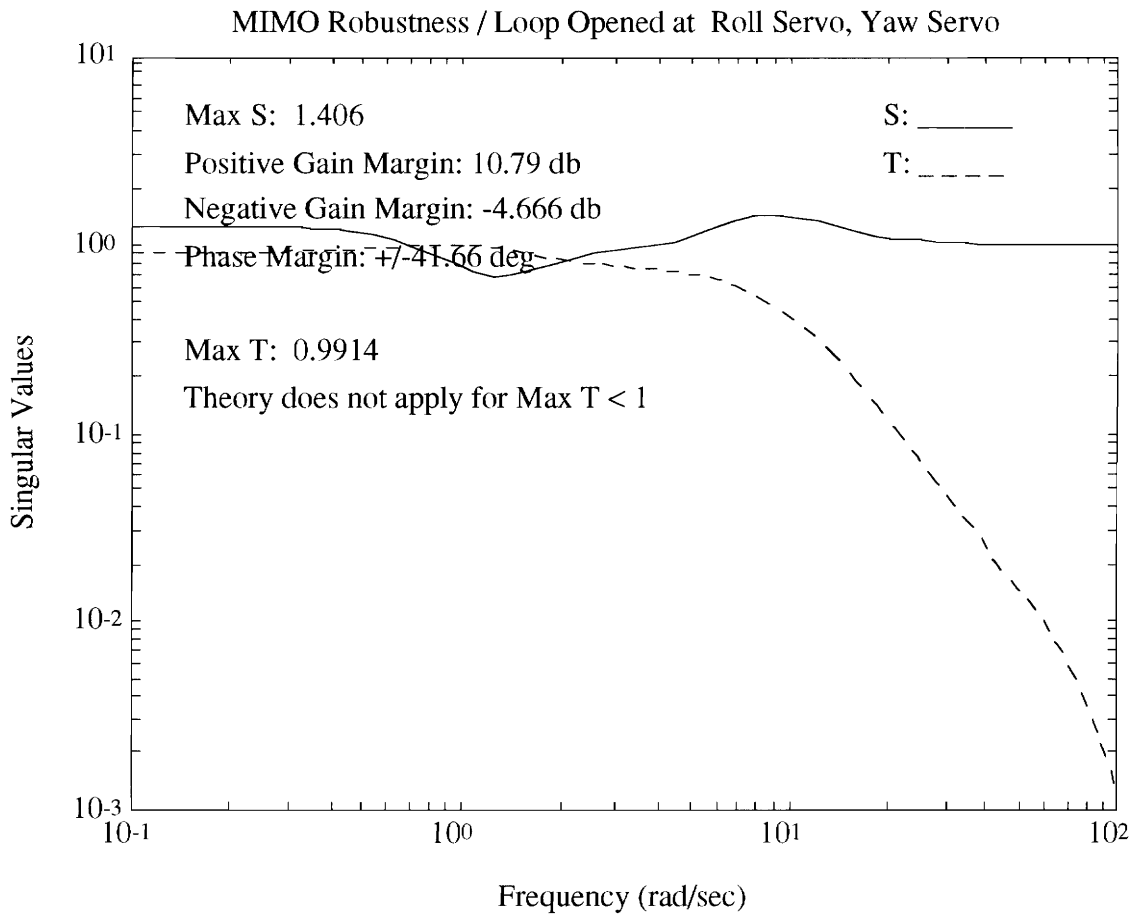


Figure 5.34 MIMO Robustness with Loop Open at Actuators

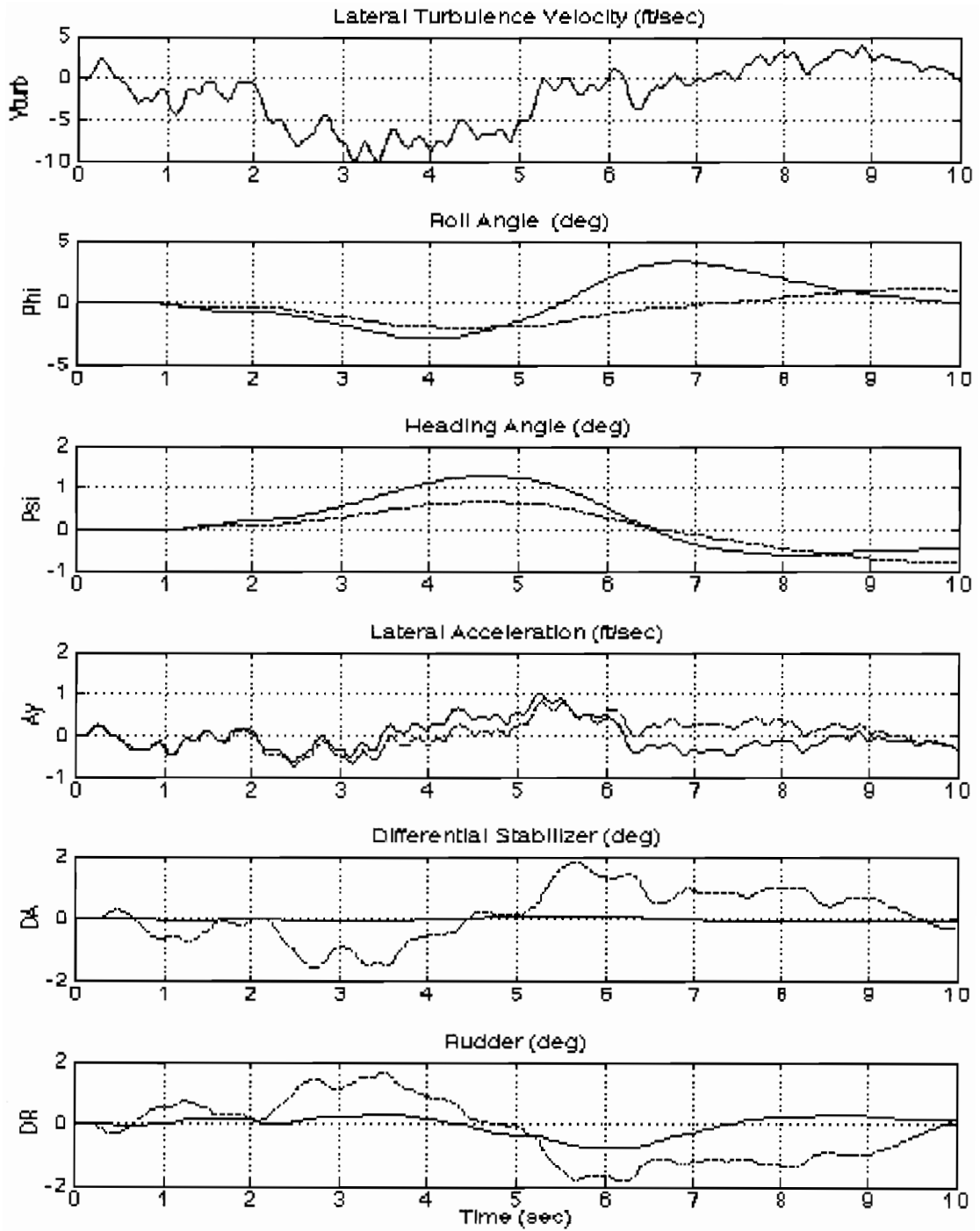
## 5.9 Response to Atmospheric Turbulence

After the linear stability analysis was complete, the nonlinear FORTRAN model was utilized to assess the turbulence rejection properties of the system. The same Von-Karman turbulence model was used for the PA ARI analysis as was used in the AFCS analysis in section 4.4.2. Figure 5.35 shows the effect of turbulence on the aircraft straight and level tracking characteristics of the PA ARI compared with the AFCS. The aircraft angular deviations from the initial condition were reduced considerably with the PA ARI control system, while the control surface activity was increased. This was the expected result, as the feedback loop gains of the PA ARI were increased substantially from the AFCS design.

## 5.10 Equivalent Systems Analysis

The PA ARI closed-loop system shown in figure 5.10 was linearized and reduced to a 4 state equivalent model required for the flying qualities specification analysis. The frequency response of the reduced order versus the full order system for lateral stick and rudder pedal inputs is shown in figures 5.36 and 5.37, respectively. Table 5.3 compares the parameters of the equivalent system model with the values specified in MIL-F-8785C and displays the flying quality level achieved. All parameters met Level 1 requirements.





AFCS: \_\_\_\_\_ PA ARI: - - - - -

Figure 5.35 AFCS vs PA ARI Response to Atmospheric Turbulence

Table 5.3 PA ARI Equivalent System Analysis Results

LOES Parameter	Definition	Level 1 Requirement	Value	Flying Quality Level
$\lambda_s = (-1/\tau_s)$	Spiral mode eigenvalue	Time to Double > 12 sec ( $\lambda_s < 0.0578$ )	0.0040	1
$\tau_R$	Roll mode time constant	$\tau_R < 1$ sec	0.52 sec	1
$\omega_{dr}$	Dutch-roll Frequency	$\omega_{dr} > 1$ rad/sec	1.10 rad/sec	1
$\zeta_{dr}$	Dutch-roll Damping	$\zeta_{dr} > 0.13^*$	0.95	1
$t_{lat}$	Lateral Axis Time Delay	$t_{lat} < 0.10$ sec	0.05 sec	1
$t_{ped}$	Yaw Axis Time Delay	$t_{ped} < 0.10$ sec	0.01 sec	1

\* Requirement computed from  $0.15 = \zeta_{dr}\omega_{dr}$  with  $\omega_{dr} = 1.1$  rad/sec

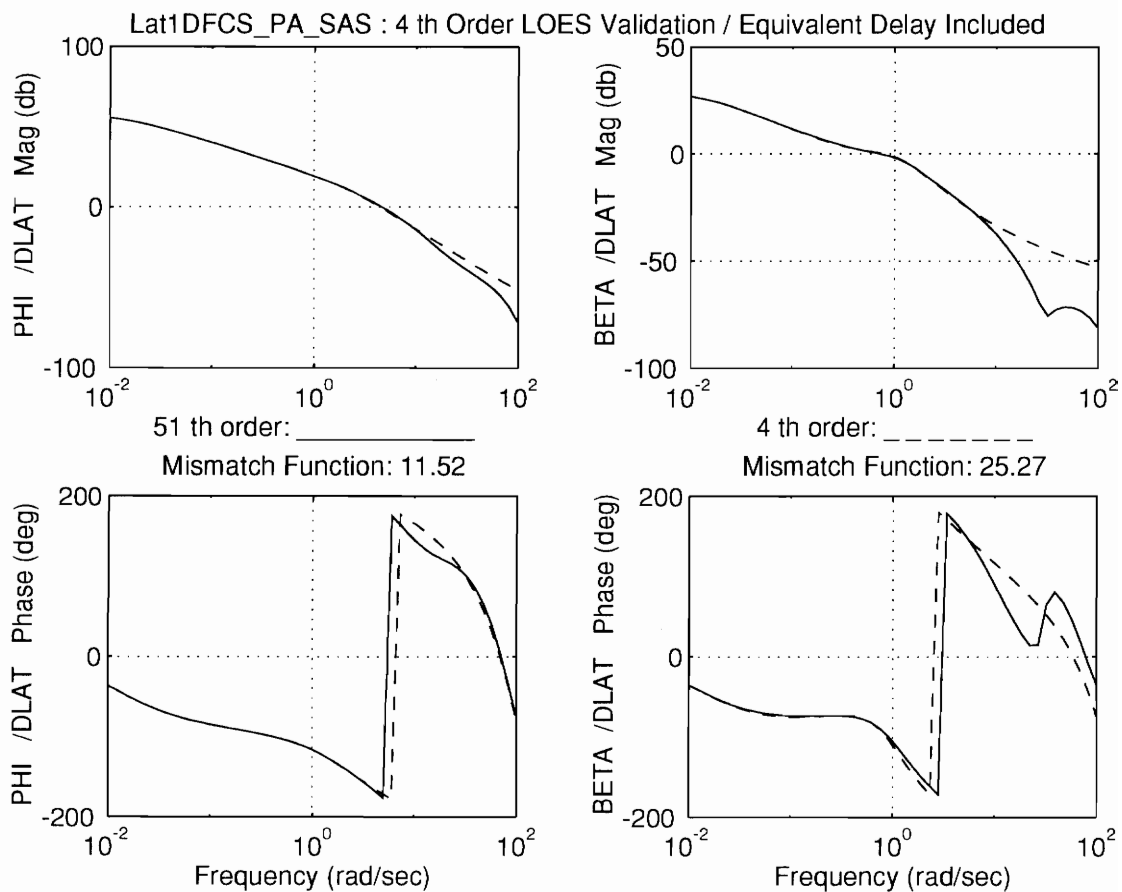


Figure 5.36 Equivalent System Model Frequency Response Validation / Lateral Stick Input

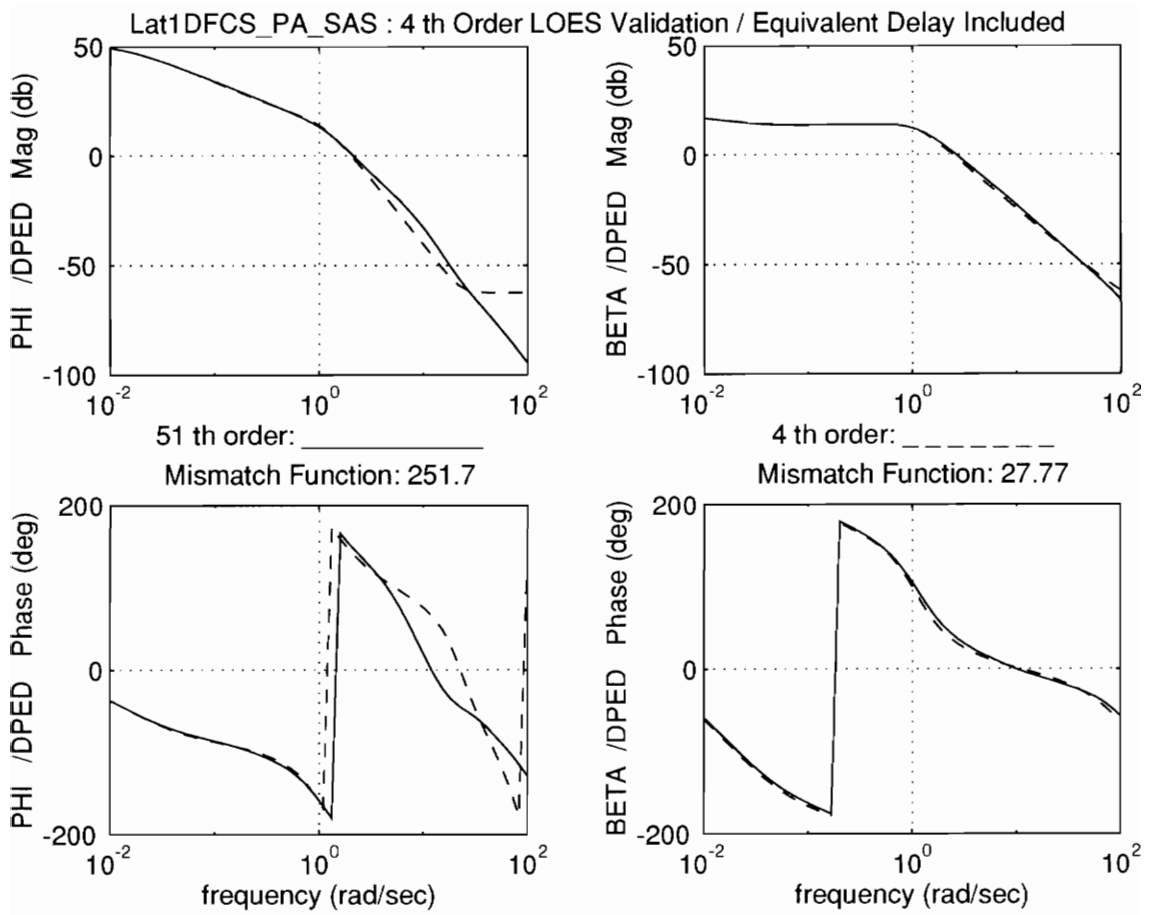


Figure 5.37 Equivalent System Model Frequency Response Validation /  
Rudder Pedal Input

## **5.11 Piloted Simulation Evaluation**

A major part of the PA ARI development was piloted simulation evaluation. As described in section 4.3 [4.1], an intensive simulation evaluation was conducted in which multiple Navy and Grumman pilots participated in evaluating the PA ARI control laws for various operational tasks. As described in section 4.3, the primary tasks performed were bank angle captures and runway lineup corrections. These tasks were designed to demonstrate the improvements in the PA ARI control law as compared with the production AFCS. Pilot handling qualities ratings (HQR's) were the primary method of system performance evaluation.

### **5.11.1 Bank Angle Captures**

The modified spoiler gearing and roll rate command/tracking system greatly enhanced the bank angle capture task as compared with the AFCS. The increased sensitivity and linearity of the roll rate response coupled with the absence of Dutch-roll oscillations enabled the pilots to perform bank angle captures in a routine manner. Average pilot HQR's for these tasks was ranged from 2 to 3.

### **5.11.2 Runway Lineup Corrections**

The PA ARI control system also greatly enhanced the pilot's ability to perform runway lineup correction maneuvers. The quick, predictable roll rate response of the aircraft combined with the absence of undesirable Dutch-roll oscillations allowed the pilots to efficiently establish the desired cross track rate required to eliminate the lateral offset. These characteristics also

enabled the pilot to roll out on centerline in a predictable fashion with few secondary corrections. The average pilot HQR's for this task ranged between 2 and 3. Table 5.4 below summarizes the HQR's obtained from the simulation evaluation of the production AFCS for the bank angle and runway lineup tasks.

Table 5.4 AFCS vs PA ARI Handling Qualities Ratings Comparison

Task	AFCS HQR	PA ARI HQR
Bank Angle Capture	6	2.5
Runway Lineup	6	2.5

## 5.12 Summary

The PA ARI control law design which is targeted for the new F-14 Digital Flight Control System resulted in substantial flying qualities enhancements over the existing AFCS control system in the PA operating regime. The feedback loop design, accomplished using discrete time SISO methods, proved to be highly effective in augmenting the aircraft damping characteristics and provided excellent disturbance rejection properties. The design was shown to possess excellent stability robustness characteristics in the face of SISO uncertainties. MIMO stability analysis showed excellent robustness properties at the actuator plane, but less robustness at the sensor plane. The primary disadvantage of the design technique was the lack of a systematic method for design of the feedforward paths.

## Chapter VI

### Multivariable Model Following Control Law Design

#### 6.1 Introduction

Although the PA ARI control law designed in chapter V resulted in greatly enhanced performance compared to the production AFCS, the use of classical SISO and “ad-hoc” design techniques raised questions regarding the optimality of the design. To determine the performance increase achievable, a multivariable model following (MMF) control law design was conceived. The MMF was designed using a combination of explicit model following, dynamic inversion, and integral linear quadratic regulation to achieve the desired closed-loop response, accurate command tracking, and stability robustness. To simplify the design process, the MMF control law was designed using continuous time methods and neglecting high frequency dynamics. However, the complete high order dynamics, discretization effects, and nonlinear simulation results were evaluated to verify the final control law design.

#### 6.2 Design Objectives

The MMF control law design objectives are essentially the same as the PA ARI design objectives. The system should meet or exceed the requirements for level 1 flying qualities defined by MIL-F-8785C as well as

the SISO stability robustness requirements defined by MIL-F-9490D. The system is designed to provide the following responses to pilot inputs:

- 1) 1st order roll rate response to lateral stick inputs with negligible sideslip excursions
- 2) roll angle hold for centered lateral stick
- 3) proportional sideslip response to rudder pedal with no roll axis coupling

### **6.3 General Description**

The primary components of the MMF are the maneuver command generator (MCG), dynamic inversion, LQ regulator, reduced order observer, and control surface selector. The MCG and dynamic inversion are designed to provide feedforward, open-loop model following. The LQ regulator is designed to operate on the error between the commanded and estimated state vector to provide accurate steady state tracking and disturbance rejection. A reduced order observer is used to compute unmeasured state trajectories. A control surface selector is used to convert generalized roll and yaw control commands into specific control surface commands. The structure of the overall system is shown in figure 6.1. A primary advantage of this type of model following structure is that the forward path (MCG and dynamic inversion) and feedback path (regulator and observer) designs are independent. In model following systems such as the F-15 S/MTD, the forward path characteristics are a function of the feedback path characteristics [1.11].



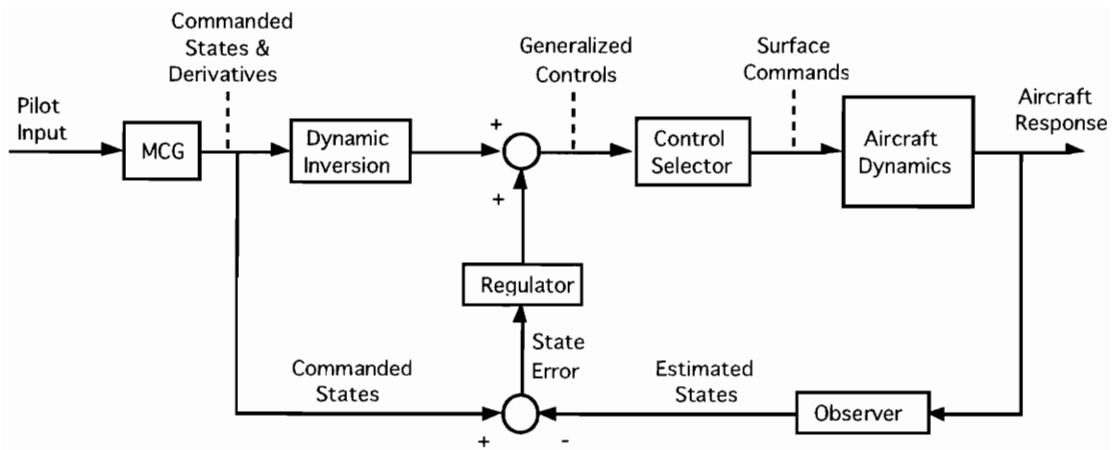


Figure 6.1 MMF Control Structure

## 6.4 Maneuver Command Generator

The first component of the MMF forward path is the maneuver command generator (MCG) [6.1]. The purpose of the maneuver command generator is to generate desired aircraft states and state derivatives in response to pilot inputs. Flying qualities requirements, desired aircraft response types, aircraft performance limitations, and kinematic relationships were used to design the MCG. The design goal of the MCG is to provide decoupled roll axis and yaw axis command responses, as specified in section 6.2. Lateral stick produces a roll rate command signal, which is integrated to form the roll angle command. Yaw rate is commanded as a function of roll rate and roll angle in order to maintain the proper kinematic relationship of these variables during transient rolling maneuvers as well as during steady state turns. Rudder pedal commands sideslip angle and yaw rate, with no change in roll rate or roll angle. The general structure of the MCG is shown in figure 6.2.

### 6.4.1 Roll Rate Command Model

The MCG is designed to command roll rate in response to lateral stick inputs. When the lateral stick is returned to zero, the aircraft roll angle will be held constant. The design parameters for the roll rate command model are the lateral stick to roll rate gain and the roll mode time constant. The command model also produces the commanded roll acceleration. Figure 6.3 shows the details of the roll rate command model. The roll rate command sensitivity is selected to produce 20 deg/sec roll rate per inch of lateral stick

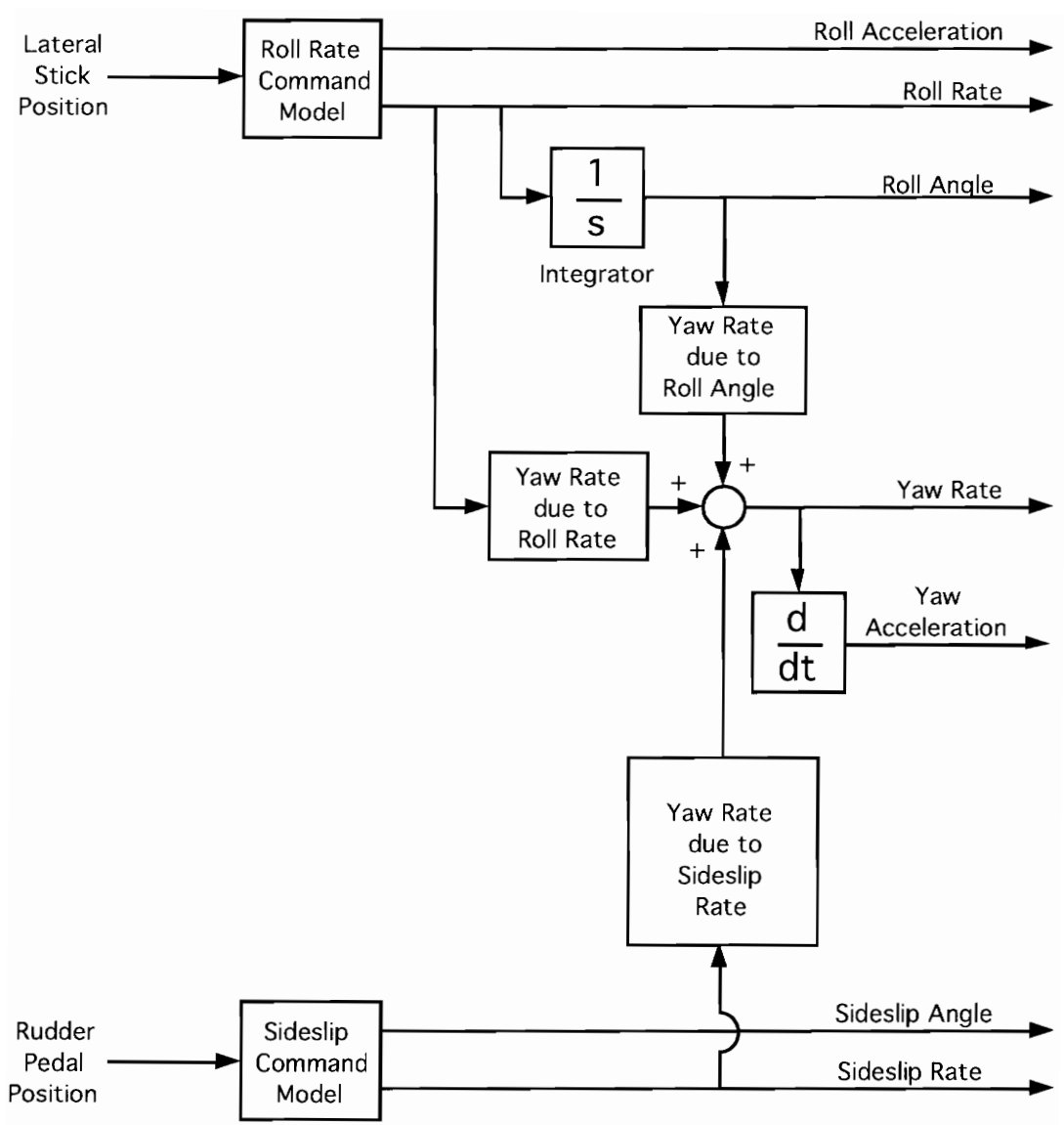
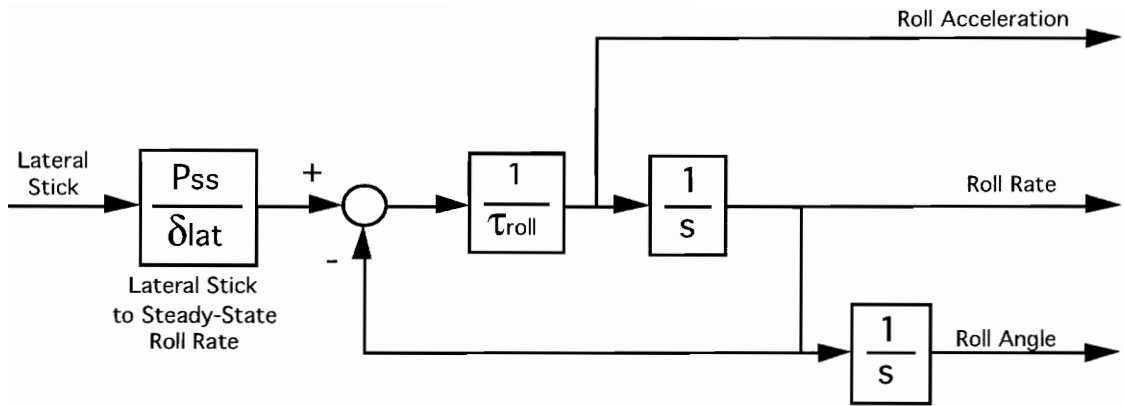


Figure 6.2 Maneuver Command Generator Structure



$$\frac{P_{ss}}{\delta_{lat}} = 20 \text{ (deg/sec)/inch} \quad \tau_{roll} = 0.5 \text{ sec}$$

Figure 6.3 Roll Rate Command Model

deflection. The first order time constant of the commanded roll response is selected to be 0.5, the same time constant used in the PA ARI design.

#### 6.4.2 Sideslip Command Model

Rudder pedal deflection is used to command sideslip angle. The sideslip command model generates the desired sideslip due to a rudder pedal input via a second-order filter as shown in figure 6.4. The frequency and damping of this filter, which equate to the aircraft's equivalent Dutch-roll frequency and damping, were selected to be 1.2 rad/sec and 0.707. The rudder pedal to sideslip sensitivity is selected such that a full pedal deflection of 3.0 inches will result in 15 degrees of commanded sideslip.

#### 6.4.3 Yaw Rate Command due to Roll Rate Command

In section 5.4, the 6-DOF lateral force equation was shown to be equivalent to:

$$\dot{\beta} = P \sin \alpha - R \cos \alpha + \frac{g \sin \Phi + A_y}{V_T} \quad (6.1)$$

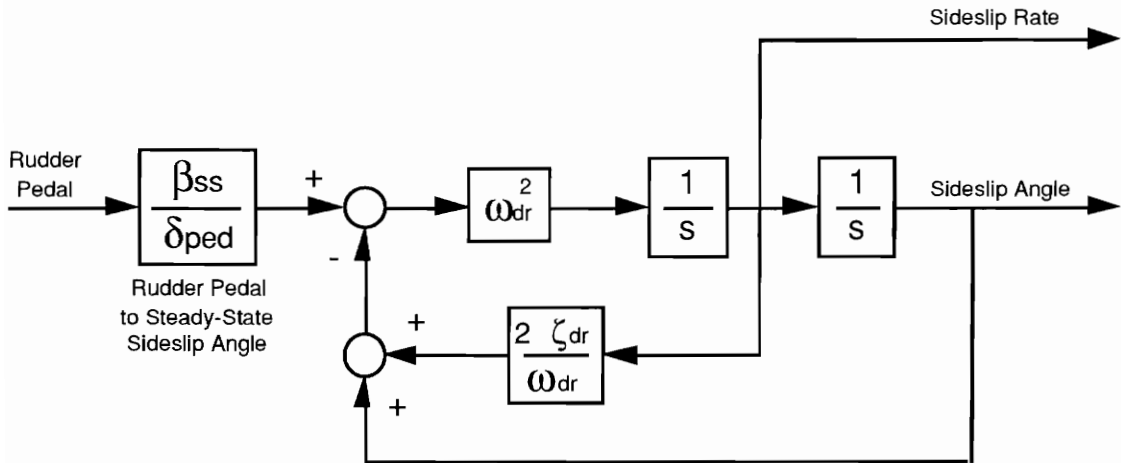
By assuming a perfectly coordinated small amplitude roll maneuvers, this expression can be reduced to:

$$P \sin \alpha = R \cos \alpha \quad (6.2)$$

or equivalently,

$$R = P \tan \alpha \quad (6.3)$$

This relationship is used in the MCG to compute the commanded yaw rate due to commanded roll rate at the measured angle-of-attack.



$$\frac{\beta_{ss}}{\delta_{ped}} = -5 \text{ deg/inch}$$

$$\omega_{dr} = 1.2 \text{ rad/sec}$$

$$\zeta_{dr} = 0.707$$

Figure 6.4 Sideslip Command Model

#### 6.4.4 Yaw Rate Command due to Roll Angle Command

By assuming the aircraft is in a steady banked turn, sideslip rate, roll rate, and lateral acceleration can be assumed close to zero. The 6-DOF lateral force equation given by (6.1) can then be reduced to:

$$R \cos \alpha = \frac{g \sin \Phi}{V_T} \quad (6.4)$$

which can be rearranged as follows:

$$R = \frac{g \sin \Phi}{V_T \cos \alpha} \quad (6.5)$$

This relationship is used in the MCG to compute the commanded yaw rate due to commanded roll angle, measured airspeed, and angle-of-attack.

#### 6.4.5 Yaw Rate Command due to Sideslip Rate Command

The final term to be derived in the MCG is the commanded yaw rate due to sideslip rate command. This term is based on the assumption that rudder pedal commands pure yaw axis motion. By assuming small perturbation transient motion in the yaw axis with no motion in the roll axis, equation (6.1) can be reduced to:

$$\dot{\beta} = -R \cos \alpha + \frac{A_y}{V_T} \quad (6.6)$$

which can be rearranged as:

$$R = \frac{\left( \frac{A_y}{V_T} - \dot{\beta} \right)}{\cos \alpha} \quad (6.7)$$

The MCG is designed to operate only on the pilot inputs and flight condition

scheduling parameters (airspeed, angle-of-attack). Therefore, the lateral acceleration term in (6.6) cannot be used. A lateral acceleration command could be derived based on the commanded sideslip, aircraft measured airspeed, and the aircraft sideslip to Y-force stability derivative ( $Y_{\beta}$ ). The degree of uncertainty in  $Y_{\beta}$  combined with the resulting insignificant performance increase does not warrant the inclusion of this term in the MCG. The yaw rate command path is therefore reduced to:

$$R = \frac{-\dot{\beta}}{\cos\alpha} \quad (6.8)$$

The sideslip rate term in equation (6.8) is supplied from the sideslip command model derived in section 6.4.2. By combining the results of sections 6.3.1 through 6.3.5, the complete MCG is formed as shown by figure 6.5.

#### 6.4.6 Response to Pilot Inputs

The characteristics of the MCG are evident when the response of the system to pilot lateral stick and rudder pedal commands is computed. The lateral stick command used is a 1 inch half-doublet which enters at time = 1 second and is neutralized at time = 2 seconds. Figure 6.6 shows the MCG state variable command response to the lateral stick input. The command response to lateral stick is termed “rate command, attitude hold”, because the steady-state roll rate is proportional to the lateral stick input (20 (deg/sec)/inch), while the roll angle is held constant when the stick input is neutralized. Figure 6.7 shows the MCG response to a 1 inch rudder pedal step. The command enters at time = 1 second and is held in until the end of the run.



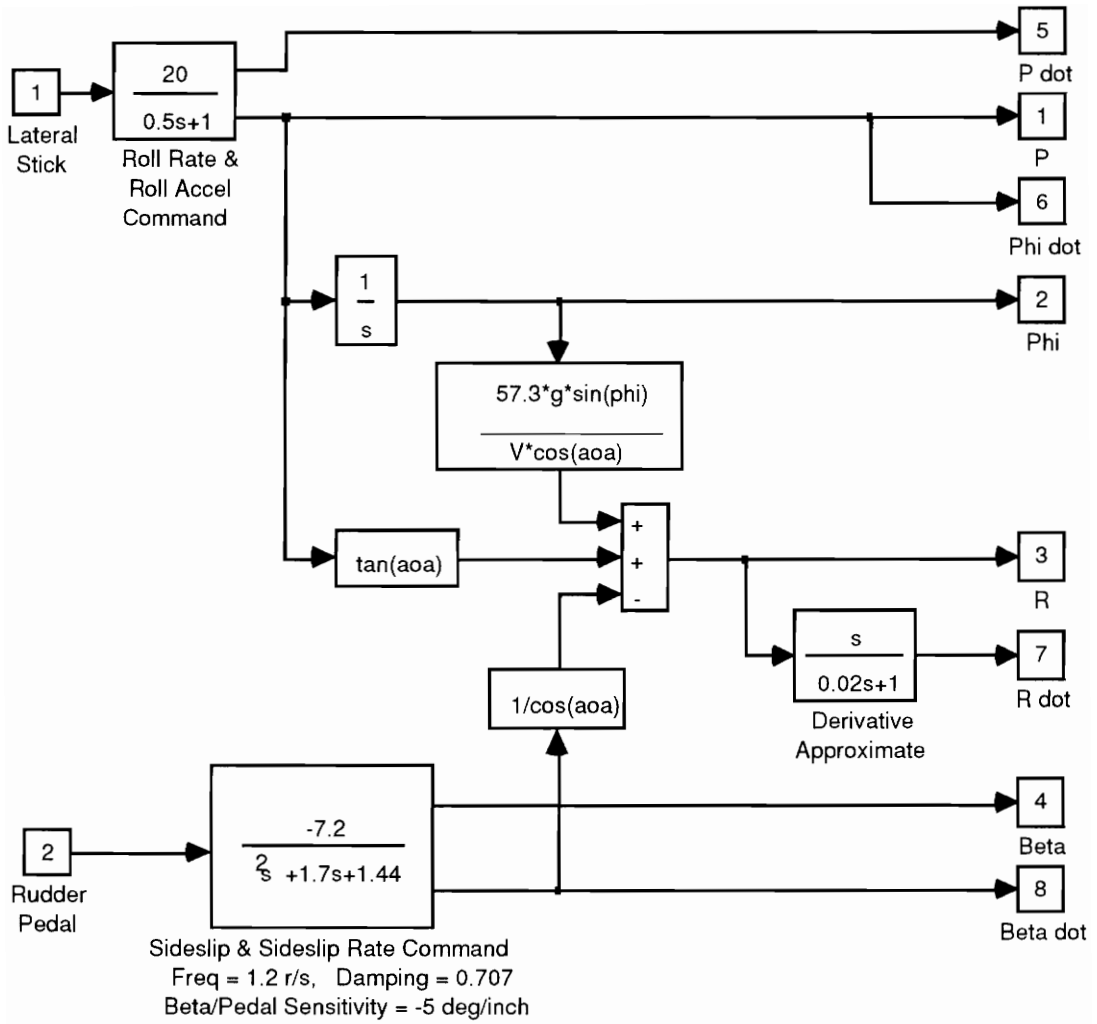


Figure 6.5 Detailed Maneuver Command Generator

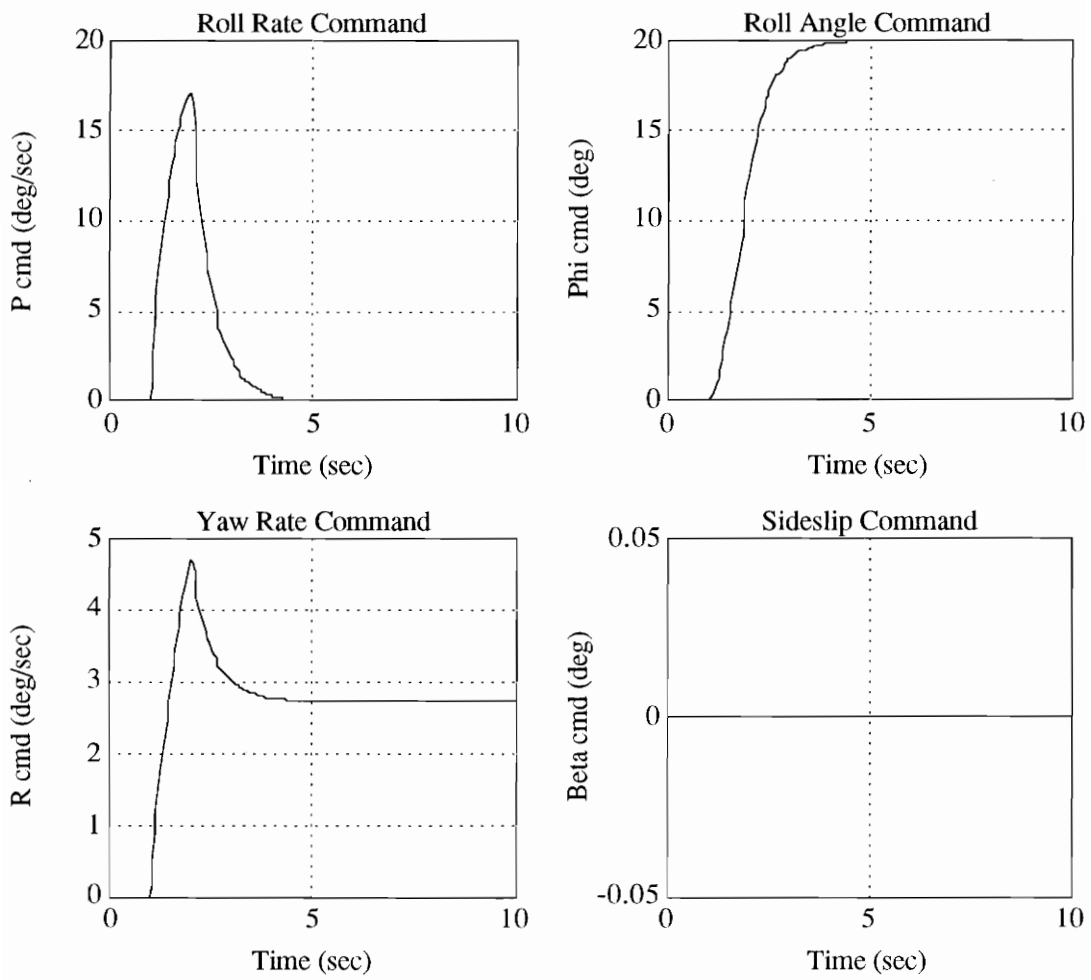


Figure 6.6 MCG Response to Lateral Stick Half Doublet

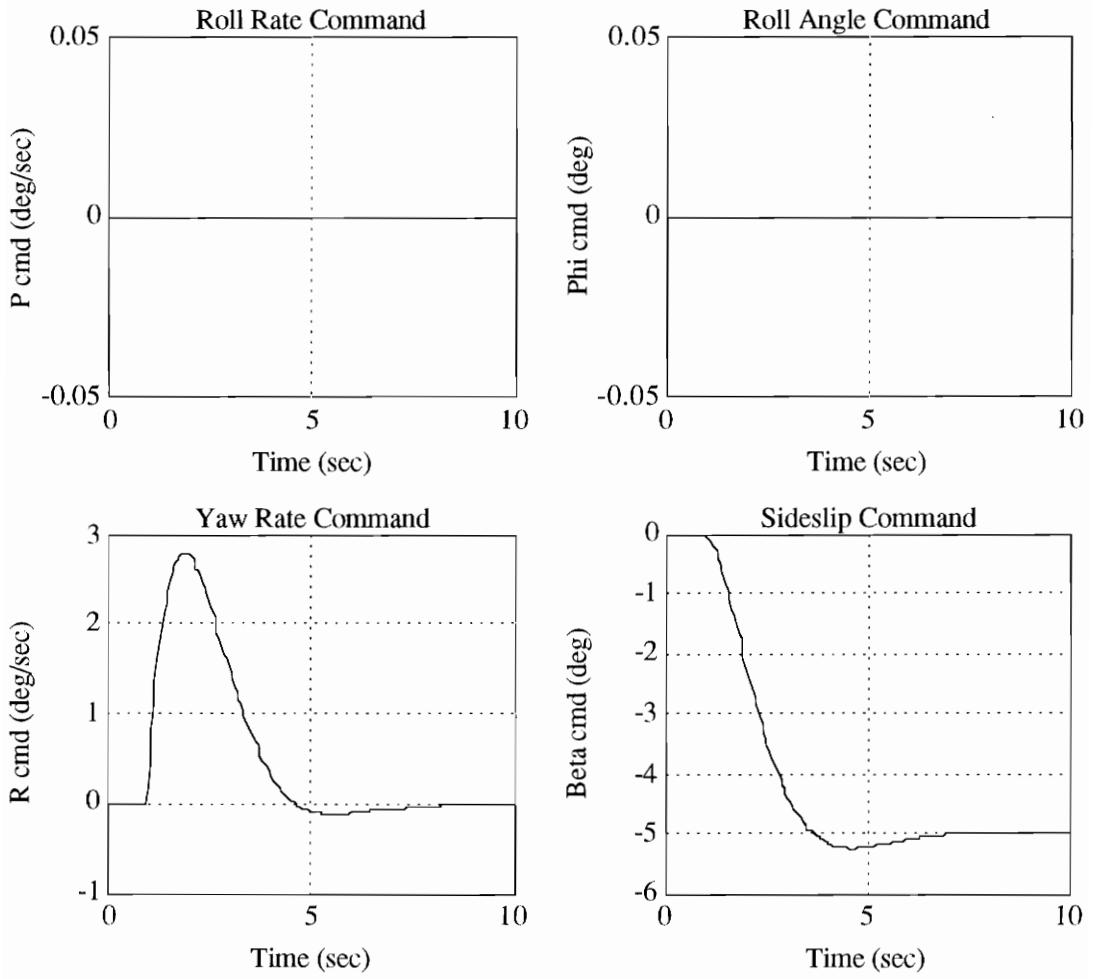


Figure 6.7 MCG Response to Rudder Pedal Step

## 6.5 Design Plant Model

The design plant model will be presented before proceeding to MMF design tasks based on the plant model. The MMF control law is designed using the 4 state rigid body aerodynamic model described in section 2.3.1. All high frequency dynamics are neglected in the design stage to reduce the complexity of the resulting control law, but are included in the final design analysis. The continuous time state-space model of the aircraft is:

$$\begin{aligned} \text{A:} & \begin{bmatrix} -0.1129 & -233.5377 & 44.1579 & 31.6331 \\ 0.0027 & -0.2520 & -0.1407 & 0 \\ -0.0206 & 0.6524 & -1.3283 & 0 \\ 0 & 0.1853 & 1.0000 & 0 \end{bmatrix} \\ \text{B:} & \begin{bmatrix} 0 & 0.0622 & 0.1012 \\ -0.0016 & -0.0052 & -0.0112 \\ -0.0193 & -0.0467 & 0.0036 \\ 0 & 0 & 0 \end{bmatrix} \\ \text{C:} & \begin{bmatrix} 0 & 0 & 57.2958 & 0 \\ 0 & 0 & 0 & 57.2958 \\ 0 & 57.2958 & 0 & 0 \\ 0.2403 & 0 & 0 & 0 \end{bmatrix} \\ \text{D:} & \begin{bmatrix} 0 & 0 & 0 \\ 0 & 0 & 0 \\ 0 & 0 & 0 \\ 0 & 0 & 0 \end{bmatrix} \end{aligned}$$

where the state vector ( $x$ ) is:

- $v$  lateral velocity (ft/sec)
- $r$  yaw rate (rad/sec)
- $p$  roll rate (rad/sec)
- $\phi$  roll angle (rad)

the input vector ( $u$ ) is:

- $\delta_{sp}$  differential spoiler (deg)
- $\delta_a$  differential horizontal stabilizer (deg)
- $\delta_r$  rudder (deg)

and the output vector ( $y$ ) is:

- $p$  roll rate (deg/sec)
- $\phi$  roll angle (deg)
- $r$  yaw rate (deg/sec)
- $\beta$  sideslip angle (deg)

### 6.5.1 Control Selector Design

The design objectives stated in section 6.2 require control about 2 axes; roll and yaw. No direct control of side force is required. The F-14 aerodynamic model has 3 control inputs, which implies that some control redundancy exists for accomplishing the desired tasks. The purpose of the control selector is to combine the redundant control inputs into a reduced control effector set. Examination of the B matrix shows that differential spoiler ( $\delta_{sp}$ ) and differential stabilizer ( $\delta_a$ ) have similar effects on the state derivatives. This is intuitively obvious, since the primary objective of these control inputs is to provide aircraft roll axis control, while the rudder is the primary yaw axis control. The singular values of the B matrix demonstrate that there are basically only two independent control effectors in the system. The singular values of B are shown below:

0.1216  
0.0451  
0.0020

The ratio between the 1st and 2nd singular values is 2.7, while the ratio between the 2nd and 3rd singular values is 22.4. Therefore, the effective rank of the B matrix is 2. This result supports the earlier observation that differential spoiler and differential stabilizer are related. To simplify the subsequent control design tasks, these two inputs are “ganged” into one control effector. The rudder input is considered the only yaw axis control effector. The relationship between the ganged controls (g), sometimes called the “generalized” controls, and the physical input vector (u) is:

$$u = Mg \tag{6.9}$$

where M is the control selector matrix. M is designed according to the physical actuator position authority limits. Since the differential spoiler limit is  $\pm 59.5$  degrees while the differential stabilizer limit is  $\pm 12$  degrees (a 5 to 1 ratio), the M matrix was defined as:

		Generalized Controls	
		$\delta_{roll}$	$\delta_{yaw}$
Physical Controls	$\delta_{sp}$	5	0
	$\delta_a$	1	0
	$\delta_r$	0	1

As shown, the generalized roll control is distributed between the differential spoiler and differential stabilizer at a 5 to 1 ratio, while the generalized yaw control and rudder control are equivalent. The control selector matrix is incorporated into the design plant model as shown by figure 6.8 below:

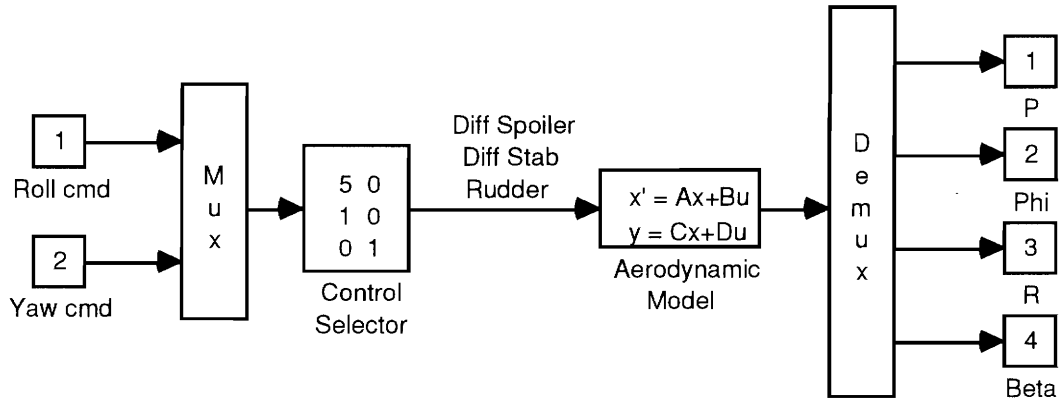


Figure 6.8 Combined Control Selector and Plant

### 6.5.2 Transformation to Sensor Coordinates

To simplify the design process, the design plant model is converted to sensor coordinates (observer canonical form). This is accomplished by performing the following similarity transformation on the design plant state-space model:

$$\begin{aligned}
 A_{dp} &= CAC^{-1} \\
 B_{dp} &= CB \\
 C_{dp} &= CC^{-1} = I \\
 D_{dp} &= D
 \end{aligned}
 \tag{6.10}$$

The resulting state space model with generalized controls is:

$$A_{dp} = \begin{bmatrix} -1.3283 & 0 & 0.6524 & -4.9049 \\ 1.0000 & 0 & 0.1853 & 0 \\ -0.1407 & 0 & -0.2520 & 0.6546 \\ 0.1852 & 0.1327 & -0.9795 & -0.1129 \end{bmatrix}$$

$$B_{dp} =$$

```

-8.2147    0.2087
      0      0
-0.7555   -0.6423
      0      0.0243

```

$C_{dp} =$

```

1.0000      0      0      0
      0    1.0000      0      0
      0      0    1.0000      0
      0      0      0    1.0000

```

$D_{dp} =$

```

0    0
0    0
0    0
0    0

```

where the state vector ( $x$ ) and output vector ( $y$ ) are:

$p$             roll rate (deg/sec)  
 $\phi$            roll angle (deg)  
 $r$             yaw rate (deg/sec)  
 $\beta$           sideslip angle (deg)

and the generalized control input vector ( $g$ ) is:

$\delta_{roll}$       roll command (deg)  
 $\delta_{yaw}$         yaw command (deg)

This is the model used for all subsequent MMF control system design tasks.



## 6.6 Feedforward Dynamic Inversion

### 6.6.1 Solution of the Dynamic Inversion Problem

The purpose of the feedforward dynamic inversion as applied in this thesis is to convert the MCG commanded states and state derivatives into control commands that will cause the aircraft states to follow the commanded states. The dynamic inversion control law is computed directly from the linear time-invariant model of the aircraft dynamics, given by:

$$\dot{\mathbf{x}} = \mathbf{A}\mathbf{x} + \mathbf{B}\mathbf{u} \quad (6.9)$$

Equation 6.9 can be rearranged to express  $\mathbf{u}$  as a function of  $\mathbf{x}$  and  $\dot{\mathbf{x}}$  as follows:

$$\mathbf{u} = \mathbf{B}^{-1} \dot{\mathbf{x}} - \mathbf{B}^{-1} \mathbf{A}\mathbf{x} \quad (6.10)$$

If the inverse of  $\mathbf{B}$  exists, this control law will theoretically accomplish exact model following. For systems with fewer inputs than state variables, exact model following of all states is not possible. In this case, the pseudo-inverse of  $\mathbf{B}$  can be used in equation 6.10 to achieve approximate model following. This method of applying feedforward dynamic inversion to achieve model following aircraft control has been successfully demonstrated on aircraft in-flight-simulators by Rynaski [6.2] and Chetty [1.14].

### 6.6.2 Application to the MMF Control Law

The design plant model presented in section 6.5.2 is used in equation 6.10 to form the MMF dynamic inversion control law. Figure 6.9 shows the implementation of the dynamic inversion control law.

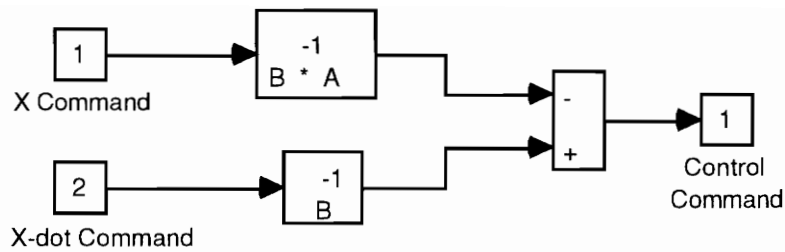


Figure 6.9 Dynamic Inversion Control Law

The dynamic inversion control law is then combined with the MCG and the design plant model, as shown in figure 6.10. The model following performance of this system is shown in figures 6.11 and 6.12. As explained in section 6.6.2, the plant state response will not track the commanded states exactly because the plant has fewer inputs than states. However, given that this controller is feedforward only and that feedback paths are yet to be added, this performance is perfectly acceptable.

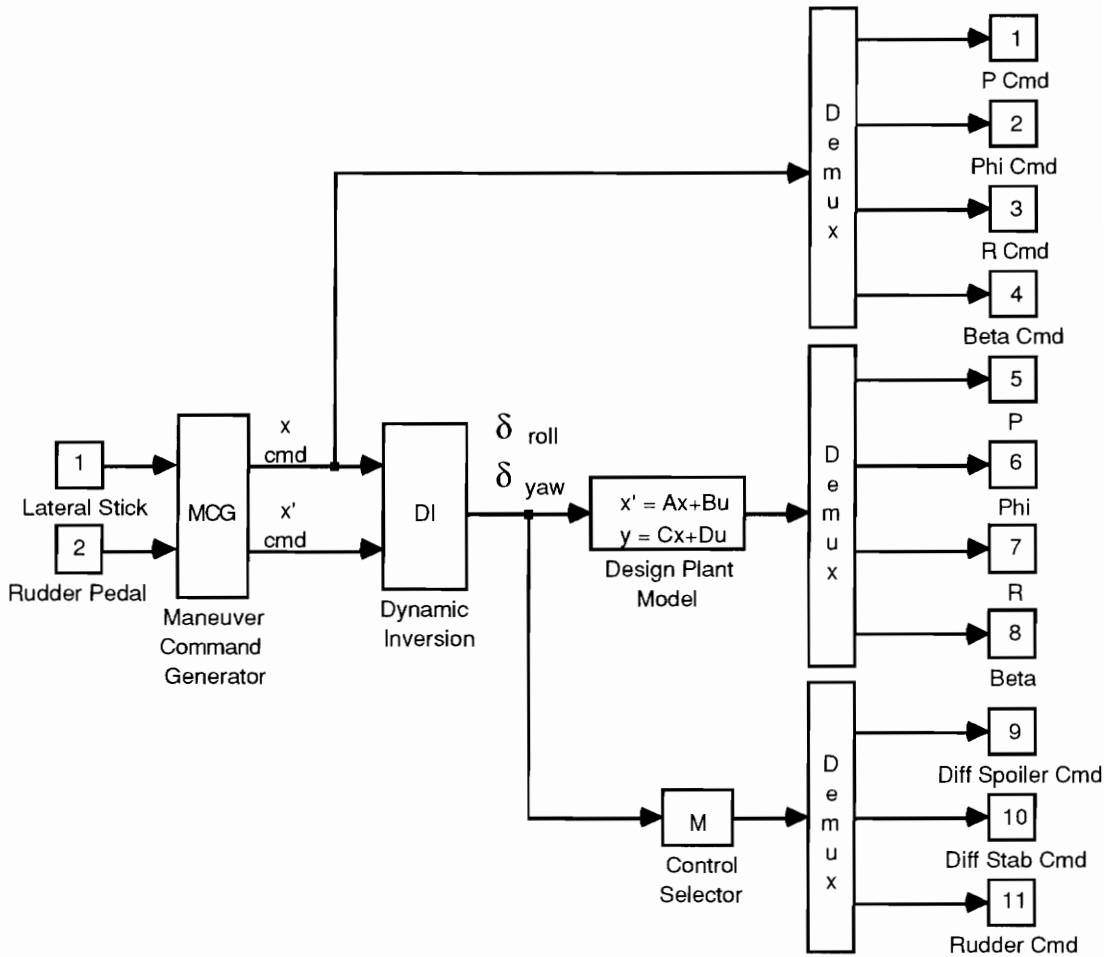


Figure 6.10 Combined MCG, Dynamic Inversion, and Design Plant Model

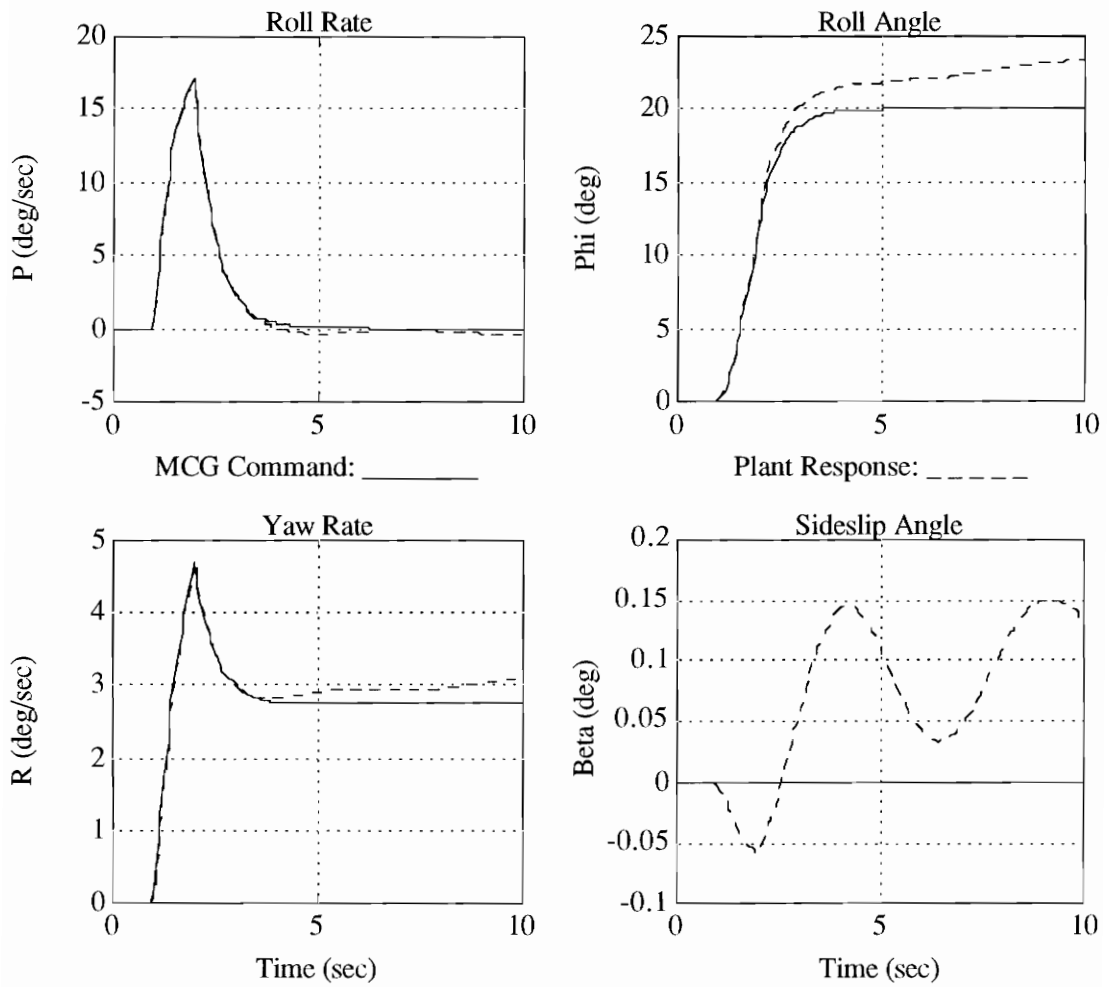


Figure 6.11 Combined MCG and Dynamic Inversion Response to Lateral Stick

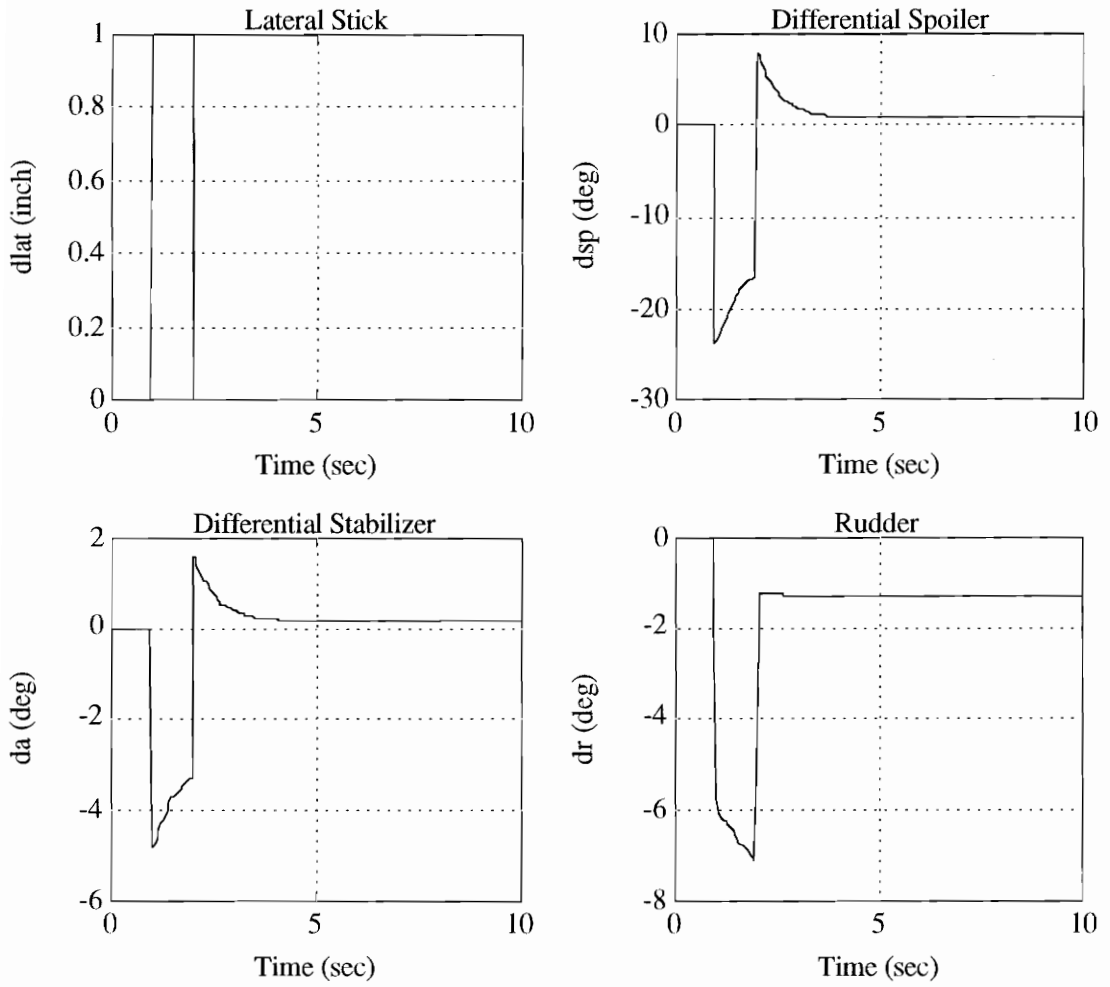


Figure 6.11 (Continued) Combined MCG and Dynamic Inversion Response to Lateral Stick

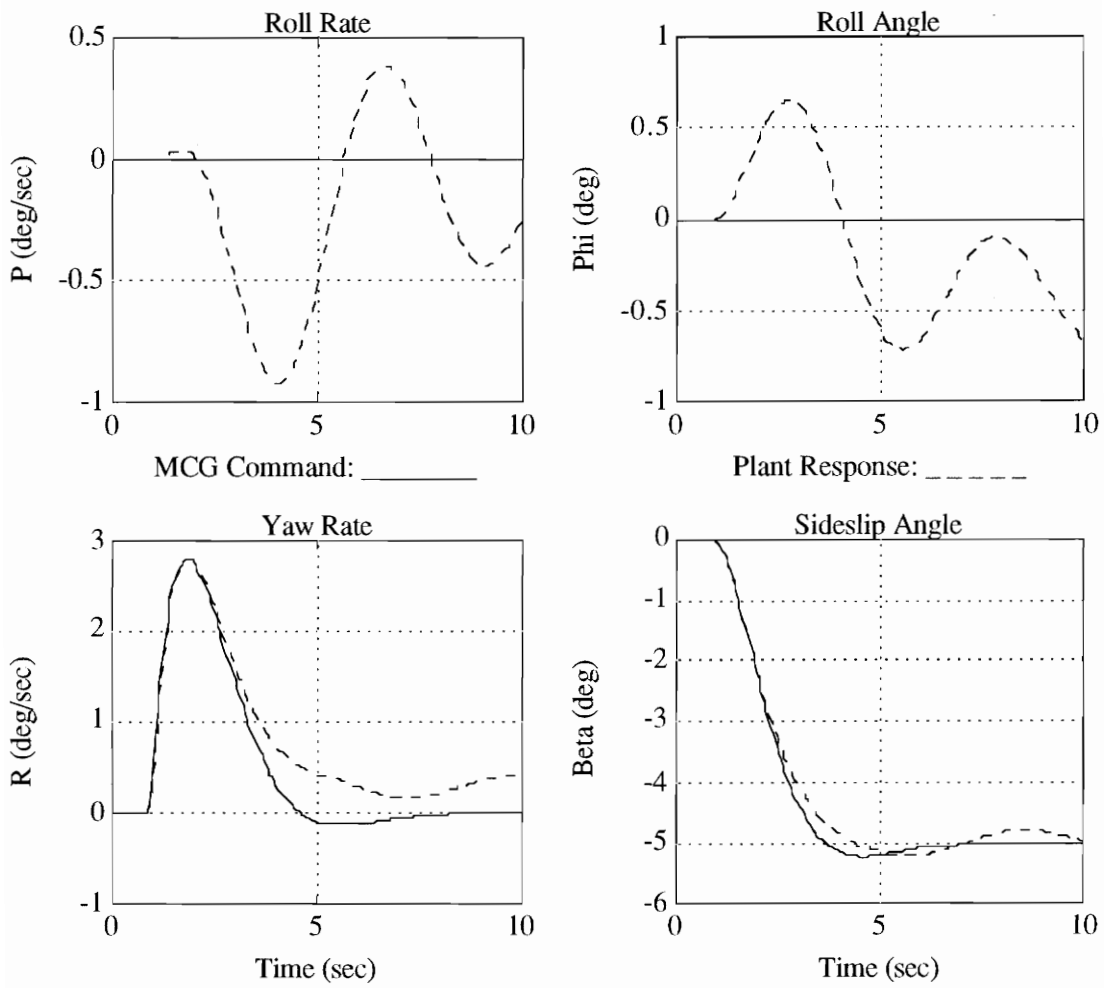


Figure 6.12 Combined MCG and Dynamic Inversion Response to Rudder Pedal

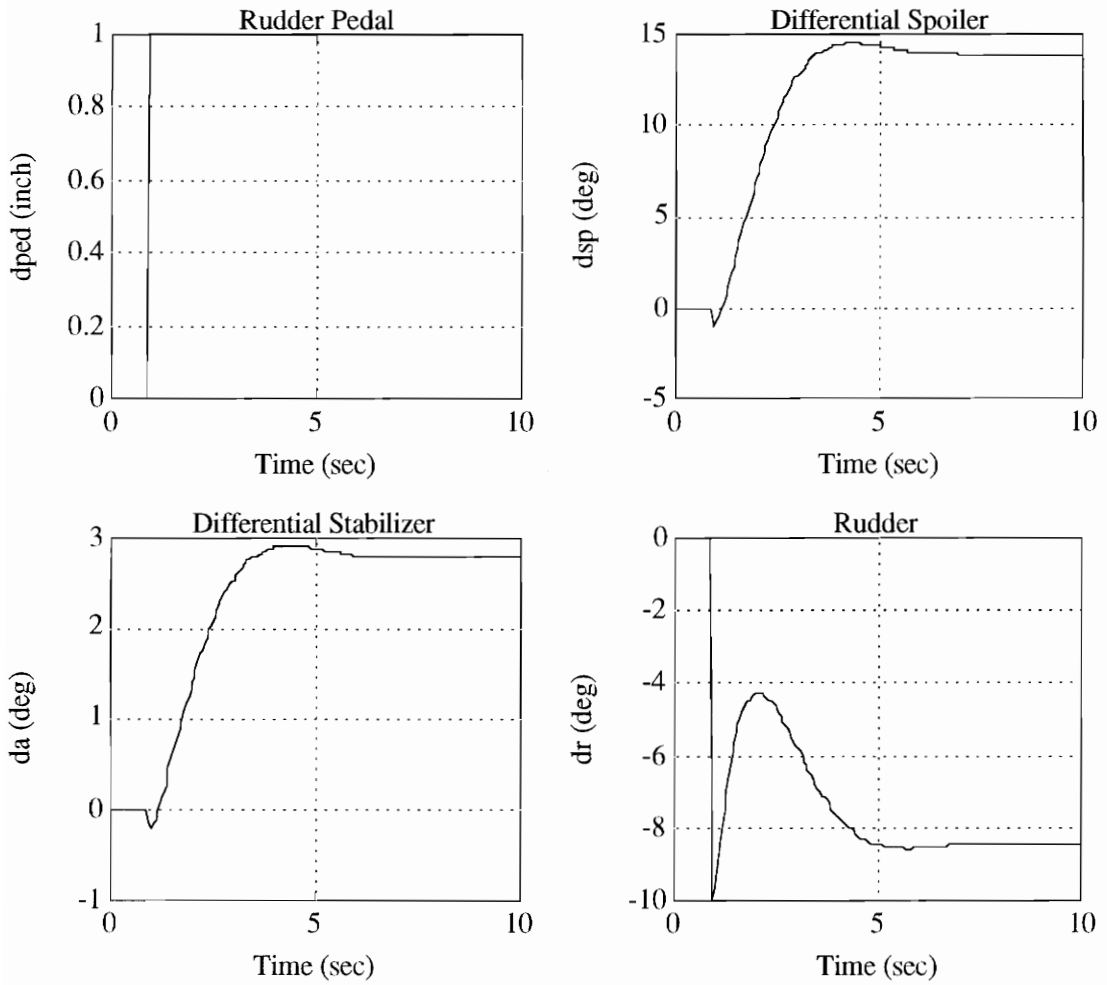


Figure 6.12 (Continued) Combined MCG and Dynamic Inversion Response to Rudder Pedal

## 6.7 Linear Quadratic Regulator Design

Linear quadratic regulator (LQR) theory is used to design a proportional plus integral regulator that operates on the error between the commanded states produced by the MCG and the plant states, which are assumed to be measurable (this assumption will be removed later when the state estimator is designed). The decision to design the regulator first, followed by the estimator was driven by the fact that one of the outputs desired to be integrally regulated (sideslip angle) was not measured.

### 6.7.1 Solution of the LQR Problem

The steady-state solution of the LQ regulator problem [6.4] is a full state feedback gain matrix for the linear time-invariant system of the form:

$$\dot{\mathbf{x}} = \mathbf{Ax} + \mathbf{Bu} \quad (6.11)$$

that minimizes a quadratic performance index given by:

$$J = \int_0^{\infty} (\mathbf{x}^T \mathbf{Q}_c \mathbf{x} + \mathbf{u}^T \mathbf{R}_c \mathbf{u}) dt \quad (6.12)$$

This performance index states that the desired control law ( $\mathbf{u}$ ) keeps the integral-squared-error of the state trajectories small without using excessive control power.  $\mathbf{Q}_c$  and  $\mathbf{R}_c$  are real, symmetric matrices chosen by the designer to determine the relative importance of each state and control to the cost function. Assuming that  $(\mathbf{A}, \mathbf{B})$  is stabilizable and  $(\mathbf{A}, \mathbf{Q}_c^{1/2})$  is detectable, the state feedback control law that minimizes the performance index is:

$$\mathbf{u} = -\mathbf{K}_c \mathbf{x} \quad (6.13)$$



where  $K_c$  is given by:

$$K_c = R_c^{-1} B^T P_c \quad (6.14)$$

and  $P_c$  is the positive definite solution to the steady-state algebraic Riccati equation:

$$0 = A^T P_c + P_c A - P_c B R_c^{-1} B^T P_c + Q_c \quad (6.15)$$

### 6.7.2 Application to the MMF Control Law

The LQ regulator is designed to track roll angle and sideslip angle commands with zero steady state error. For good performance, the minimum bandwidth of the regulator is chosen to be 2.0 rad/sec, while the maximum crossover frequency is limited to 10.0 rad/sec to insure robustness against unmodeled high frequency dynamics. These requirements on the LQ regulator return ratio are shown in figure 6.13.

The singular values of the design plant model are shown in figure 6.14. These singular values indicate that integration in each loop will be necessary to meet the design requirements. To accomplish this, integrators are augmented to the roll angle and sideslip angle outputs of the design plant model, as shown below:

$$\begin{bmatrix} \dot{x}_{dp} \\ \dot{x}_{\phi_1} \\ \dot{x}_{\beta_1} \end{bmatrix} = \begin{bmatrix} A_{dp} & 0 & 0 \\ C_{dp}(\phi) & 0 & 0 \\ C_{dp}(\beta) & 0 & 0 \end{bmatrix} \begin{bmatrix} x_{dp} \\ x_{\phi_1} \\ x_{\beta_1} \end{bmatrix} + \begin{bmatrix} B_{dp} \\ 0 \\ 0 \end{bmatrix} u_{dp} \quad (6.14)$$

$$\begin{bmatrix} \phi_1 \\ \beta_1 \end{bmatrix} = \begin{bmatrix} 0 & 1 & 0 \\ 0 & 0 & 1 \end{bmatrix} \begin{bmatrix} x_{dp} \\ x_{\phi_1} \\ x_{\beta_1} \end{bmatrix}$$

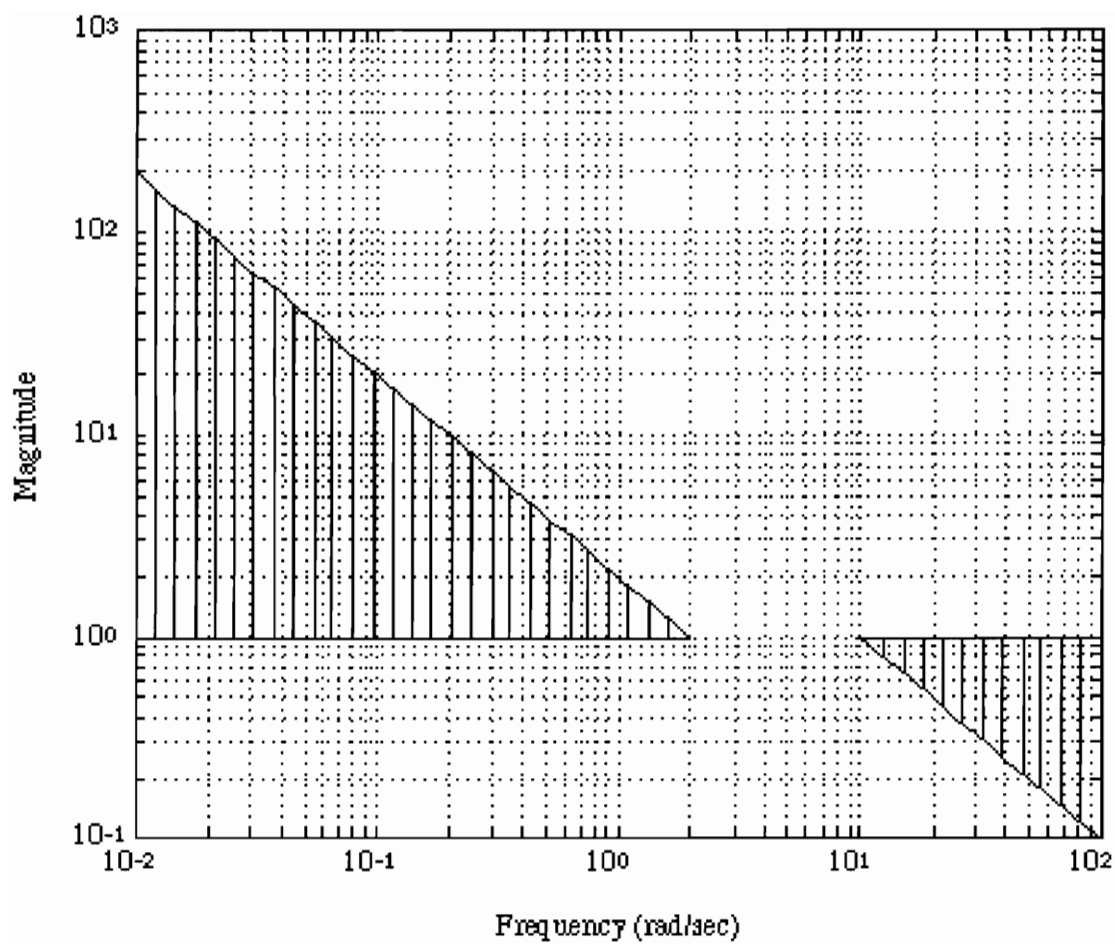


Figure 6.13 Performance and Robustness Specification

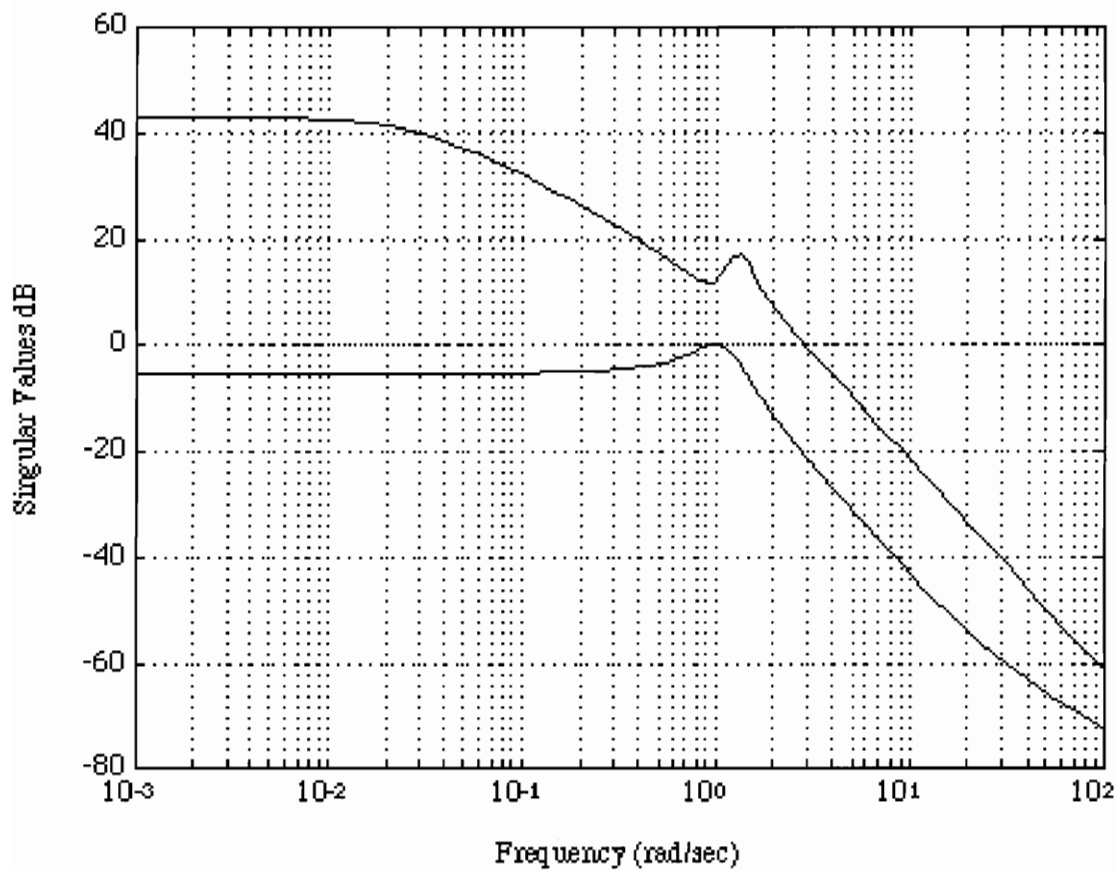


Figure 6.14 Open-loop Plant Singular Values

where  $C_{dp}(\phi)$  and  $C_{dp}(\beta)$  are the rows of  $C_{dp}$  associated with the  $\phi$  and  $\beta$  outputs. The state space quadruple defined by (6.14) shall be denoted  $A_a, B_a, C_a, D_a$ . The augmented plant is also shown below in figure 6.15.

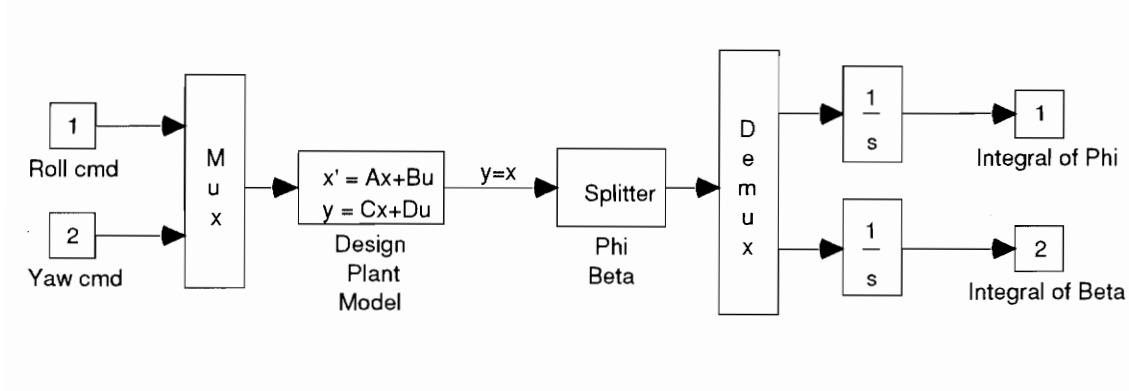


Figure 6.15 Plant Augmented with Integrals of Phi and Beta

The open-loop singular values of the augmented plant are shown in figure 6.16. These singular values show that each loop can now achieve zero steady-state tracking error. Once the augmented plant is formed, the state and control input weighting matrices,  $Q_c$  and  $R_c$  are defined. A common technique [6.4] for the selection of  $Q_c$  is to define a set of performance outputs as follows:

$$z = Hx \quad (6.15)$$

The performance outputs are a linear combination of the plant states. The state weighting matrix is then computed from the performance output matrix as follows:

$$Q_c = H^T H \quad (6.16)$$

The quadratic cost function can also be expressed in terms of the performance outputs as follows:

$$J = \int_0^{\infty} (z^T z + u^T R_c u) dt \quad (6.17)$$

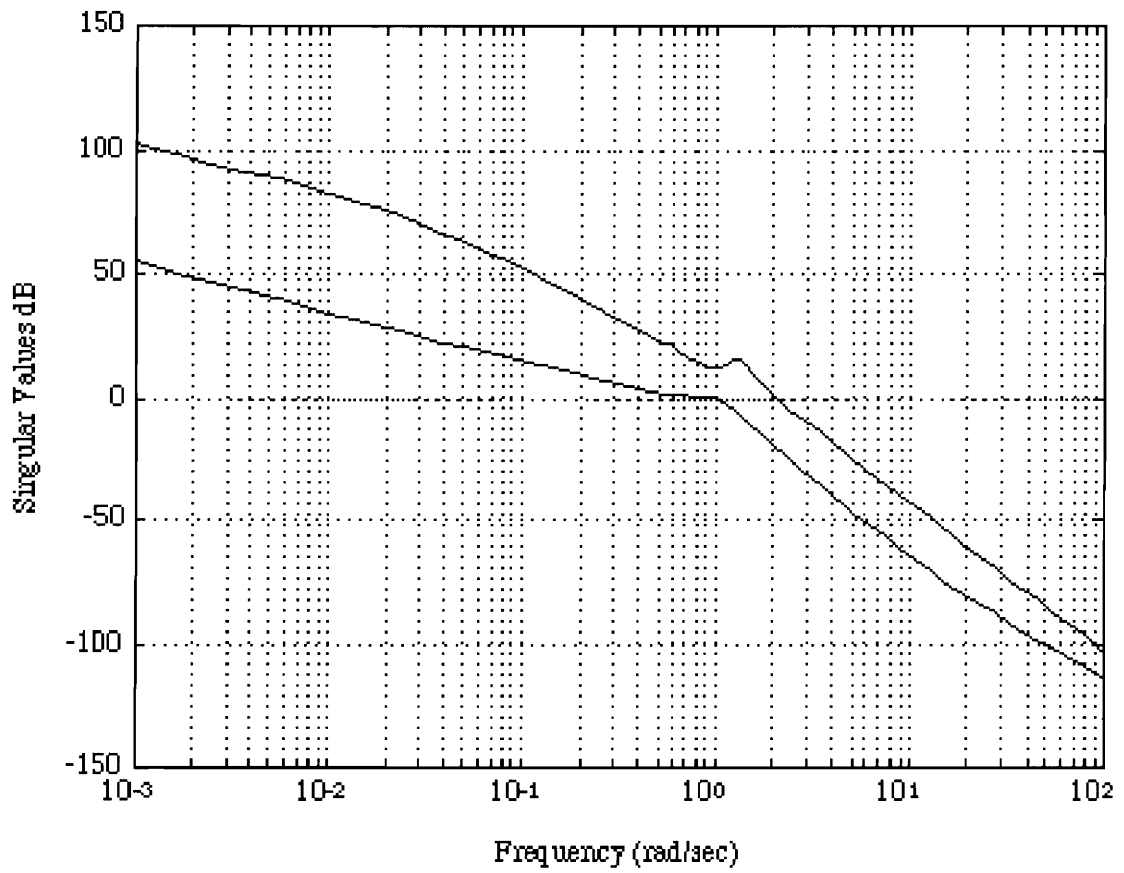


Figure 6.16 Augmented Plant Singular Values

which shows that choosing  $Q_c = H^T H$  results in the regulation of the system responses given by (6.15). Preliminary designs were performed using  $H = C_a$ . The performance outputs for this case are:

$$\begin{aligned} z_1 &= \frac{\phi}{s} \\ z_2 &= \frac{\beta}{s} \end{aligned} \tag{6.18}$$

After a few iterations, the desired results were obtained using the following performance outputs:

$$\begin{aligned} z_1 &= \phi + 2\frac{\phi}{s} \\ z_2 &= 6\beta + 10\frac{\beta}{s} \end{aligned} \tag{6.19}$$

These performance outputs are specified by the following H matrix:

H =

$$\begin{bmatrix} 0 & 1 & 0 & 0 & 2 & 0 \\ 0 & 0 & 0 & 6 & 0 & 10 \end{bmatrix}$$

This choice of H results in the following  $Q_c$ :

$Q_c =$

$$\begin{bmatrix} 0 & 0 & 0 & 0 & 0 & 0 \\ 0 & 1 & 0 & 0 & 2 & 0 \\ 0 & 0 & 0 & 0 & 0 & 0 \\ 0 & 0 & 0 & 36 & 0 & 60 \\ 0 & 2 & 0 & 0 & 4 & 0 \\ 0 & 0 & 0 & 60 & 0 & 100 \end{bmatrix}$$

The input weighting matrix,  $R_c$ , is selected to be identity, as follows:

$$R_c = \begin{bmatrix} 1 & 0 \\ 0 & 1 \end{bmatrix}$$

For this  $Q_c$  and  $R_c$  the LQ regulator gains are:

$$K_c = \begin{bmatrix} -0.6701 & -1.8997 & 0.6644 & -3.4383 & -1.7945 & -4.4156 \\ 0.4925 & -0.5018 & -4.3205 & 8.7971 & -0.8831 & 8.9723 \end{bmatrix}$$

The singular values of  $K_c(sI - A)^{-1}B$  are shown below in figure 6.17, which shows that the required specifications are satisfied. The guaranteed stability robustness properties of the LQ regulator are demonstrated by computing the singular values of the sensitivity function (S) and complementary sensitivity function (T), as defined below:

$$S = (I + G)^{-1} \quad (6.20)$$

$$T = G(I + G)^{-1} \quad (6.21)$$

where  $G = K_c(sI - A)^{-1}B$ . The maximum singular values of the S and T functions are shown in figure 6.18. The Kalman inequality [6.4] guarantees that the regulator gain and phase margins are at least:

$$1/2 < GM < \infty \quad (6.22)$$

$$-60^\circ < PM < 60^\circ \quad (6.23)$$

Due to numerical precision, the computed gain margin is only 211.8.

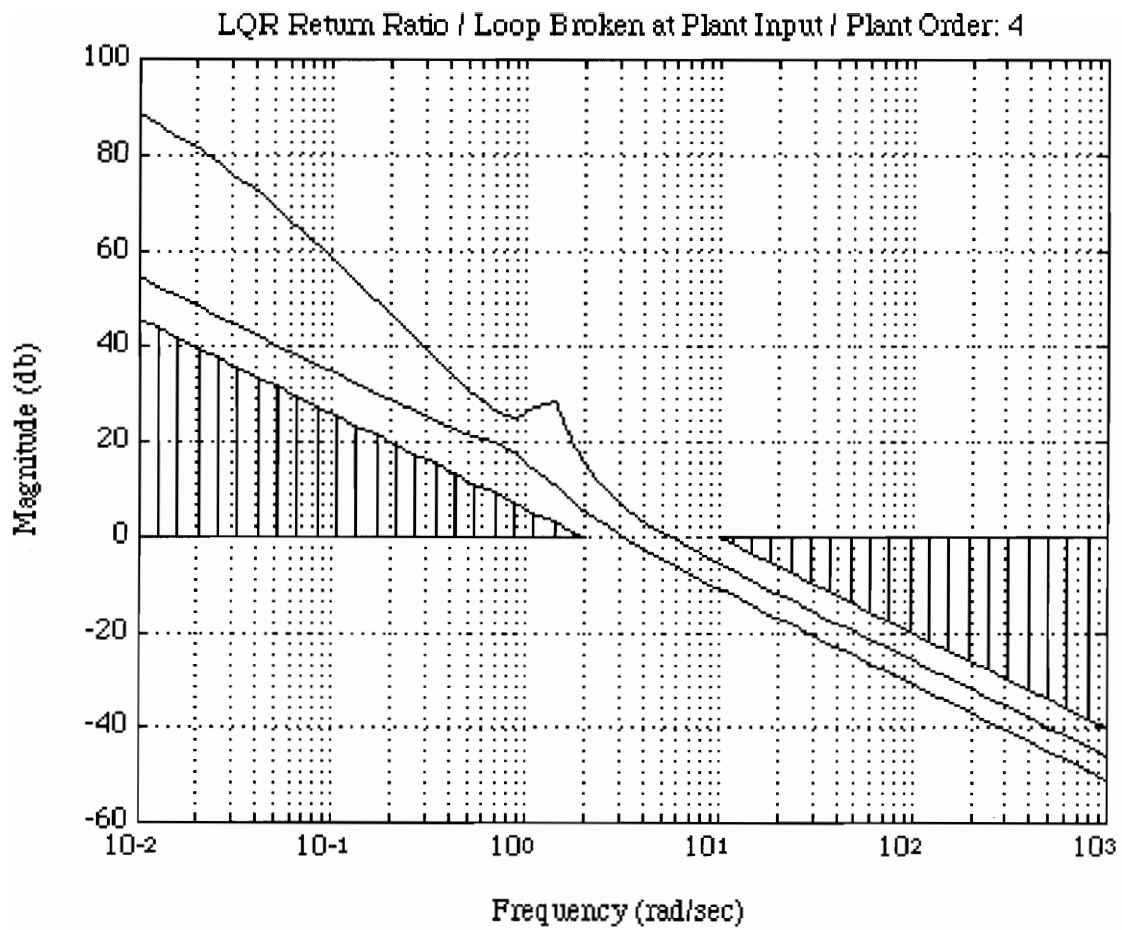


Figure 6.17 LQR Input Return Ratio Singular Values



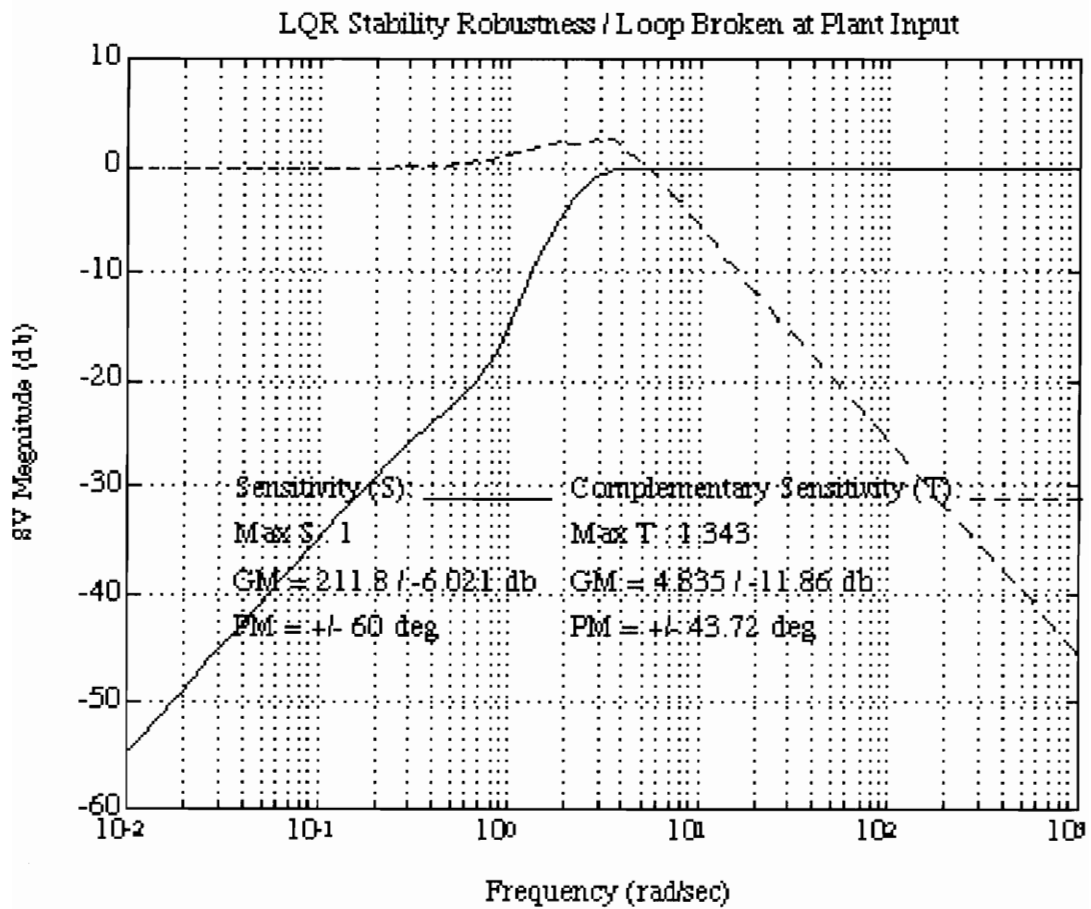


Figure 6.18 LQR MIMO Stability Robustness

The closed-loop modes of the regulator are:

Eigenvalue	Damping	Freq (r/s)	Mode
-2.0201 + 2.5185i	0.6257	3.2286	Dutch-roll
-2.0201 - 2.5185i	0.6257	3.2286	Dutch-roll
-1.2212 + 1.6298i	0.5996	2.0365	Integrator
-1.2212 - 1.6298i	0.5996	2.0365	Integrator
-1.8984	1.0000	1.8984	Roll
-1.3555	1.0000	1.3555	Spiral

The modes of the closed-loop regulator were identified by plotting the root-locus of the regulator as a scalar multiplier on the state feedback gain matrix was varied from 0 to 1, as shown in figure 6.19. This is not a symmetric root-locus, as would be obtained from the variation of the regulator cost function Q to R ratio. For closed-loop time response evaluation of the regulator, the system is modeled as shown in figure 6.20. This requires that the state feedback gains be partitioned into the integrator gains and the aircraft state gains, as shown below:

$K_i =$

$$\begin{bmatrix} -1.7945 & -4.4156 \\ -0.8831 & 8.9723 \end{bmatrix}$$

$K_x =$

$$\begin{bmatrix} -0.6701 & -1.8997 & 0.6644 & -3.4383 \\ 0.4925 & -0.5018 & -4.3205 & 8.7971 \end{bmatrix}$$

The closed-loop responses to roll angle and sideslip angle command steps are shown in figures 6.21 and 6.22, respectively. The roll angle response to roll angle command is essentially deadbeat, with a settling time of approximately 3 seconds and with very little sideslip excursion. The sideslip response to sideslip command is also deadbeat, with a settling time of approximately 3 seconds.

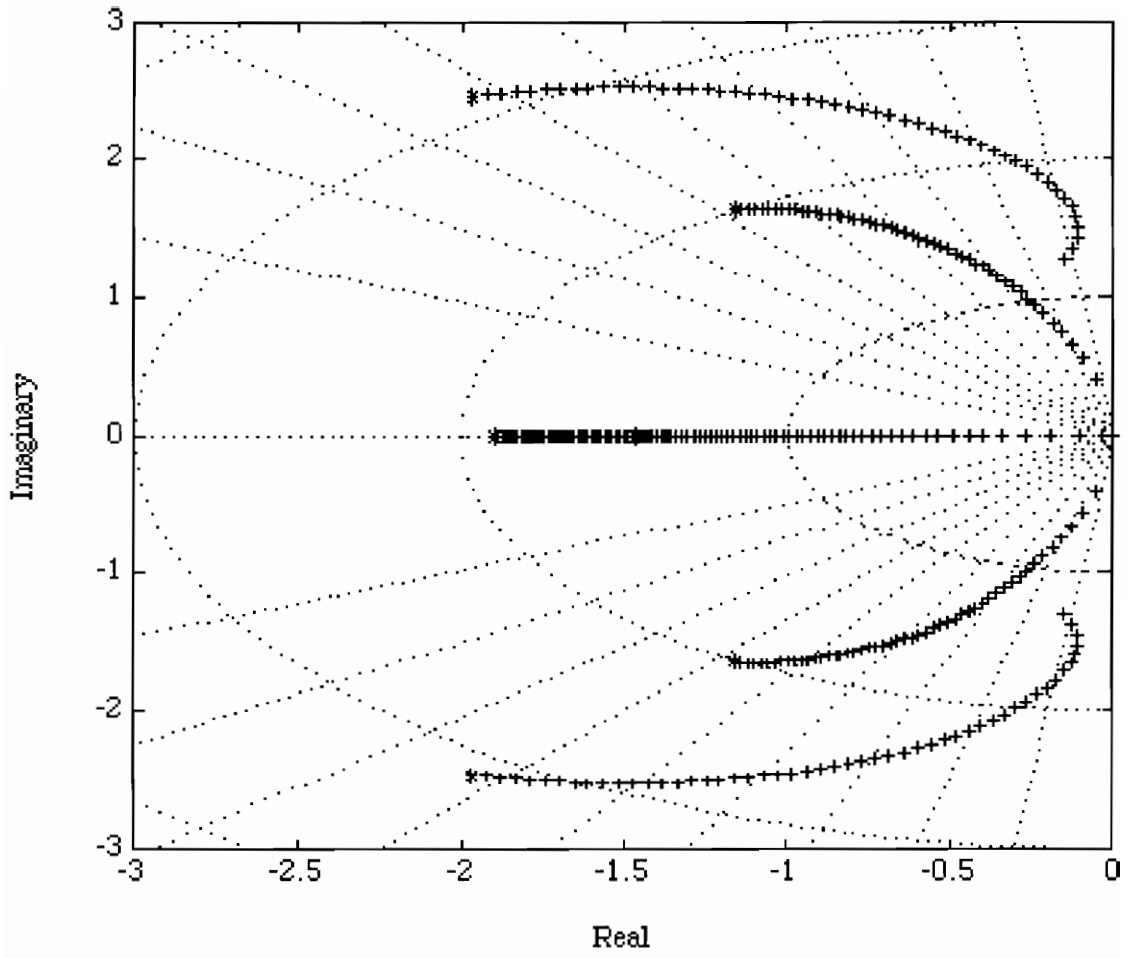


Figure 6.19 Regulator Root-Locus

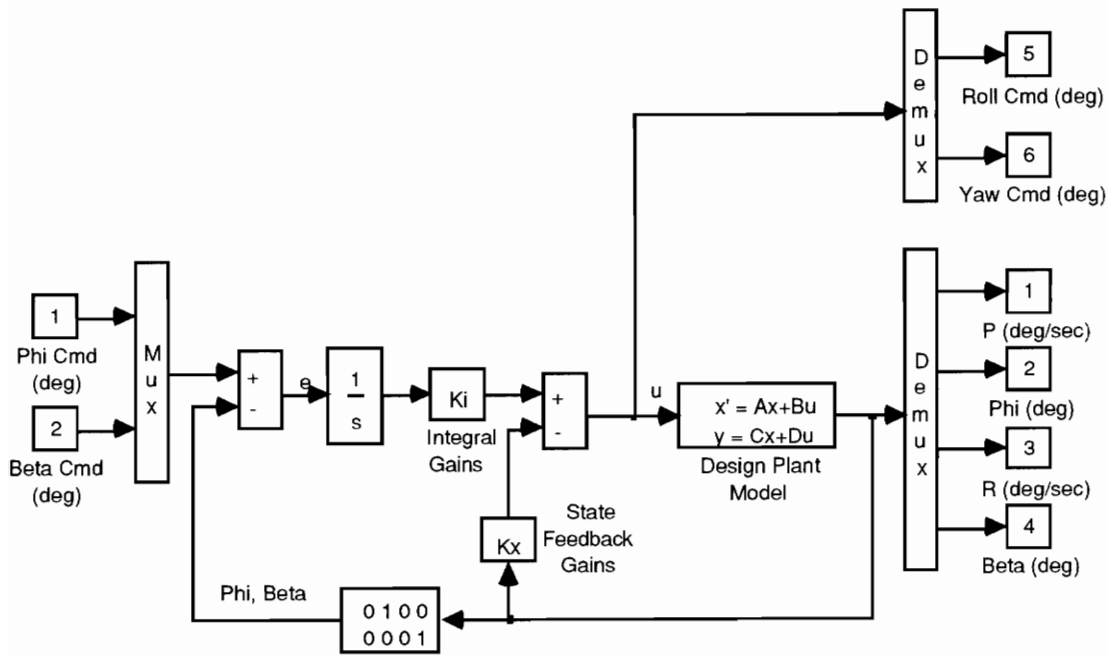


Figure 6.20 Closed-loop LQ Regulator

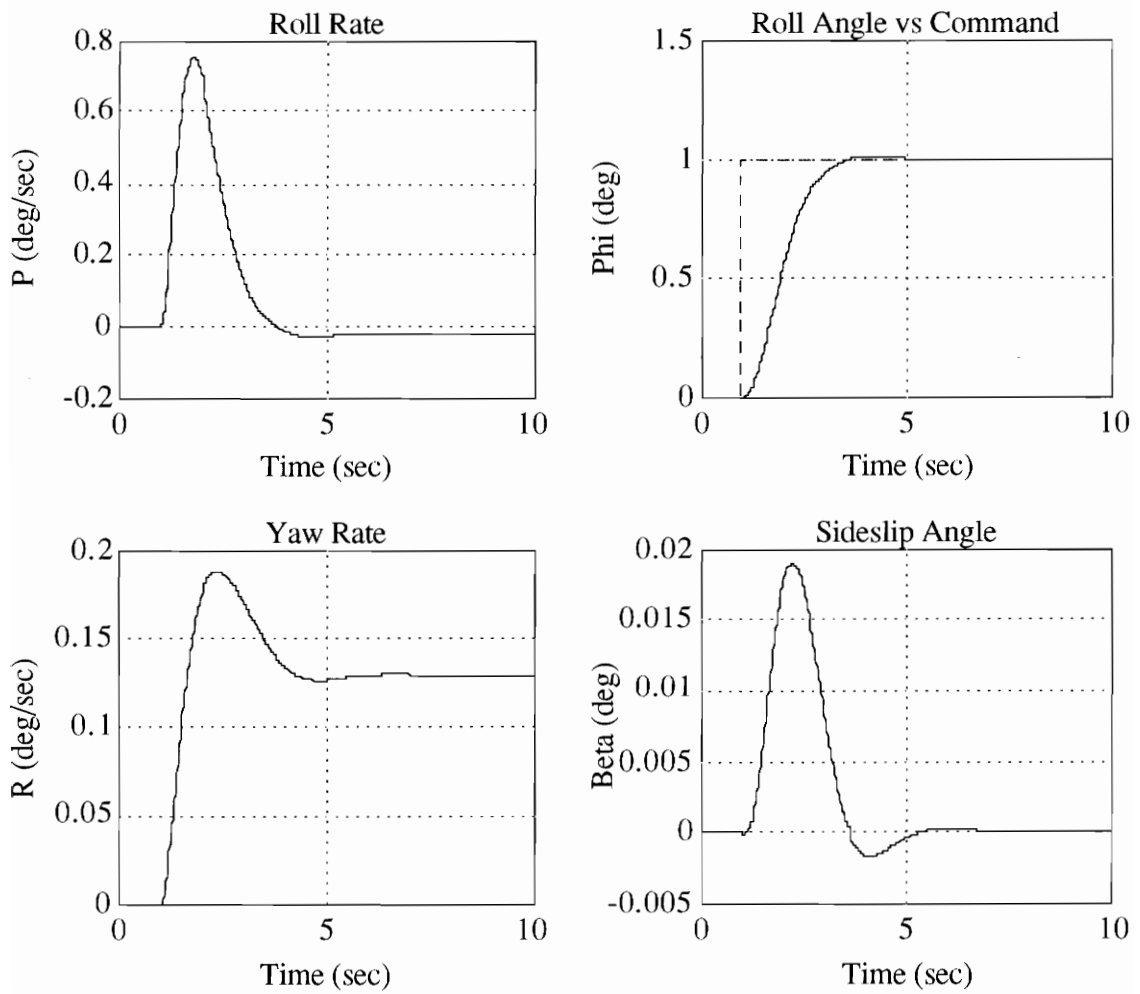


Figure 6.21 LQR Response to Roll Angle Step Command

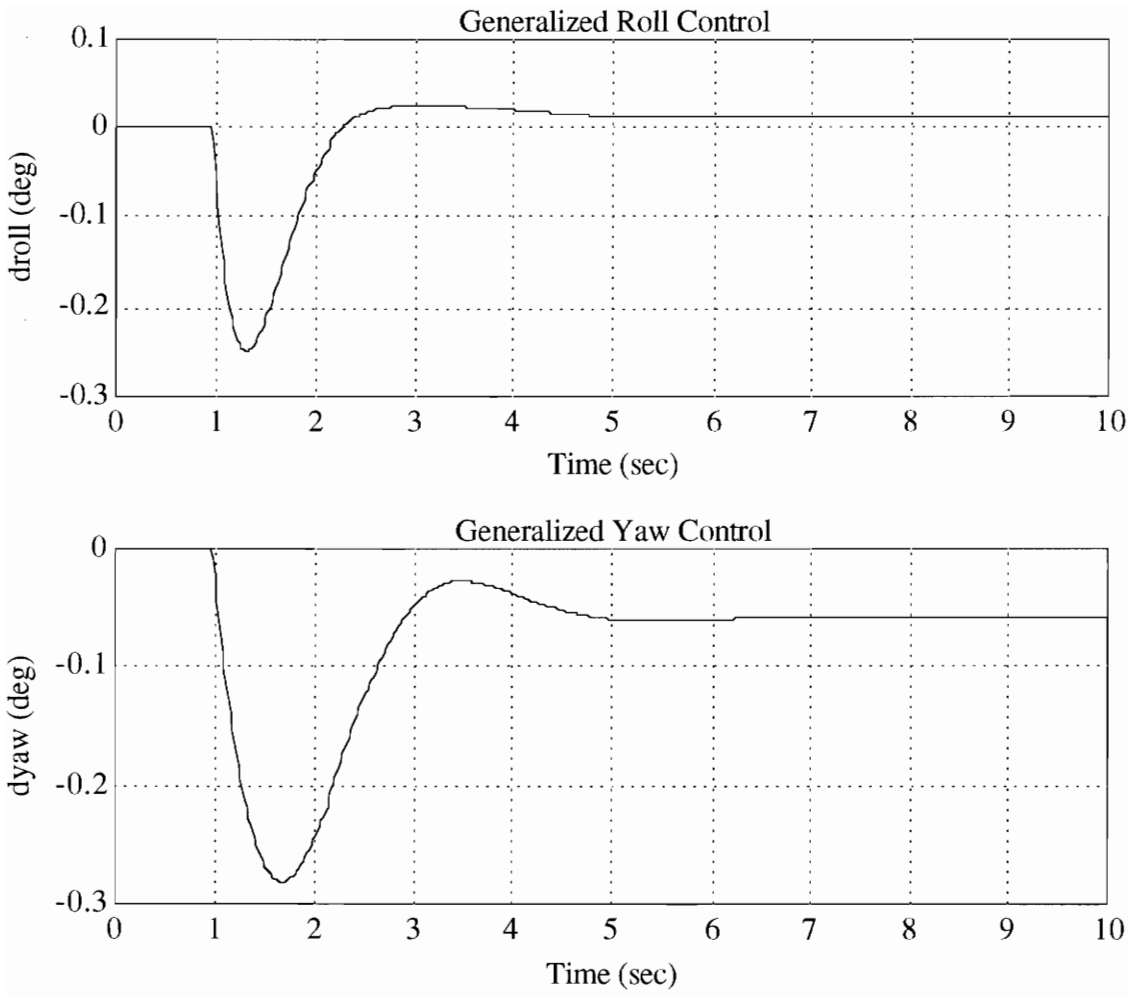


Figure 6.21 (Continued) LQR Response to Roll Angle Step Command

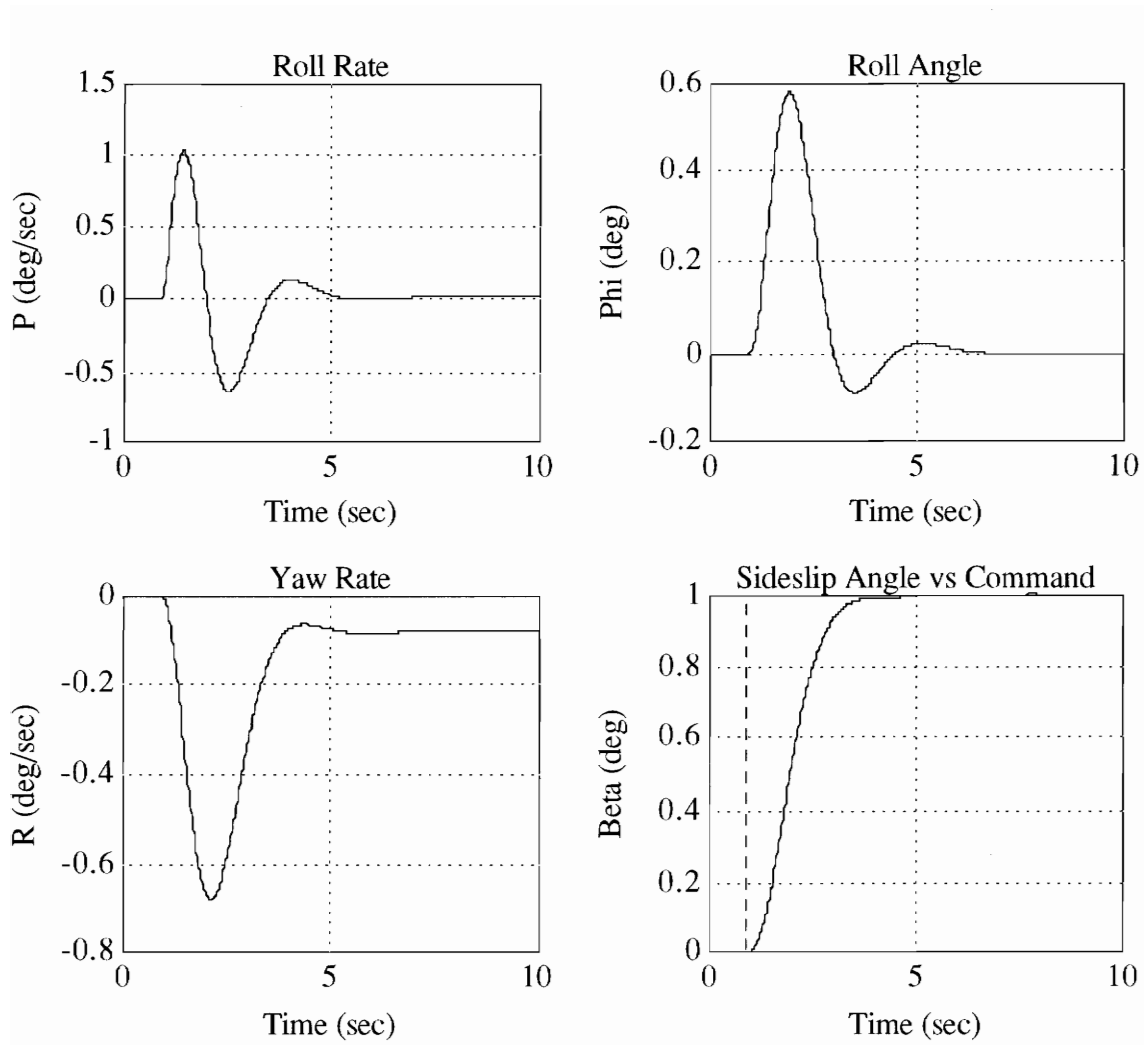


Figure 6.22 LQR Response to Sideslip Angle Step Command

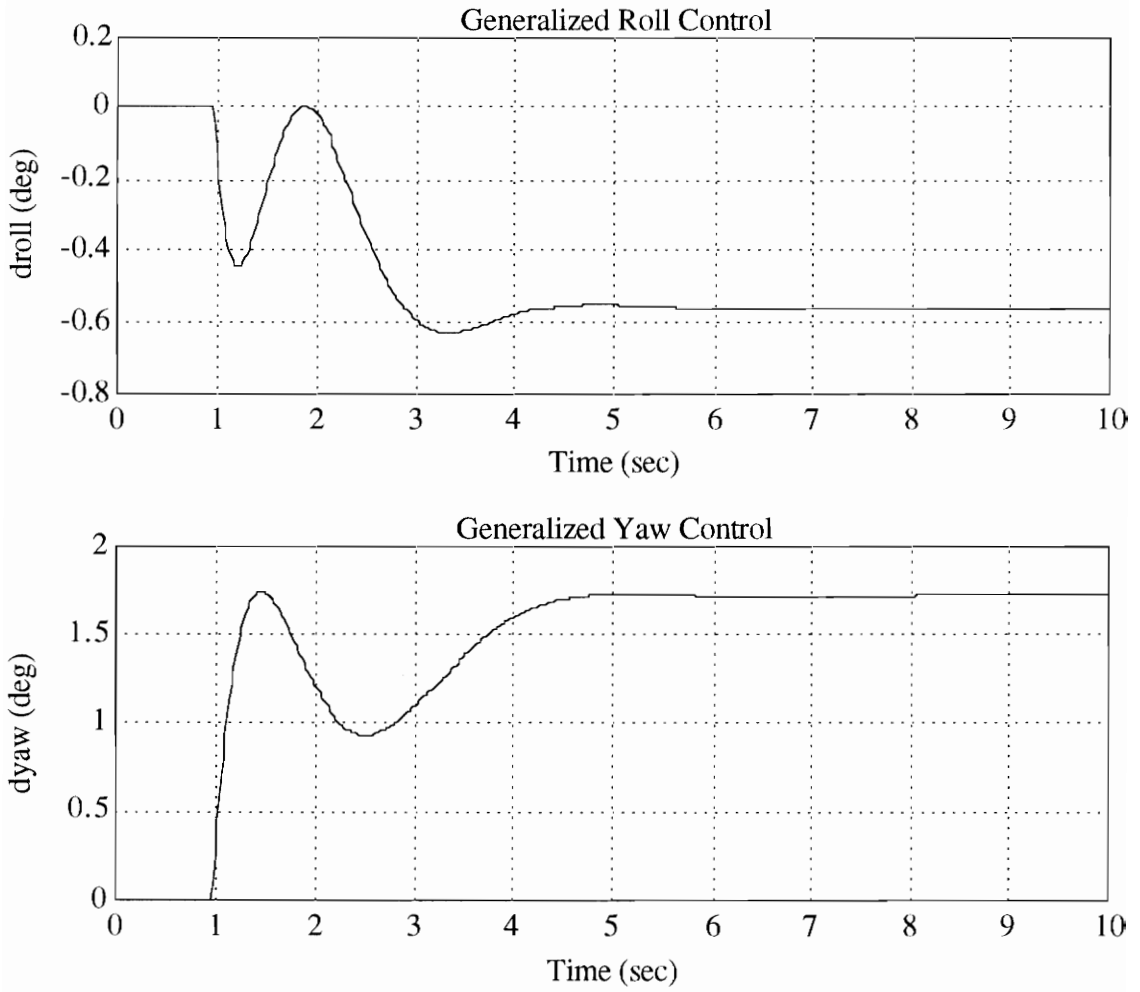


Figure 6.22 (Continued) LQR Response to Sideslip Angle Step Command



However, the transient roll response for a sideslip command is somewhat greater than desired (almost 0.6 deg). This characteristic will disappear once the regulator is combined with the MCG and dynamic inversion forward path.

## 6.8 Reduced Order Estimator with Loop Transfer Recovery

### 6.8.1 Design Procedure

The regulator designed in the previous section assumed that all states were available for feedback. The reality of the situation is that roll rate, roll angle, and yaw rate are measured while sideslip is not. To complete the feedback controller design, a sideslip estimate is required. The typical approach to estimator design that preserves the robustness properties of the regulator is called Loop Transfer Recovery (LTR). LTR consists of designing a full-state Kalman filter using the modified process noise intensity matrix:

$$Q_f = Q_o + q^2 BB^T \quad (6.24)$$

As the parameter  $q$  is increased towards infinity, the robustness of the LQG compensated system asymptotically approaches that of the pure regulator. If the  $n$ -th order plant has  $z$  minimum phase transmission zeros, the resulting compensator will have  $z$  poles at these locations and  $n-z$  poles approaching infinity. An iterative process is then required to decide how high to increase  $q$  at the cost of noise sensitivity and compensator realizability. Compensator poles approaching infinity are normally truncated.

Recognizing the iterative process inherent in a typical LTR design, Bacon suggested [6.5] an alternate approach that directly achieves loop transfer recovery in the form of a reduced order observer. The key assumption in applying the Bacon technique is that the product of the system matrices  $CB$  is full rank, i.e.,

$$\det(CB) \neq 0 \quad (6.25)$$

This condition will be satisfied for any system where the number of transmission zeros is equal to or exceeds the number of states minus the number of measurements. The following 3 step procedure is then used to find the reduced order observer:

- 1: Compute the singular value decomposition of  $B$

$$B = [U_1 \quad U_2] \begin{bmatrix} \Sigma_B \\ 0 \end{bmatrix} V^T \quad (6.26)$$

- 2: Define  $T = U_2^T$  and

$$\begin{bmatrix} T \\ C \end{bmatrix}^{-1} = [L_1 \quad L_2] \quad (6.27)$$

- 3: The reduced order observer equations are then

$$\begin{aligned} \dot{x}_{\text{roo}} &= A_{\text{roo}} x_{\text{roo}} + B_{\text{roo}} u_{\text{roo}} \\ y_{\text{roo}} &= C_{\text{roo}} x_{\text{roo}} + D_{\text{roo}} u_{\text{roo}} \end{aligned} \quad (6.28)$$

where

$$\begin{aligned} A_{\text{roo}} &= T A L_1 \\ B_{\text{roo}} &= T A L_2 \\ C_{\text{roo}} &= L_1 \\ D_{\text{roo}} &= L_2 \end{aligned} \quad (6.29)$$

The unaugmented plant with generalized controls given in section 6.5.2 is used to compute the reduced order observer. However, the C and D matrices are truncated to reflect the fact that sideslip is not measured. The resulting plant model used for the reduced order observer design is:

A =

$$\begin{bmatrix} -1.3283 & 0 & 0.6524 & -4.9049 \\ 1.0000 & 0 & 0.1853 & 0 \\ -0.1407 & 0 & -0.2520 & 0.6546 \\ 0.1852 & 0.1327 & -0.9795 & -0.1129 \end{bmatrix}$$

B =

$$\begin{bmatrix} -8.2147 & 0.2087 \\ 0 & 0 \\ -0.7555 & -0.6423 \\ 0.0149 & 0.0243 \end{bmatrix}$$

C =

$$\begin{bmatrix} 1.0000 & 0 & 0 & 0 \\ 0 & 1.0000 & 0 & 0 \\ 0 & 0 & 1.0000 & 0 \end{bmatrix}$$

D =

$$\begin{bmatrix} 0 & 0 \\ 0 & 0 \\ 0 & 0 \end{bmatrix}$$

where the state vector (x) is:

p	roll rate (deg/sec)
$\phi$	roll angle (deg)
r	yaw rate (deg/sec)
$\beta$	sideslip angle (deg)

the generalized control input vector ( $g$ ) is:

$\delta_{roll}$	roll command (deg)
$\delta_{yaw}$	yaw command (deg)

and the measured output vector ( $y$ ) is:

$p$	roll rate (deg/sec)
$\phi$	roll angle (deg)
$r$	yaw rate (deg/sec)

The plant model has 1 transmission zero located at:

-0.0805

Since 3 measurements are available, the rank requirements of CB should be satisfied. The singular values of the matrix product CB are:

8.2507  
0.6586

which shows that CB is full rank. Application of the 3 step algorithm outlined above results in the following reduced order observer:

$A_{roo} =$

-0.0805

$B_{roo} =$

0.1443      0.1295      -0.9925

$C_{roo} =$

0  
0  
0

$$1.0014$$

$$D_{\text{roo}} = \begin{bmatrix} 1.0000 & 0 & 0 \\ 0 & 1.0000 & 0 \\ 0 & 0 & 1.0000 \\ 0.0016 & 0.0375 & -0.0374 \end{bmatrix}$$

The closed-loop LQG system is shown in figure 6.23. The eigenvalues of the closed-loop system are:

Eigenvalue	Damping	Freq (r/s)	Mode
-2.0201 + 2.5185i	0.6257	3.2286	Dutch-roll
-2.0201 - 2.5185i	0.6257	3.2286	Dutch-roll
-1.2212 + 1.6298i	0.5996	2.0365	Integrator
-1.2212 - 1.6298i	0.5996	2.0365	Integrator
-1.8984	1.0000	1.8984	Roll
-1.3555	1.0000	1.3555	Spiral
-0.0805	1.0000	0.0805	Observer

The eigenvalues for the LQG system are simply the union of the eigenvalues of the regulator (section 6.7.2) only plus the lone observer pole, which is a result of the separation theorem.

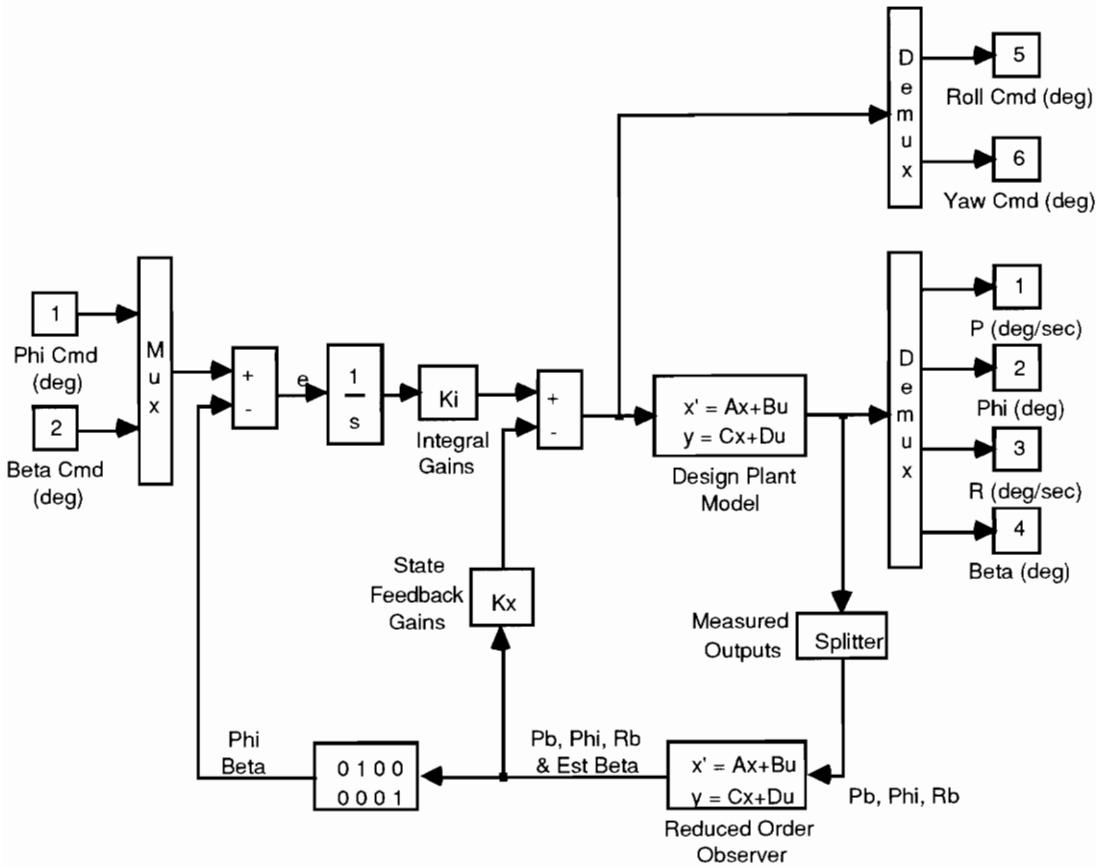


Figure 6.23 Closed-loop LQG System

### 6.8.2 Robustness Analysis

The robustness recovery achieved by the reduced order observer is demonstrated by computing the plant input open-loop return ratio singular values. The system model used for this analysis is shown in figure 6.24. Figure 6.25 shows the LQR vs the LQG input return ratio singular values. As expected, the LQG system achieves perfect loop transfer recovery. However, there are no guarantees for the loop properties at the plant output. To investigate the stability robustness properties at the plant output, the open-loop model shown in figure 6.26 is used. Figure 6.27 shows the LQG output return ratio singular values. Since 3 measurements are being used to regulate 2 variables (roll angle and sideslip), a certain degree of redundancy exists in the measurements which results in the near singularity of the return ratio. The 2 channels which carry the majority of the energy also fail to meet the required specifications (albeit the input return ratio specifications). The resulting reduced robustness at the outputs is demonstrated by the sensitivity and complementary sensitivity functions, as shown in figure 6.28.

### 6.8.3 Transient Response

The closed-loop LQG system in figure 6.23 is used to compute the closed-loop response to command inputs. The responses are overplotted with the same responses obtained from the closed-loop LQR system. As expected, the response to roll angle and sideslip angle commands is identical to that obtained with the LQ regulator alone, as shown in figures 6.29 and 6.30.

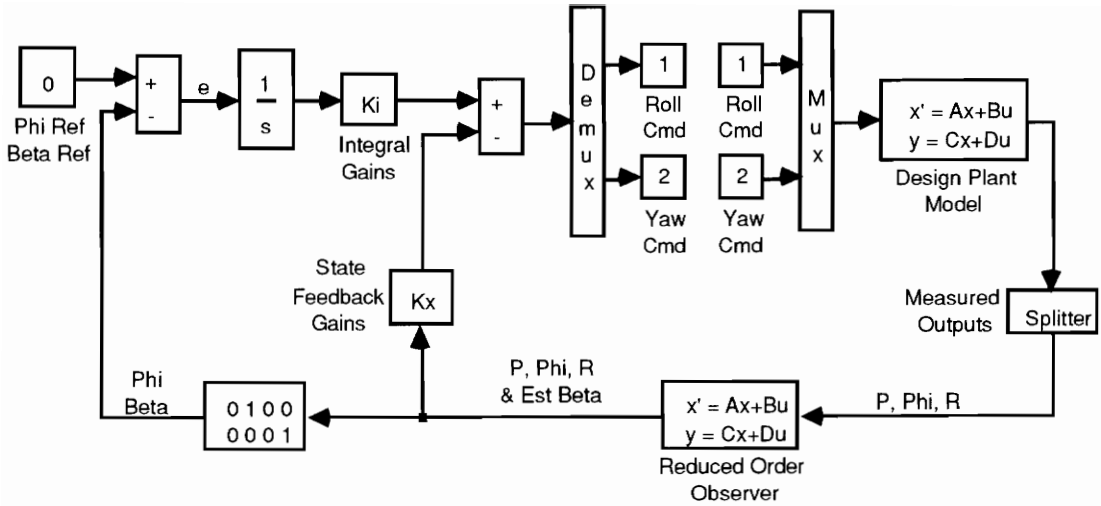


Figure 6.24 LQG System with Loop Opened at Plant Input



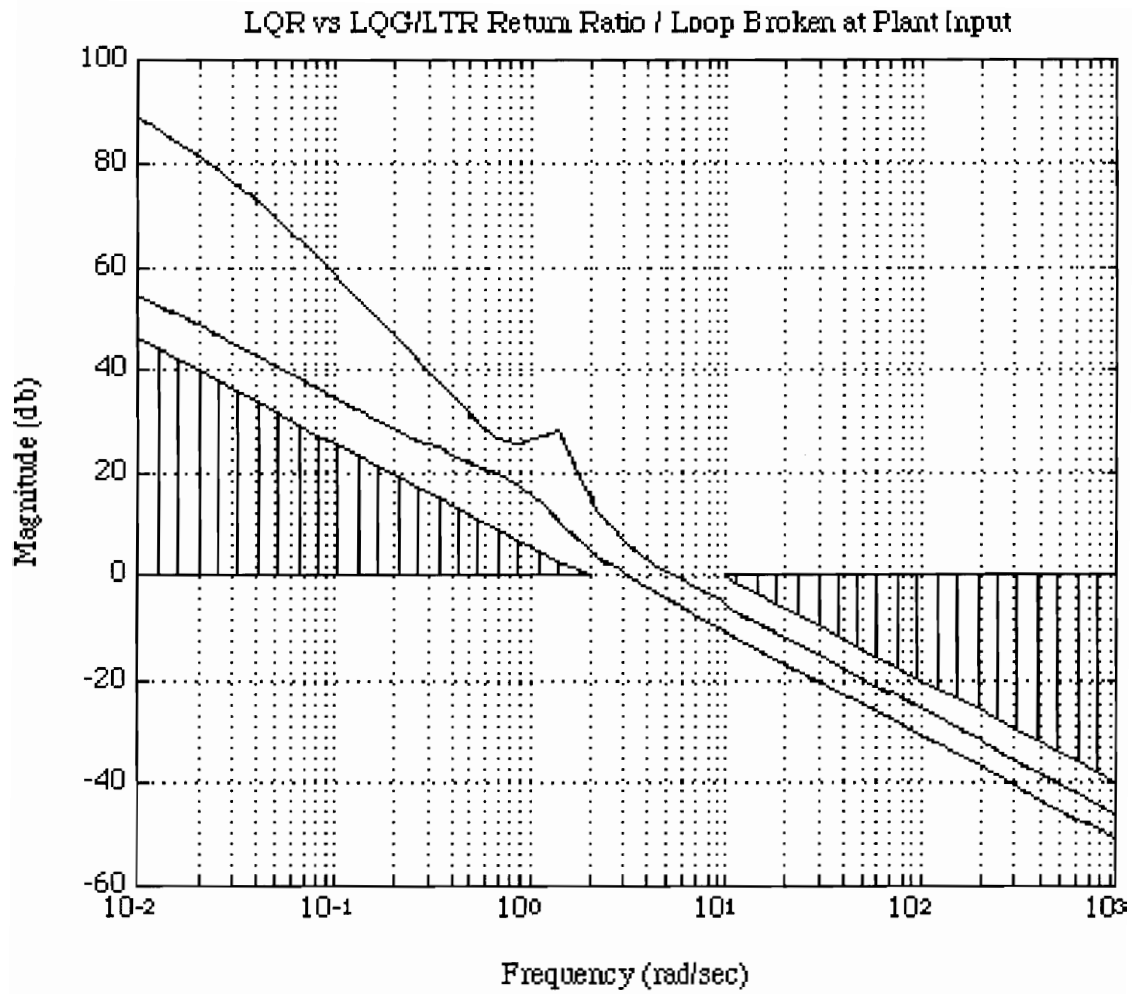


Figure 6.25 LQR vs LQG/LTR Input Return Ratio Singular Values

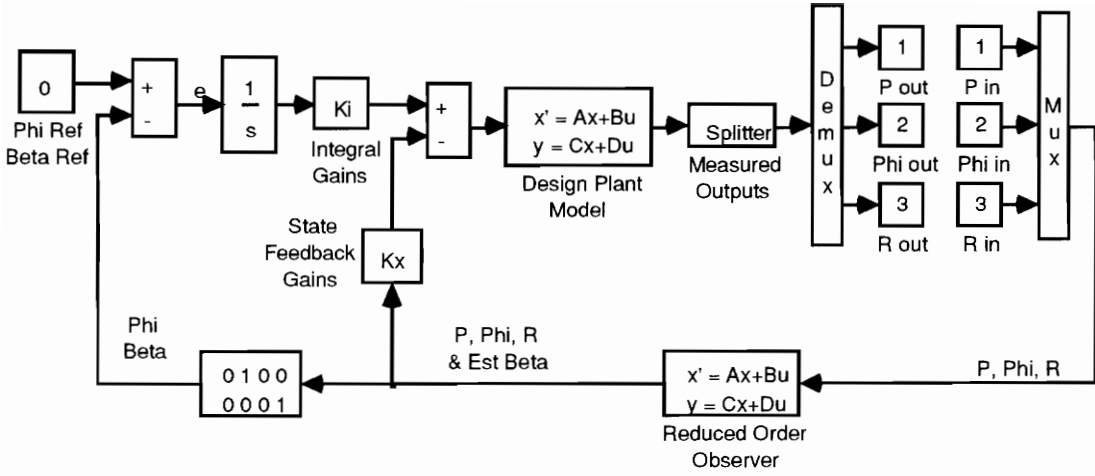


Figure 6.26 LQG/LTR System with Loop Opened at Plant Output

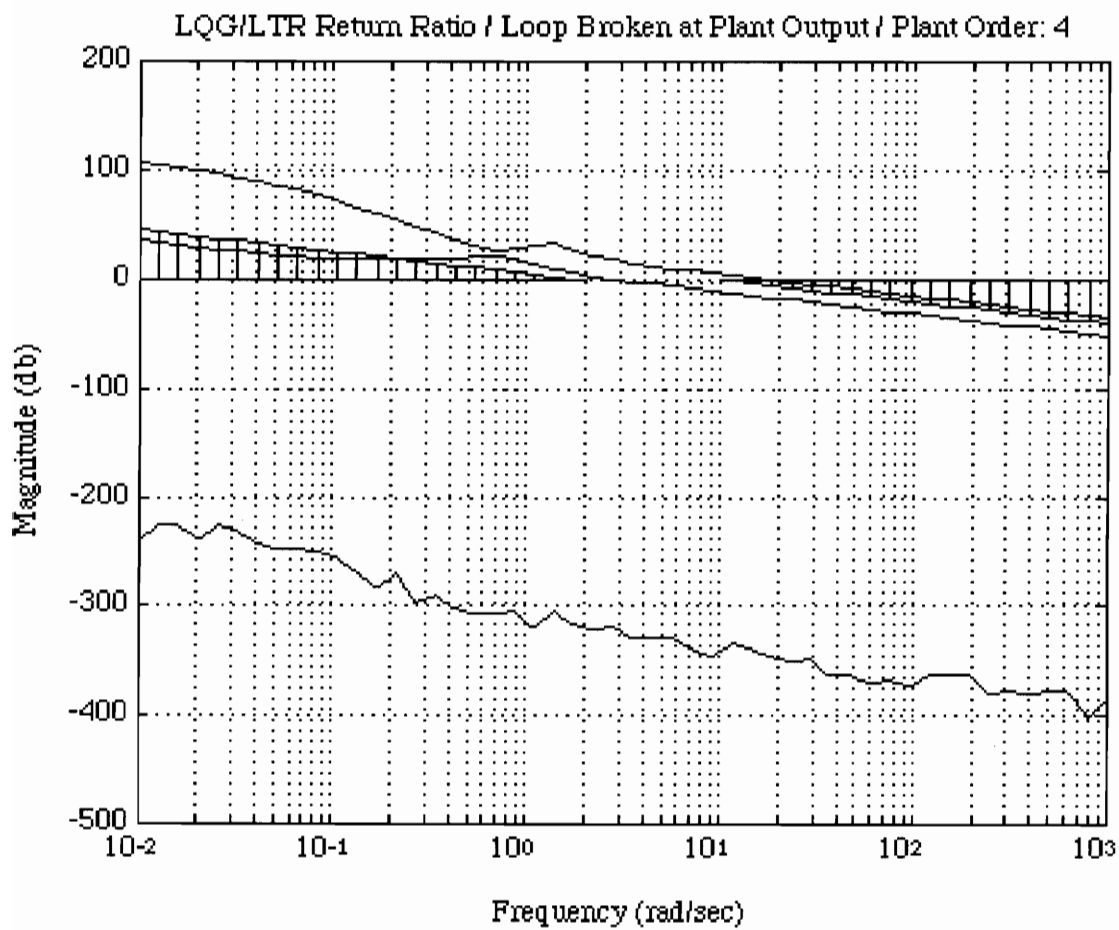


Figure 6.27 LQG/LTR Output Return Ratio Singular Values

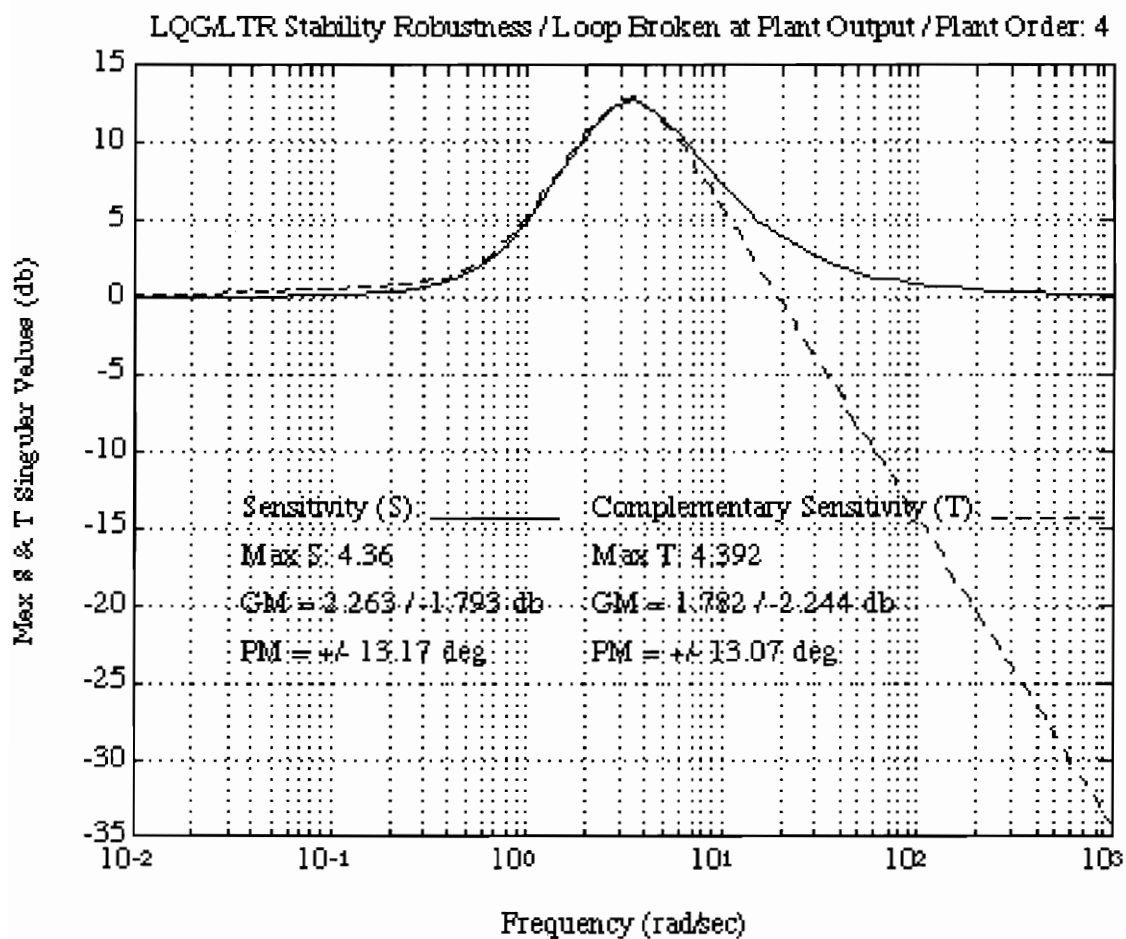


Figure 6.28 LQG/LTR Output MIMO Robustness

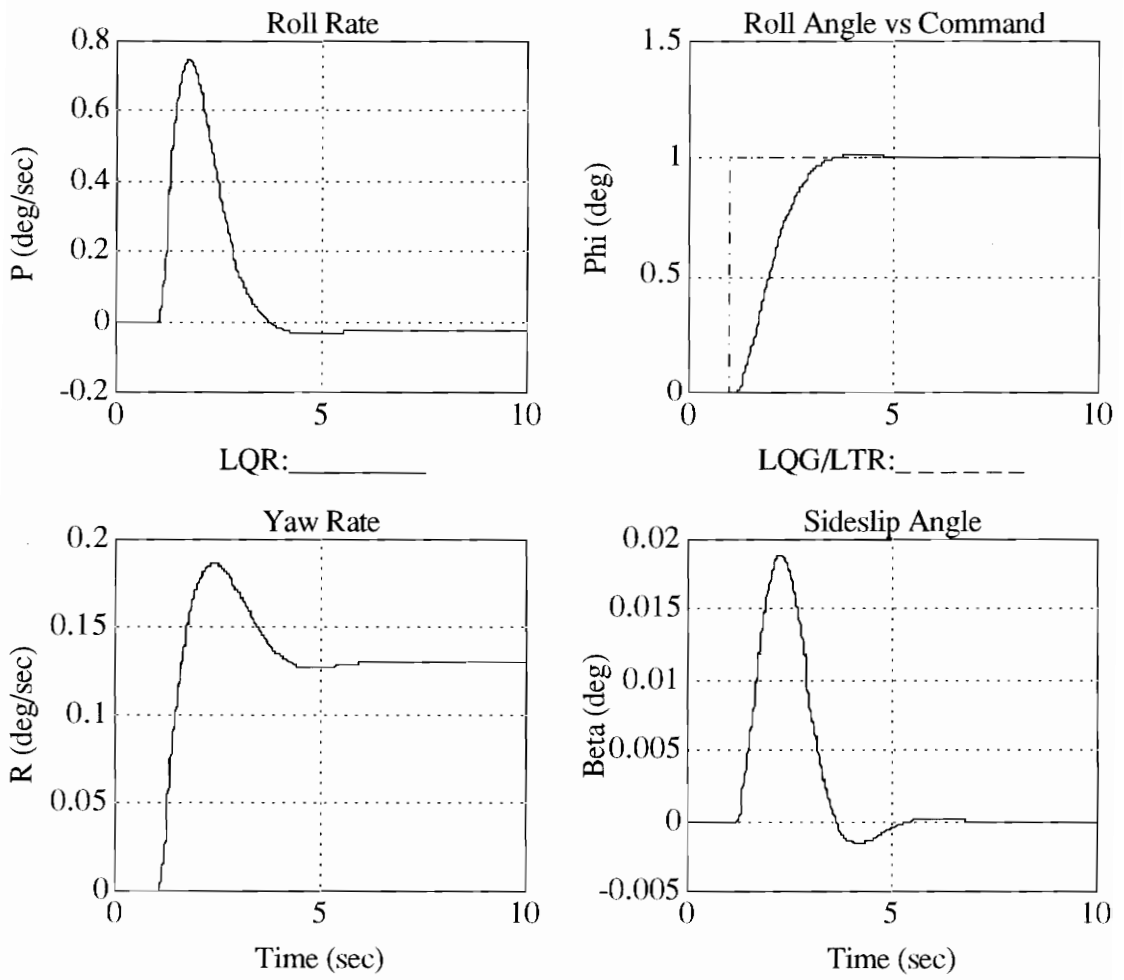


Figure 6.29 LQR vs LQG/LTR Response to Roll Angle Command

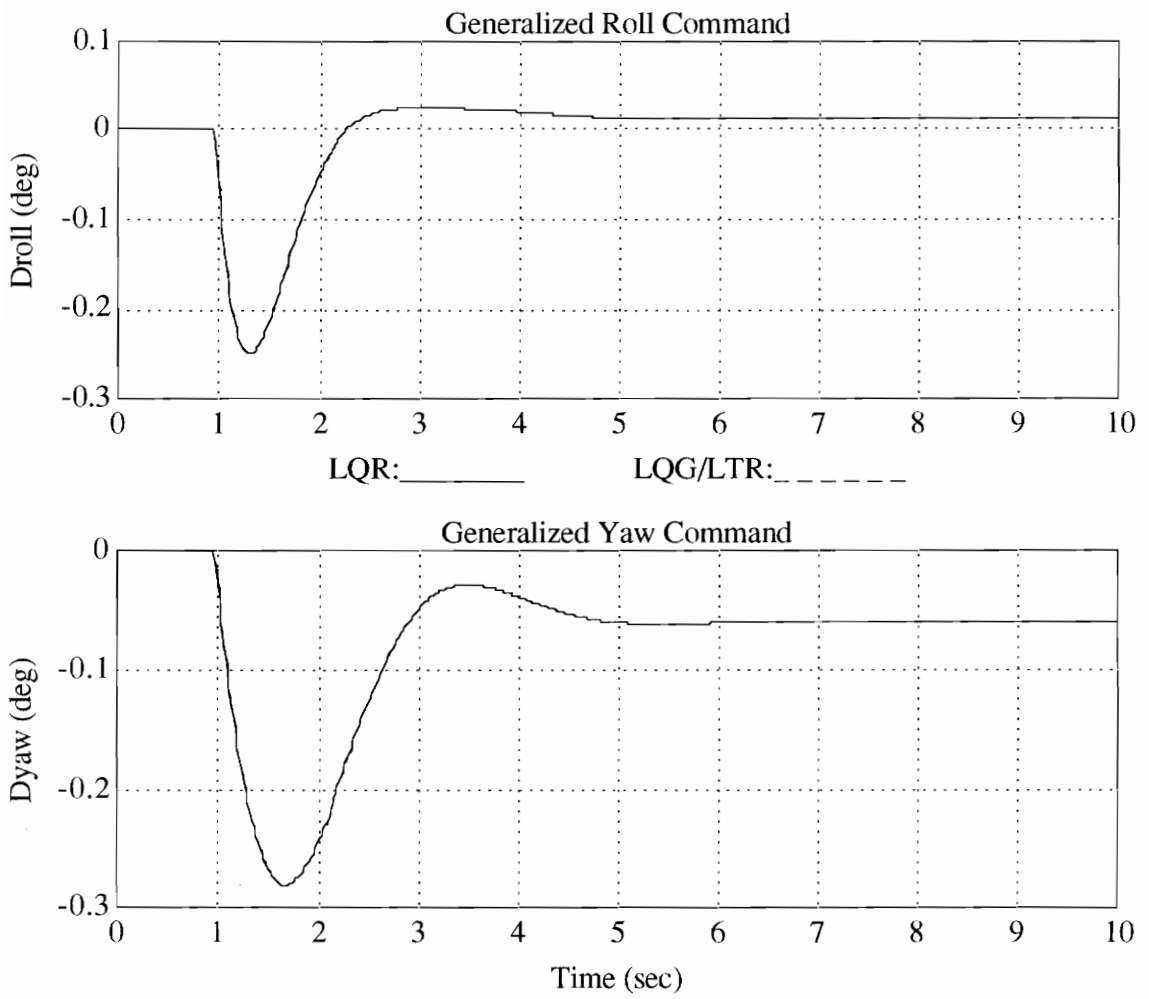


Figure 6.29 (Continued) LQR vs LQG/LTR Response to Roll Angle Command

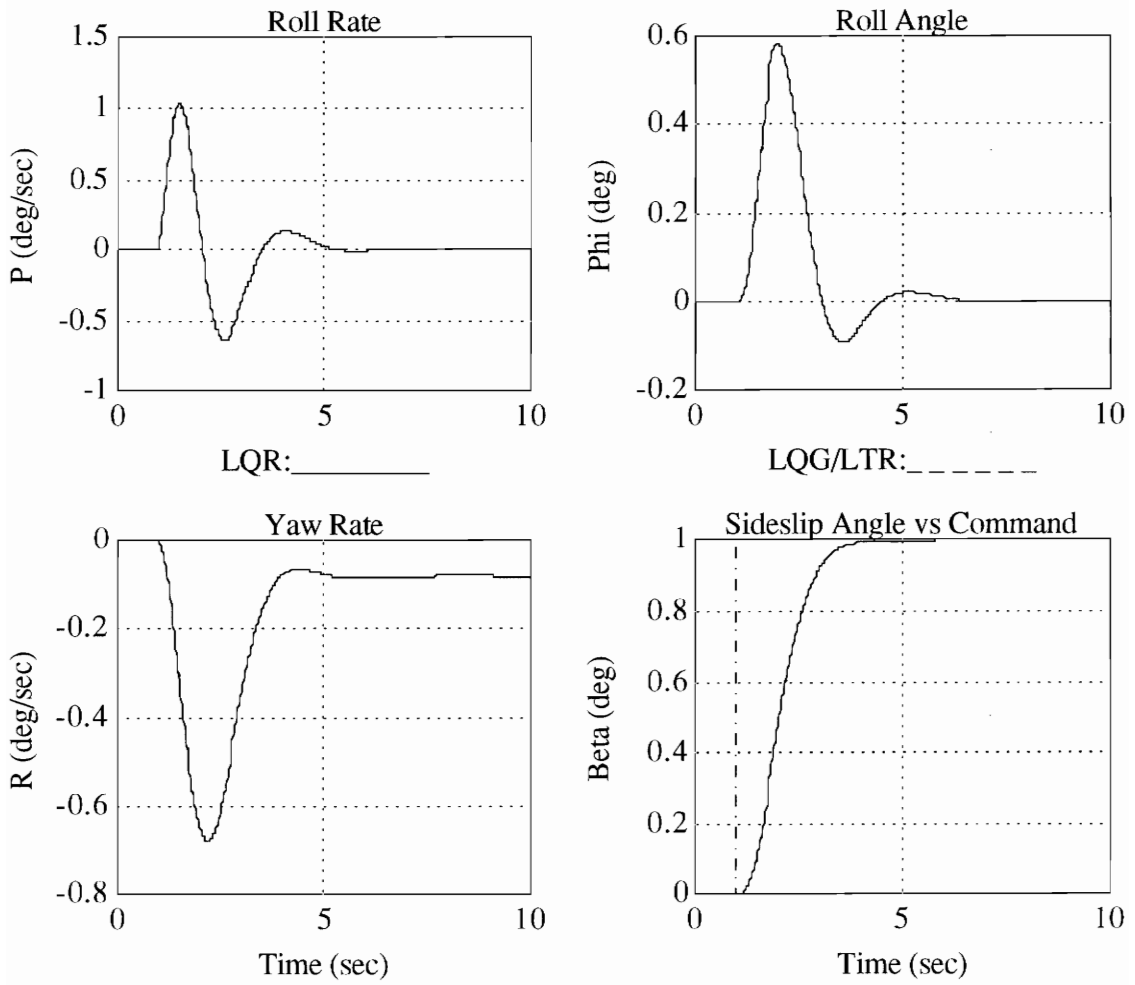


Figure 6.30 LQR vs LQG/LTR Response to Sideslip Command

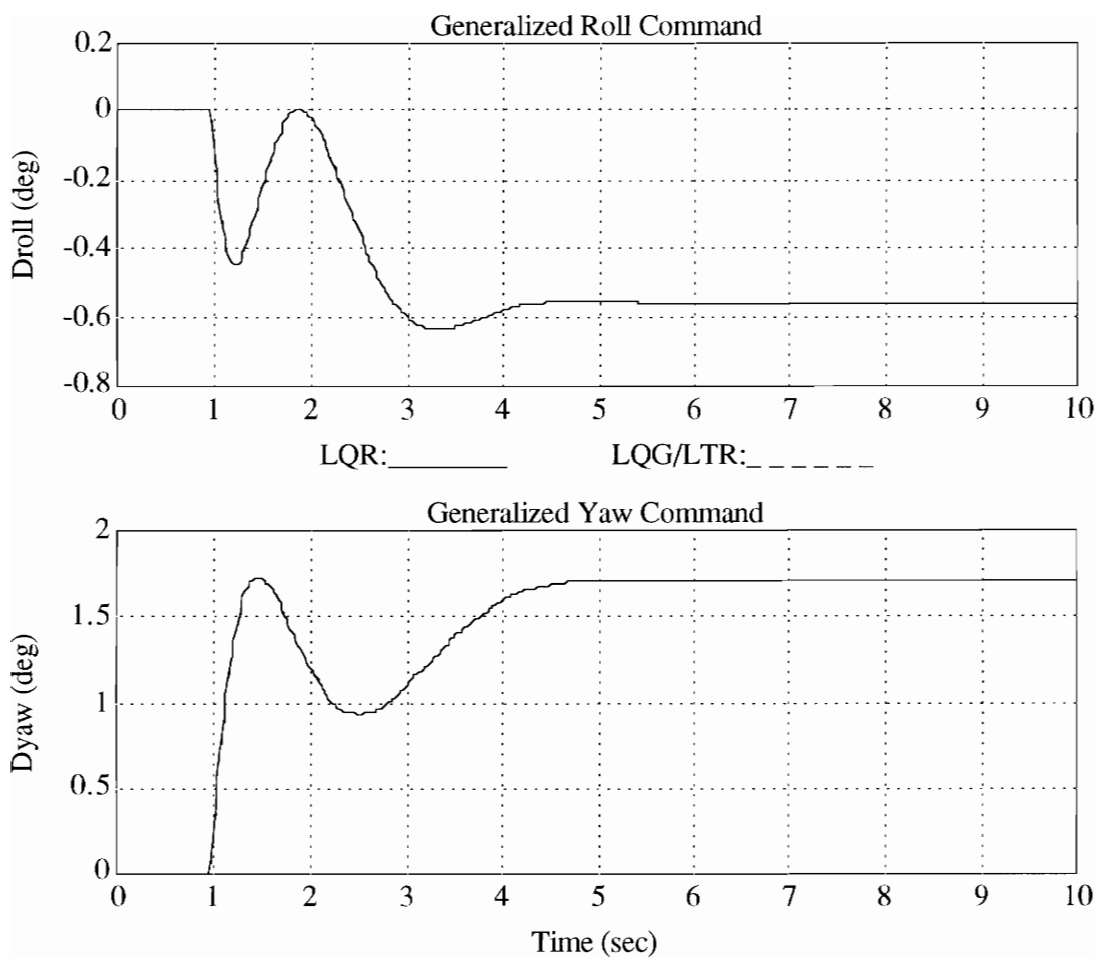


Figure 6.30 (Continued) LQR vs LQG/LTR Response to Sideslip Command



## 6.9 Consolidated MMF Control System

### 6.9.1 "Fly-by-wire" Implementation

All of the individual components for the MMF control law have now been designed. The next step in the design process is to integrate these components into a complete system and demonstrate the model following characteristics. Figure 6.31 shows the resulting closed-loop MMF control system. This system is currently configured as a "fly-by-wire" control system, with no mechanical links between the pilot inputs and the control surfaces. This system configuration will be referred to as the "Stage 1" design. The "Stage 2" design (next section) will incorporate the MMF control law into the actual F-14 mechanical control system framework.

As figure 6.31 shows, the input to the LQ regulator is the error between the commanded states generated by the MCG and the measured/estimated states generated by the reduced order observer. However, the command inputs to the LQ regulator designed in section 6.7.2 are only roll angle and sideslip angle. Therefore, the regulator structure is modified such that the regulator input is the full state vector error, as shown in figure 6.32. This modification has no effect on the location of the closed-loop eigenvalues of the system, as shown below:

Eigenvalue	Damping Freq (r/s)		Mode
0	1.0000	0.0000	Phi Cmd (MCG)
-0.0805	1.0000	0.0805	Observer
-0.8485 + 0.8485i	0.7071	1.2000	Beta Cmd (MCG)
-0.8485 - 0.8485i	0.7071	1.2000	Beta Cmd (MCG)
-1.2212 + 1.6298i	0.5996	2.0365	LQR Integrator
-1.2212 - 1.6298i	0.5996	2.0365	LQR Integrator
-1.3555	1.0000	1.3555	Spiral

-1.8984		1.0000	1.8984	Roll
-2.0000		1.0000	2.0000	P Cmd (MCG)
-2.0201 + 2.5185i		0.6257	3.2286	Dutch-roll
-2.0201 - 2.5185i		0.6257	3.2286	Dutch-roll
-50.0000		1.0000	50.0000	R-dot cmd (MCG)

The performance of the MMF control law is demonstrated by computing the response to pilot inputs. Figures 6.33 and 6.34 show the response of the combined MMF to lateral stick and rudder pedal inputs. The response to the lateral stick input shows that roll angle model following is exact, sideslip excursions are minimal, and small errors exist in the roll rate and yaw rate responses, which were not integrally regulated. The response to the pedal input shows that sideslip tracking is excellent, with minimal roll axis excursions. A steady state error exists in the yaw rate response due to the simplified MCG model for yaw rate due to rudder pedal, as described in section 6.4.5.

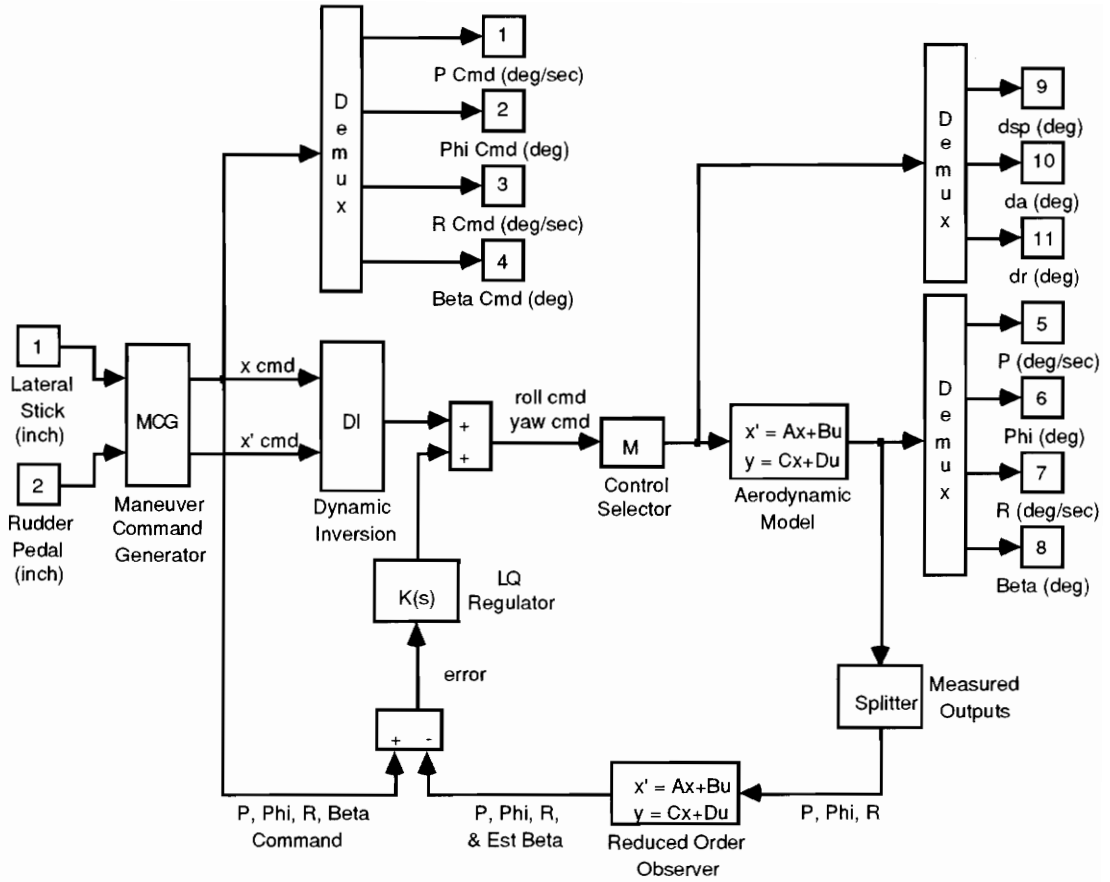


Figure 6.31 Stage 1 MMF Control Architecture

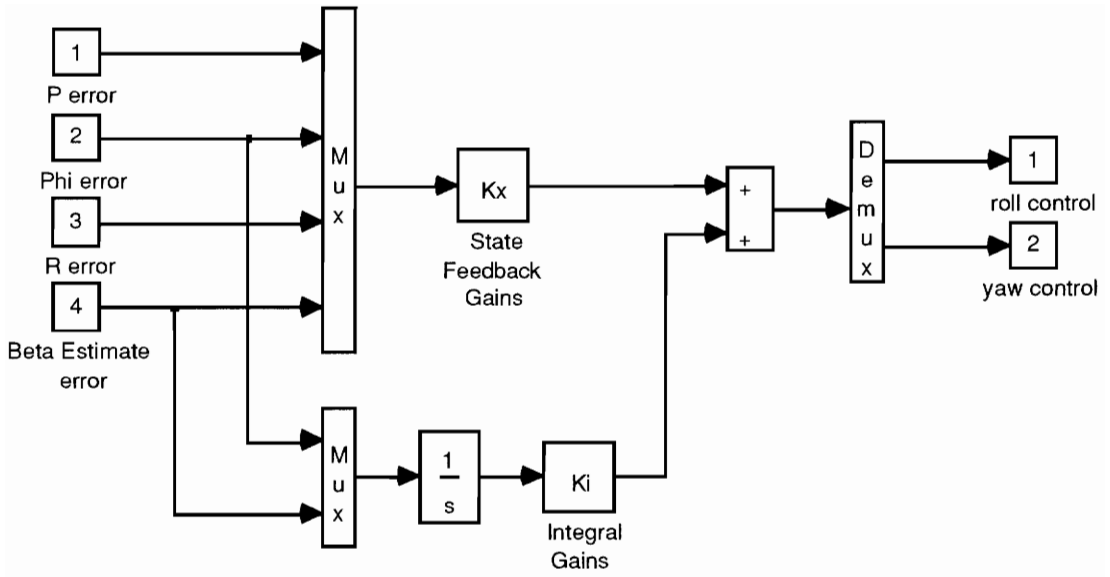


Figure 6.32 Modified LQ Regulator Structure

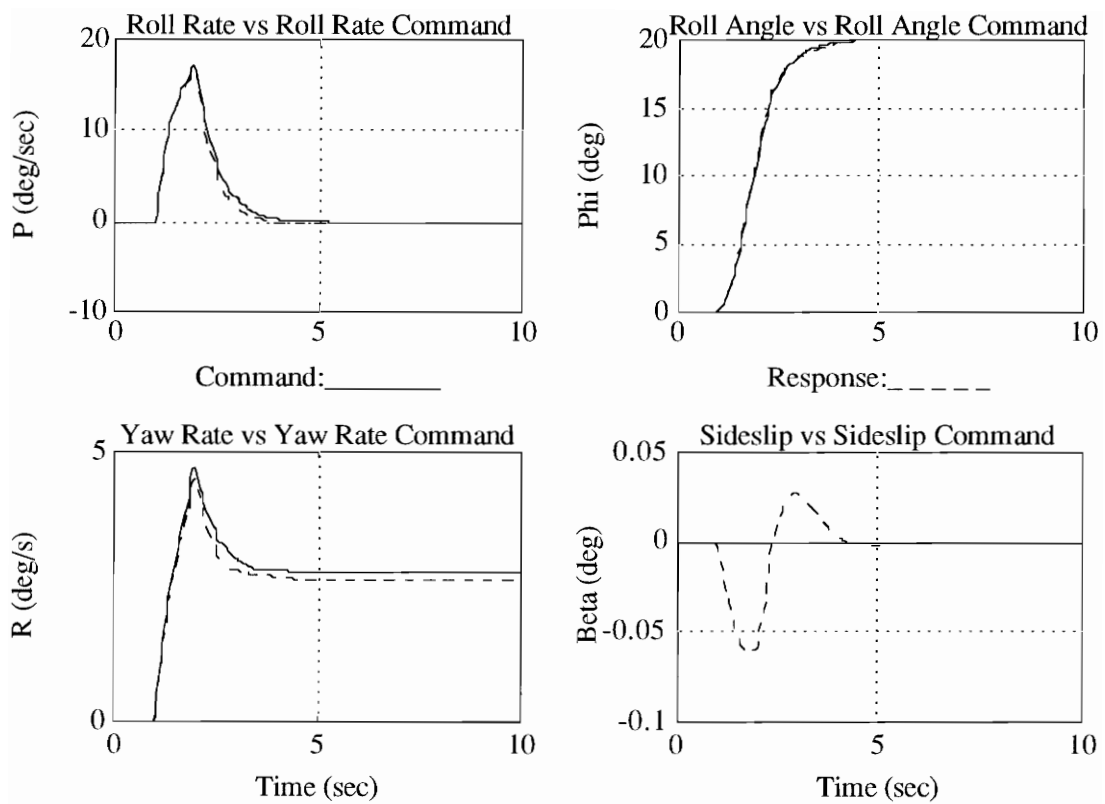


Figure 6.33 Stage 1 MMF Response to Lateral Stick

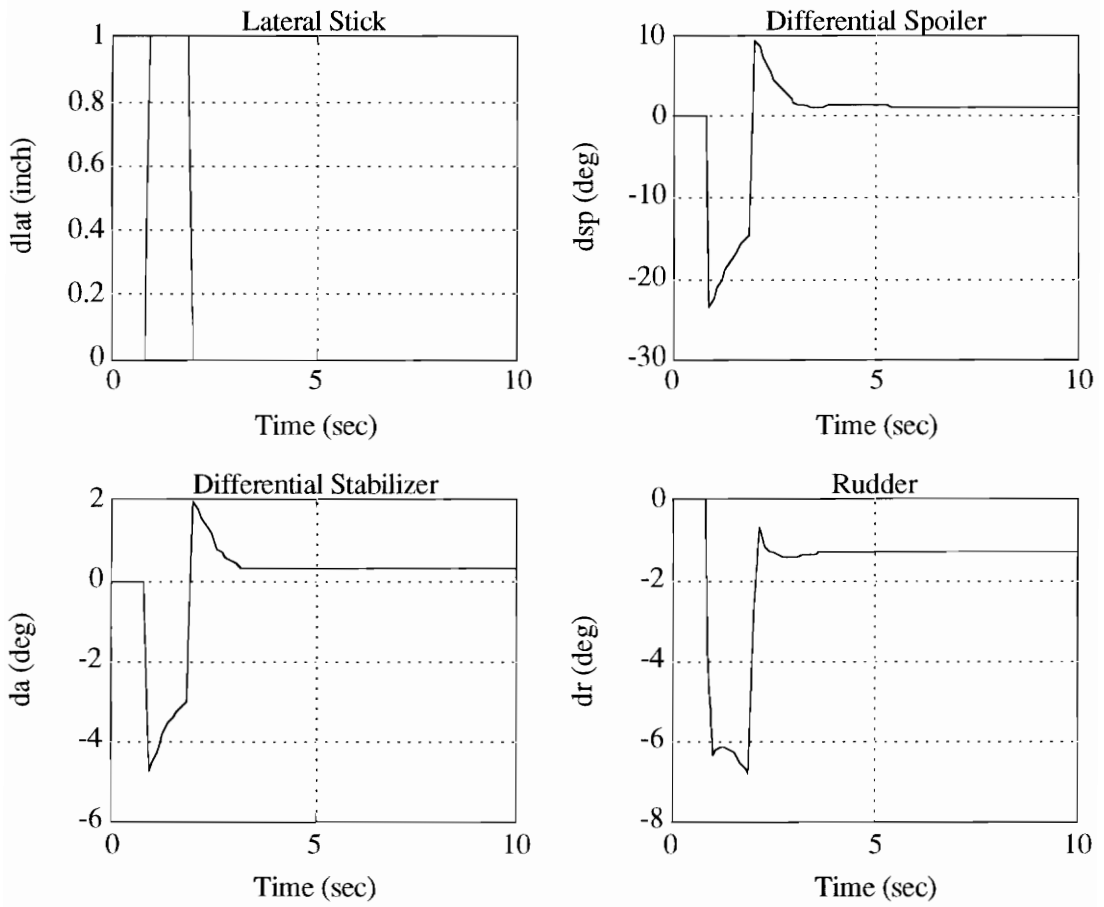


Figure 6.33 (Continued) Stage 1 MMF Response to Lateral Stick

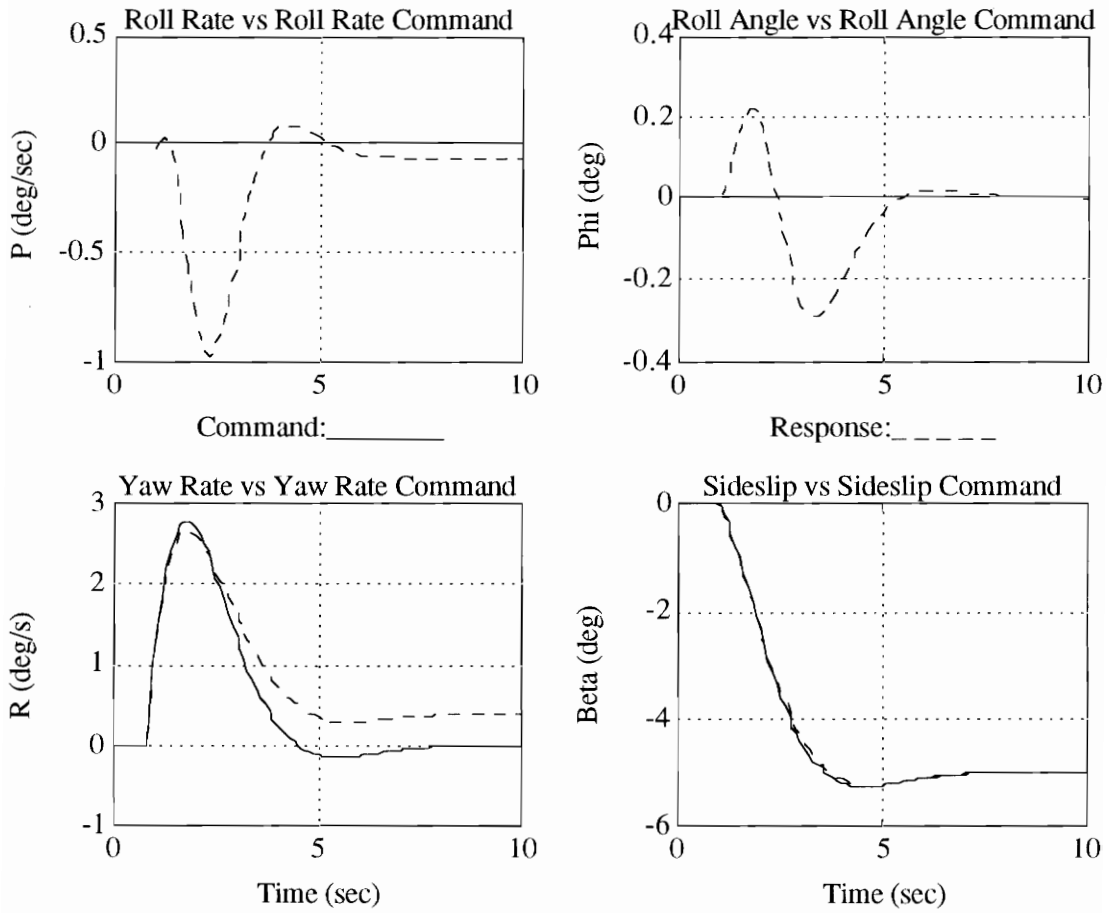


Figure 6.34 Stage 1 MMF Response to Rudder Pedal

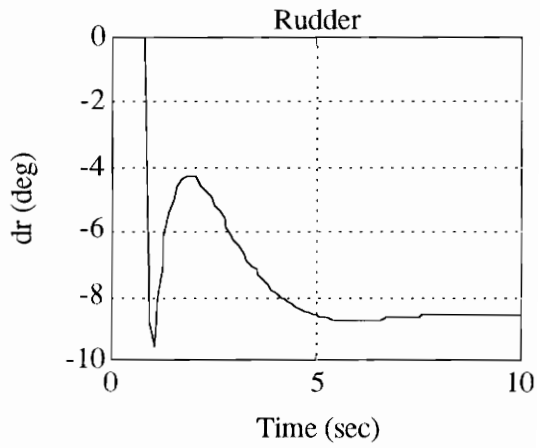
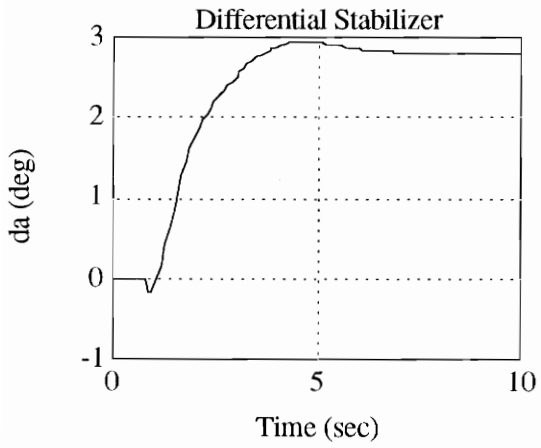
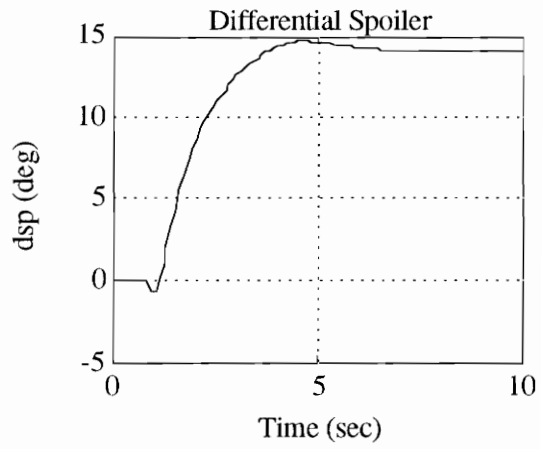
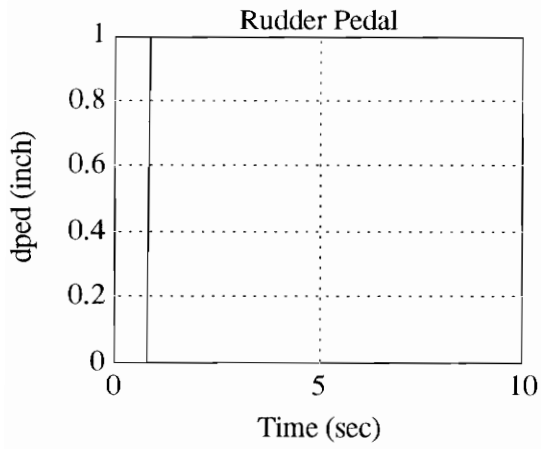


Figure 6.34 (Continued) Stage 1 MMF Response to Rudder Pedal



## 6.9.2 Integration with the Mechanical Control System

The final design task for the MMF is to reconfigure the control law structure to be consistent with the F-14 mechanical flight control system. Specifically, the F-14 mechanical control system contains direct mechanical links from the pilot lateral stick and rudder pedal inputs to the differential stabilizer and rudder surface actuators which have been ignored thus far in the MMF design process. When these paths are included in the closed-loop system, the effective gain from the pilot inputs to the surface actuators will be different than the intended design unless the contribution of the mechanical paths is subtracted out from the digital control system. Figure 6.35 shows the modification required to the MMF for integration with the F-14 mechanical control system. The block labeled “Mechanical Path Gain” has been added to compensate for the gain mechanical control system. This block computes the mechanical path commands resulting from lateral stick and rudder inputs and subtracts them from the series servo commands, thereby preserving the closed-loop gain of the Stage 1 MMF configuration.

Figure 6.36 shows the MMF control system integrated with the mechanical control system, and includes the discrete time model of the MMF (Tustin transform at 50 hz), high order actuator, sensor, and anti-aliasing filter dynamics. This detailed model will be referred to as the “Stage 2” MMF configuration. The response of the Stage 2 configuration to lateral stick and rudder pedal inputs is shown in figures 6.37 and 6.38. Roll angle and sideslip tracking performance is unchanged from the Stage 1 configuration, but the effect of the added high frequency dynamics is apparent in the actuator responses.

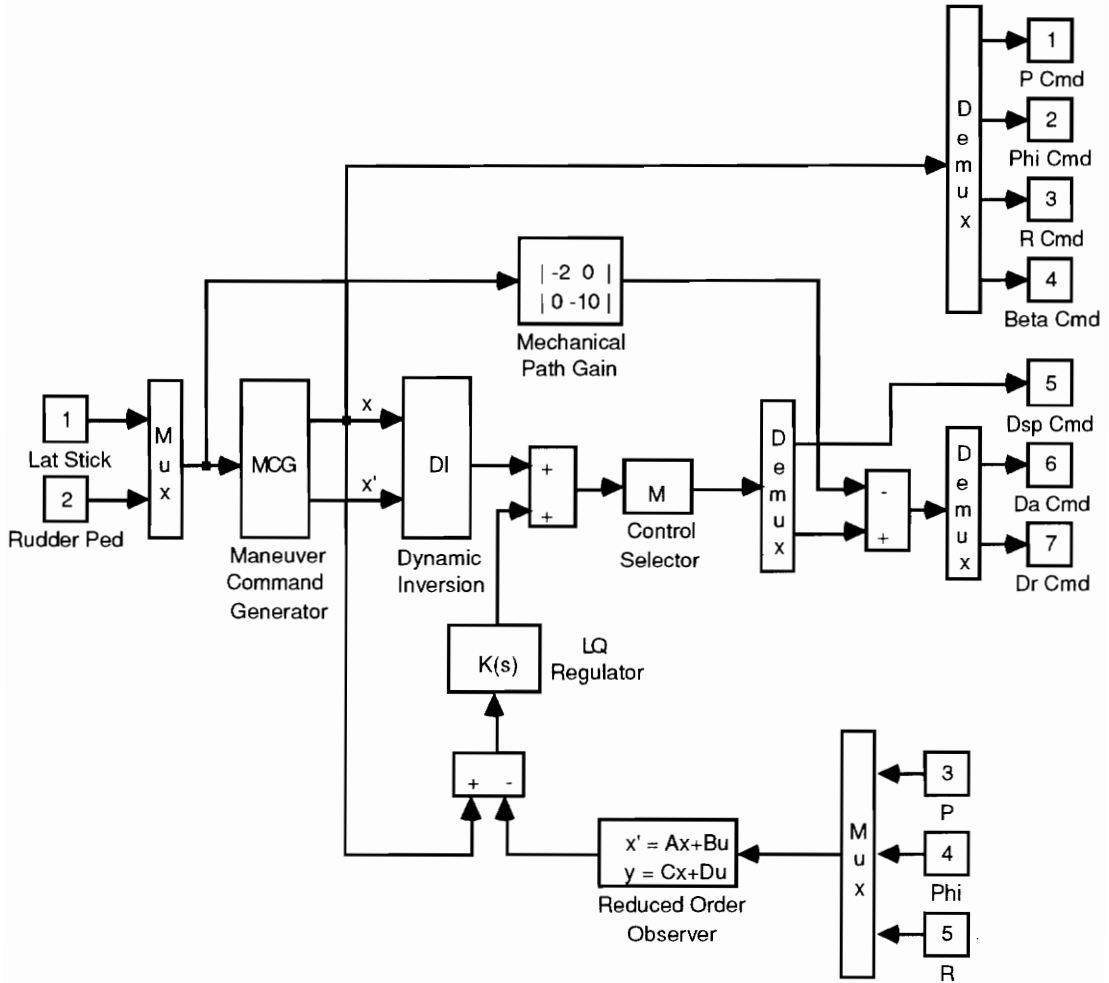


Figure 6.35 MMF with Mechanical Path Compensation

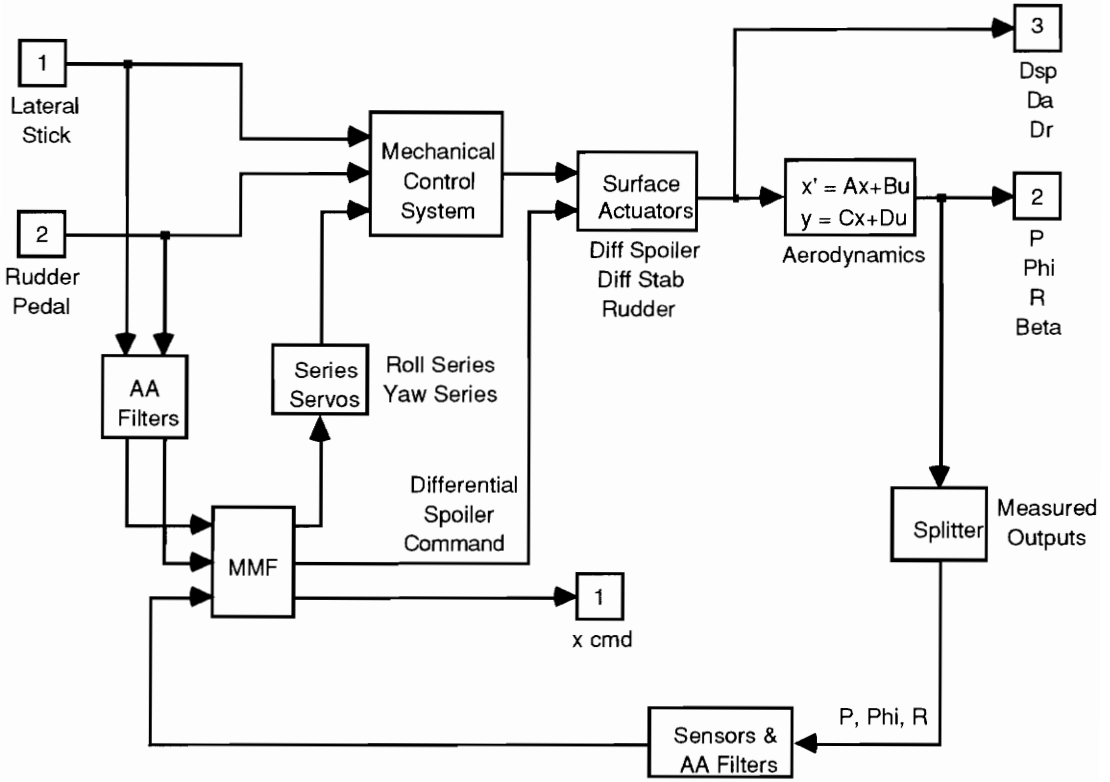


Figure 6.36 Stage 2 MMF Closed-loop System

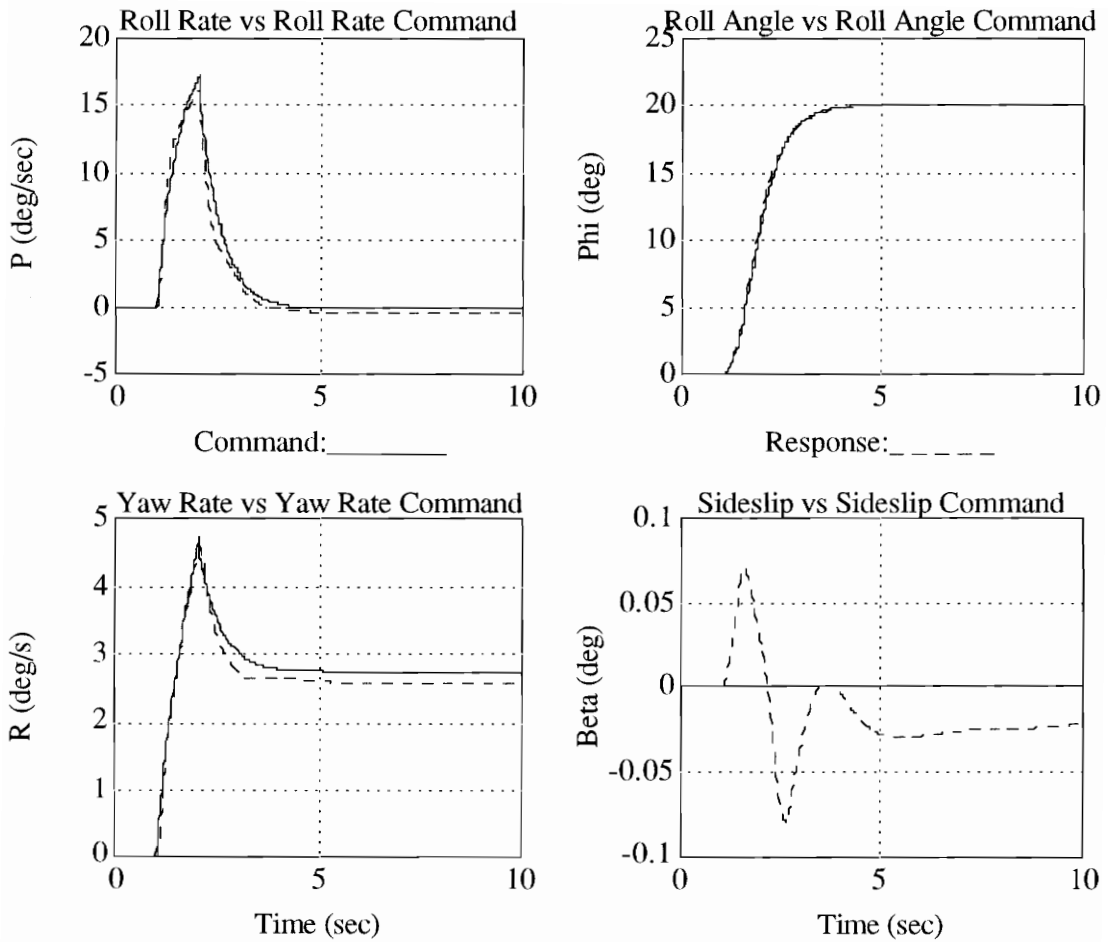


Figure 6.37 Stage 2 MMF Response to Lateral Stick

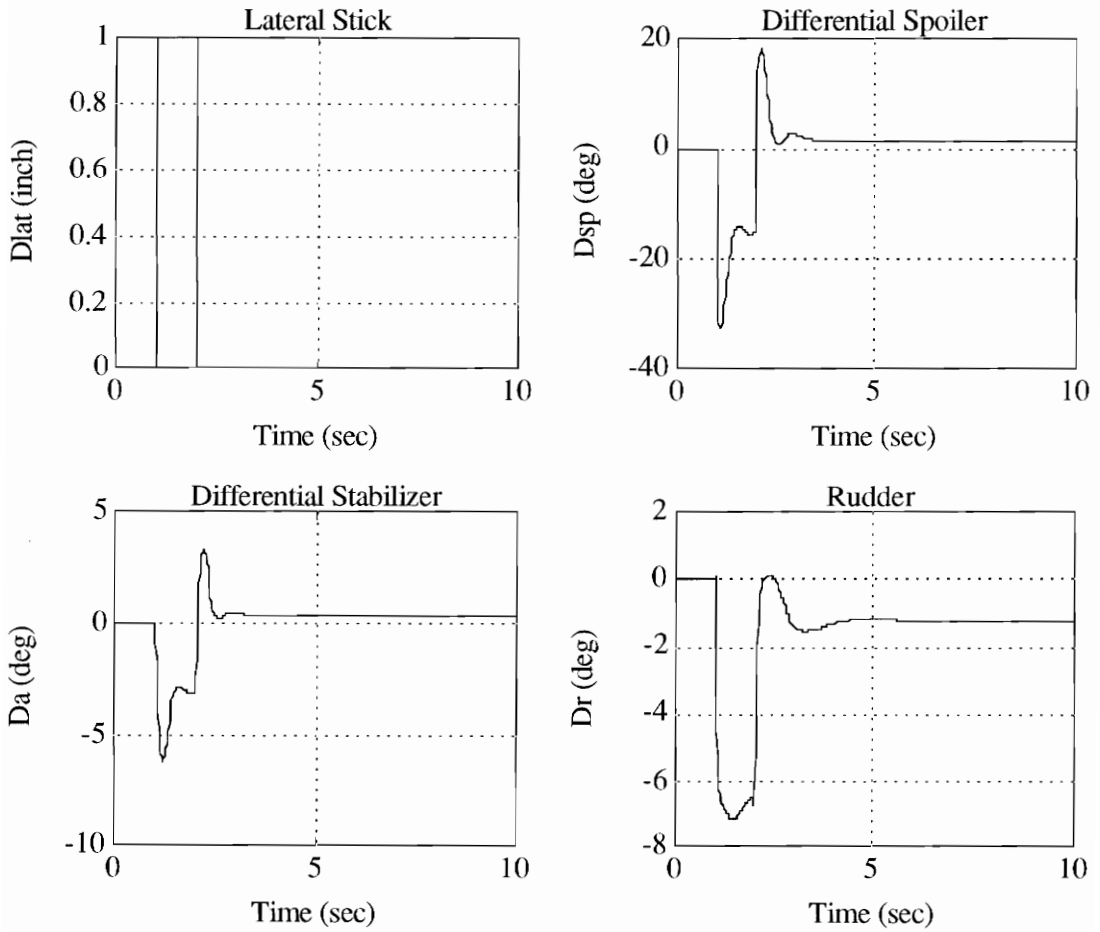


Figure 6.37 (Continued) Stage 2 MMF Response to Lateral Stick

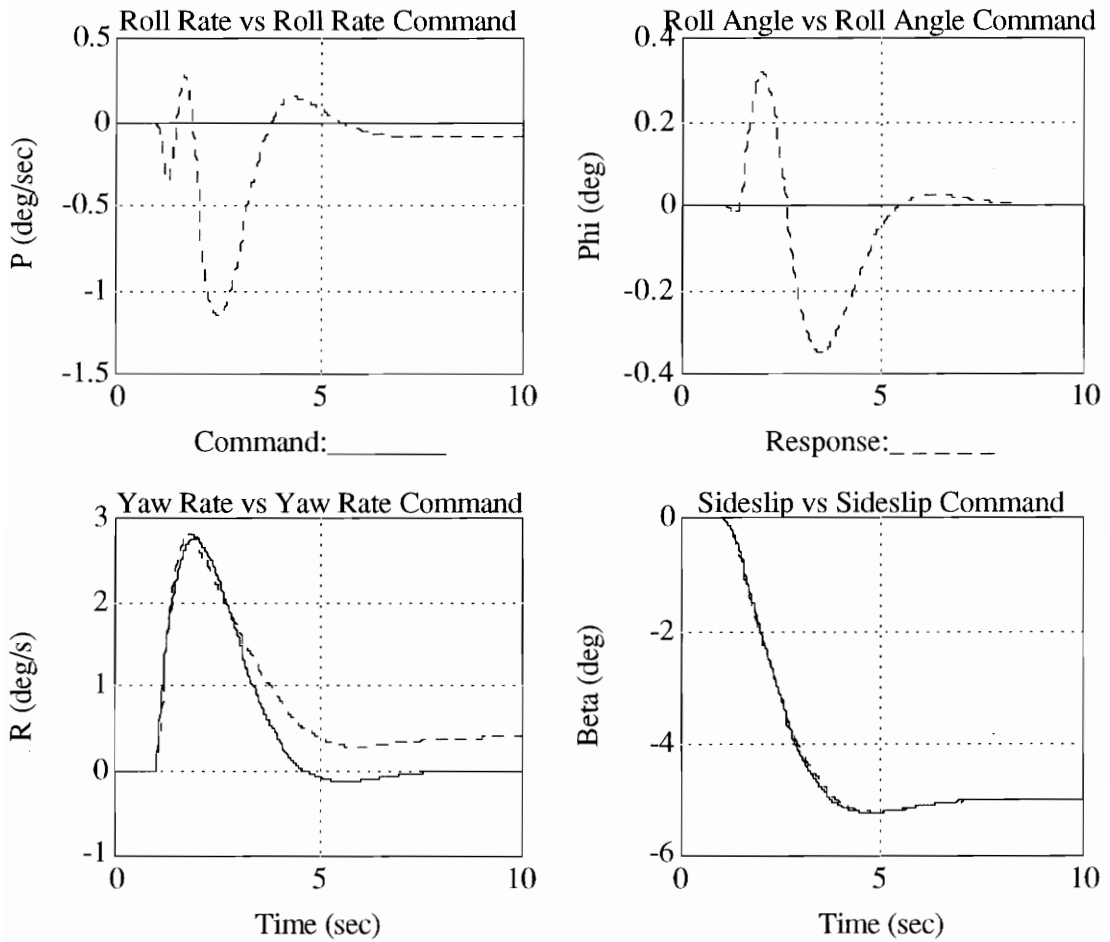


Figure 6.38 Stage 2 MMF Response to Rudder Pedal

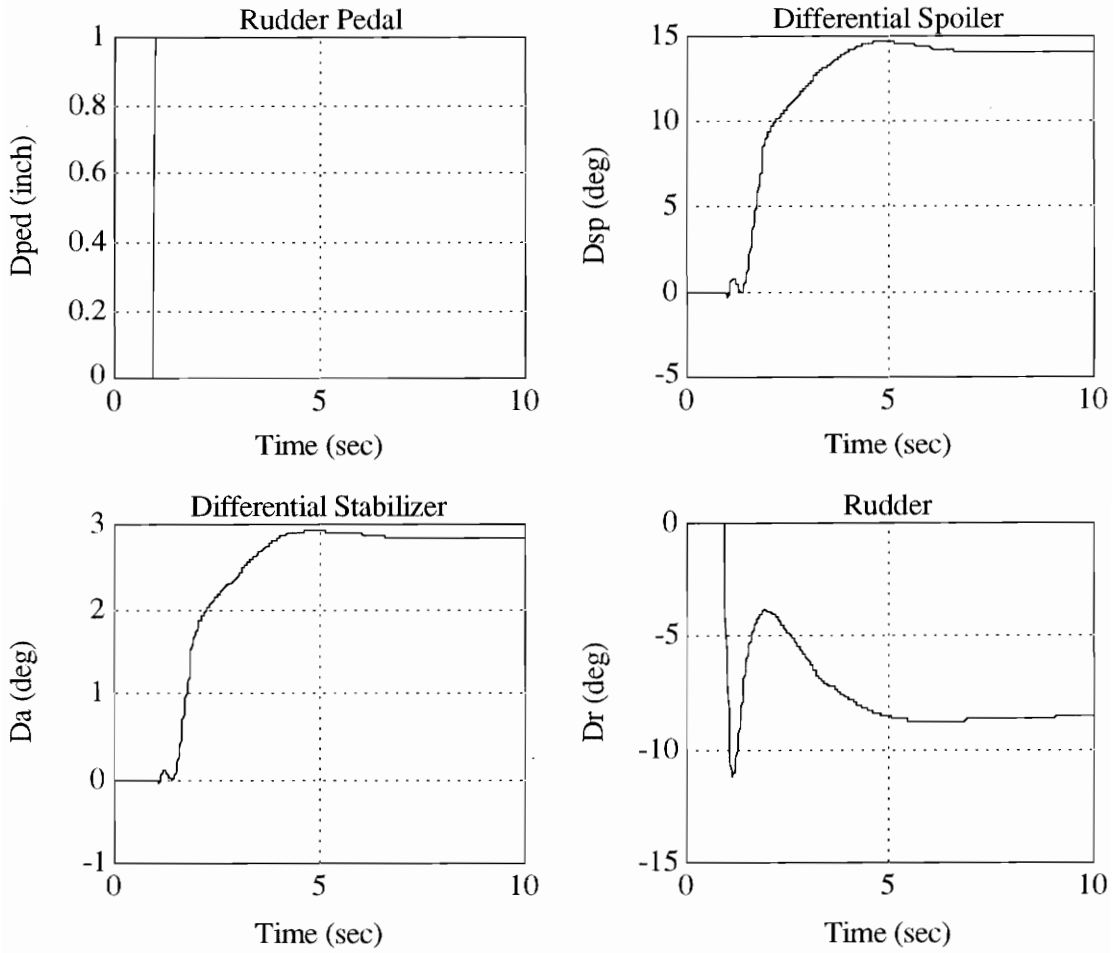


Figure 6.38 (Continued) Stage 2 MMF Response to Rudder Pedal

## 6.10 High Order Stability Robustness Analysis

To complete the MMF design analysis, the SISO and MIMO stability robustness properties are analyzed for the full order system model. The open-loop model used to perform this analysis is shown in figure 6.39, which includes digitization effects and all known high frequency dynamics. For the single loop analysis, the frequency response is computed at each loop break while the others are closed. The bode plots for these cases are shown in figures 6.40 through 6.45, and the stability margin results are tabulated in table 6.1. All margins meet the requirements of MIL-F-9490D except for the roll rate and yaw rate phase margin. The roll rate gain margin reported is negative because the system is unstable with the loop open, so the negative gain margin indicates the amount of gain decrease the loop can tolerate and remain stable.

Table 6.1 MMF SISO Gain and Phase Margins

Loop	Gain Margin (db)	Phase Margin (deg)
Diff Spoiler	9.88	46.35
Diff Stabilizer	12.39	N/A
Rudder	14.88	50.22
Roll Rate	-8.83	32.79
Roll Angle	10.12	52.55
Yaw Rate	17.00	42.68



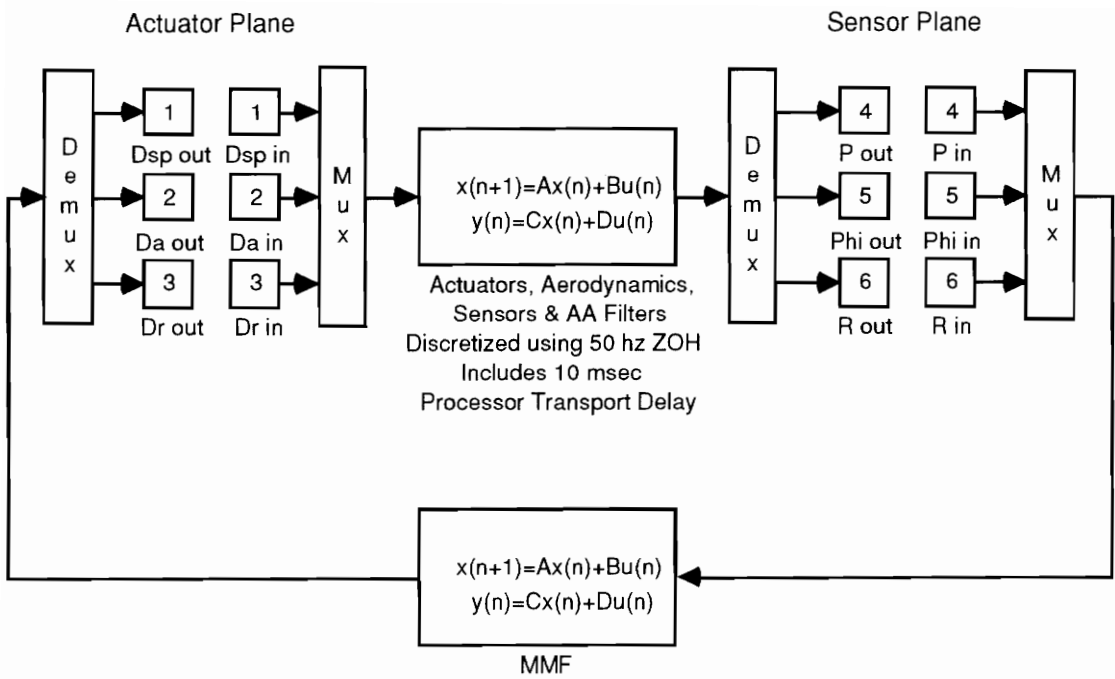


Figure 6.39 Open-loop MMF Control System

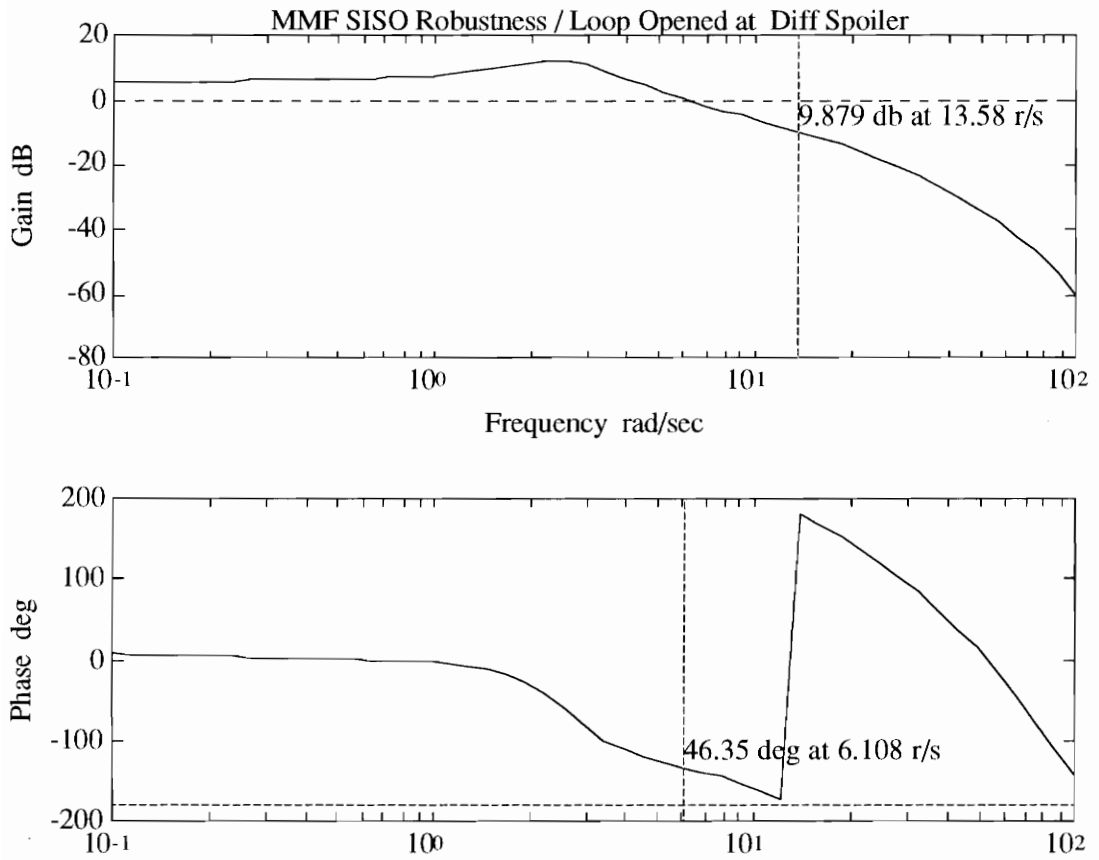


Figure 6.40 MMF Open-loop Frequency Response with Loop Opened at Differential Spoiler

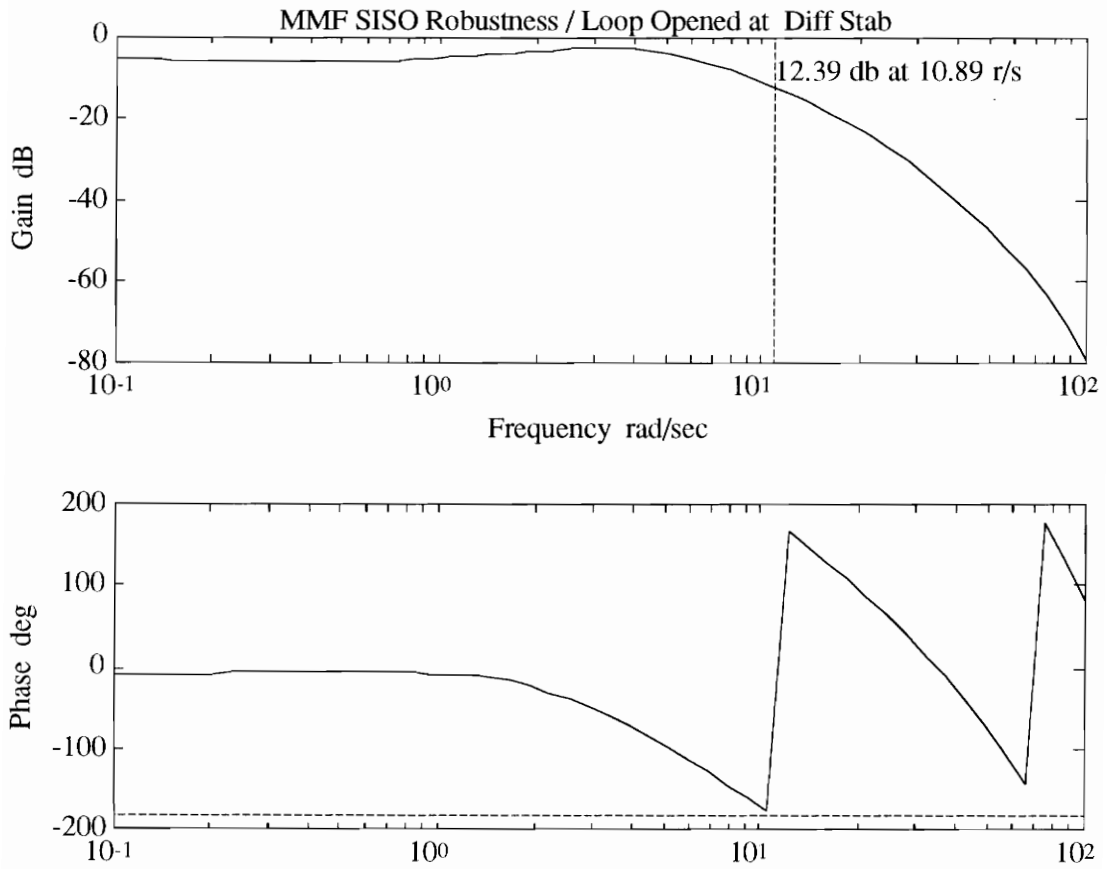


Figure 6.41 MMF Open-loop Frequency Response with Loop Opened at Differential Stabilizer

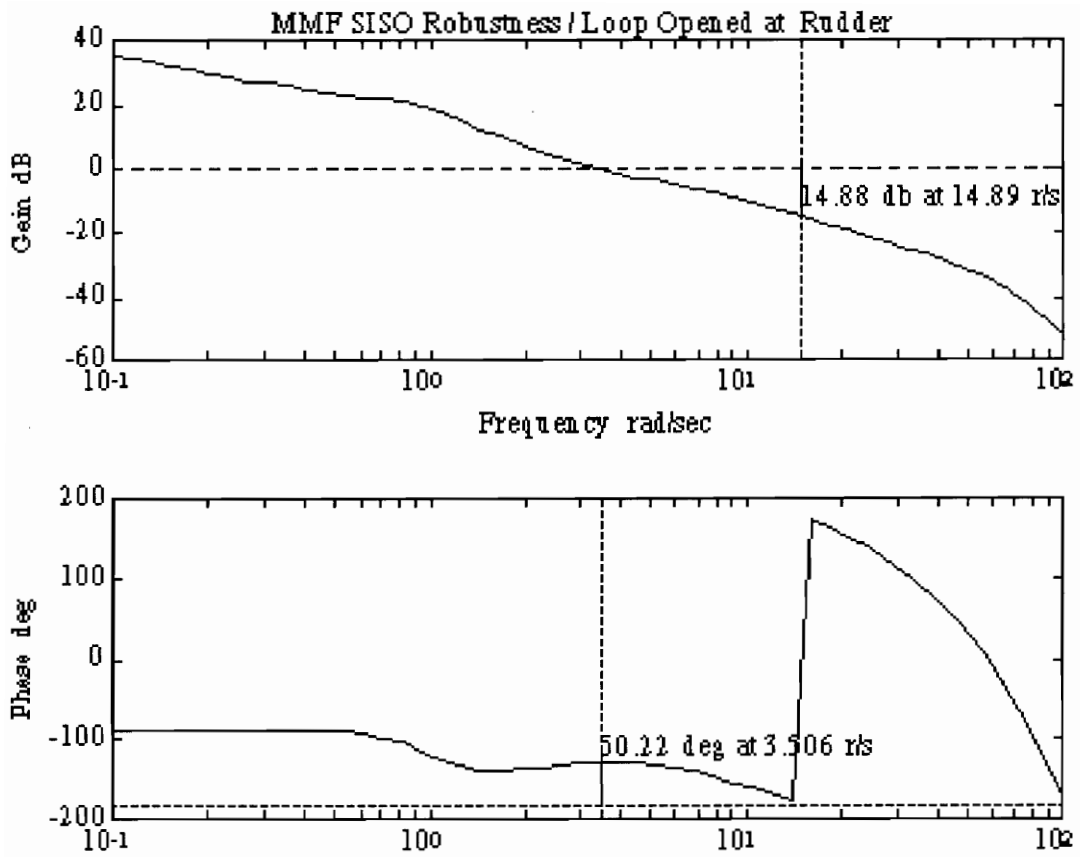


Figure 6.42 MMF Open-loop Frequency Response with Loop Opened at Rudder

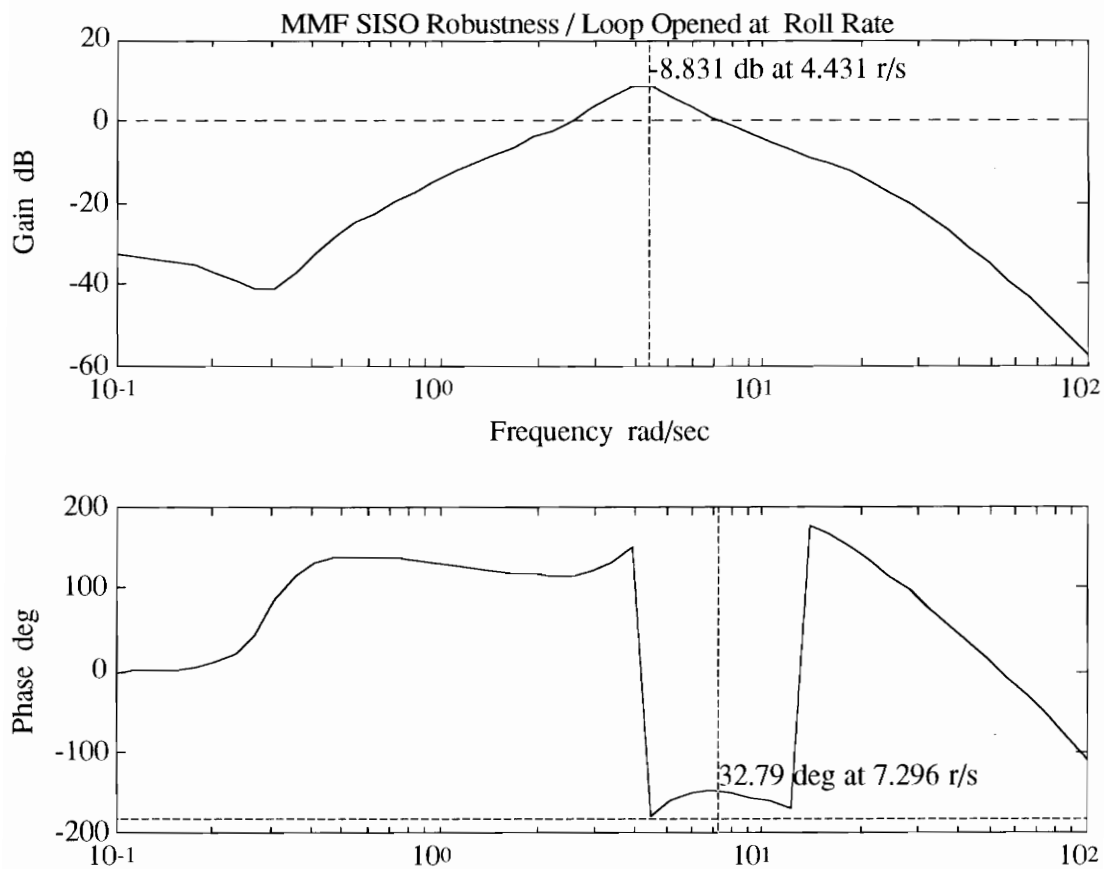


Figure 6.43 MMF Open-loop Frequency Response with Loop Opened at Roll Rate

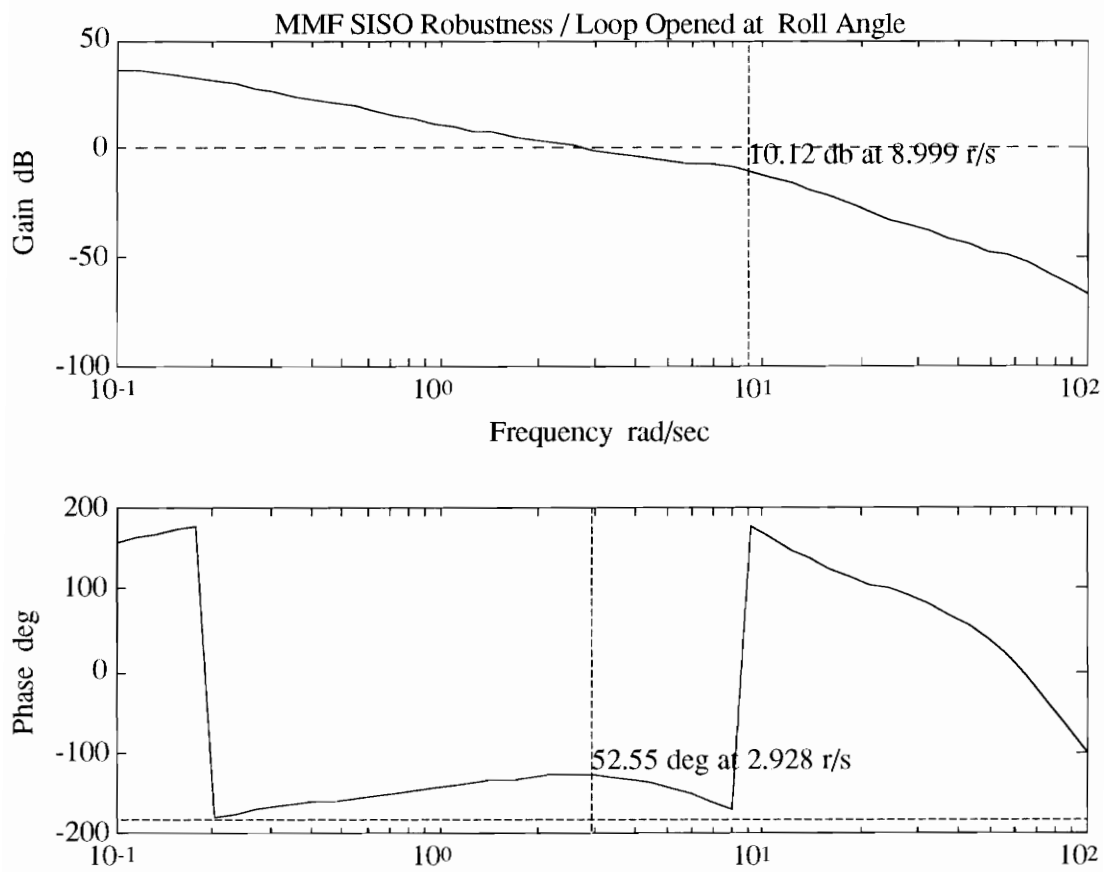


Figure 6.44 MMF Open-loop Frequency Response with Loop Opened at Roll Angle

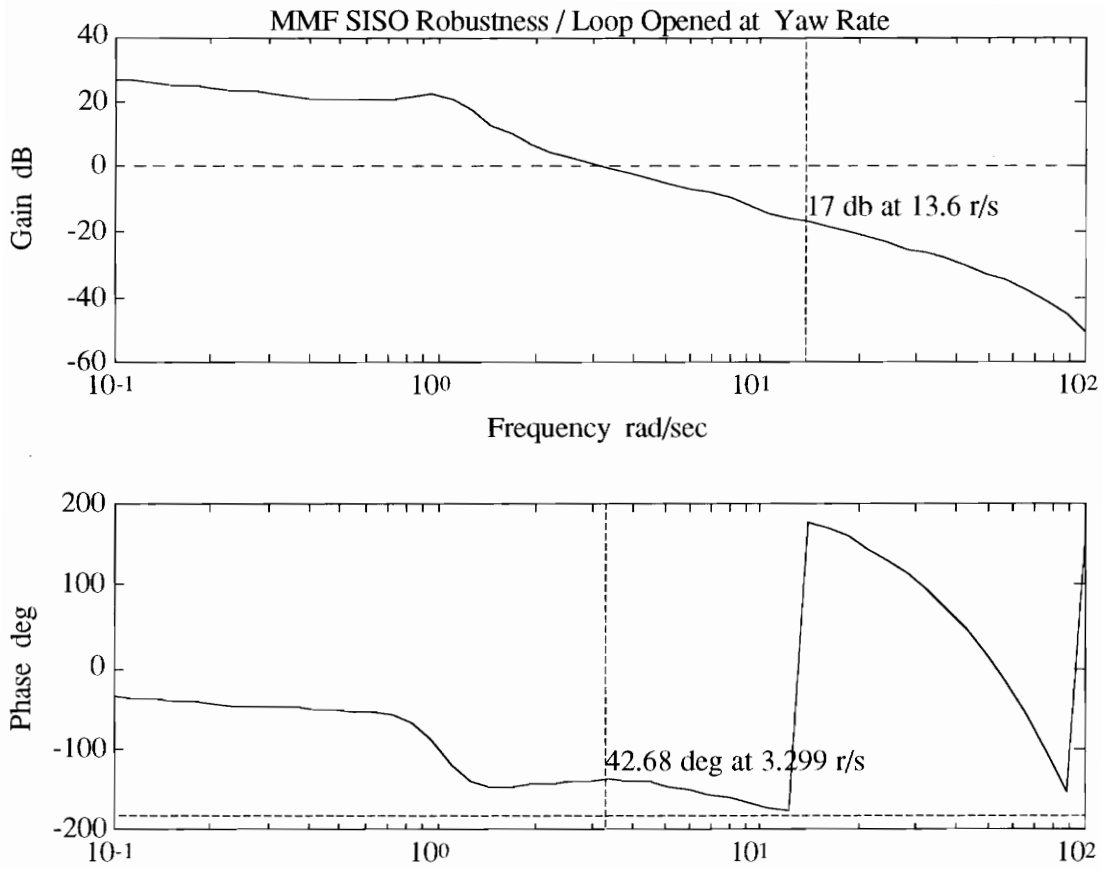


Figure 6.45 MMF Open-loop Frequency Response with Loop Opened at Yaw Rate

In addition to the SISO stability analysis, the MIMO stability robustness properties are analyzed for the high order system model. The open-loop model used to perform the MIMO analysis is the same one used for the SISO analysis, shown in figure 6.39. The MIMO robustness characteristics are evaluated at the actuator plane and the sensor plane using the sensitivity and complementary sensitivity functions. The singular value plots for these cases are shown in figures 6.46 and 6.47, and the results are summarized in table 6.2. The actuator plane robustness is considerably less than the design plant input robustness demonstrated during the design phase. This is because the design plant inputs were the generalized roll and yaw commands, while the actuator plane signals are differential spoiler, differential stabilizer, and rudder. The added pathway for uncertainty therefore results in reduced MIMO robustness. The sensor plane robustness estimates are only marginally worse than those estimated for the design model, which did not include high frequency dynamics or digitization effects.

Table 6.2 MMF MIMO Gain and Phase Margins

Loop Break Plane	GM (db)	PM (deg)
Actuators	+2.64 /-2.80	±15.84
Sensors	+1.47 /-1.47	±9.07



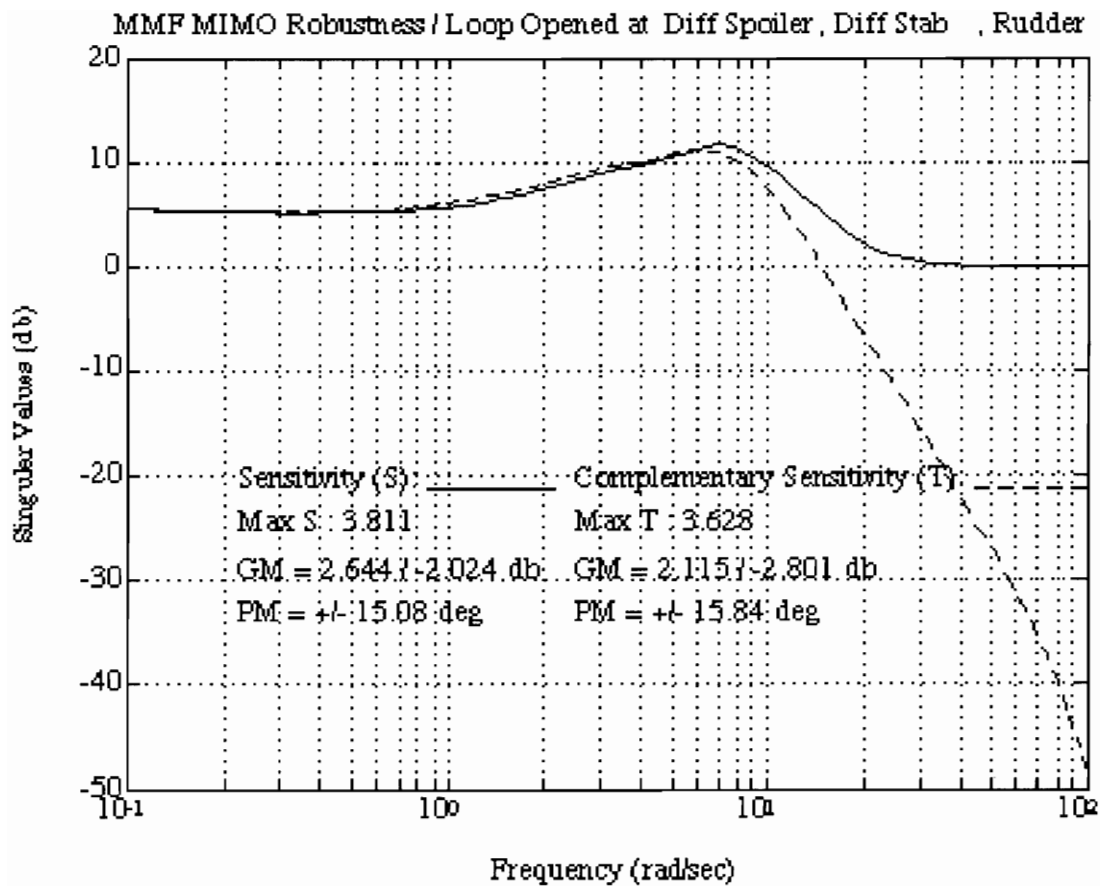


Figure 6.46 High Order MMF Actuator Plane Stability Robustness

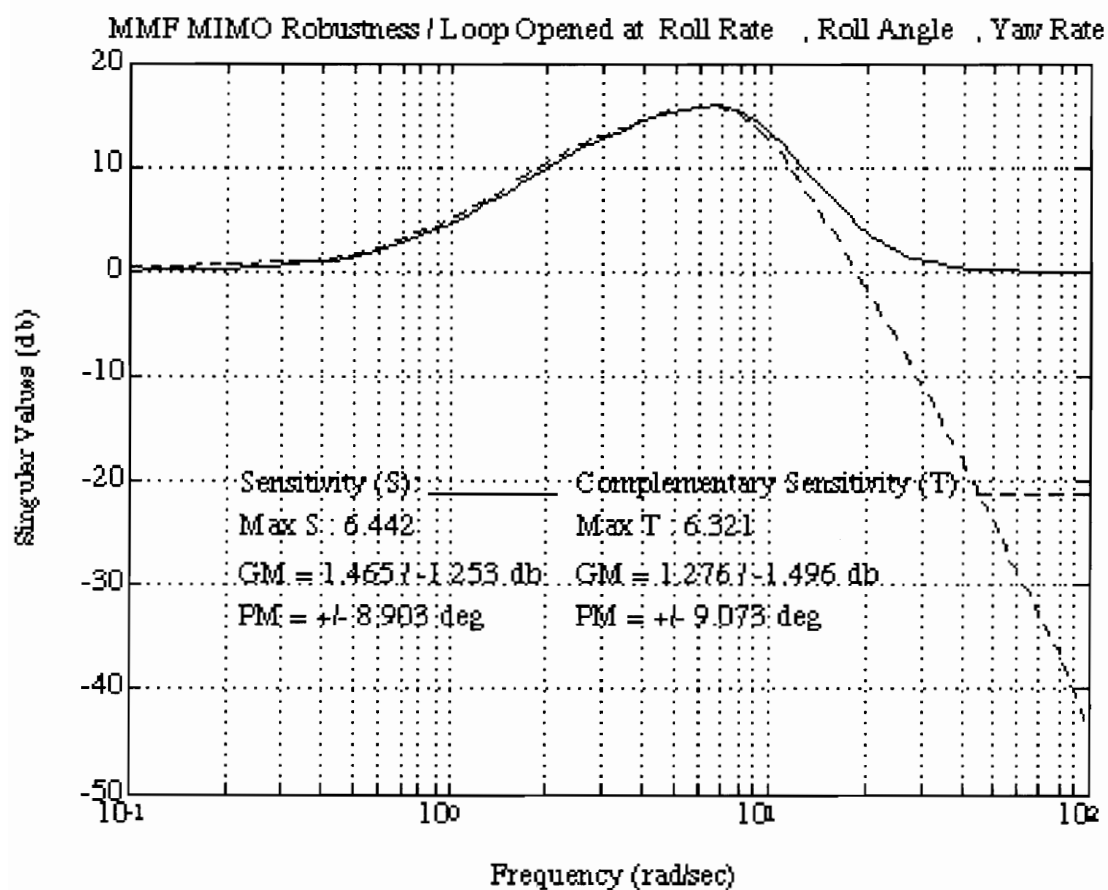


Figure 6.47 High Order MMF Sensor Plane Stability Robustness

## 6.11 Equivalent Systems Analysis

The MMF closed-loop system shown in figure 6.36 was linearized and reduced to a 4 state LOES model required for the flying qualities specification analysis. The frequency response of the reduced order versus the full order system for lateral stick and rudder pedal inputs is shown in figures 6.48 and 6.49, respectively. The fidelity of the LOES model was significantly degraded for the “cross-axis” responses, namely the lateral stick to sideslip and rudder pedal to roll angle transfer functions. This is because the reduction process emphasizes transfer functions with higher magnitudes. The mismatch of these responses does not significantly affect the modal properties used to analyze flying qualities. Table 6.3 compares the parameters of the equivalent system model with the values specified in MIL-F-8785C and displays the flying quality level achieved. As expected, the modal parameters are very close to the response characteristics designed into the maneuver command generator. As a result, all parameters meet Level 1 requirements.

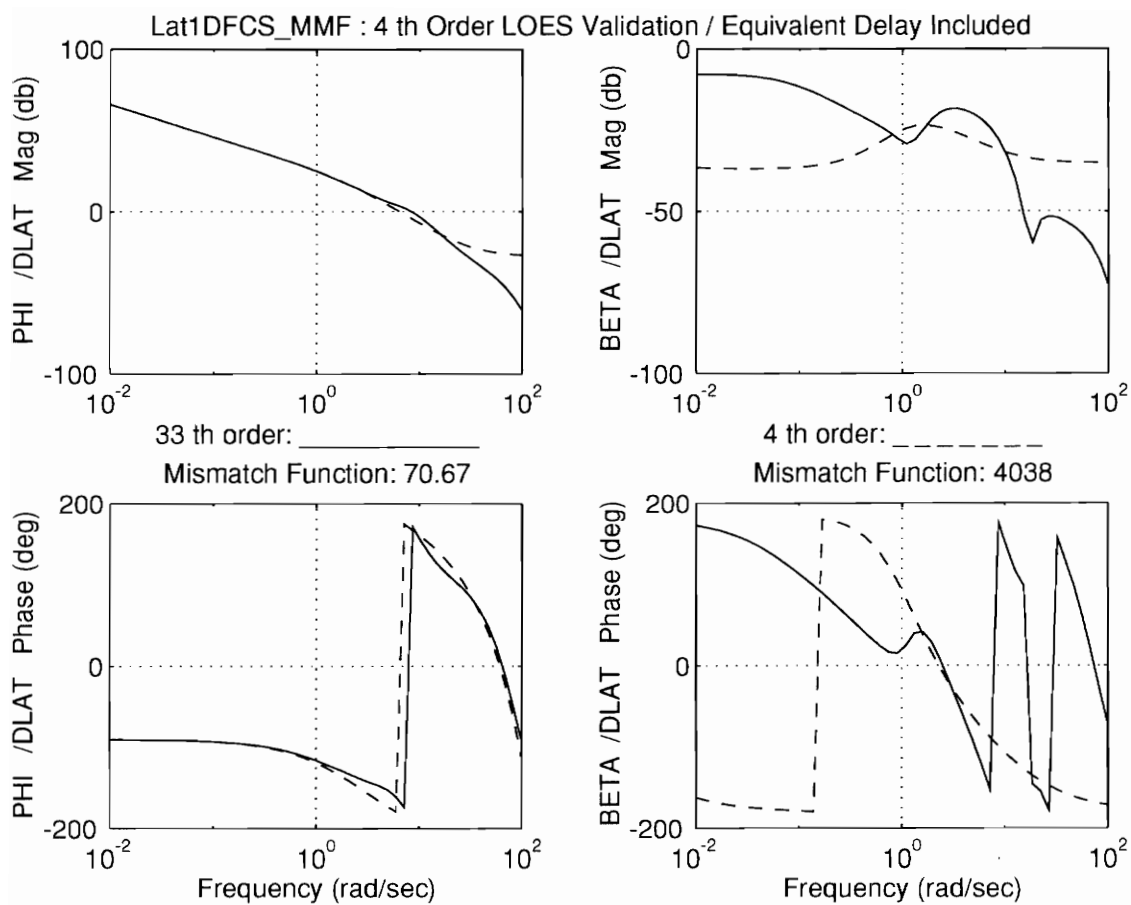


Figure 6.48 MMF LOES Frequency Response Validation / Lateral Stick Input

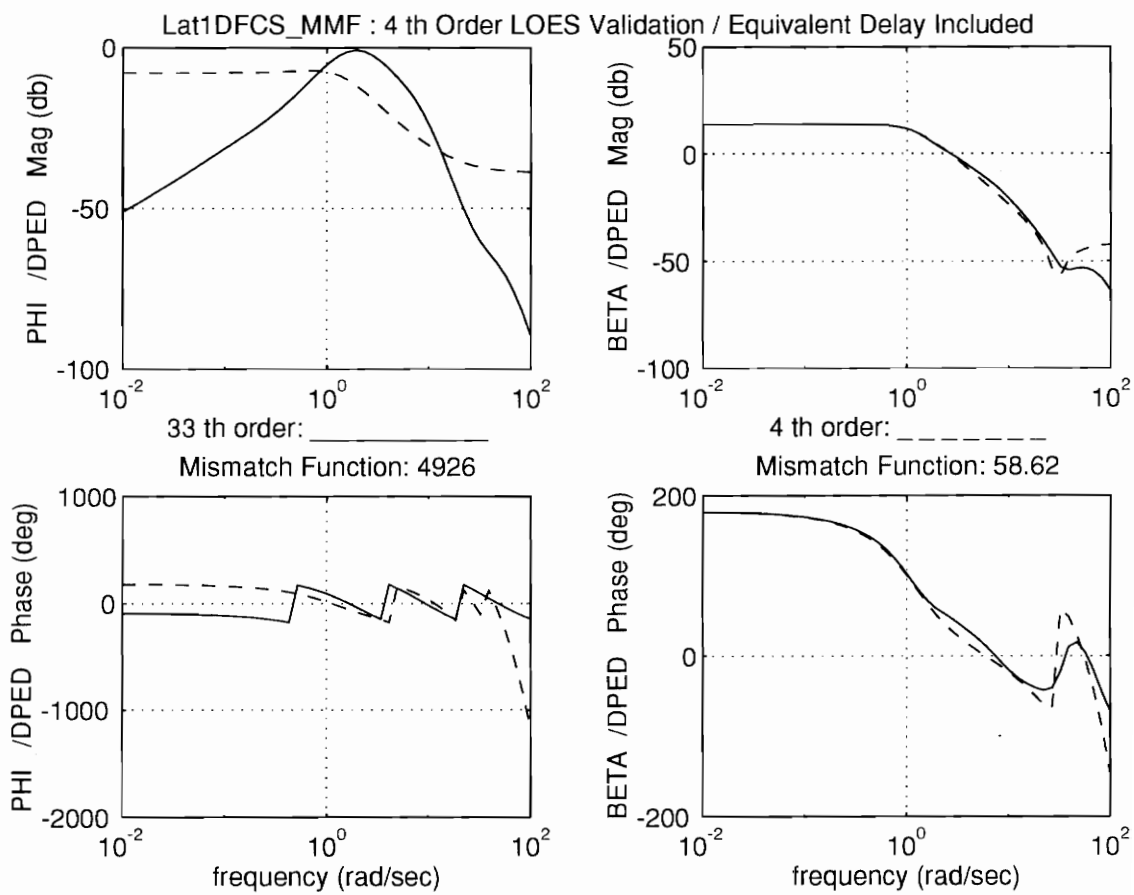


Figure 6.49 MMF LOES Frequency Response Validation / Rudder Pedal  
Input

Table 6.3 MMF Equivalent System Analysis Results

LOES Parameter	Definition	Level 1 Requirement	Value	Flying Quality Level
$\lambda_s = (-1/\tau_s)$	Spiral mode eigenvalue	Time to Double > 12 sec ( $\lambda_s < 0.0578$ )	0.000	1
$\tau_R$	Roll mode time constant	$\tau_R < 1$ sec	0.47 sec	1
$\omega_{dr}$	Dutch-roll Frequency	$\omega_{dr} > 1$ rad/sec	1.20 rad/sec	1
$\zeta_{dr}$	Dutch-roll Damping	$\zeta_{dr} > 0.125^*$	0.75	1
$t_{lat}$	Lateral Axis Time Delay	$t_{lat} < 0.10$ sec	0.05 sec	1
$t_{ped}$	Yaw Axis Time Delay	$t_{ped} < 0.10$ sec	0.05 sec	1

\* Requirement computed from  $0.15 = \zeta_{dr}\omega_{dr}$  with  $\omega_{dr} = 1.2$  rad/sec

## 6.12 Nonlinear Simulation Evaluation

The final step in the evaluation of the MMF control law is to validate its performance in the F-14 nonlinear simulation. To accomplish this task, the MMF control laws were coded in FORTRAN and linked with the F-14 nonlinear simulation. Figures 6.50 and 6.51 show the response of the MMF control law to lateral stick and rudder pedal inputs. As predicted by the linear analysis, roll response tracking is excellent with less sideslip excursions than experienced with the PA ARI, and direct sideslip command maneuvers can be accomplished with no lateral axis corrections required.

The turbulence response characteristics of the MMF were evaluated in the identical fashion as for the AFCS and PA ARI systems, as described in chapters 4 and 5. Figure 6.52 shows the MMF vs the PA ARI response to turbulence. The turbulence rejection properties of the MMF are shown to be superior to those of the classically designed PA ARI.

A formal piloted evaluation of the MMF control laws was not performed. However, this researcher performed an informal piloted evaluation to verify the basic flying qualities and response characteristics. As expected, the roll axis response was crisp and predictable with small sideslip excursions, while the sideslip response to pedal inputs was equally predictable with no requirement for the pilot to maintain a wings level roll attitude. A major advantage of the MMF control law design is the ability to change the response characteristics of the airplane by changing the MCG parameters, with no change required to the feedback regulator. The MCG parameters can be easily tuned during piloted simulation testing to provide optimal flying qualities. An example of tuning the roll mode time constant is demonstrated in figure 6.53.

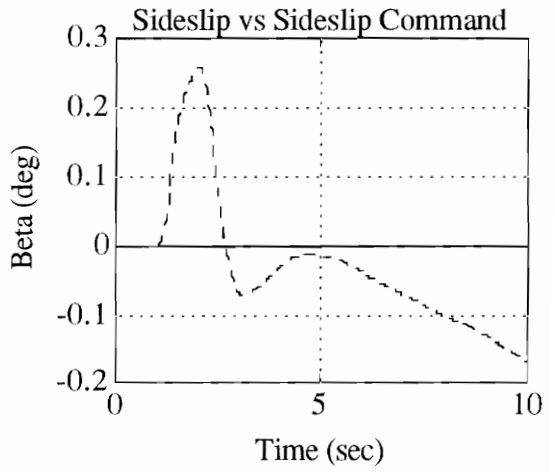
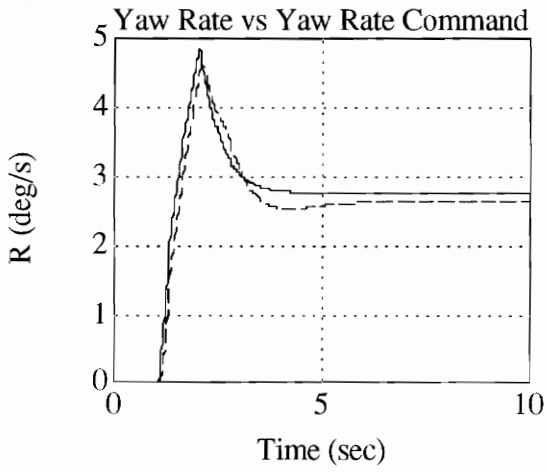
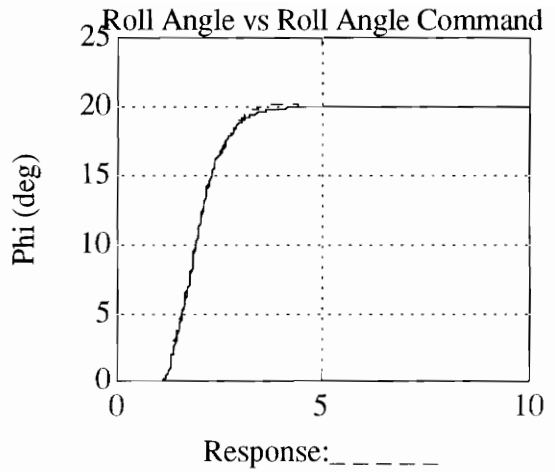
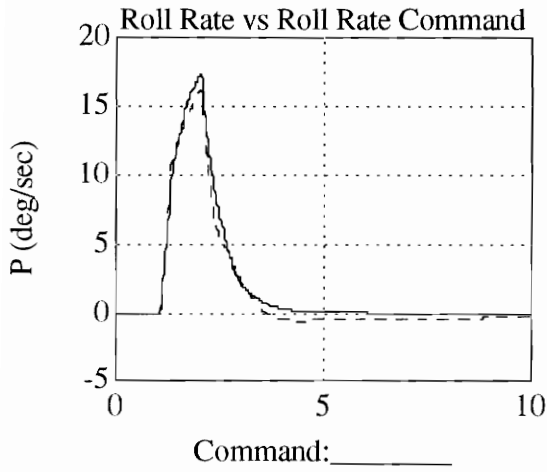


Figure 6.50 Nonlinear MMF Response to Lateral Stick



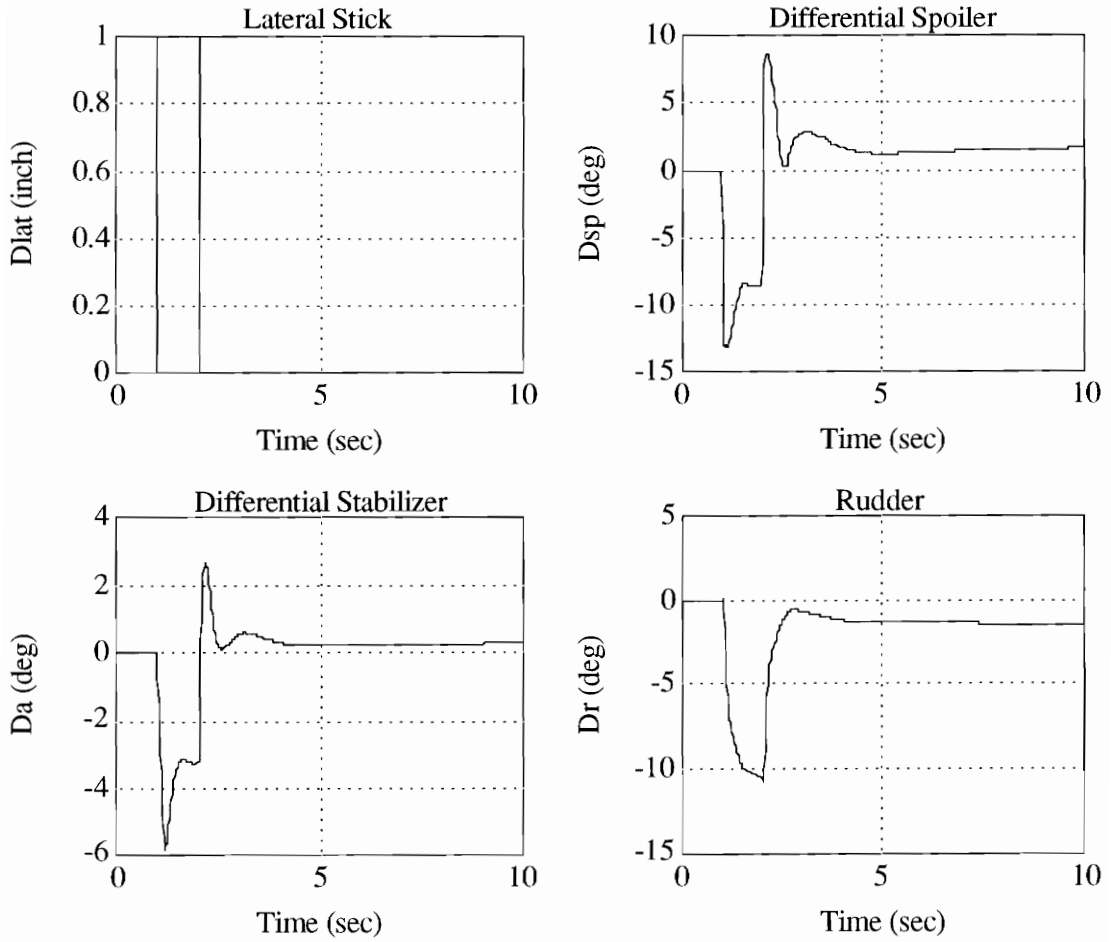


Figure 6.50 (Continued) Nonlinear MMF Response to Lateral Stick

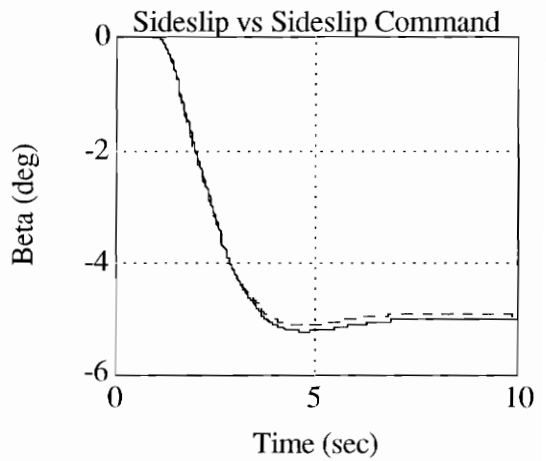
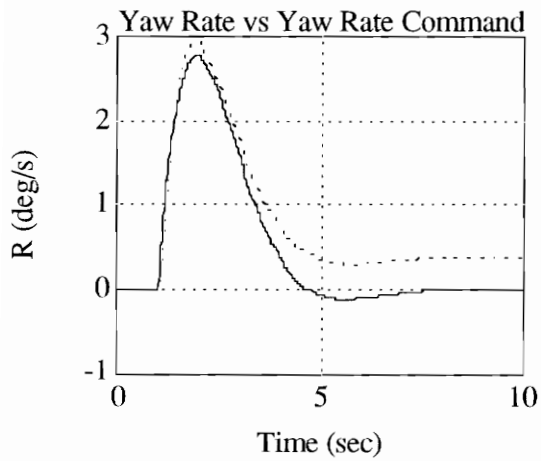
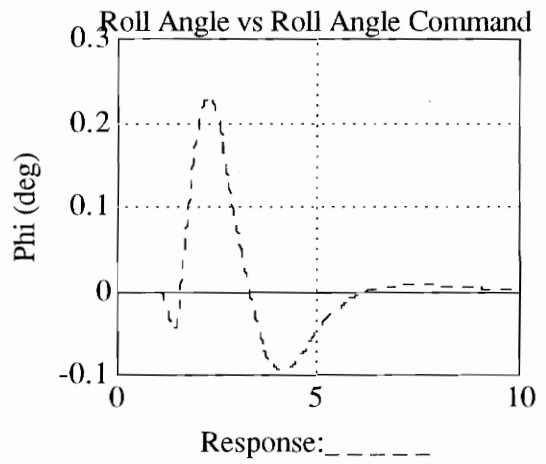
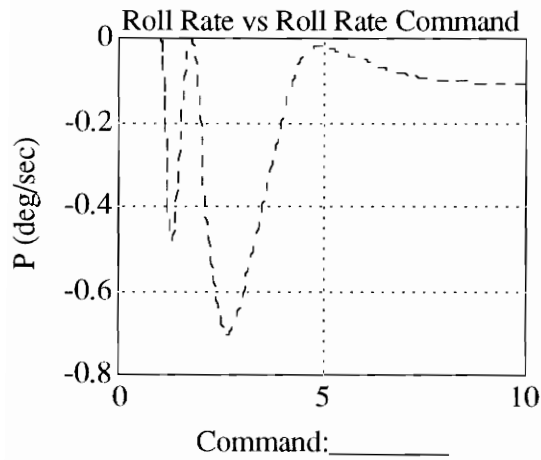


Figure 6.51 Nonlinear MMF Response to Rudder Pedal

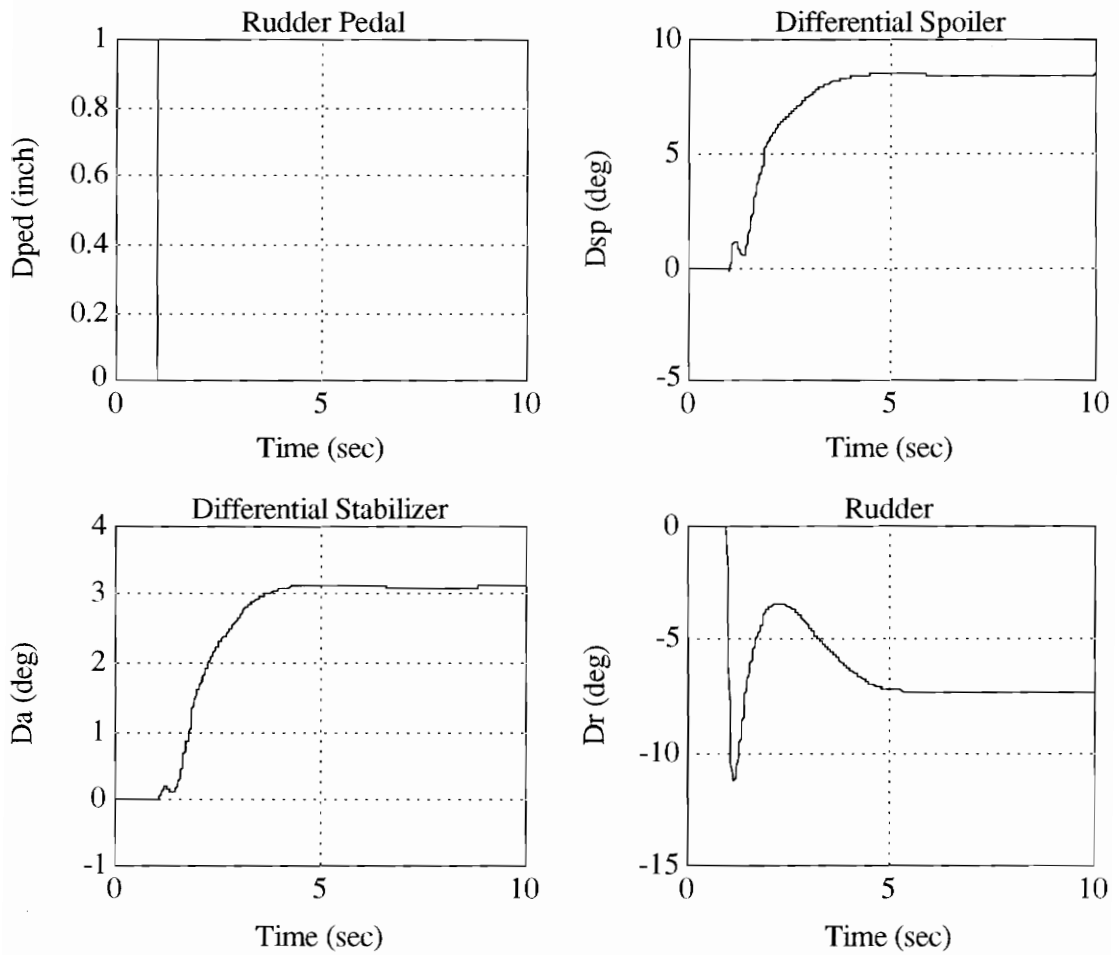


Figure 6.51 (Continued) Nonlinear MMF Response to Rudder Pedal

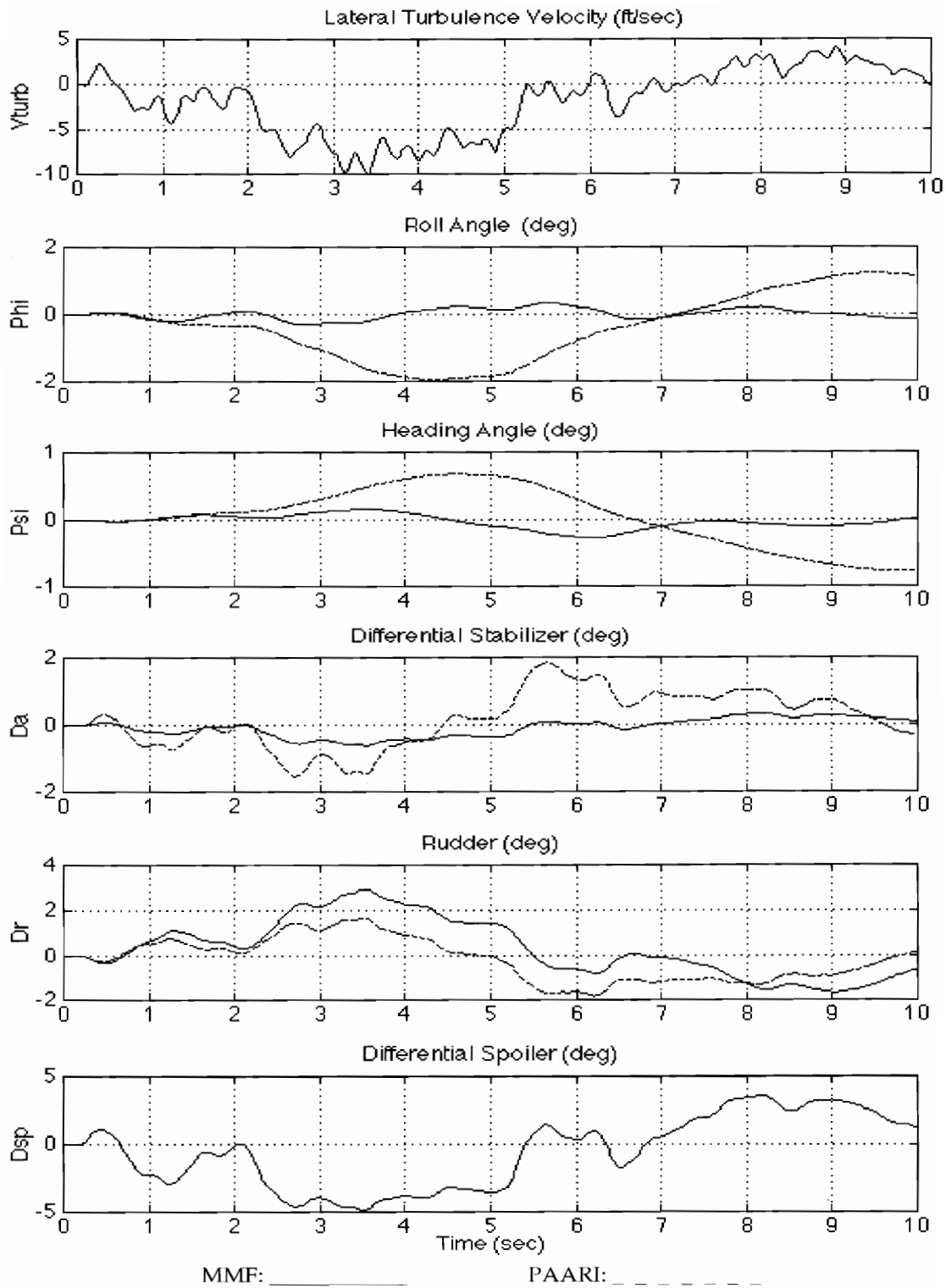


Figure 6.52 MMF vs PAARI Response to Atmospheric Turbulence

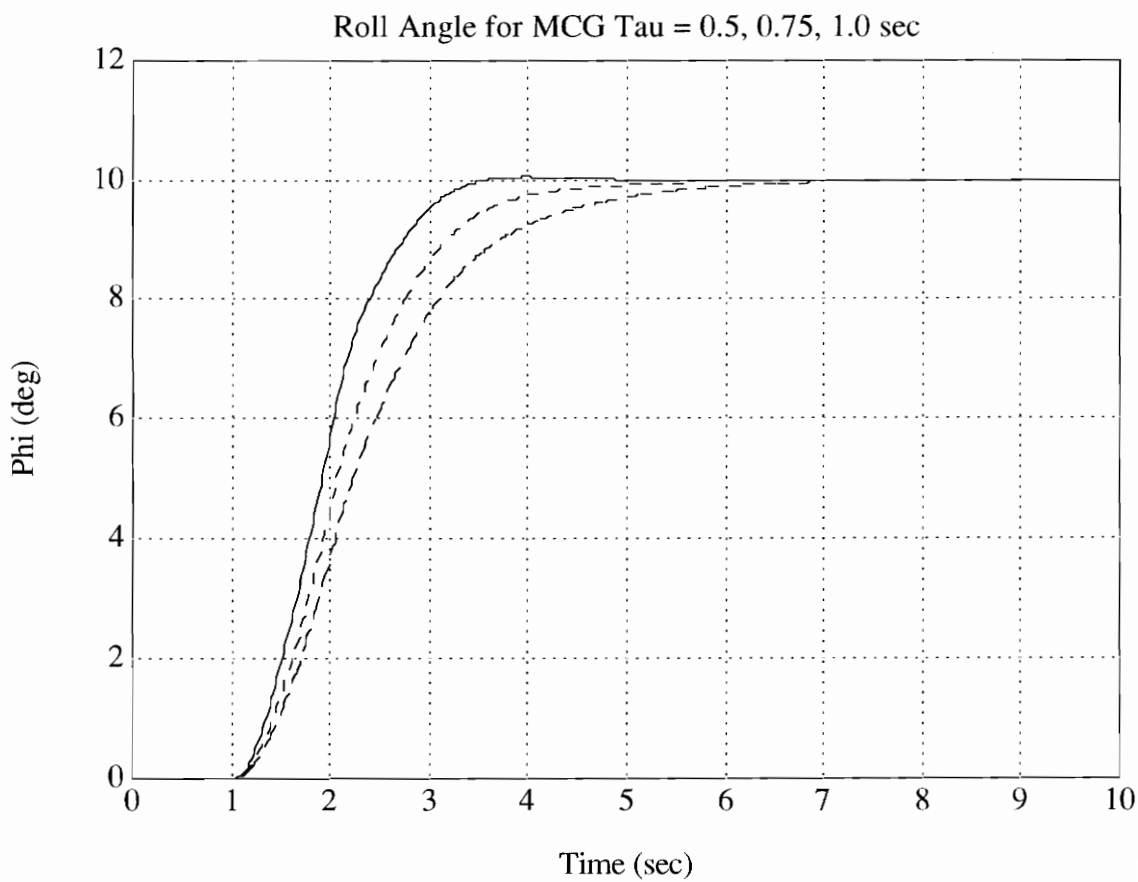


Figure 6.53 Response to Lateral Stick Half-Doublet showing Effect of Variation of MCG Roll Command Time Constant

### 6.13 Summary

Multivariable synthesis techniques have been used to design a control law for the F-14 aircraft in the powered approach configuration. Linear quadratic regulator theory was used to develop a state-feedback regulator with integral error control of roll angle and sideslip. The unmeasured sideslip angle state was estimated using a reduced order observer featuring exact LTR. Flying qualities requirements were directly incorporated into the design using an explicit model following scheme combining a Maneuver Command Generator with dynamic inversion. The SISO and MIMO robustness properties were evaluated for the full order system including digital effects and high order dynamics. The closed-loop performance and flying qualities of the system were demonstrated using equivalent systems analysis, off-line nonlinear 6-DOF simulation, and pilot-in-the-loop 6-DOF nonlinear simulation. The flying qualities were found to be roughly equivalent to the PA ARI. Areas where the MMF outperformed the PA ARI were in sideslip suppression for lateral stick inputs and turbulence rejection characteristics. The model following structure of the MMF also enabled easy evaluation of different closed-loop response characteristics by changing the parameters of the MCG.

## Chapter VII

### Summary and Conclusions

Piloted simulation, nonlinear simulation analysis, and linear stability analysis of the production AFCS control system confirmed the known flying qualities deficiencies of the aircraft in the powered approach configuration. The deficiencies were shown to be due to the nonlinear lateral stick to spoiler gearing, the lack of automatic coordinating rudder due to lateral stick inputs, and the low feedback gains which do not sufficiently augment the bare airframe characteristics in the low-speed PA regime.

To improve the flying qualities, the PA ARI control system was designed. The PA ARI design, which is targeted for the new F-14 Digital Flight Control System, resulted in substantial flying qualities enhancements over the existing AFCS control system, as demonstrated using equivalent systems analysis as well as extensive pilot-in-the-loop simulation. The feedback loop design, accomplished using discrete time SISO methods, proved to be highly effective in augmenting the aircraft damping characteristics and provided excellent disturbance rejection properties. The system was shown to possess excellent SISO robustness properties. The MIMO robustness properties were found to be good at the actuator plane, but not at the sensor plane. The primary disadvantage of

the design technique was the use of ad-hoc trial and error methods for the design of the feedforward paths.

To determine the relative optimality of the PA ARI control law design, multivariable synthesis techniques were applied to the F-14 PA design problem. The multivariable model following (MMF) system combined dynamic inversion and LQG/LTR techniques, resulting in a relatively systematic design process. The SISO robustness was shown to be acceptable, while the MIMO robustness properties were poorer than desired. The lack of MIMO robustness of the MMF system resulted from the fact that the LQG/LTR design procedure utilized for this problem only guarantees robustness at the input of the design plant model. Since generalized control inputs were used in the design process, no guaranteed margins exist for the physical plant inputs. The closed-loop performance and flying qualities of the system were demonstrated using equivalent systems analysis, off-line nonlinear 6-DOF simulation, and pilot-in-the-loop 6-DOF nonlinear simulation.

No major differences in flying qualities were observed between the PA ARI and the MMF control systems. The main difference in the response characteristics between the two systems was the MMF's response to rudder inputs, which allowed direct control of sideslip with no lateral stick input required to maintain a wings level attitude. Also, the model following architecture and integral feedback regulation resulted in a higher degree of sideslip suppression for lateral maneuvering than was achieved by the PA ARI. Based on an informal piloted evaluation of the MMF, this degree of performance does not noticeably enhance the flying



qualities. The primary benefit of the MMF over the PA ARI control system was the ease of which the closed-loop response characteristics could be tuned by changing parameters in the maneuver command generator. To perform the equivalent modifications in the PA ARI would require time consuming trial and error iteration of the forward path gains. However, the software implementation requirements of the MMF are considerably higher than for the PA ARI and far outweigh the increased flexibility in tuning the closed-loop response. In conclusion, the difference in performance between the classically designed PA ARI and the modern MMF design does not warrant the application of modern control theory.

## References

- 1.1 Nelson, Robert C., *Flight Stability and Automatic Control*, McGraw-Hill, New York, 1989
- 1.2 Mclean, Donald, *Automatic Flight Control Systems*, Prentice Hall International (UK) Ltd, 1990
- 1.3 NAVAIRTESTCEN Technical Report TPS-15R-85, Skidmore, M. A., "Phase II-A Developmental Testing of the F-14A Airplane", 2 December 1985.
- 1.4 NASA TM-81833, Kelly, W., and Brown, P., "Simulator Results of an F-14A Airplane Utilizing an Aileron-Rudder Interconnect During Carrier Approaches and Landings," May 1980
- 1.5 NASA TM-81972, Kelly, W., and Enevoldson, E., "Limited Evaluation of an F-14A Airplane Utilizing an Aileron-Rudder Interconnect Control System in the Landing Configuration," December 1981
- 1.6 NAVAIRTESTCEN Report of Test Results SA-3R-80, Lewis, J., and Hildreth, B., "Navy Evaluation of NASA Developed Automatic Rudder Interconnect (ARI) for the F-14A Airplane," 14 February 1980
- 1.7 Gangsaas, D., Bruce, K., and Blight, J., "Application of Modern Synthesis to Aircraft Control: Three Case Studies," IEEE Transactions on Automatic Control, Vol. AC-31, No. 11, November 1986
- 1.8 Doyle, J., and Stein, G.: "Multivariable Feedback Design: Concepts for a Classical/Modern Synthesis," IEE Transactions on Automatic Control, Vol. AC-26, No. 1, February 1981

- 1.9 Moorhouse, D. J., "Lessons Learned from the STOL and Maneuver Technology Demonstrator," WL-TR-92-3027, June 1993
- 1.10 Thompson, C., Coleman, E., and Blight, J., "Integral LQG Controller Design for a Fighter Aircraft," AIAA Paper 87-2452, AIAA Guidance, Navigation, and Control Conference, Monterey, CA, August 1987
- 1.11 Adams, R., Buffington, J., Sparks, A., and Banda S., "An Introduction to Multivariable Flight Control System Design," WL-TR-92-3110, October 1992
- 1.12 Chetty, S., and Henschel, F., "Model Following Flight Control System Design for ATTAS, DFVLR's New In-Flight Simulator," AIAA Paper 87-2451, AIAA Guidance, Navigation, and Control Conference, Monterey, CA, August 1987
- 2.1 Nichols, J., "The Generic Simulation Executive at Manned Flight Simulator," AIAA paper 94-3429-CP, AIAA Flight Simulation Technologies Conference, Scottsdale, AZ, August 1994
- 2.2 Bachner, S., and Wachter, B., "F-14 Aerodynamic Model Description", Report No. NAWC23, June 30, 1994
- 2.3 Etkin, B., *Dynamics of Atmospheric Flight*, Wiley, New York, 1972
- 3.1 Cooper, G.E., and Harper, R.P., Jr., "The Use of Pilot Rating in the Evaluation of Aircraft Handling Qualities," NASA TN D-5153, NASA, Washington D.C., April 1969
- 3.2 Ashkenas, I.L., "Twenty-five Years of Handling Qualities Research," AIAA J. Aircraft, vol. 21, no. 5, May 1984, pp. 289-301

- 3.4 Rabin, U.H., and Anderson, M.R., "V-22 Flight Control System Analysis (Revision D DFCS Control Laws)," SCT Report No. 4522-440-001, September 1988
- 3.5 MIL-F-9490D, "Flight Control Systems, Design, Installation and Test of, Piloted Aircraft, general Specification for", June 1975
- 3.6 Lehetomaki, N., Sandell, N., and Athans, M., "Robustness Results in Linear-Quadratic Gaussian Based Multivariable Control Designs," IEEE Transactions on Automatic Control, Vol. AC-26, No. 1, Feb. 1981, pp 75-92
- 3.7 Chiang, R., and Safonov, M., "Robust Control Toolbox Users Guide", The Mathworks, Inc., 1992
- 4.1 Minnich, S., and Ryberg, E., "Piloted Simulation Flying Qualities Evaluation of a DFCS equipped F-14 Airplane," Report No. NAWCAD17, Preliminary Draft
- 5.1 MIL-STD-1797A, "Military Specification - Flying Qualities of Piloted Vehicles," March 1987
- 6.1 Shaw, P., Haiges, K., "Design Methods for Integrated Control Systems," AFWAL-TR-88-2061, Aero Propulsion Laboratory, AFWAL, Wright-Patterson Air Force Base, Ohio, June 1988
- 6.2 Rynaski, E., "The Total In-Flight Simulator, 'TIFS', 20 Years of Flight Experience," a tutorial, IEEE Conference on Control Applications, Dayton, Ohio, 13 Sept 1992
- 6.4 Ridgely, D., Banda, S., "Introduction to Robust Multivariable Control," AFWAL-TR-85-3102, February 1986

- 6.5 Bacon, Barton J., "Closed-Form Solution for Loop Transfer Recovery via Reduced-Order Observers," AIAA Paper 89-3455-CP, AIAA Guidance, Navigation, and Control Conference, Boston, MA, August 1989

## Vita

Although Mr. Renfrow was born in White Plains, New York in October, 1963, he spent the majority of his formative years in rural Johnston County, North Carolina. From August 1981 to May 1985 he attended North Carolina State University where he received his Bachelor of Science degree in Aerospace Engineering. Since June 1985 he has been employed at the Naval Air Warfare Center - Aircraft Division in Patuxent River, Maryland where he has served as flight control system analyst on the V-22 and F-14 Digital Flight Control System programs. He began his graduate studies at the Virginia Polytechnic Institute and State University in August 1989, and finished in December 1994, receiving his Master of Science in Mechanical Engineering.

*Joseph A. Renfrow*